

AN ABSTRACT OF THE THESIS OF

Guang Xiao for the degree of Doctor of Philosophy in Chemistry  
presented on December 13, 1989

Title: The Analytical Chemistry of Pentazocine Metabolites Produced by  
the Greyhound

Redacted for privacy

Abstract approved: \_\_\_\_\_

 E. H. Piepmeier  
Redacted for privacy

 A. M. Craig

This thesis concerns itself mainly with analytical methods development and analytical applications in the field of drug metabolism studies. The determination of the analgesic pentazocine and its metabolites in the greyhound are studied.

Pentazocine and all of its possible metabolites are isolated from the greyhound urine by a the multi-solvent extraction and XAD-2 column after enzymatic hydrolysis. The optimization of subsequently applied chromatographic separation techniques are studied, and a useful strategy for the separation of analgesics like pentazocine and its metabolites is devised. As a result, nine pentazocine metabolites were recovered from the greyhound urine and metabolic isomers were successfully separated by the HPLC assay developed.

Mass spectroscopic fragmentations of trimethylsilylated pentazocine upon electron impact (EI) are described. The identification of positional isomers due to different functional group attachment to the end of the side chain is achieved by the fragmentations proposed. The EI mass spectra of nine pentazocine metabolites including three pairs of new metabolic isomers are interpreted based on the fact that the biotransformation of a drug results in structurally similar metabolites.

A complete NMR assignment of pentazocine is conducted emphasizing the choice and utilization of selected 1D and 2D NMR methods to determine the molecular structure and conformation of a complex organic molecule. An NMR analysis protocol is proposed whereby a pentazocine metabolite can be characterized without a synthetic reference.

A newly discovered pentazocine metabolite is identified as 8-methoxyl pentazocine by using the NMR analysis strategies devised. These results show three pairs of new metabolic isomers of pentazocine in greyhound urine. Three of the new isomers have a methoxyl group attached to the aromatic ring at the 8-position and a hydroxyl group at the 9-position. Their isomers are formed by interchanging these two groups between these two sites. It is concluded that, in addition to oxidative metabolism on the side chain observed in most other species, pentazocine has also undergone the hydroxylation and methylation of the aromatic ring in the greyhound metabolism.

ANALYTICAL CHEMISTRY OF PENTAZOCINE METABOLITES  
PRODUCED BY THE GREYHOUND

by

Guang Xiao

A THESIS

submitted to

Oregon State University

in partial fulfillment of  
the requirements for the  
degree of  
Doctor of Philosophy

Completed December 13, 1989

Commencement June, 1990

APPROVED:

Redacted for privacy

---

Co-Professor of Chemistry in Charge of Major

Redacted for privacy

---

Co-Associate Professor of Veterinary Medicine in Charge of Major

Redacted for privacy

---

Chairman of Department of Chemistry

Redacted for privacy

---

Dean of the Graduate School

Date thesis is presented December 13, 1989

To my fellow students in Beijing and Beijing (Peking) University, who fought for a free China with their future and even with their lives in June 1989.

## Acknowledgments

I would like to sincerely thank Dr. E. H. Piepmeier and Dr. A. M. Craig for their patience, encouragement, constant support and guidance throughout my stay in graduate school. Their enthusiasm for science and profound knowledge in both chemistry and real life have set an example for me to be a capable scientist.

My special thanks go to a number of people for their assistance in the preparation of this thesis: Mr. Rodger Kohnert for his invaluable guidance and assistance on the NMR study of pentazocine and one of its metabolites; Mr. Dan Bilich for his patience and neverending technical assistance; Drs. Linder Blythe and Lori Walker for their special assistance in this project; Mr. Ben Shen for his suggestions at various times.

I extend my thanks to all my committee members for their guidance, to the members of "Craig's Lab", and the Chemistry Department for their help and support. I should also thank Hector, Jack, and many friends in the United State, Cheng, Yi, and many many other friends in China for providing me with diversions necessary to keep my faith in science, and life filled with excitement.

Finally, I would like to express my deepest gratitude to Shun-Wen Chang for her never failing love, understanding, guidance in matters in which she is naturally superior than I; to our parents, Lun and Louisa Rong Chung, Henry and Mei for their immeasurable love and enormous quantities of support to both Shun-Wen and I; to my brother, my aunt and my grandmother for their affection, patience and encouragement.

## TABLE OF CONTENTS

	Page
I. INTRODUCTION	1
1. Historical	1
2. Metabolism of Analgesics	6
3. Analytical Chemistry in Metabolism Studies	9
II. DEVELOPMENT OF TOTAL ISOLATION OF THE DRUG AND ITS METABOLITES FROM BIOLOGICAL SAMPLE MATRIX	14
1. Abstract	15
2. Introduction	16
3. Materials and Reagents	19
4. Methods	20
5. Results and Discussion	36
III. HIGH-PERFORMANCE LIQUID CHROMATOGRAPHIC SEPARATION OF PENTAZOCINE METABOLITE ISOMERS FROM GREYHOUND URINE	42
1. Introduction	43
2. Experimental	48
3. Materials and Reagents	52
4. Results and Discussion	52
5. Conclusion	65

IV.	STRUCTURAL CHARACTERIZATION OF PENTAZOCINE METABOLITES IN THE GREYHOUND BY GAS CHROMATOGRAPHY/ELECTRON IMPACT MASS SPECTROMETRY	71
	1. Introduction	72
	2. Experimental	74
	3. Results and Discussion	76
	4. Conclusion	115
V.	INTRODUCTION AND GENERAL THEORY OF TWO-DIMENSIONAL NMR	121
	1. Introduction	122
	2. $^1\text{H}$ and $^{13}\text{C}$ NMR Fundamentals	123
	3. Two-Dimensional NMR	135
	4. Experimental	164
	5. Conclusion	165
VI.	NUCLEAR MAGNETIC RESONANCE STUDY OF PENTAZOCINE	167
	1. Introduction	168
	2. Discussion and Results	170
	3. Strategic Implications for Metabolite NMR Analysis	200
	4. Experimental	203

VII. COMPLETE STRUCTURAL ELUCIDATION OF A PENTAZOCINE METABOLITE	205
1. Introduction	206
2. Discussion and Results	208
3. Experimental	250
VIII. CONCLUSION	255
IX. REFERENCES	262

## LISTS OF FIGURES

<u>Figure</u>		<u>Page</u>
I.1	Major pentazocine metabolites found in various species.	4
II.1	Extraction scheme of pentazocine and its metabolites in greyhound urine with base hydrolysis.	21
II.2	Extraction scheme of pentazocine and its metabolites in greyhound urine with acid hydrolysis.	23
II.3	Extraction scheme of pentazocine and its metabolites in greyhound urine with enzymatic hydrolysis.	25
II.4	Extraction scheme of pentazocine and its metabolites in greyhound urine under different pH values after enzymatic hydrolysis.	26
II.5	Extraction scheme of pentazocine and its metabolites in greyhound urine with enzymatic hydrolysis and back-extraction.	28
II.6	Extraction scheme of pentazocine and its metabolites in greyhound urine with increasing solvent polarity.	30
II.7	XAD-2 resin column extraction scheme of pentazocine and its metabolites in greyhound urine after multi-solvent extraction.	32
II.8	XAD-2 extraction column.	34
II.9	Schematic representation of a Thin-Layer Chromatogram (pre-coated silica gel plates, 60F <sub>254</sub> , 0.25 mm. thick, EM Science) of Fraction C, Fraction B and Fraction D in developing solvent system:chloroform/methanol/ammonia, 97/3/0.015%, v/v/v.	38

<u>Figure</u>	<u>Page</u>
II.10	40
<p>Gas chromatographic and mass spectroscopic testing results of XAD-2 column extracts: (a) Chromatogram of XAD-2 extracts after trimethylsilylated derivatization; (b) Mass spectrum of trimethylsilylated derivative of pentazocine metabolite, MET7; (c) Mass spectrum of trimethylsilylated derivative of pentazocine metabolite, MET8; (d) Mass spectrum of trimethylsilylated derivative of pentazocine metabolite, MET9.</p>	
II.11	41
<p>Overall flow diagram of isolation of pentazocine and its metabolites from greyhound urine.</p>	
III.1	49
<p>Extraction scheme of pentazocine and its metabolites from greyhound urine for separation of metabolites MET1 and MET2.</p>	
III.2	55
<p>Schematic representation of pentazocine metabolites separation by TLC (pre-coated silica gel plates, 60F<sub>254</sub>, 0.25 mm. thick, EM Science). Developing solvents: (a) Hexane; (b) Hexane/Methanol (9/1, v/v); (c) Ethyl acetate; (d) Ethyl acetate/Methanol (9/1, v/v).</p>	
III.3	57
<p>Schematic representation of pentazocine metabolites separated by TLC (pre-coated silica gel plates, 60F<sub>254</sub>, 0.25 mm. thick, EM Science); Developing solvent system: chloroform/methanol/ammonia (97/3/0.015%, v/v/v): (a) Application of combined solvent extracts; (b) Application of individual extracts.</p>	

<u>Figure</u>	<u>Page</u>
III.4 Normal phase chromatograms of (a) pentazocine metabolite MET1 and (b) pentazocine metabolite MET2 with mobile phase: chloroform/methanol/ammonia (95/5/0.015%, v/v/v), stationary phase: 5 $\mu$ m silica, and flow rate: 2 ml/min: (A) Sample injection of equivalent to 10 ml urine extracts; (B) Sample injection of actual collection for subsequent NMR analysis of MET1.	62
III.5 Normal phase chromatogram of (a) pentazocine with mobile phase: chloroform/methanol/ammonia (95/5/0.015%, v/v/v), stationary phase: 5 $\mu$ m silica, and flow rate: 2ml/min.	63
III.6 GC/MS chromatograms of (a) interference, (b) MET1 and (c) MET2: (A) GC/MS chromatogram obtained for collected TLC eluting band before HPLC analysis; (B) Close-up of chromatogram (A).	64
III.7 Mass spectra of pentazocine metabolites MET1 and MET2: (a) mass spectrum of pentazocine metabolite MET1 trimethylsilylated derivative; (b) mass spectrum of pentazocine metabolite MET2 trimethylsilylated derivative.	66
III.8 Mass spectrum of pentazocine trimethylsilylated derivative.	67
III.9 Structures of pentazocine metabolites MET1 and MET2.	68
III.10 GC/MS chromatograms of (a) pentazocine metabolite MET1: (A) GC/MS chromatogram obtained for the fraction collected for MET1 after HPLC separation; (B) Close-up of chromatogram (A).	69

<u>Figure</u>		<u>Page</u>
IV.1	Structure of pentazocine.	73
IV.2	Mass spectrum of pentazocine trimethylsilylated derivative.	77
IV.3	Fragmentation pathway producing ion m/z 73.	79
IV.4	Fragmentation Pathway I.	80
IV.5	Fragmentations of (a) secondary cleavage of ion m/z 357; (b) Pathway II; and (c) Pathway III.	82
IV.6	Fragmentation Pathway IV.	83
IV.7	Fragmentation Pathway V.	85
IV.8	Fragmentation Pathway VI: (a) producing ion m/z 244; (b) producing ion m/z 245; and (c) producing ion m/z 246.	87
IV.9	Mass spectrum of pentazocine metabolite MET1 trimethylsilylated derivative.	94
IV.10	Mass spectrum of pentazocine metabolite MET2 trimethylsilylated derivative.	96
IV.11	GC/MS chromatogram of pentazocine metabolites (a) MET1 and (b) MET2.	98
IV.12	Structures of pentazocine metabolites MET1 and MET2.	99
IV.13	Mass spectrum of pentazocine metabolite MET3 trimethylsilylated derivative.	100
IV.14	Fragmentation Pathway VII.	101
IV.15	Mass spectrum of pentazocine metabolite MET4 trimethylsilylated derivative.	103
IV.16	Structures of pentazocine metabolites MET3 and MET4.	104

<u>Figure</u>	<u>Page</u>
IV.17 Mass spectrum of pentazocine metabolite MET5 trimethylsilylated derivative.	105
IV.18 Mass spectrum of pentazocine metabolite MET6 trimethylsilylated derivative.	107
IV.19 Structures of pentazocine metabolites MET5 and MET6.	108
IV.20 Mass spectrum of pentazocine metabolite MET7 trimethylsilylated derivative.	109
IV.21 Fragmentation pathway producing ion m/z 370 in pentazocine carboxylic acid metabolites.	111
IV.22 Fragmentation Pathway VIII.	112
IV.23 Fragmentation Pathway IX.	113
IV.24 Structure of pentazocine metabolite MET7.	114
IV.25 Mass spectrum of pentazocine metabolite MET8 trimethylsilylated derivative.	116
IV.26 Mass spectrum of pentazocine metabolite MET9 trimethylsilylated derivative.	117
IV.27 Structures of pentazocine metabolites MET8 and MET9.	118
V.1 Pascal's triangle for relative intensities of first-order multiplets.	127
V.2 Proton NMR spectrum of aromatic protons in pentazocine.	128
V.3 Different representations of three NMR signals recieved simultaneously: (a) the sum of three sine waves; (b) three separate sine waves; (c) the Fourier transform of (a).	133
V.4 The microscopic ( $\mu$ ) and macroscopic (M) magnetizations in the stationary and rotating frames.	137

<u>Figure</u>	<u>Page</u>
V.5	139
<p>Schematic representations of the Spin-echo experiment for a simple AX system: (a) macromagnetization vector before applying the 90° pulse; (b) application of the 90° pulse transverses the magnetization; (c) transversed magnetization splits into its components; (d) application of the 180° pulse causes interchange of magnetizations; and (e) Spin-echo information after time <math>\tau</math> due to refocusing of magnetizations.</p>	
V.6	144
<p>Timing sequence for 2D NMR spectroscopy.</p>	
V.7	147
<p>Pulse sequence and its effect on magnetization components in homonuclear 2D J-resolved spectroscopy: (A) Pulse sequence in homonuclear 2D J-resolved spectroscopy; (B) Effect of the pulse sequence on a <math>^1\text{H}</math> doublet; and (C) Effect of the pulse sequence on two magnetization components that are not coupled to each other.</p>	
V.8	149
<p>Schematic representation of a 2D J-resolved spectrum for a proton spectrum containing two overlapped doublets.</p>	
V.9	151
<p>Pulse sequence for COSY.</p>	
V.10	153
<p>COSY spectrum of pentazocine.</p>	
V.11	155
<p>Pulse sequence and its effect on magnetization components in heteronuclear 2D-shift correlated experiment: (A) Pulse sequence in heteronuclear 2D-shift correlated experiment; (B) Effect of the pulse sequence on a <math>^1\text{H}</math> doublet coupled with a bound C; and (C) Effect of the pulse sequence on the bound <math>^{13}\text{C}</math> magnetization component.</p>	

<u>Figure</u>	<u>Page</u>	
V.12	Schematic representation of the HETCOR spectrum of ethanol	158
V.13	Schematic representation of the long range heteronuclear correlation spectrum of ethanol.	160
V.14	Pulse sequence for NOESY.	162
V.15	NOESY spectrum of pentazocine metabolite MET1.	163
VI.1	Pentazocine molecular structure.	169
VI.2	400-MHz $^1\text{H}$ NMR spectrum of pentazocine in D-chloroform.	171
VI.3	Proton broadband-decoupled $^{13}\text{C}$ NMR spectrum of pentazocine in D-chloroform.	178
VI.4	Structures of (a) pentazocine; and five smaller molecules with similar nuclear environments to that of N-ring portion in pentazocine: (b) piperidine; (c)-(f) piperidine derivatives.	181
VI.5	COSY spectrum of pentazocine in D-chloroform.	187
VI.6	Heteronuclear shift correlated (direct C-H bond) spectrum of pentazocine in D-chloroform.	196
VI.7	Schematic representation of the assignment strategy for the complete NMR analysis of pentazocine metabolite.	201
VII.1	400-MHz $^1\text{H}$ NMR spectrum of pentazocine metabolite MET1 in D-chloroform.	209
VII.2	NMR spectra of pentazocine metabolite MET1 in D-acetone: (a) 400-MHz $^1\text{H}$ NMR spectrum; (b) $^{13}\text{C}$ NMR spectrum; and (c) COSY spectrum.	211
VII.3	400-MHz $^1\text{H}$ NMR spectrum of pentazocine metabolite MET1 in D-methanol.	213

<u>Figure</u>	<u>Page</u>
VII.4 Proton broadband-decoupled $^{13}\text{C}$ NMR spectrum of pentazocine metabolite MET1 in D-methanol.	217
VII.5 COSY spectrum of pentazocine metabolite MET1 in D-methanol	221
VII.6 Heteronuclear shift correlated (direct C-H bond) spectrum of pentazocine metabolite MET1 in D-chloroform.	227
VII.7 Heteronuclear shift correlated (long range C-H coupling) spectrum of pentazocine metabolite MET1 in D-methanol.	232
VII.8 The possible structure of the aromatic ring portion of pentazocine metabolite MET1 based on long range C-H coupling information.	236
VII.9 The possible structure of the aromatic ring portion of pentazocine metabolite MET1 based on heteronuclear shift correlated spectral information.	237
VII.10 $^1\text{H}$ NMR difference spectrum of pentazocine metabolite MET1 in D-methanol (irradiation of resonance j & e): (a) proton difference spectrum of MET1 in D-methanol; (b) off-resonance proton NMR spectrum of MET1 in D-methanol.	239
VII.11 $^1\text{H}$ NMR difference spectrum of pentazocine metabolite MET1 in D-methanol (irradiation of resonance k,l): (a) proton difference spectrum of MET1 in D-methanol (upon irradiation of k); (b) proton difference spectrum of MET1 in D-methanol (upon irradiation of l); and (c) off-resonance proton NMR spectrum of MET1 in D-methanol.	241

<u>Figure</u>	<u>Page</u>
VII.12 <sup>1</sup> H NMR difference spectrum of pentazocine metabolite MET1 in D-methanol (irradiation of resonance g,o): (a) proton difference spectrum of MET1 in D-methanol (upon irradiation of g); (b) proton difference spectrum of MET1 in D-methanol (upon irradiation of o); and (c) off-resonance proton NMR spectrum of MET1 in D-methanol.	242
VII.13 The structure of aromatic ring portion of pentazocine metabolite MET1 deduced from NOE experiments.	246
VII.14 NOESY spectrum of pentazocine metabolite MET1 in D-methanol.	247
VII.15 The structure of aromatic ring portion of pentazocine metabolite MET1 and its connection to the rest of the molecule deduced from COSY and NOESY spectral information	249
VII.16 Molecular structure of pentazocine metabolite MET1.	252
VIII.1 Structures of pentazocine and its metabolites produced by the side chain oxidative metabolism in the greyhound: (a) pentazocine, (b) metabolite MET3 (cis-alcohol), (c) MET4 (trans-alcohol), and (d) MET7 (trans-acid).	257
VIII.2 Structures of pentazocine and its metabolites produced by hydroxylation and methylation of aromatic ring and oxidation of side chain metabolism in the greyhound: (a) metabolite MET1, (b) MET2, (c) MET5, (d) MET6, (e) MET8 and (f) MET9.	259
VIII.3 The probable metabolic pathway of pentazocine in the greyhound.	261

## LIST OF TABLES

<u>Table</u>		<u>Page</u>
I.1	Summary of pentazocine metabolism studies conducted in different species.	5
III.1	Summary of TLC developing solvent systems.	53
III.2	R <sub>f</sub> values of pentazocine and its metabolites in TLC.	59
IV.1	Important mass spectral fragment ions (m/z) and the structural implications for the trimethylsilylated derivative of pentazocine.	89
IV.2	GC relative retention time of the trimethylsilylated derivatives of pentazocine metabolites.	91
IV.3	Important fragment ions (m/z) in mass spectra of trimethylsilylated derivatives of pentazocine and its metabolites.	92
IV.4	Percent abundances of important fragment ion peaks relative to base peak.	93
VI.1	The probable pentazocine <sup>1</sup> H NMR resonance assignments	177
VI.2	The possible assignments of <sup>13</sup> C NMR resonances of pentazocine.	179
VI.3a	Proton J-couplings in pentazocine observed by COSY experiment.	188
VI.3b	Proton J-coupling constants observed in pentazocine.	191
VI.3c	The <sup>1</sup> H resonance assignments of pentazocine supported by COSY experiment.	194

<u>Table</u>		<u>Page</u>
VI.4	Heteronuclear chemical shift correlation (direct C-H bond) NMR results for pentazocine.	197
VI.5	$^1\text{H}$ and $^{13}\text{C}$ NMR resonance assignments for pentazocine in D-chloroform.	199
VII.1	The probable $^1\text{H}$ NMR resonance assignments for pentazocine metabolite MET1.	214
VII.2	The observed $^1\text{H}$ NMR resonance of pentazocine metabolite MET1 in three different deuterated solvents.	215
VII.3	The possible assignments of $^{13}\text{C}$ resonances of pentazocine metabolite MET1.	219
VII.4a	Proton J-couplings in pentazocine metabolite MET1 observed by COSY experiment.	222
VII.4b	The $^1\text{H}$ resonance assignments of pentazocine metabolite MET1 supported by COSY experiment.	224
VII.5	Heteronuclear chemical shift correlation (via coupling through direct C-H bond) NMR results for pentazocine metabolite MET1.	228
VII.6	Heteronuclear chemical shift correlation (long range C-H coupling) NMR results for pentazocine metabolite MET1.	233
VII.7	Intensity changes observed by NOE experiments upon selective proton resonance irradiation.	244
VII.8	Proton couplings observed by both NOESY and COSY experiments for pentazocine metabolite MET1.	248

TablePage

VII.9	Comparison of $^1\text{H}$ and $^{13}\text{C}$ NMR spectra data obtained for pentazocine in D-chloroform and pentazocine metabolite MET1 in D-methanol.	251
-------	---	-----

# THE ANALYTICAL CHEMISTRY OF PENTAZOCINE METABOLITES

PRODUCED BY THE GREYHOUND

## I. INTRODUCTION

It was discovered more than a century ago that drugs or other foreign compounds are excreted either unchanged or chemically modified by living tissues. The importance of this biotransformation process in determining the pharmacological activity, clinical efficiency, and toxicological profile of drug molecules has since led to the emergence of specialties from its parent sciences of chemistry, biochemistry, pharmacology, and toxicology.

However, the advances in the selectivity, sensitivity, and accuracy of the analytical chemistry tools, as well as the development of analytical methods specifically designed for drug metabolism studies play a major role in formulating the science of drug metabolism. The primary aim in this thesis is to investigate the analgesic drug pentazocine metabolism in greyhounds, particularly the separation of pentazocine and its metabolites from urine samples and the structural elucidation of these compounds by chromatographic and spectroscopic methods.

### 1. Historical

The problem of how to relieve pain has always been a major

interest. As far back as thousands of years ago, Egyptians had written many references to opium preparations for pain relief. Many analgesically active alkaloids were isolated from opium by the beginning of the nineteenth century, and became popular to use. These opium alkaloids nonetheless are highly addictive, and can promote dangerous side effects physically, psychologically, and socially.

The unwanted and dangerous side effects of opium alkaloid analgesics encouraged a search for new drugs that would be as potent but free from side effects. Pentazocine was originally one of the many chemicals synthesized as part of a deliberate effort to develop such an effective analgesic with little or no abuse potential<sup>[1]</sup>. The pharmacology of pentazocine has been described as having both agonistic actions and weak opioid antagonistic activity<sup>[2]</sup>.

Nevertheless, pentazocine produces side effects similar to those associated with the morphine-like analgesics. Psychic and physical dependences of pentazocine have been reported in humans. Abuse of pentazocine involves the intravenous administration of a liquid mixture of crushed tablets and certain antihistamine tablets. It has been widely used by "street addicts" in combination with tripeleminamine referred as "T's and Blues"<sup>[3]</sup>. In particular, pentazocine has been reported repeatedly used in the racing business by both jockeys and thoroughbreds<sup>4</sup>, and it is also thought to be used in greyhound racing to relieve pain in greyhound muscles. The abuse of such an analgesic can cause restlessness of a racing greyhound at the race track, and eventually lead to its death.<sup>[4]</sup>

Pentazocine (1,2,3,4,5,6-Hexahydro-6,11-dimethyl-3-(3-methyl-2-

butenyl)-2,6-methano-3-benzazocine-8-ol, Fig. I.1a) is extensively metabolized following oral, intravenous and intramuscular administration in man<sup>[5]</sup>. The previous metabolism studies of pentazocine in monkey, mouse, and rat liver homogenates<sup>[6]</sup> found that pentazocine was mainly metabolized through oxidation of the terminal methyl groups of the dimethylallyl side chain to yield a pair of isomeric cis- (1,2,3,4,5,6-Hexahydro- 8-hydroxy- $\alpha$ ,6,11-trimethyl-2,6-methano-3-benzazocine-3-cis-2-buten-1-ol, Fig. I.1b) and trans-alcohol (1,2,3,4,5,6-Hexahydro- 8-hydroxy- $\alpha$ ,6,11-trimethyl-2,6-methano-3-benzazocine-3-trans-2-buten-1-ol, Fig. I.1c), and one of a corresponding trans-carboxylic acid (1,2,3,4,5,6-Hexahydro-8-hydroxy- $\alpha$ ,6,11-trimethyl-2,6-methano-3-benzazocine-3-crotonic acid, Fig. I.1d). Norpentazocine (Fig. I.1e), a metabolite produced by the N-dealkylation, was identified in the bile of mice<sup>[7]</sup>. In a study of benzomorphans in the rat liver, it was indicated that hydroxylation and methylation on the aromatic ring might happen, but the positions where hydroxylation and methylation occurred could not be clarified<sup>[8]</sup>. A metabolite formed by reductive metabolism, pentazocine hydrate (Fig. I.1f), was also detected in human urine by GLC/MS<sup>[9]</sup>. As summarized in Table I.1, different animal species show different metabolic behavior for pentazocine.

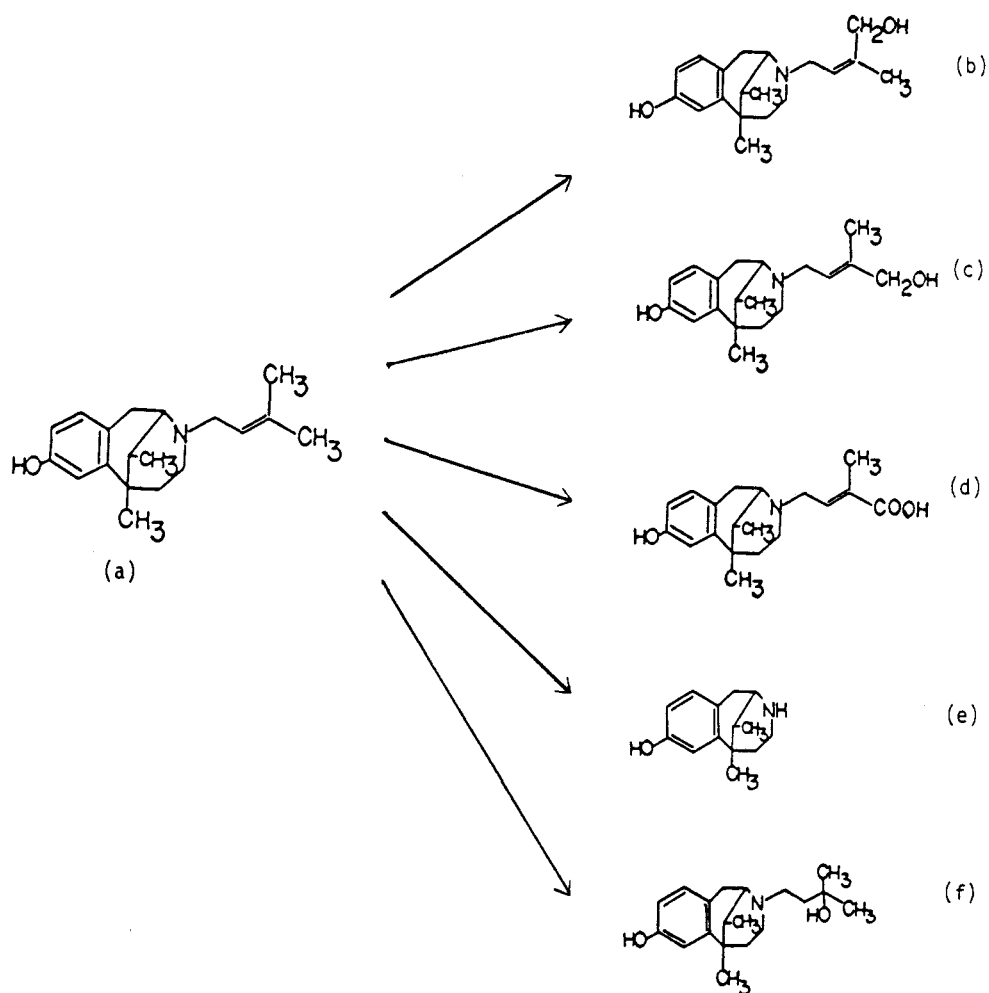


Figure I.1 Major pentazocine (a) metabolites found in various species: pentazocine (b) cis-alcohol, (c) trans-alcohol (d) trans-acid, (e) norpentazocine and (f) pentazocine hydrate.

Table I.1. Summary of Pentazocine Metabolism Studies Conducted in Different Species.

SPECIES	SAMPLE	RESULTS	METABOLITES				
			trans-OH	cis-OH	trans-Acid	nor-Pent	others
Human	Urine Blood	MS N/A	N	Y	Y	N	*
Monkey	Urine	MS/NMR/IR	Y	Y	Y	N	N
Rat	Liver	MS	Y	Y	Y	N	**
Mouse	Bile Blood Brain	GC N/A N/A	Y	Y	Y	Y	N
Horse	Urine	N/A					
Rabbit	Blood	N/A					
Dog	Urine	N/A					

Y --- The metabolite was found.

N --- The metabolite was not found.

N/A--- No metabolism information available, other studies conducted.

\* --- Pentazocinehydrate.

\*\* --- hydroxylation of aromatic ring was suspected (no actual structure).

## 2. Metabolism of Analgesics

Biotransformation is the major factor limiting the intensity and duration of the effects of analgesics<sup>[10]</sup>. In some cases, biotransformation may become essential for the activation as well as the detoxification of the analgesics. It is a detoxification process because after biotransformation, analgesics are transformed to their metabolites, which are usually pharmacologically less active and/or more easily excreted than the parent compound.

The development of new analgesics is therefore dependent upon studies of the drug metabolism to understand the pharmacological effects and eventually eliminate the side effects of analgesics.

When molecules undergo biotransformation, they interact with biological systems (enzymes, enzymic systems, cells, tissues, organs, or organisms). Thus, the metabolism of a drug is governed by the relationship between the nature of the biological system encountered and the inherent properties of the drug molecule. Distinct but closely related drugs may have different metabolisms, or the same drug may have different metabolic behavior in different species, and may give different metabolites at different rates by competitive pathways.

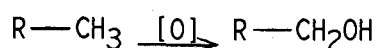
It is therefore interesting and worthwhile to study pentazocine metabolism in the greyhound urine, because the metabolism of pentazocine in a greyhound may be different from those in the other species previously studied.

Although individual compounds may undergo different metabolic

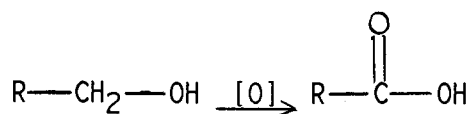
alterations due to their different structural properties, in general, various metabolic transformations are classified into two categories: Phase I processes, reactions of functionalization, involving oxidation, reduction, and hydration/hydrolysis; and Phase II processes, reactions of conjugation, involving a foreign compound or a metabolite combined with an endogenous molecule<sup>[11]</sup>. It is essential to understand the basics of the metabolic transformation to establish strategies which aid in the development of analytical methods for metabolites studies.

Among Phase I processes, oxidative functionalization reactions (monooxygenase-mediated oxygenations) are most important, and can be described as an activated enzymic species transferring an oxygen atom (oxene) to the substrate (drug or other foreign compound). As a consequence of such an oxidative metabolism, hydroxylation of drugs occurs, resulting in the production of alcohols, as well as carboxylic acids upon further oxidation.

The overall chemical reactions are:



and further oxidation to



It is quite clear that any alteration by oxidative functionalization reactions would result in a more polar metabolite than the parent drug. The implication herein is very important for the development of a strategy to isolate drugs and their metabolites from biological tissues or fluids.

Phase II reactions, conjugation reactions, are a group of

synthetic pathways in which a drug or its metabolite with a suitable functional group (which may be added by oxidative functionalization reactions) is combined with an endogenous molecule to give a conjugate. It is most common that Phase II reactions are preceded by Phase I reactions in the biotransformation, although the direct conjugations or even Phase II preceding Phase I reactions are observed<sup>[12]</sup>. Phase II reactions are major metabolic pathways for analgesics and their metabolites produced by such reactions as oxidative functionalization reactions, and are very important for the detoxication and excretion of drugs and foreign compounds.

More than seven kinds of conjugation reactions have been described in the literature. Glucuronidation is one of the major conjugation reactions. This process involves glucuronic acid combined with functional groups such as hydroxyl, carboxyl, amino, or sulfhydryl, catalyzed by an enzyme to form glucuronides. The mechanism can be described as involving the enzymic transfer of the glucuronic acid moiety from uridine diphosphate glucuronic acid (UDPGA) to the metabolite by the enzyme, UDP-glucuronyltransferase. The conjugates formed are usually extremely water soluble under physiological conditions and are rapidly assimilated by the kidney and excreted in the urine.

Glucuronides may be enzymatically hydrolyzed to the non-conjugated compound by  $\beta$ -glucosiduronidase. Using this method, non-glucuronided structures of pentazocine metabolites have been studied.

Methylation is another Phase II reaction undergone by metabolites containing hydroxyl, amino, or sulfhydryl groups. As a result, a methyl group is added to the functional group of a metabolite to form

for example, a methoxy group with a hydroxyl functional group. The source of the methyl group is generally the high-energy nucleotide S-adenosylmethionine. Unlike most other conjugations, the methylation may actually reduce the polarity and hydrophilicity of the metabolites.

### 3. Analytical Chemistry in Metabolism Studies

In addition to knowledge of the metabolic transformations and the chemistry of functional groups, it is most important in drug metabolism studies to have a good appreciation of the analytical techniques that are used so as to ensure that they are applied thoughtfully and the data obtained are interpreted accurately. Also, problems solved in a real sample analysis help to further the development of the field of analytical chemistry. In the studies of pentazocine metabolism in the greyhound, numerous analytical techniques were examined, and analytical strategies were developed. Problems encountered were studied from the analytical chemistry point of view and solved with practical solutions applicable to drug metabolism studies.

In most drug metabolism studies, it is essential to first isolate a drug and its metabolites from biological media, followed by the separation of the isolated components, and then the identification of each component. In some cases quantification of the recovered drug and each metabolite is also involved.

The strategy of the isolation procedure is to use the unique chemical properties of drugs and their metabolites to remove them from the biological samples which have different chemical properties. There

are many ways to achieve the isolation, the two most common are solvent extraction and the use of resins and adsorbents. Basically, both methods are based on the idea that the biological samples are extracted in a intermediate phase, which has similar chemical properties as those of the drugs and/or their metabolites, but is easily separated from the biological samples. Thus, by simply removing this intermediate phase, drugs and/or their metabolites will be brought out of the biological samples.

An efficient isolation procedure would eliminate most of the analytical interferences and greatly simplify the separation of the metabolites from each other in the steps that follow. Since drugs and their metabolites can be neutral, acidic, basic, or amphoteric compounds, the total recovery of the metabolites in the isolation step requires that the whole spectrum of acidity or alkalinity be considered. By manipulating the pH conditions, it is also possible to separate metabolites into different groups according to their acidity during the isolation step. This thesis examined the various isolation procedures for pentazocine and its metabolites, aimed at the development of a procedure that selectively recovers pentazocine and all of its metabolites from greyhound urine.

The purpose of the separation procedure following the initial isolation step is to separate the mixtures of drugs and metabolites into individual components. Most separations are carried out by chromatography techniques. The overall separation strategy and the specific chromatographic techniques to be applied depend upon whether the identification of a metabolite and determination of its concentration is needed, or substantial quantities of one or more of

metabolites are to be separated for further structural characterization.

Depending on the degree of the separation and the amount of the materials to be separated, preliminary separations of a mixture prior to the use of more specific separation procedures can be done. This is necessary when separations of all the metabolites are required, since their structures may be so closely related that specific separations may be difficult especially if a large number of metabolites is involved. In the case where structures of individual components are to be identified, relatively large sample sizes are required for some of the spectrometers. One-step separation under such circumstances may turn out to be unnecessarily time consuming depending on the number of individual components involved. Thus, a preliminary separation by a low efficiency but quick chromatographic technique can be performed first to "group" the metabolites into several subgroups according to their chemical or structural similarities. The final specific separations by high efficiency chromatographic techniques can then be done for individual subgroups obtained from the initial separations. In this way, the specific separation conditions may be easier to find, because fewer components are involved and their chemical properties are more clearly defined. For the very same reason, the separation time may be significantly shortened, and the preparative steps may be done by analytical scale techniques for final structural identification purposes. Part of this thesis is focused on the development of this separation strategy and its application to the separations of pentazocine and its metabolites for their structural determinations.

The identification of structures of drug metabolites is dependent upon the degree of the knowledge of metabolite structures expected and

whether or not synthetic reference compounds are available for direct comparison of their chemical or physical properties. A tentative identification of the unknown compound structure is always possible by mass spectrometric analysis. If metabolites are not expected to be too much different from their parent drug structure, the study of the parent drug mass spectral fragmentation can help the metabolites structural elucidation by tracing the characteristic fragments in the metabolites mass spectra. This thesis proposes various fragmentation pathways for the formation of the trimethylsilylated pentazocine mass spectrum, and by identifying the corresponding characteristic fragments in the trimethylsilylated derivative mass spectra of the metabolites, structures of pentazocine metabolites in greyhound urine are elucidated. With the help of the extensively studied fragmentation mechanisms such as the hydrogen-rearrangement, it is also possible to identify the steric isomer structures by mass spectral information alone.

With modern NMR techniques available today, any structural identification can be achieved in which little needs to be known prior to the analysis; it relies on the characterization of a compound by such powerful NMR techniques as homonuclear and heteronuclear chemical shift correlation and NOE experiments. Although much larger sample size, and therefore tedious sample preparation may be required compared to that of GC/MS, when little else is known about a compound structure, or when mass spectroscopy provides little information about some part of a molecule, then NMR techniques, especially the powerful 2D NMR techniques, become indispensable. This thesis explores the advantages of modern NMR techniques in the identification of metabolite structures

in which neither a synthetic reference compound nor prior structural information are needed. The complete structural elucidation of a new pentazocine metabolite is achieved by using a combination of one and two dimensional NMR techniques, and an analysis strategy is proposed for such a procedure.

Metabolism studies are the joint efforts from fields such as analytical chemistry, biochemistry, and pharmacology. The potential metabolic alterations of drugs have been studied extensively. For example the possibility of the metabolic oxidation of aromatic hydrocarbons to phenols during drug metabolism has been theoretically predicted and proven in some examples of drug metabolism<sup>[13]</sup>. Such information from the science of metabolism pathways may be used to assist the structural elucidations of the metabolites. In the study of the pentazocine metabolism in the greyhound, the structures of pentazocine metabolites are thus characterized by using spectroscopic and chromatographic information combined with knowledge of the drug metabolism.

II. DEVELOPMENT OF THE TOTAL ISOLATION OF PENTAZOCINE AND ITS  
METABOLITES FROM A BIOLOGICAL SAMPLE MATRIX

by

Guang Xiao and Edward H. Piepmeier

Department of Chemistry

Oregon State University

Corvallis, OR 97331

and

A. Morrie Craig

School of Veterinary Medicine

Oregon State University

Corvallis, OR 97331

## 1. Abstract

### **Analytical Procedures for the Isolation and Separation of Pentazocine Metabolites from Greyhound Urine**

The proposed investigation of pentazocine metabolism in the greyhound needs the development of a selective and sensitive analytical procedure for the determination of such analgesics and their metabolites in biological fluids. The present work in Chapter II & III examines various analytical techniques and describes the analytical assay development for the drug metabolism study of pentazocine and its metabolites in the greyhounds.

There are many procedures that can be used to isolate drugs and their metabolites from biological fluids. In chapter II, the isolation of analgesics and their metabolites from other biological interferences in the urine sample is examined, and in particular, the development of the isolation of pentazocine and all of its possible metabolites from greyhound urine is described.

Various chromatographic techniques can be applied to separate a mixture of drugs and their metabolites into individual components after isolation from biological fluids. The assay development for a particular separation depends upon the required sensitivity and specificity. In chapter III, the development of the separation of isomeric pentazocine metabolites is described, and some of the analytical topics in the area of chromatography are discussed.

## 2. Introduction

The purpose of isolation is to remove interferences for subsequent separation and the final analysis. In the case of this pentazocine metabolism study, the assay development should be focused on both the parent drug pentazocine and all the possible metabolites in greyhound urine. Thus, the isolation procedure should not only exclude a large portion of the endogenous impurities in the urine sample, but also recover pentazocine and all of its metabolites.

The most common isolation procedure is a solvent extraction, where drugs and/or their metabolites are removed from biological fluids by suitable water-immiscible organic solvents. The development of an extraction procedure for a drug metabolism study should be based on three principles:

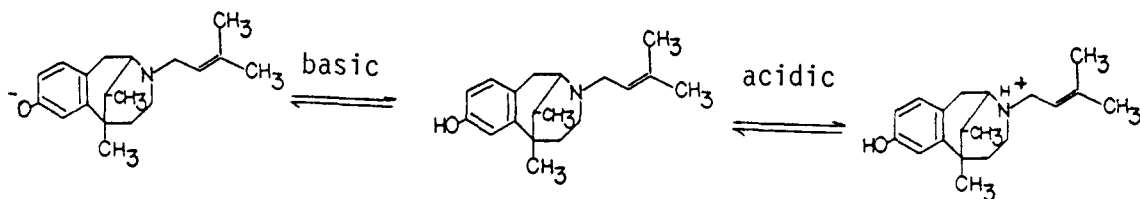
1. Any organic compound (a drug or a metabolite) is most readily extracted at an appropriate pH, under which the compound is not ionized.
2. An organic compound is most likely to be extracted by an organic solvent whose polarity is similar to that of the compound.
3. Most metabolites of a drug are more polar than the parent compound (a metabolite produced by the methylation is an exception<sup>[14]</sup>).

Although a knowledge of the dissociation constant of the parent drug is helpful in determining the pH for the extraction, in the case

of a total metabolite extraction where functional groups of the metabolites are unknown, the best pH condition should be determined by trial experiments covering most of the pH range to ensure the best metabolite recovery.

The choice of the proper solvent is important in determining the specificity of an isolation procedure. The polarity differences among the metabolites and between the metabolites and their parent drug may be exploited to facilitate their separation during isolation. Since most of the metabolites are more polar than their parent drug, by starting the extraction with the least polar organic solvent, and by subsequently increasing the solvent polarity, selective separation of a drug from its metabolites and some metabolites from the others can be achieved.

Analgesic alkaloids like pentazocine contains both phenolic and amino functional groups in their structures. Under either appropriate acidic or basic pH, pentazocine exists in an ionized form and is therefore soluble in the aqueous phase of an extraction:



Thus, such compounds present in the first organic extract from an aqueous phase can be "back-extracted" into another acidic or basic aqueous phase under an appropriate acidic condition. This should reduce the amount of neutral material contaminating the extract, since neutral molecules remain in the first organic extract. After the back-extraction, the pH of the aqueous phase is readjusted to that of the first extraction, and the compounds of the interests are re-extracted into a second organic solvent.

Many drugs and their metabolites are excreted in urine as glucuronide conjugates that are very polar and cannot be readily extracted into organic solvents for the isolation. It is therefore necessary to hydrolyse the conjugates to release the parent compounds for the extraction. The hydrolysis can be either chemical, with acids such as hydrochloric acid, or enzymatic, with enzymes such as  $\beta$ -glucuronidase. The enzymatic approach is mild compared to that of chemical hydrolysis, and hence is less likely to cause degradation of the compounds.

Solvent extraction is not effective for the isolation a compound of interest if the compound is water-soluble at all pH values and not readily extractable by water-immiscible organic solvents. Liquid-solid extraction can then be used for the isolation. There are many types of resins and adsorbents that can be used, and they basically work on chromatographic principles: biological samples are passed through a column packed with solid adsorbent, and the compounds of interest are retained on the adsorbent surface. Then, when eluted with appropriate solvents, only the analytes will be selectively removed from the column and the isolation is achieved. The solvent used can be either

water-miscible or -immiscible, thus very polar organic solvents such as methanol can be used.

In the following section, isolation procedures are examined, and a selective isolation scheme aimed at the recovery of pentazocine and all of its possible metabolites in greyhound urine is developed.

### 3. Materials and Reagents

$\beta$ -glucuronidase (1,400,000 units/g, Sigma Chemical Company).

polypropylene column (65 x12 mm, syringe barrel).

Pencil electrode (No. S803A, Beckman).

pH meter (model 130, Corning).

Amberlite XAD-2 resin (Eastman Kodak)

TLC plates (pre-coated silica gel, 60F<sub>254</sub>, 0.25 mm. thick, EM Science)

Chromato-Vue cabinet (model CC-60, UVP, Inc.), containing lamps emitting "long uv" light at 366 nm, and "short uv" at 254nm.

Gas chromatograph, (Perkin Elmer Sigma 3B) equipped with a 30 m x 0.25 mm i.d. DB-5 capillary column (J & W Scientific, Inc.).

Mass spectrometer (Finnigan 1020B mass spectrometer).

pH 5.0 acetate buffer: 30 ml glacial acetic acid and 82 g sodium acetate in 800 ml distilled water; adjust to pH 5.0 with concentrated sodium hydroxide solution or glacial acetic acid; top up to 1000 ml.

5000 units/ml  $\beta$ -glucuronidase solution: dissolve 250,000 units in

50 ml distilled water.

0.6 N ammonium hydroxide solution.

0.2 N sulfuric acid solution.

3:1 (v/v) methylene chloride and isopropanol solution.

Dragendorff reagent: Dissolve 1.3 g of bismuth subnitrate in a mixture of 60 ml distilled water and 15 ml glacial acetic acid.

Dissolve 12.0 g of potassium iodide in 30 ml of distilled water. Mix these two solutions and dilute with 100 ml distilled water and 25 ml glacial acetic acid.

cupric chloride solution: dissolve 25 g of cupric chloride in 75 ml distilled water and 25 ml methanol.

5% (w/v) sodium nitrite solution.

#### 4. Methods

Extraction with base hydrolysis (Fig. II.1). Two 5-ml aliquots of greyhound urine collected 4 hours after the intravenous administration of pentazocine were each mixed with 5 ml 0.1 N sodium hydroxide in a 150 x 16 mm culture tube, and set for 10 minutes. After the hydrolysis, 4 ml of pH 3.3 phosphate buffer was added to each urine sample. One urine sample was then made acidic to pH 4.0, and the other was adjusted to pH 9.0 with concentrated ammonia hydroxide. The pH values were measured with a "pencil" electrode and pH meter. 5 ml of pre-mixed extracting solvent consisting of methylene chloride and isopropanol (3:1, v/v) were added to each of the urine samples, the tube then was capped, and the mixture rotated on a Rotorack for 5 minutes to partition pentazocine and its metabolites into the organic

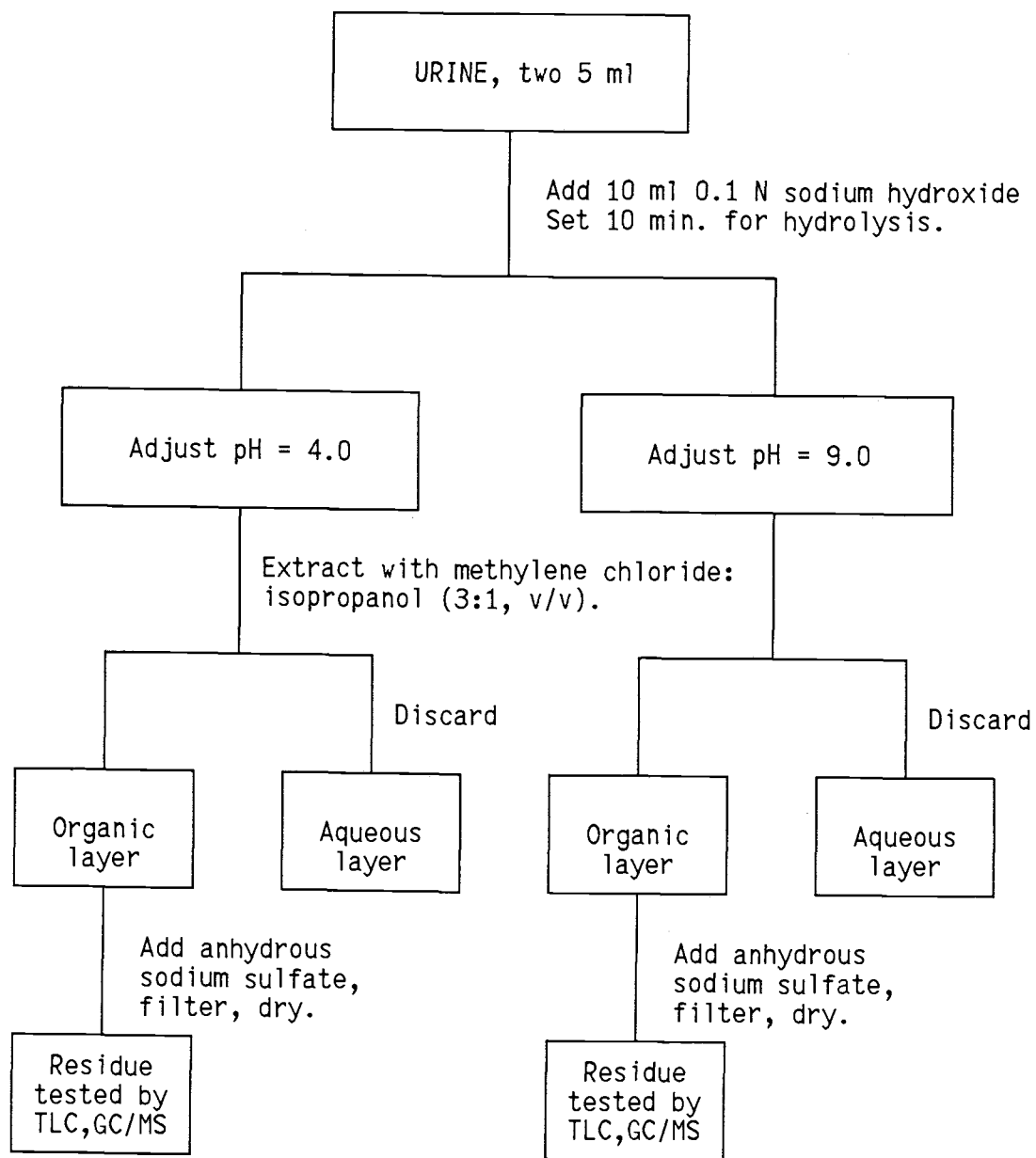


Figure II.1 Extraction scheme of pentazocine and its metabolites in greyhound urine with base hydrolysis.

phase. Each mixture was then centrifuged, and the organic layer was transferred to a clean 100 x 13 mm culture tube. After dehydration with anhydrous sodium sulphate, the organic phase was filtered and carefully dried under a nitrogen stream in a 35°C water bath. Two sample blanks were made for comparison by two-5 ml aliquots of greyhound urine collected before the administration of pentazocine (0 hour) and subject to the same extraction procedure described. Two other samples were also made for comparison by the same extraction procedures without the base hydrolysis step.

Extraction with acid hydrolysis (Fig. II.2). A 5-ml aliquot of greyhound urine collected 4 hours after the intravenous administration of pentazocine was mixed with 0.5 ml concentrated hydrochloric acid in a 150 x 16 mm culture tube, the tube was then lightly capped, and the contents were incubated for 30 minutes at 115°C in a water bath. After the hydrolysis, the urine was adjusted to pH 9.0 with the dropwise addition of concentrated ammonium hydroxide. The pH values were measured with a "pencil" electrode and pH meter. 5 ml of pre-mixed extracting solvent consisting of methylene chloride and isopropanol (3:1, v/v) were added to the urine, the tube then was capped, and the mixture rotated on a Rotorack for 5 minutes to partition pentazocine and its metabolites into the organic phase. The mixture was then centrifuged, and the organic layer was transferred to a clean 100 x 13 mm culture tube. After dehydration with anhydrous sodium sulphate, the organic phase was filtered and carefully dried under a nitrogen stream in a 35°C water bath. A sample blank was also made from a 5-ml aliquot of greyhound urine collected before the administration of pentazocine (0 hour) and subjected to the same extraction procedure described.

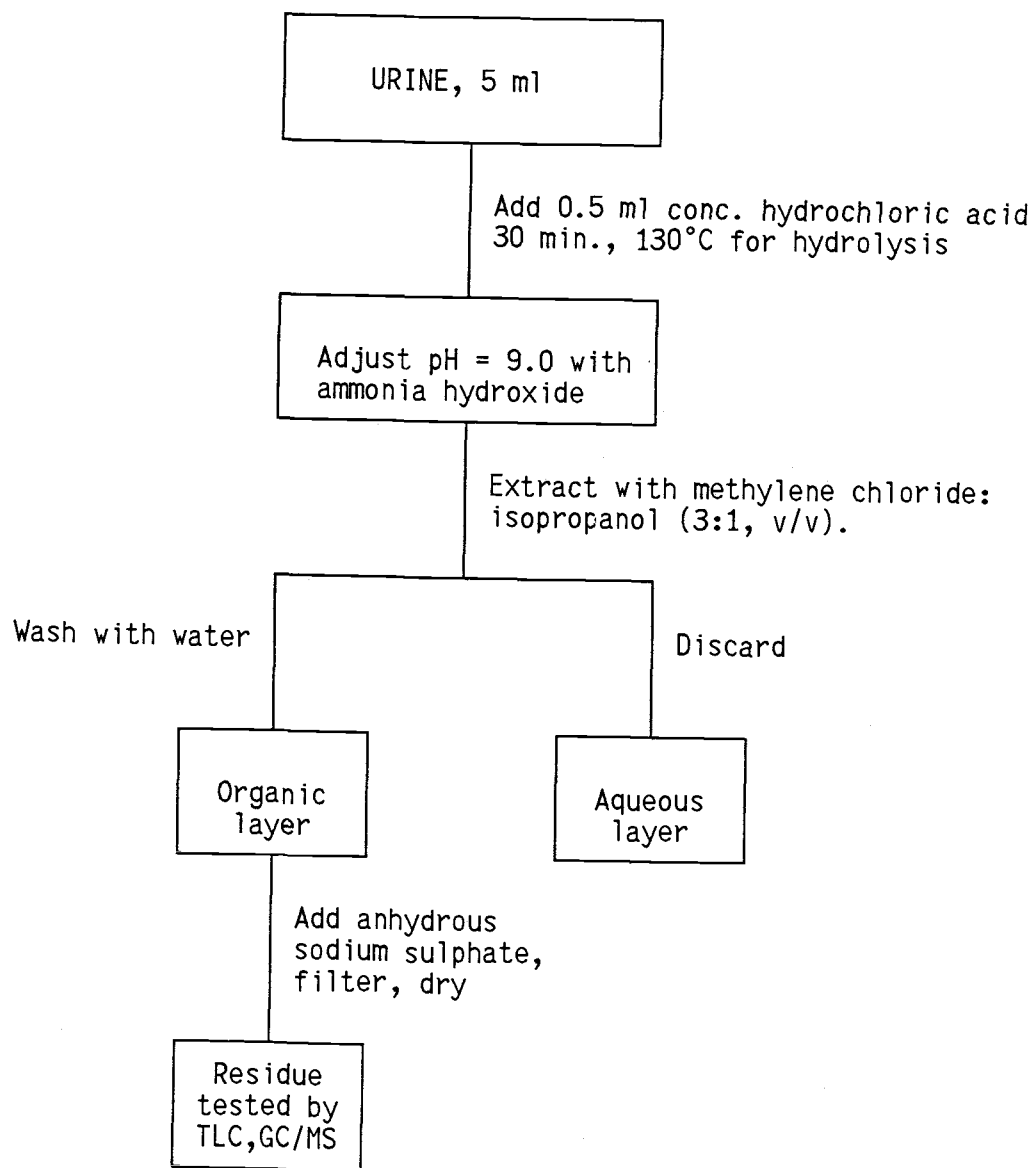


Figure II.2 Extraction scheme of petazocine and its metabolites in greyhound urine with acid hydrolysis.

Another sample was also made for comparison purposes by using the same extraction procedure without the acid hydrolysis step.

Extraction with enzymatic hydrolysis (Fig. II.3). A 5-ml aliquot of urine collected 4 hours after the intravenous administration of pentazocine was mixed with 2 ml of pH 5 acetate buffer and 1 ml of  $\beta$ -glucuronidase solution (5000 units) in a 150 x 16 mm culture tube, and then capped. The urine was incubated for 3 hours at 63°C in a water bath. After the hydrolysis, the urine was adjusted to pH 9.0 by the dropwise addition of concentrated ammonium hydroxide. The pH values were measured with a "pencil" electrode and pH meter. 5 ml of pre-mixed extracting solvent consisting of methylene chloride and isopropanol (3:1, v/v) were added to the urine, the tube then was capped, and the mixture rotated on a Rotorack for 5 minutes to partition pentazocine and its metabolites into the organic phase. The mixture was then centrifuged, and the organic layer was transferred to a clean 100 x 13 mm culture tube. After dehydration with anhydrous sodium sulphate, the organic phase was filtered and carefully dried under a nitrogen stream in a 35°C water bath. A sample blank was also made using a 5-ml aliquot of greyhound urine collected before the administration of pentazocine (0 hour) and subjected to the same extraction procedure described. Another sample was also made for comparison purposes by using the same extraction procedure without the enzymatic hydrolysis step.

Extraction under different pH conditions after enzymatic hydrolysis (Fig. II.4). Six 5-ml aliquots of greyhound urine samples collected 4 hours after the intravenous administration of pentazocine were each mixed with 2 ml of pH 5 acetate buffer and 1 ml of

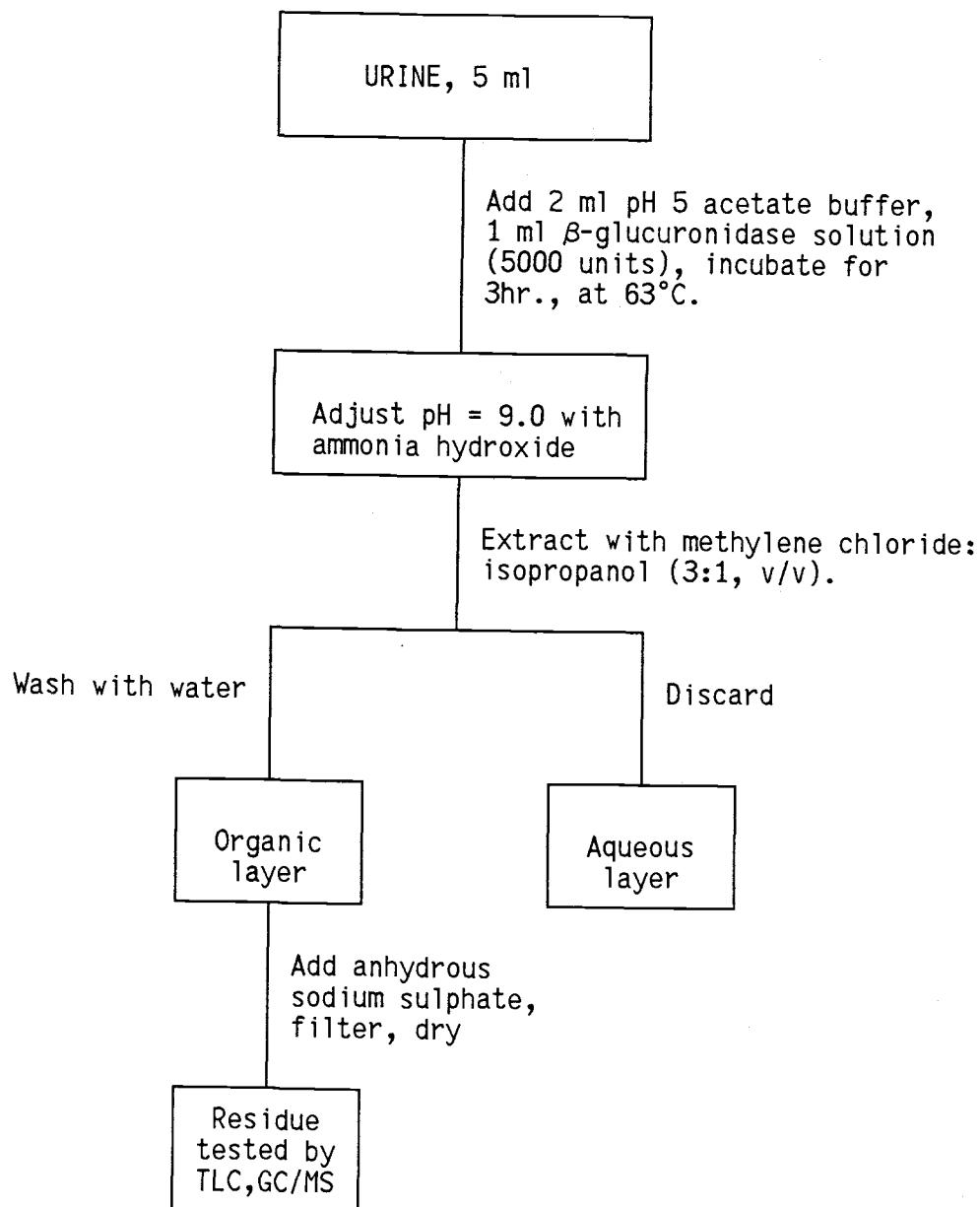


Figure II.3 Extraction scheme of petazocine and its metabolites in greyhound urine with enzymatic hydrolysis.

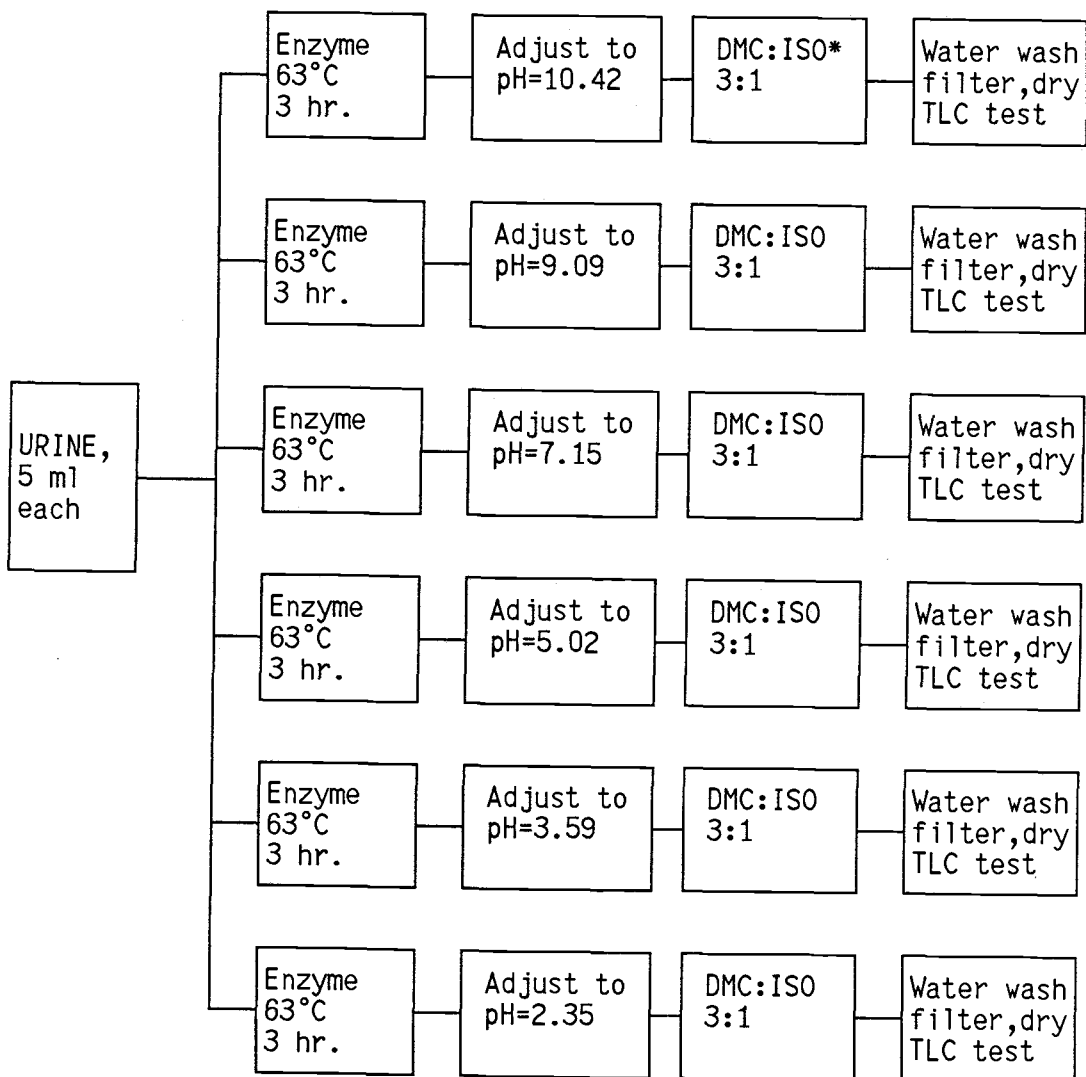


Figure II.4 Extraction of pentazocine and its metabolites in greyhound urine under different pH values after enzymatic hydrolysis.

\* DMC:ISO - methylene chloride:isopropanol (3:1, v/v).

$\beta$ -glucuronidase solution (5000 units) in separate 150 x 16 mm culture tubes, and then capped. The urine samples were incubated for 3 hours at 63°C in a water bath. After the hydrolysis, the samples were adjusted to pH values of 10.42, 9.0, 7.15, 5.0, 3.59, and 2.35. The pH values were measured with a "pencil" electrode and pH meter. 5 ml of pre-mixed extracting solvent consisting of methylene chloride and isopropanol (3:1, v/v) were added to each of the samples, the tubes then were capped, and the mixture rotated on a Rotorack for 5 minutes to partition pentazocine and its metabolites into the organic phase. The mixtures were then centrifuged, and each of the organic layers was transferred to a clean 100 x 13 mm culture tube. After dehydration with anhydrous sodium sulfate, each organic extract was filtered and carefully dried under a nitrogen stream in a 35°C water bath. Six sample blanks were also made from six 5-ml aliquots of greyhound urine collected before the administration of pentazocine (0 hour) and subjected to the same extraction procedures described.

Extractions with enzymatic hydrolysis and back-extraction (Fig. II.5). A 5-ml aliquot of urine collected 4 hours after the intravenous administration of pentazocine was mixed with 2 ml of pH 5 acetate buffer and 1 ml of  $\beta$ -glucuronidase solution (5000 units) in a 150 x 16 mm culture tube, and then capped. The urine was incubated for 3 hours at 63°C in a water bath. After the hydrolysis, the urine was adjusted to pH 9.0 with the dropwise addition of concentrated ammonium hydroxide. The pH values were measured with a "pencil" electrode and pH meter. 5 ml of pre-mixed extracting solvent consisting of methylene chloride and isopropanol (3:1, v/v) were added to the urine, the tube then was capped, and the mixture rotated on a Rotorack for 5 minutes to

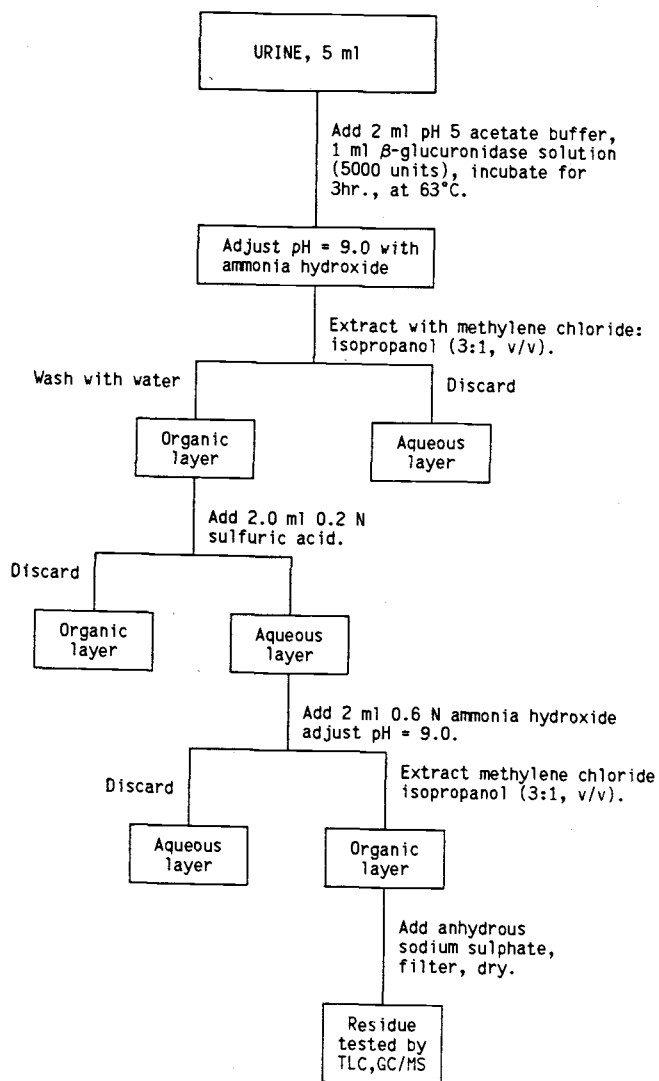


Figure II.5 Extraction of pentazocine and its metabolites in greyhound urine with enzymatic hydrolysis and back-extraction.

partition pentazocine and its metabolites into the organic phase. The mixture was then centrifuged, and the organic layer was transferred to a clean 120 x 16 mm culture tube, and then 2.0 ml of 0.2 N sulfuric acid was added to the same tube. The tube was capped and the mixture was rotated on a Rotorack for 5 minutes. The organic layer was discarded, and 2 ml of 0.6 N ammonium hydroxide were added and the solution was adjusted to pH 9.0. 5 ml of pre-mixed extracting solvent consisting of methylene chloride and isopropanol (3:1, v/v) were added to the urine, the tube then was capped, and the mixture rotated on a Rotorack for 5 minutes to partition pentazocine and its metabolites into the organic phase. The mixture was then centrifuged, and the organic layer was transferred to a clean 100 x 13 mm culture tube. After dehydration with anhydrous sodium sulphate, the organic phase was filtered and carefully dried under a nitrogen stream in a 35°C water bath. A sample blank was also made using a 5-ml aliquot of greyhound urine collected before the administration of pentazocine (0 hour) and subjected to the same extraction procedure described.

Multi-solvent extraction with increasing solvent polarity (Fig. II.6). A 5-ml aliquot of urine collected 4 hours after the intravenous administration of pentazocine was mixed with 2 ml of pH 5 acetate buffer and 1 ml of  $\beta$ -glucuronidase solution (5000 units) in a 150 x 16 mm culture tube, and then capped. The urine was incubated for 3 hours at 63°C. After the hydrolysis, the urine was adjusted to pH 9.0 with the dropwise addition of concentrated ammonium hydroxide. The pH values were measured with a "pencil" electrode and pH meter. 5 ml of cyclohexane was added to the urine, the tube then was capped, and the mixture was rotated on a Rotorack for 5 minutes. The mixture was then

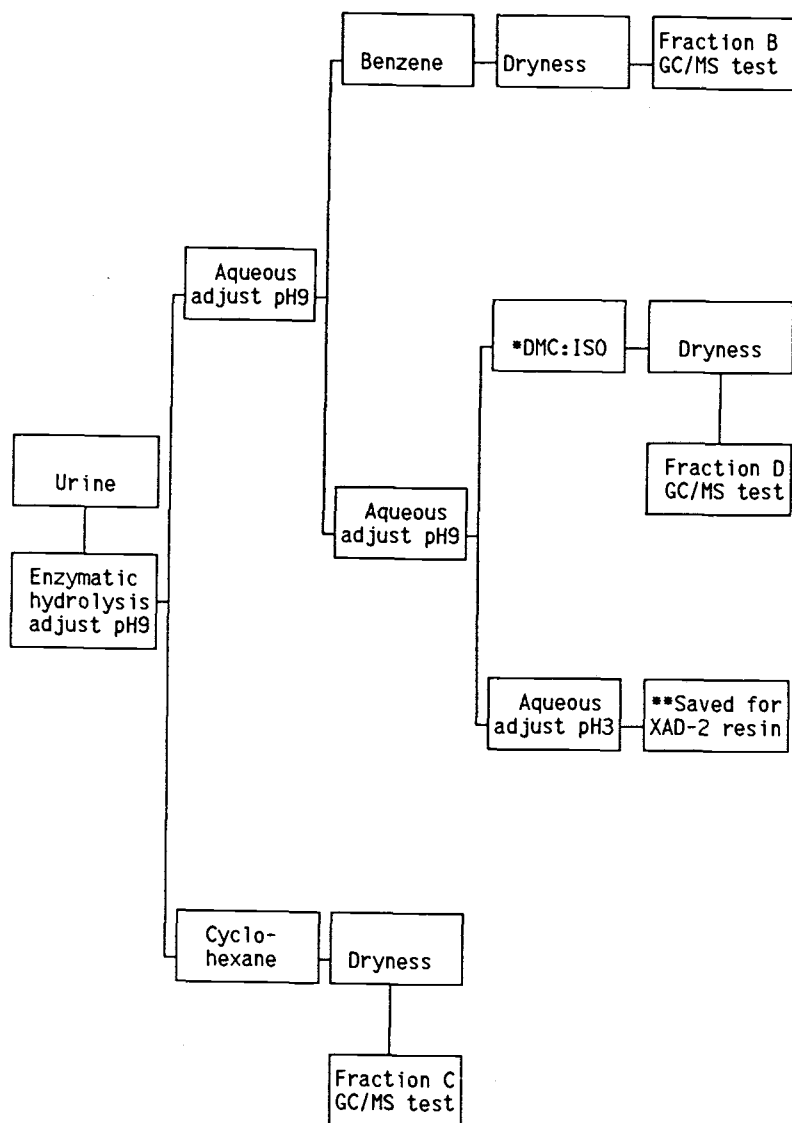


Figure II.6 Extraction of pentazocine and its metabolites in greyhound urine with increasing solvent polarity.

\* DMC:ISO - methylene chloride:isopropanol (3:1, v/v).

\*\* Referring to XAD-2 resin column extraction (Fig. II.7).

centrifuged, the cyclohexane layer was transferred to a clean 120 x 16 mm culture tube and washed with 2 ml of water; the remaining urine sample after the first extraction was also transferred to another clean 150 x 16 mm culture tube, and 5 ml of benzene was added to the tube, the tube was then capped, and the mixture was rotated on a Rotorack for 5 minutes. The mixture was centrifuged, the benzene layer was transferred to a second clean 120 x 16 mm culture tube and washed with 2 ml of water; the remaining urine sample after the second extraction was transferred to a third clean 150 x 16 mm culture tube, and 5 ml of pre-mixed extracting solvent consisting of methylene chloride and isopropanol (3:1, v/v) were added to the urine, the tube then was capped, and the mixture rotated on a Rotorack for 5 minutes. The mixture was then centrifuged, the organic layer was transferred to a clean 120 x 16 mm culture tube and washed with 2 ml of water. After dehydration with anhydrous sodium sulphate, all organic phases collected were filtered and carefully dried under a nitrogen stream in a 35°C water bath. The urine sample after all extractions was then subjected to XAD-2 resin column described next. Sample blanks were also made from a 5-ml aliquot of greyhound urine collected before the administration of pentazocine (0 hour) and subjected to the same extraction procedures described.

Isolation of pentazocine carboxylic acid metabolites from greyhound urine (Fig. II.7).

(a) Amberlite XAD-2 resin column preparation. The resin was prepared by rinsing with 4 bed volumes of acetone, 3 bed volumes of methanol and 3 bed volumes of distilled water two times. The washed resin slurry in the millipore water was transferred into the 65 x 12 mm

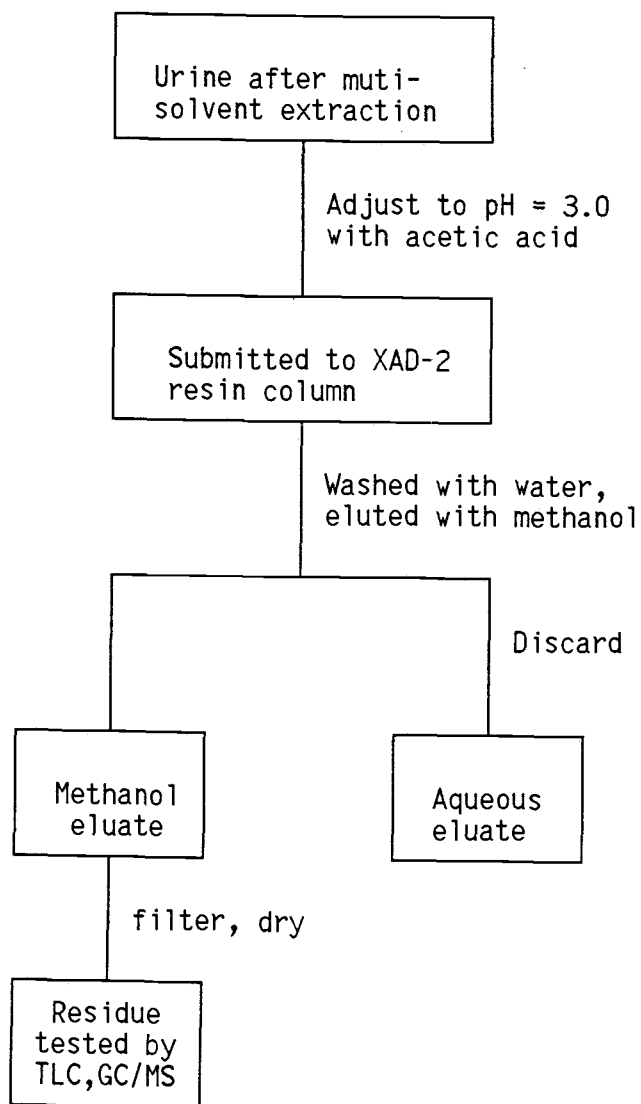


Figure II.7 XAD-2 resin column extraction scheme of pentazocine and its metabolites in greyhound urine after multi-solvent extraction.

polypropylene column plugged with glass wool, to provide a resin bed height of 55 mm (Fig. II.8).

(b) Metabolite isolation. The urine samples saved after the multi-solvent extraction for the increasing solvent polarity study were adjusted to pH 3.0 with dropwise addition of acetic acid, and filtered. A 15-ml aliquot of the acidified urine samples was applied to the top of the column, and the column was rinsed with 20 ml of distilled water twice. The metabolites were then eluted from the column with 20 ml methanol nonselectively, the eluate was collected in small tubes, after discarding the first 5-ml fraction. The collected eluate was carefully dried under a nitrogen stream in a 35°C water bath. A urine sample blank was also made from the 0 hour urine sample after multi-solvent extractions and subjected to the same XAD-2 resin clean-up procedure.

The efficiencies of the isolation procedures were examined by chromatographic techniques including TLC and GC/MS.

(a) TLC. Each hour-4 urine extraction residue was dissolved in 25  $\mu$ l of methylene chloride. The entire methylene chloride solution for each extract was then applied equally to two TLC plates. The samples were applied as a thin band 1 cm from the bottom edge of TLC plate. The plates were developed 5 cm from the origin in a tank previously saturated in the freshly prepared developing solvents for about 30 minutes. The sample blanks (0 hour) were treated in the same way and applied to each TLC plate along with hour-4 urine extracts for the direct comparison. One of the two TLC plates was developed in a solvent system consisting of chloroform:methanol:ammonia hydroxide (80:15:5, v/v/v) (system A), and the other was developed in a solvent

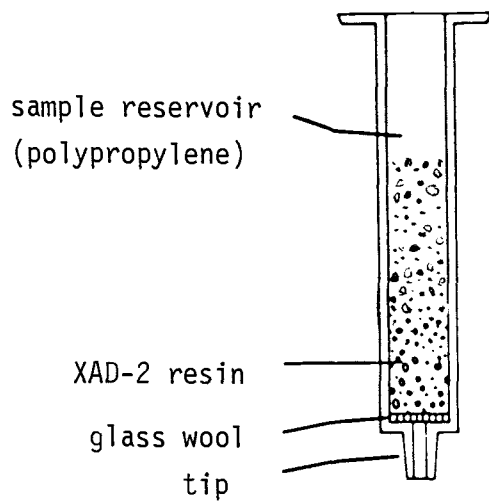


Figure II.8 XAD-2 resin extraction column.

system consisting of chloroform:methanol:propionic acid (80:15:5 v/v/v) (system B). The developed plates were then dried with hot air.

Quenching spots indicating the presence of compounds that quench the background fluorescence produced by the fluorophore incorporated in the TLC coating material were marked and compared with sample blank under 254 nm and 366 nm ultraviolet light. The plates were then subjected to different spray reagents in the following order: 1. Dragendorff reagent; 2. 5% sodium nitrite; 3. cupric chloride solution. The colored spots on TLC plates produced by the nitrogen containing compounds after each spray were compared with sample blanks after being dried and pictured by a Polaroid camera

(b) GC/MS. Each urine extraction residue was dissolved into 5 ml of methylene chloride, and a 100- $\mu$ l volume of methylene chloride solution was evaporated to dryness under a nitrogen stream at 35°C. The residues were then dissolved in 10 mg/ml sodium acetate in methanol, and evaporated again under a nitrogen stream. A 100- $\mu$ l volume of Sylon BFT (Supelco) was then added and the solution was heated at 60°C for 25 minutes to form the trimethylsilylated derivatives for gas chromatographic-mass spectrometric (GC/MS) analysis. After the silylation reaction was completed, the solutions were evaporated under a nitrogen stream, and the residues were dissolved in 50  $\mu$ l of methylene chloride. A 2.5- $\mu$ l volume of the trimethylsilylated sample in methylene chloride was injected into the gas chromatograph of the GC/MS system (Finnigan 1020B mass spectrometer equipped with a Perkin Elmer Sigma 3B gas chromatograph). The chromatograph was equipped with a 30 m x 0.25 mm i.d. DB-5 capillary column (J & W Scientific, Inc.). Operating temperatures were as

follows: injector, 260°C, GC temperature program was from 165 to 210°C at 3°C/minute; interface, 280°C; source, 80°C. The carrier gas was helium, at a flow-rate of 33 cm/sec. The mass spectra were obtained at an ionization energy of 70 eV and scanned from 45 to 500 a.m.u..

Pentazocine was identified by comparison with the mass spectrum of an analytical standard. The metabolites were identified by the characteristic fragments in their spectra as discussed later. The sample blanks were also treated and injected in the same way for comparison purposes.

## 5. Results and Discussion

Hydrolysis procedures. The TLC tests for different hydrolysis procedures show that pentazocine and its metabolites are excreted in both conjugated and nonconjugated forms in the greyhound urine. After spraying with the sequence described, by comparing the intensities and numbers of spots on the TLC plates for the blanks and the hour-4 urine extracts with and without hydrolysis, it was found that the highest number of intense spots showed after the enzymatic hydrolysis. It was estimated by GC/MS that the conjugated form of pentazocine was about 40% of the total drug excreted. It was also noted that the amount of pentazocine was significantly less after the acid hydrolysis, which agrees with previous findings<sup>[15,16]</sup>. However, pentazocine seemed to be stable when incubated at 63°C, pH 5 for enzymatic hydrolysis.

pH conditions for the extraction. The extracts obtained at different pH conditions were examined by GC/MS. It was found that most of the pentazocine metabolites were basic and best extracted into an

organic phase using pH 9-10, but a suspected metabolite (a trans acid), which was found in other animal species, was only slightly extracted under acidic conditions.

Back-extraction. The recovery of pentazocine and its metabolites after back-extraction was very good. The amount of the neutral material contaminating the extract was reduced. It was also noticed that the single step extraction produced a clean extract which was suitable for direct GC/MS analysis without further cleanup. Therefore, the necessity of the back-extraction would depend upon the requirements of subsequent separation studies.

Multi-solvent extraction with increasing solvent polarity. The extraction scheme developed was to isolate pentazocine and its metabolites into three fractions, fraction C produced by the cyclohexane extraction, fraction B produced by the benzene extraction, and fraction D produced by the methylene chloride extraction. Each one of the extracts was tested by TLC and GC/MS. As shown on the TLC plates (Fig. II.9), pentazocine and two of its metabolite suspects were extracted into fraction C by cyclohexane, three other metabolites were extracted into fraction B by benzene, and fraction D extracted by methylene chloride again contained the same metabolites as fraction B. These results indicate that benzene extraction is not sufficient. Therefore, this study indicates that pentazocine metabolites can be separated by using two fractions, by extracting first with cyclohexane and then with methylene chloride and isopropanol (3:1, v/v).

Isolation of water-soluble pentazocine metabolites by XAD-2 resin column. Amberlite XAD-2 resin, a styrene-divinylbenzene copolymer with high surface area, can adsorb many water-soluble organic compounds

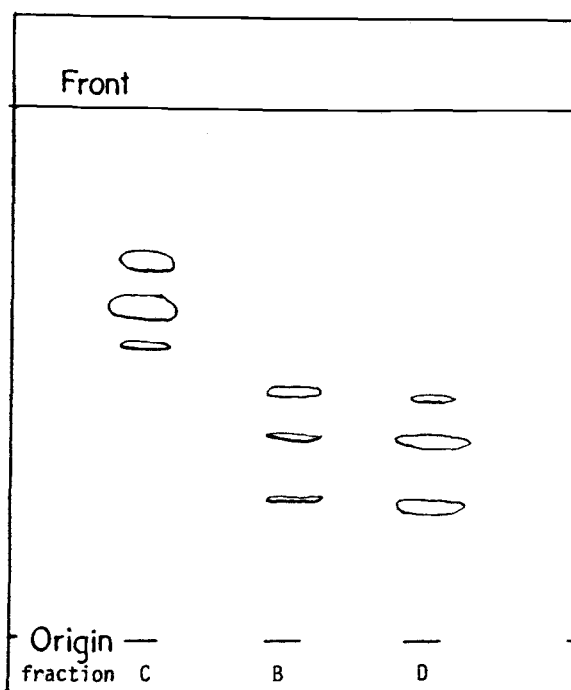


Figure II.9 Schematic representation of Thin-Layer Chromatogram (pre-coated silica gel plates, 60F<sub>254</sub>, 0.25 mm. thick, EM Science) of Fraction C, Fraction B and Fraction D in Developing solvent system: Chloroform/Methanol/Ammonia, 97/3/0.015%, v/v/v.

by Van der Waals' interaction<sup>[17]</sup>. The eluate residue was silylated and tested by GC/MS. As shown in Fig. II.10, the results show three additional pentazocine metabolite suspects isolated from the greyhound urine sample, which were not extractable by water-immiscible organic solvents of various polarities and over a pH range from basic to acidic (Fig. II.4). Since the pH of the sample submitted to the XAD-2 column was adjusted to pH 3.0 (based on the consideration that XAD-2 resin most efficiently binds the nonionized species of weak organic acids and bases<sup>[17]</sup>), the unextractable pentazocine metabolites are most likely the carboxylic acid derivatives of pentazocine.

Overall performance and the general scheme of the total isolation of pentazocine and its metabolites from greyhound urine. This study indicates that the incorporation of the multi-solvent extractions and a homemade XAD-2 resin column provide an efficient method for the isolation of the analgesic drug pentazocine and its metabolites from greyhound urine samples after enzymatic hydrolysis. The overall procedures are shown in Fig. II.11. The method separates extracts into three fractions, each containing different pentazocine metabolites, and produces clean extracts which are suitable for direct GC/MS analysis without further cleanup.

The preliminary TLC and GC/MS results also indicate that pentazocine metabolites consist of basically two different classes: those metabolites with basic properties, which can be extracted under basic pH conditions; and those metabolites with acidic properties, which can be isolated from the urine sample by XAD-2 resin. The isolation scheme proposed provides for the total isolation of all pentazocine metabolites from the greyhound urine samples.

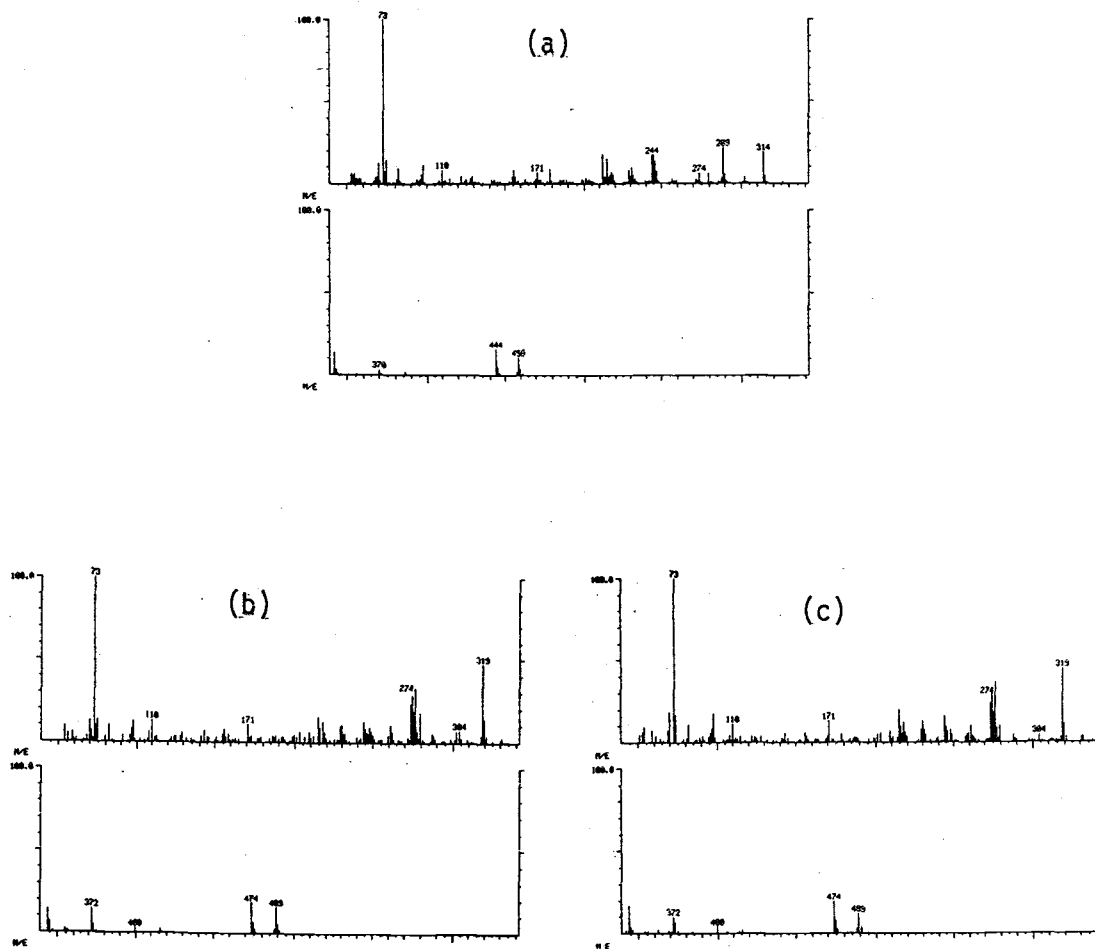


Figure II.10 Gas chromatographic and Mass spectroscopic testing results of XAD-2 column extracts: (a) Mass spectrum of trimethylsilylated pentazocine metabolite, MET7; (b) Mass spectrum of trimethylsilylated pentazocine metabolite, MET8; (c) Mass spectrum of trimethylsilylated of pentazocine metabolite, MET9.

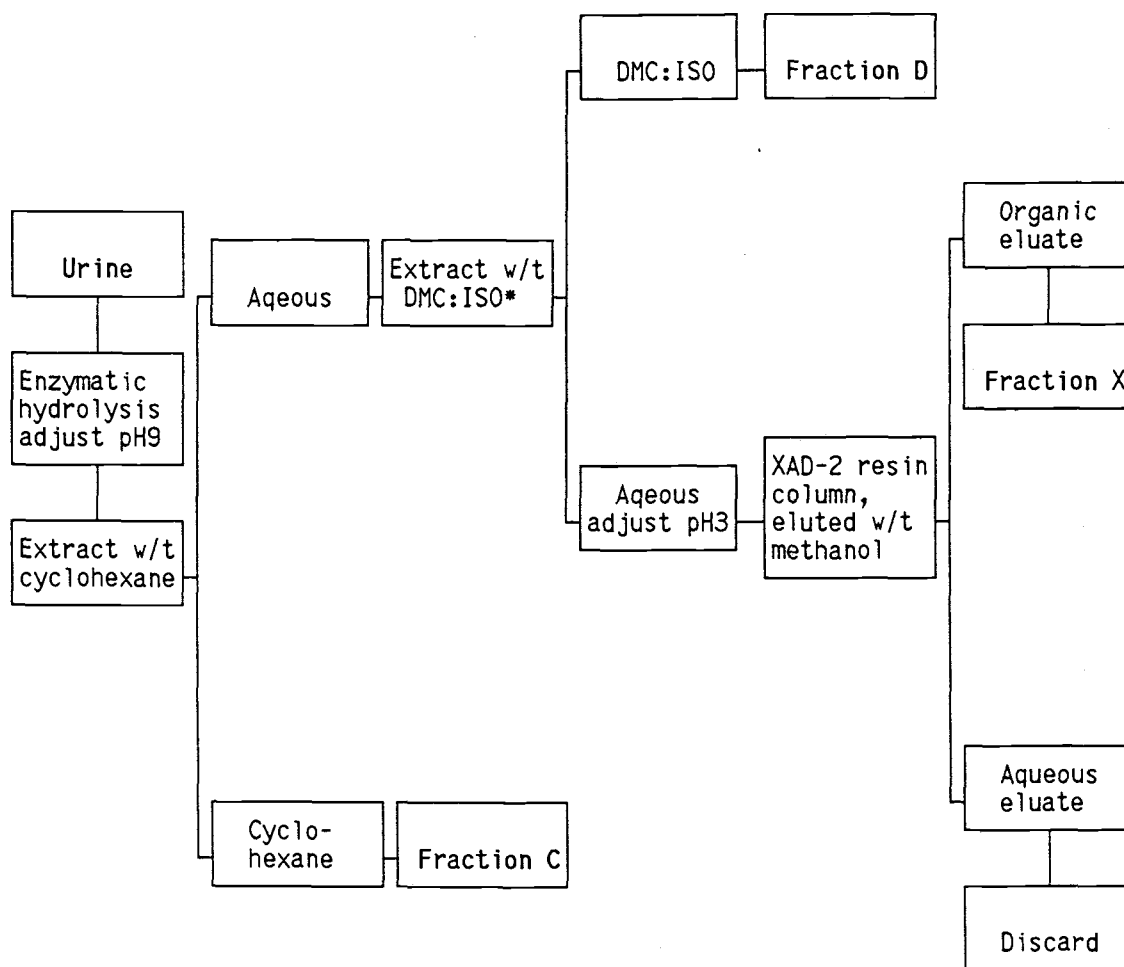


Figure II.11 Overall flow diagram of isolation of pentazocine and its metabolites in greyhound urine.

\* DMC:ISO - methylene chloride:isopropanol (3:1, v/v).

III. HIGH-PERFORMANCE LIQUID CHROMATOGRAPHIC SEPARATION OF  
PENTAZOCINE METABOLITE ISOMERS FROM GREYHOUND URINE

by

Guang Xiao and Edward H. Piepmeier

Department of Chemistry

Oregon State University

Corvallis, OR 97331

and

A. Morrie Craig

School of Veterinary Medicine

Oregon State University

Corvallis, OR 97331

For submission to Journal of Chromatography

## 1. Introduction

In the GC/MS studies of pentazocine metabolism in the greyhound<sup>[18]</sup>, nine metabolites have been found in greyhound urine. In addition to the metabolites produced by biotransformation through oxidation of the side-chain of pentazocine to either alcohol or carboxylic acid, as previously discovered in other species, a new branch of metabolites has been found, which is apparently produced by the hydroxylation and methylation of the aromatic ring of pentazocine. As a result, an additional methoxy group is attached to the aromatic ring of each of these metabolites, and two different placements of this methoxy group on the aromatic ring also causes pairs of isomers among the metabolites. There is evidence for a pair of isomers whose structures are the same as pentazocine except for an additional methoxy group attached to the aromatic ring. It is also clear that some metabolites in this new branch of metabolites have undergone oxidative biotransformation, that is, some of those metabolites have either alcohol or carboxylic acid attached to the side-chain. Although the structural changes on the side-chain of pentazocine after the biotransformation can be identified from mass spectra, the position of the methoxy group attached to the aromatic ring cannot be determined by GC/MS data only. Therefore, the identification of the methoxy group position in the metabolites by more powerful spectroscopic tools such as NMR is crucial for the complete structure elucidation of the metabolites in this new branch of pentazocine metabolites. In this

chapter, the development of an overall separation strategy is described to enable the separation of a pair of pentazocine metabolic isomers (both having a suspected structure with only a methoxy group attached to different positions on the aromatic ring of the pentazocine parent structure<sup>[18]</sup> ) in sufficient quantities for subsequent NMR analysis.

The major problems in isolation and separation of drug metabolites in urine samples arise from the low concentration of metabolites, and the high content of endogenous compounds in such biological materials. The physico-chemical properties of more strongly polar metabolites could further complicate the chromatographic separation of metabolites in high purity for structural characterization. However, the biotransformation of a drug may result in many metabolites with very different physico-chemical properties. Consequently, a complete separation covering all possible metabolites can be difficult for a single HPLC run, and the repeated runs can be extremely time consuming. Therefore, besides the hydrolysis of the conjugates and isolation of the drug and its metabolites from biological materials, pre-separation of drugs and their metabolites into several groups on a preparative scale can greatly ease the difficulties in the subsequent specific separation of a drug and its metabolites into individual components. Since pentazocine metabolites in greyhound urine are found to be in a fairly small amount<sup>[19]</sup>, an enrichment step where metabolites are pre-concentrated is therefore also necessary prior to the use of more specific separation by HPLC for further purification.

Most separations are carried out by various chromatographic

techniques, and high-performance liquid chromatography (HPLC) provides very selective separation results. There have been numbers of different HPLC systems used for the study of the pentazocine parent drug itself in biological samples: a reversed-phase HPLC system ( $C_{18}$  column; acetonitrile-water-ammonium chloride, pH 8, mobile phase) was first used to investigate pentazocine in blood samples<sup>[20]</sup>; a different ion-pair reversed-phase HPLC system ( $C_{18}$  column; sodium octanesulfonate-methanol-phosphoric acid, mobile phase) and a normal phase HPLC system (5  $\mu$ m Silica column; chloroform-methanol-isopropylamine, mobile phase) was applied for the analysis of pentazocine hydrochloride in tablets<sup>[21]</sup>; pentazocine tablets were also assayed by a method using a nitrile-bonded reverse phase column, a methanol-0.003 M ammonium acetate (90 + 10) mobile phase<sup>[22]</sup>; while another reversed-phase HPLC system ( $C_{18}$  column; citrate buffer-acetonitrile-pyridine, mobile phase) was used to analyze pentazocine in human blood<sup>[23]</sup>.

Among all of the factors contributing to the separation assay development, the type of chromatography applied is considered first. Reversed-phase systems (non-polar bonded-phase columns) are more commonly used in pharmaceutical analysis due to, for example, the aqueous mobile phase used that is compatible with biological materials and particularly suitable for the quantitative analysis of conjugates of drugs and metabolites<sup>[24]</sup>. However, using bonded stationary phase materials with aqueous methanol or acetonitrile eluents containing inorganic salts, pairing ions and/or organic amines in the analysis of basic drugs was noted to have difficulties<sup>[25]</sup>, and hence may not be

appropriate for the proposed study.

Normal-phase systems frequently offer better resolution of isomers and functional classes than reversed-phase systems<sup>[26,27]</sup>. The selective separation of isomers in the normal-phase system is achieved because the polar functional groups are adsorbed by the silanol surface, and isomeric compounds which have different polarities due to different attachments of the functional group are therefore readily separated<sup>[27]</sup>. In addition, because the mobile phases used in normal phase HPLC systems are volatile, it has another advantage that allows simpler, more efficient concentration by evaporation and transfer steps for subsequent spectroscopic structural characterizations of the separated components.

Mobile phase composition in normal-phase liquid chromatography is critical to selectivity and retention of analytes<sup>[28,29,30]</sup>. Therefore the selection of the mobile phase solvent becomes the first and major decision in a successful separation development. The most comprehensive and widely accepted method for characterizing mobile phase solvent selectivity is the Snyder solvent selectivity triangle concept<sup>[28,29,30]</sup>. This method categorizes solvents into three classes according to their interaction with analyte: proton acceptor, proton donor, and large dipole. All commonly used solvents fall into eight different groups, and the solvents with similar selectivities (but perhaps different solvent strength) should be within the same group. The optimization of mobile phase selectivity therefore can be readily achieved by picking the appropriate solvents from different groups after an appropriate solvent strength is obtained by varying percentages of a pilot solvent in the mobile phase solvent system.

The initial selection of the mobile phase composition can be carried out by pilot TLC separation, which has been commonly applied in liquid-solid column chromatography, for example, flash column chromatography<sup>[31]</sup> for preparative separations. However, based on the Snyder adsorption model<sup>[32]</sup>, TLC plates coated with silica should have the same retention mechanism as normal-phase HPLC for the separation, and mobile phase solvents for normal-phase HPLC can be pre-selected by TLC for their selectivity, and then an appropriate retention time can be achieved by slightly adjusting the percentages of the solvents.

In the present study, a normal-phase HPLC system with polar eluents has been developed for the separation of a pair of pentazocine metabolic isomers in greyhound urine. After the hydrolysis and extraction to isolate pentazocine metabolites from the greyhound urine, a pre-TLC separation was conducted first, which served two purposes: (1) the enrichment and group separation of pentazocine metabolite isomers of interest from the urine extract, and (2) initial scouting for an appropriate mobile phase for later normal-phase HPLC separation of this pair of isomers. Therefore, the elution of the TLC band corresponding to the pair of metabolic isomers not only provided a relatively clean extract, but also pre-selected the mobile phase composition for further complete separation of the isomers by a normal-phase HPLC system. The specificity of the HPLC separation developed in this manner is further validated by mass spectrometry (MS).

## 2. Experimental

Extraction of pentazocine and its metabolites (Fig. III.1). The greyhound urine (1000 ml) collected after the intravenous administration of pentazocine was mixed with 400 ml of pH 5 acetate buffer and 0.71 g of  $\beta$ -glucuronidase (1,400,000 units/g, Sigma Chemical Company). The urine was incubated for 36 hours at 37°C. After the hydrolysis, the urine was cooled to the room temperature and adjusted to pH 9.0 with the addition of concentrated ammonium hydroxide. The solution was then extracted twice with 500 and 250 ml of cyclohexane, and the organic phase was removed and washed with water. After dehydration with anhydrous sodium sulphate, the combined cyclohexane phase was filtered and evaporated to dryness.

The urine remaining after the first extraction was extracted again twice with 500 and 250 ml of pre-mixed extracting solvent consisting of methylene chloride and isopropanol (3:1, v/v), the organic phase was removed and washed with water. After dehydration with anhydrous sodium sulphate, the combined methylene chloride and isopropanol phase was filtered and evaporated to dryness.

The urine after all extractions was sealed under nitrogen in a freezer for further treatment by XAD-2 resin.

Thin Layer Chromatography. TLC analyses were performed on Kieselgel 60/ Kieselgel<sub>254</sub> silica gel plates (EM Science). The samples were spotted as a band 1 cm from the bottom edge of each of the plates. The plates were developed 5 cm from the origin in a tank previously saturated in freshly prepared developing solvents for about

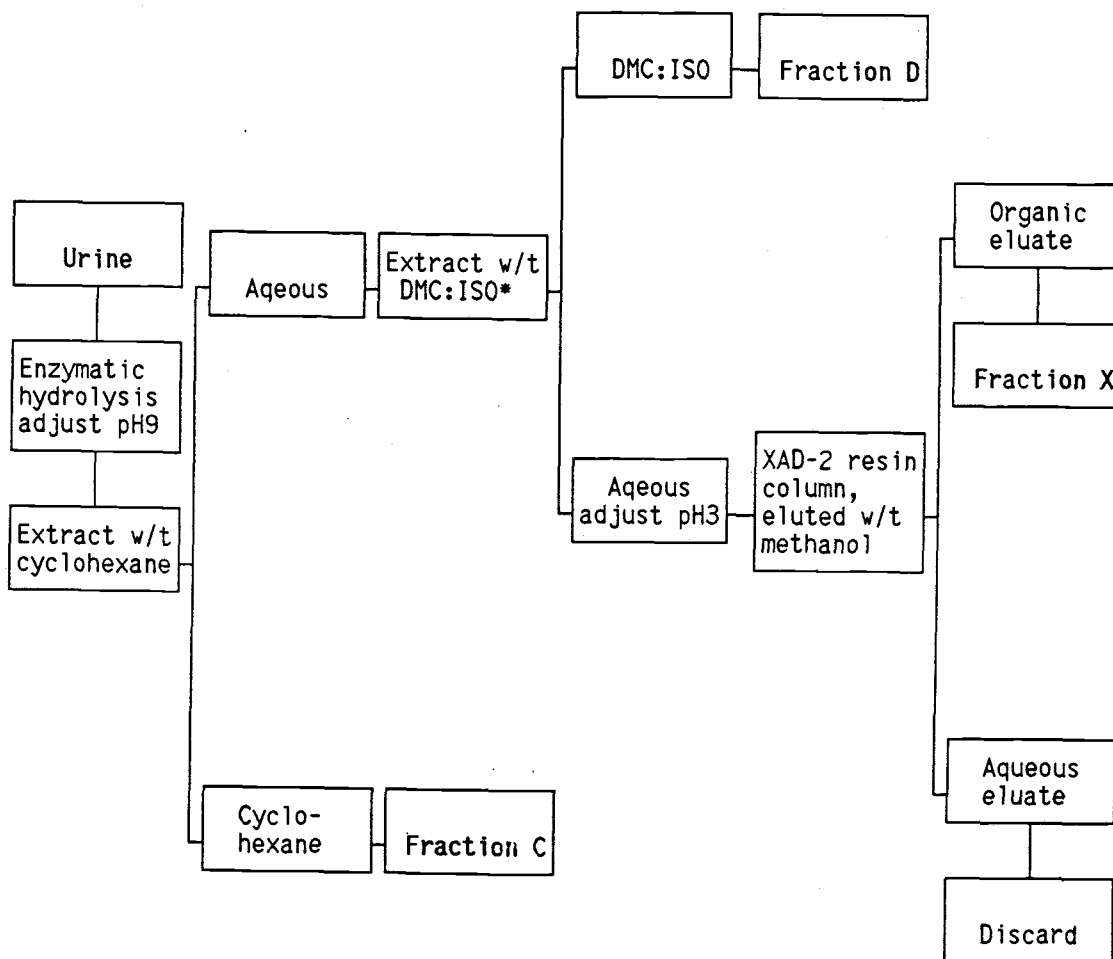


Figure III.1 Extraction scheme of pentazocine and its metabolites in greyhound urine for separation of metabolites MET1 and MET2.

30 minutes. The plates were visualized under 254 nm and 366 nm ultraviolet light in a Chromato-Vue cabinet (model CC-60, UVP Inc.), and subjected to different spray reagents in the following order: (1) Dragendorff reagent, (2) 5% sodium nitrite, and (3) cupric chloride solution. The colored bands produced by the nitrogen containing compounds after each spray were noted and compared with sample blanks after being dried. The suspected metabolite elution bands were also subjected to GC/MS analysis.

The elution bands obtained after TLC separation were prepared for further HPLC separation as follows: while being observed under UV light the band of interest was scraped off the plate onto a weighing paper, transferred to a 100 x 13 mm tube and extracted twice by 2 ml methanol with 30  $\mu$ l ammonium hydroxide. The tube was centrifuged after mixing. The supernatant was transferred to another clean tube and evaporated to dryness by a Speed Vac Concentrator (model SVC100H, Savant Instruments Inc., Hicksville, NY). The residue was dissolved in HPLC mobile phase, filtered and subjected to HPLC separation.

High-performance liquid chromatography. Analyses were performed using a Beckman (Beckman, Berkely, CA, U.S.A.) HPLC system Model 110A pump, Becman Model 160 variable wavelength detector set at 280 nm, Altex 210 injector (Altex-Beckman, San Ramone, CA, U.S.A.) and Altex Ultrasphere-Si column (25 x 4.5 mm I.D.; 5  $\mu$ m particle size). The mobile phase of chloroform-3% methanol-0.015% ammonium hydroxide, and chloroform-5% methanol-0.015% ammonium hydroxide was pumped at a flow-rate of 2 ml/min.

Gas chromatography-Mass spectrometry. In order to analyze the TLC

plates and confirm the HPLC results, the TLC elution bands and the fractions collected from HPLC were analyzed by MS. Each of the samples obtained from either TLC or HPLC in amounts equivalent to analytes contained in approximately 5 ml urine sample, were dried under a stream of nitrogen. Each of the residues were then dissolved in 10 mg/ml sodium acetate in methanol, and evaporated again under a nitrogen stream. A 100- $\mu$ l volume of Sylon BFT (Supelco) was added, and the solution was heated at 60°C for 25 minutes to form the trimethylsilylated derivatives for gas chromatographic-mass spectrometric (GC/MS) analysis. After the silylation reaction was completed, the solutions were evaporated under a nitrogen stream, and the residues were dissolved in 50  $\mu$ l of methylene chloride. A 2.5- $\mu$ l volume of the sample in methylene chloride was injected into the gas chromatograph of the GC/MS system (Finnigan 1020B mass spectrometer equipped with a Perkin Elmer Sigma 3B gas chromatograph). The chromatograph was equipped with a 30 m x 0.25 mm i.d. DB-5 capillary column (J & W Scientific, Inc.). Operating temperatures were as follows: injector, 260°C, GC temperature program was from 165 to 210°C at 3°C/minutes; interface, 280°C; source, 80°C. The carrier gas was helium, at a flow-rate of 33 cm<sup>3</sup>/sec. The mass spectra were obtained at an ionization energy of 70 eV and scanned from 45 to 500 a.m.u.. Pentazocine was identified by comparison with a mass spectrum of an analytical standard. The metabolites were identified by the characteristic fragments in their spectra<sup>[18]</sup>.

### 3. Materials and Reagents

J.T.Baker HPLC grade methanol, chloroform, methylene chloride, 2-propanol(isopropanol), cyclohexane (VWR Scientific, Denver, CO, U.S.A.). Pentazocine (Sterling, USA).  $\beta$ -glucuronidase (1,400,000 units/g, Sigma Chemical Company). TLC plates (pre-coated silica gel, 60F<sub>254</sub>, 0.25 mm. thick, EM Science). Dragendorff reagent: Dissolve 1.3 g of bismuth subnitrate in a mixture of 60 ml distilled water and 15 ml glacial acetic acid, dissolve 12.0 g of potassium iodide in 30 ml of distilled water, mix these two solutions diluted with 100 ml distilled water and 25 ml glacial acetic acid. Cupric chloride solution: dissolve 25 g of cupric chloride in 75 ml distilled water and 25 ml methanol. All other chemicals were of analytical reagent grade.

### 4. Results and Discussion

TLC pre-separation and HPLC mobile phase initial scouting. Table III. 1 summarizes the developing solvent systems tested and the separation results along with  $R_f$  values for pentazocine for each TLC development. The  $R_f$  value is defined as:

$$R_f = \frac{\text{distance of pentazocine spot from origin}}{\text{distance of solvent front from origin}}$$

One of the purposes of performing TLC pre-separation prior to the

Table III.1 Summary of TLC developing solvent systems.

Solvent	Composition (v/v/v)	Rf for Pent.	Metabolites Separation *
EtOAc/MeOH	9/1	0.28	C
CHCl <sub>3</sub> /MeOH	9/1	0.24	C
DMC/MeOH	9/1	0.22	C
ACETONE/MeOH	9.5/0.5	0.25	C
HEXANE/MeOH	9/1	0.03	C
EtOAc	PURE	0.10	C
HEXANE	PURE	0.00	C
EtOAc/MeOH/NH <sub>4</sub> OH	20/2/0.5	0.71	A
ACETONE/MeOH/NH <sub>4</sub> OH	16/4/0.5	0.74	B
CHCl <sub>3</sub> /MeOH/NH <sub>4</sub> OH	20/2/0.5	0.66	A
DMC/MeOH/NH <sub>4</sub> OH	18/2/0.5	0.75	A
EtOAc/MeOH/NH <sub>4</sub> OH	8.5/1/0.5	0.68	-
EtOAc/MeOH/HOAc	8.5/1/0.5	0.17	-
EtOAc/MeOH/H <sub>2</sub> O	8.5/1/0.5	0.16	-

\* The separation of pentazocine metabolites on TLC plates in different solvent systems are rated as: A - good, B - bad, C - worst.

final HPLC separation is to estimate approximately the polarity of the mobile phase composition for subsequent HPLC analysis. In drug metabolite analysis in biological samples, the analytes and interferences to be separated after the solvent extraction often have medium polarity. Therefore, this pilot separation by TLC was helpful because normal-phase HPLC to be applied later, uses a polar stationary phase, silica, which will strongly adsorb any compounds with polar functional groups. In normal-phase chromatography, it is customary to add small amounts of a "polar modifier" such as methanol to a non-polar mobile phase such as hexane<sup>[27]</sup>. However, as shown in Table III.1 and Fig. III.2a, III.2b, under both pure hexane and hexane with methanol developing solvent systems, pentazocine is barely eluted. Obviously, a modified mobile phase composition is needed.

A proper mobile phase composition can be obtained under the guidance of chromatographic retention theory, which describes the interactions in a given chromatographic system. There are many theories that have been developed attempting to explain the interactions within the normal phase HPLC system, and hence to predict retention of analytes and their separation. Snyder and co-workers have developed an adsorption theory based on the displacement of mobile phase solvent molecules by analyte molecules from the sites on the stationary phase<sup>[32]</sup>. In the hexane based solvent systems, the slow elution of pentazocine observed would thus be due to insufficient solvent polarity according to Snyder's theory, and a solvent system consisting of more polar solvents, which would pre-adsorb on the surface of the silica, should give faster elution for pentazocine. The reason is that the free energy required for displacement of polar solvent molecules

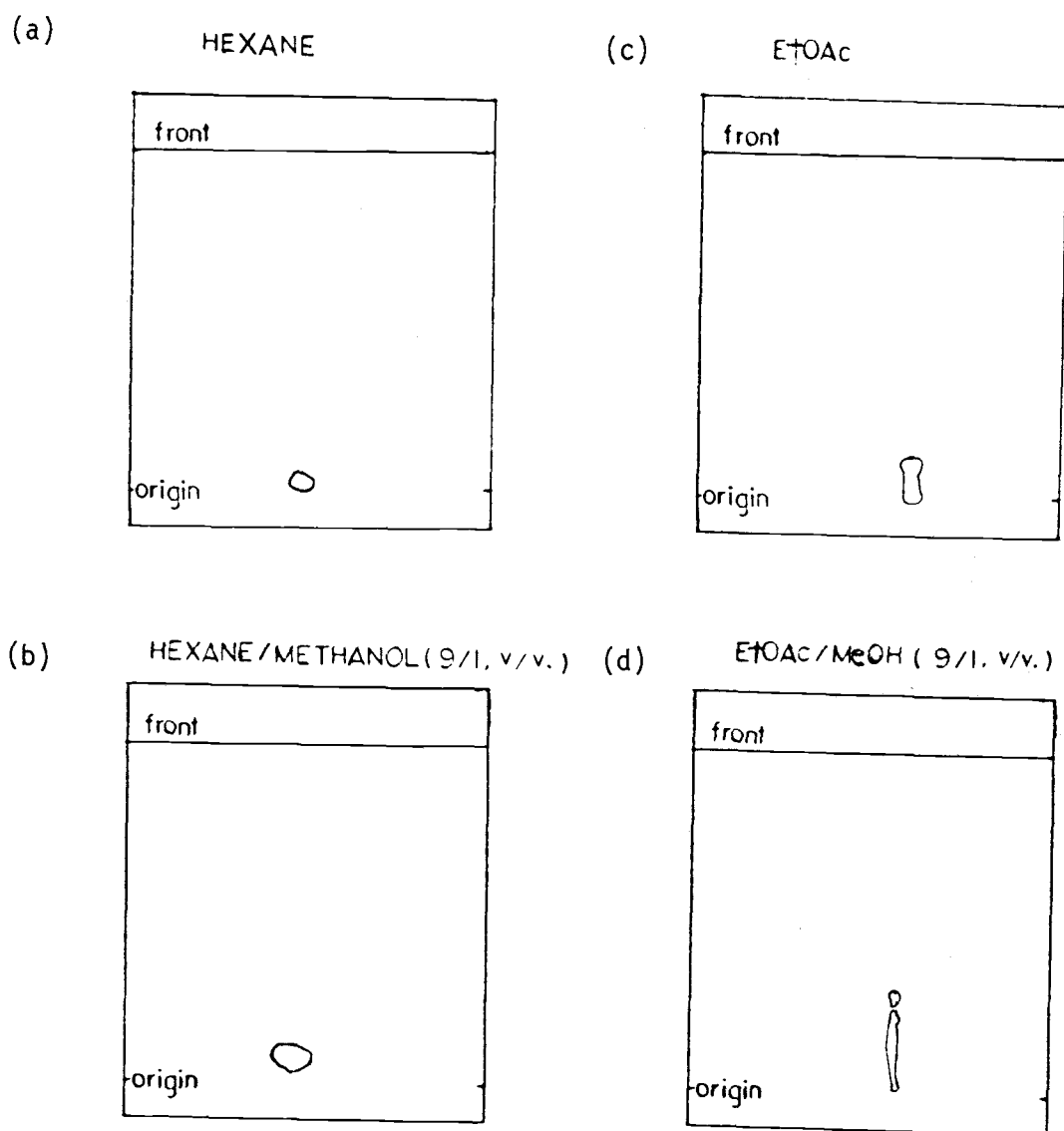


Figure III.2 Schematic representation of pentazocine metabolites separation by TLC (pre-coated silica gel plates, 60F<sub>254</sub>, 0.25 mm. thick, EM Science). Developing solvents: (a) Hexane; (b) Hexane/Methanol (9/1, v/v); (c) Ethyl acetate; (d) Ethyl acetate/Methanol (9/1, v/v).

pre-adsorbed on the surface of silica by pentazocine molecules must be greater than that of displacement of non-polar solvents molecules, and pentazocine molecules therefore will be less likely to be adsorbed by the silica surface. This prediction proved to have a pronounced effect, as shown in Table III.1 and Fig. III.2c, III.2d; the solvents with polar functional groups showed faster elution for the pentazocine on the silica TLC plates, and the elution rate increased as the polarity of the solvent increased.

Although faster elution is achieved using polar solvents with a methanol modifier, as shown in Fig. III.2c and III.2d, the separation is severely damaged by band tailings. There are several different phenomena that can lead to band tailings<sup>[27]</sup>. By carefully examining these different causes of band tailings and applying them to the separation of pentazocine metabolites, it was decided that the tailings should be suppressed by adding acid, base or water to the mobile phase depending on whether acidic or basic compounds are to be separated or some other problem such as the "system mismatch" is encountered<sup>[27]</sup>. As shown in Fig. III.3 and Table III.1, by adding ammonia to the mobile phase, the tailings are cured and the separations are dramatically improved. Also note from Table III.1 that the additions of either acid or water have relatively small effects on the elution rate of pentazocine. The better separation for the solvent extracts (the XAD-2 fraction is excluded) provided by the addition of the base into the mobile phase may be attributed to both the basic properties of the metabolites, and the change of the silanol surface of the column by the basic modifier in the mobile phase.

The best selectivity can be obtained by changing the mobile phase

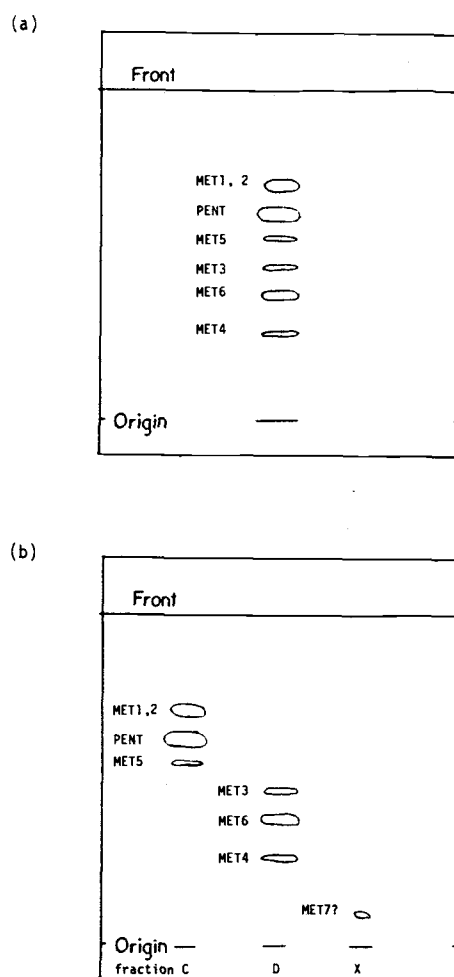


Figure III.3 Schematic representation of pentazocine metabolites separation by TLC (pre-coated silica gel plates, 60F<sub>254</sub>, 0.25 mm. thick, EM Science); Developing solvent system: Chloroform/Methanol/Ammonia (97/3/0.015%, v/v/v): (a) Application of combined solvent extracts; (b) Application of individual extracts.

solvent to a solvent from a different solvent group, according to the Snyder solvent selectivity triangle theory (which states that solvents belonging to the same group should produce similar selectivities, whereas solvents from different groups exhibit different selectivity<sup>[27]</sup>). Four solvents from different solvent groups in the triangle are selected to optimize the separation: methylene chloride (group V), chloroform (group VIII), ethyl acetate (group VIa), and acetone (group VIa). The findings in the solvent selectivity studies for the pentazocine metabolite separation are rather different from those predicted from the theory. For example, the separation using solvent system A ( $\text{CHCl}_3/\text{MeOH}/\text{NH}_4\text{OH}$ ) is similar to that of solvent system C ( $\text{CH}_2\text{Cl}_2/\text{MeOH}/\text{NH}_4\text{OH}$ ), as shown in Table III.2, despite the fact that methylene chloride and chloroform belong to two different solvent selectivity groups in the triangle and are supposed to exhibit different selectivities for a given separation. Also a solvent system consisting of ethyl acetate, methanol and ammonia shows quite different selectivity from that of a solvent system consisting of acetone, methanol and ammonia of a similar solvent strength for the separation of pentazocine and its metabolites, despite the fact that both ethyl acetate and acetone come from the same solvent group in the Snyder selective solvent triangle. Fig. III.3 shows the schematic representation of the TLC separation of pentazocine and its metabolites (after extractions) using developing solvent system A.

The failure of the Snyder solvent selectivity triangle to predict the separation of pentazocine and its metabolites in normal-phase chromatography with polar solvents might be attributed to the assumptions in this concept. The triangle concept assumes that the

Table III.2  $R_f$  values of pentazocine and its metabolites in TLC.

Spots (Metabolites)	Rf (a) Solvent System		
	A *	B **	C ***
PENTAZOCINE	1.00	1.00	1.00
MET1	1.13	0.76	1.07
MET2	1.13	0.76	1.07
MET3	0.74	0.51	0.64
MET4	0.43	0.11	0.49
MET5	0.88	0.70	0.79
MET6	0.60	0.22	0.53

\* Solvent system A:  $\text{CHCl}_3/\text{MeOH}/\text{NH}_4\text{OH}$ : 97/3/0.5 (v/v/v).

\*\* Solvent system B:  $\text{EtOAc}/\text{MeOH}/\text{NH}_4\text{OH}$ : 85/5/0.5 (v/v/v).

\*\*\* Solvent system C:  $\text{DMC}/\text{MeOH}/\text{NH}_4\text{OH}$ : 90/10/0.5 (v/v/v).

(a).  $R_f$  values are relative to the  $R_f$  of authentic pentazocine.

$$R_f(\text{relative}) = R_f(\text{metabolites})/R_f(\text{pentazocine}).$$

$R_f$  - The fractional movement of a solute band, relative to the distance moved by the solvent front.

selectivity of a given separation is mainly determined by the various intermolecular interactions between the solvent and analyte molecules, and therefore the solvents are grouped by using three probe analytes each representing proton-donor, proton-acceptor, and large dipole interaction. It is also assumed that the stationary phase in a given chromatography system and the nature of analytes to be separated play a less important role in a separation<sup>[33]</sup>. This is in direct contradiction to the solvent/analytes displacement theory<sup>[32]</sup>, where a change in the ability of solvent molecules to interact with a silica surface should create profound differences in solvent selectivity for given analytes.

Furthermore, the observed discrepancy for the solvent selectivity triangle may result from the fact that pentazocine and its metabolites contain both proton-donor (-OH) and proton-acceptor (-NR<sub>2</sub>) functional groups, which should be more complicated in terms of the chromatographic interactions than those probe compounds (each contains only a single functional group) used to establish the Snyder solvent triangle. The implication is that, perhaps, solvents can be grouped by using new probe compounds which contain both acidic and basic functional groups for a particular drug analysis and other more complex molecules, and/or the solvent selectivity may be categorized according to a given stationary phase. For example, the solvent selectivity can be categorized according to the interaction between solvent molecules and silica surface for a silica stationary phase.

The Snyder solvent triangle concept is still by far one of the most comprehensive and widely accepted techniques for characterizing solvent selectivity. The concept of the Snyder solvent triangle

might be extended to drug analysis, where drugs and their metabolites are in the same class (e.g. morphine analgesics). That is, the solvent selectivity can be characterized by selecting probe drugs which represent a typical functionality for a class of drugs, or drugs can be similarly characterized in terms of their interaction with both the solvent and the stationary phases by using probe solvents.

High-performance liquid chromatography. A normal-phase HPLC system was eluted first with a mobile phase composition optimized by TLC analysis (chloroform/methanol/ammonia, 97/3/0.015%, v/v/v), and then with a slightly adjusted composition to produce shorter analysis time (chloroform/methanol/ammonia, 95/5/0.015%, v/v/v). The chromatographic separation of MET1 and MET2 in the samples collected after TLC pre-separation is shown in Fig. III.4. Pentazocine was also injected under the same chromatographic conditions and the chromatogram is shown in Fig. III.5. The symmetric shape of pentazocine peak again indicates a well managed chromatographic condition under normal-phase column elution with a polar solvent system for a moderately polar drug analysis.

In order to confirm the HPLC results, the collected fractions before and after the HPLC separation of pentazocine metabolite isomers MET1 and MET2 were analyzed by GC/MS. Fig. III.6 shows a GC/MS chromatogram obtained before HPLC separation of MET1 and MET2. The peak at 1500 scan counts is a major interference in the same eluting band as MET1 and MET2 in the TLC pre-separation. The peak at 1778 scan counts is the pentazocine parent drug injected with the sample as a reference. The peaks at 1876 and 1902 scan counts are MET1 and MET2, respectively. The mass spectra of MET1 and MET2 trimethylsilylated

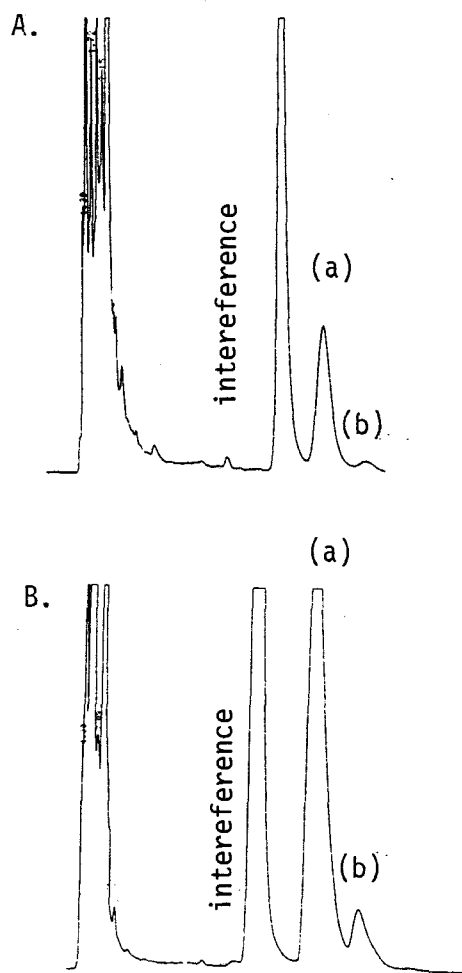


Figure III.4 Normal phase chromatograms of (a) pentazocine metabolite MET1 and (b) pentazocine metabolite MET2 with mobile phase: Chloroform/Methanol/Ammonia (95/5/0.015%, v/v/v), stationary phase: 5  $\mu$ m silica, and flow rate: 2 ml/min: (A) Sample injection of equivalent to 10 ml urine extracts; (B) Sample injection of actual collection for subsequent NMR analysis of MET1.

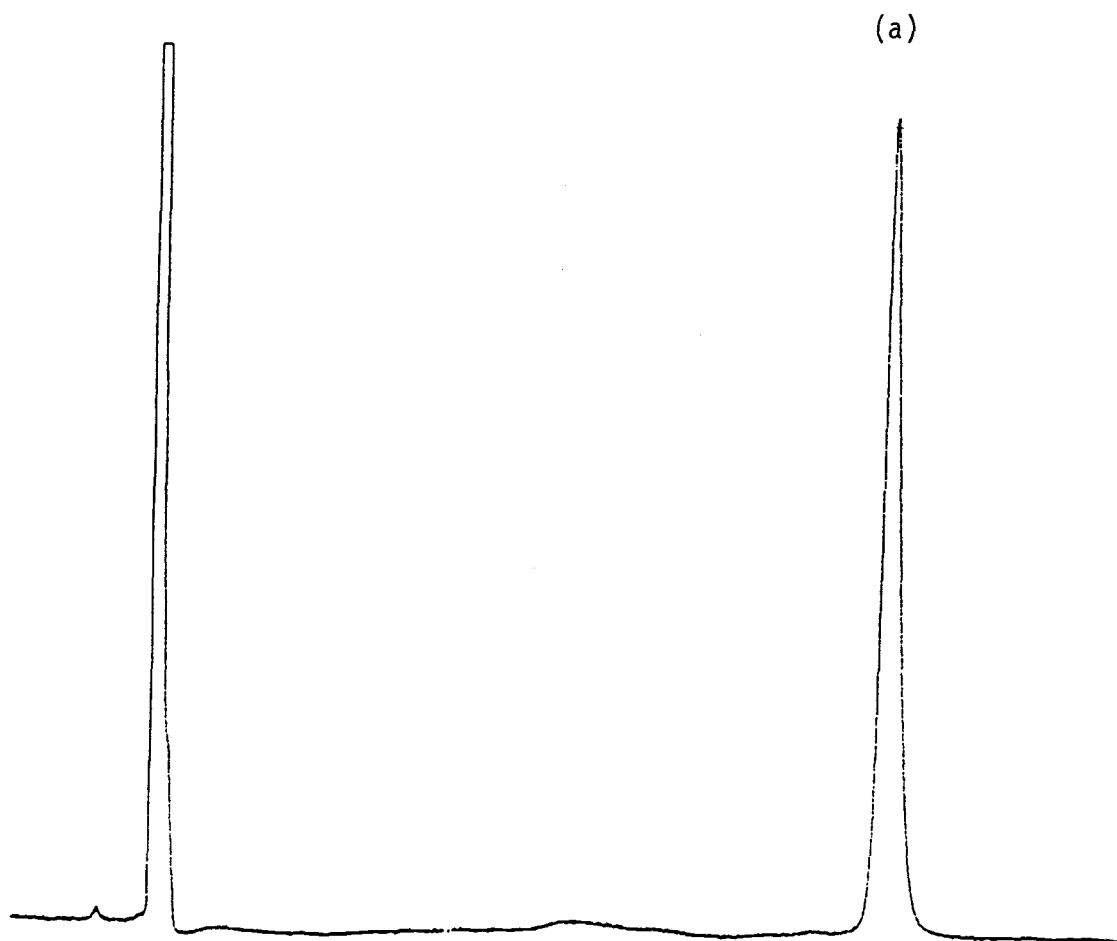


Figure III.5 Normal phase chromatogram of (a) pentazocine with mobile phase: Chloroform/Methanol/Ammonia (95/5/0.015%, v/v/v), stationary phase: 5  $\mu$ m silica, and flow rate: 2ml/min.

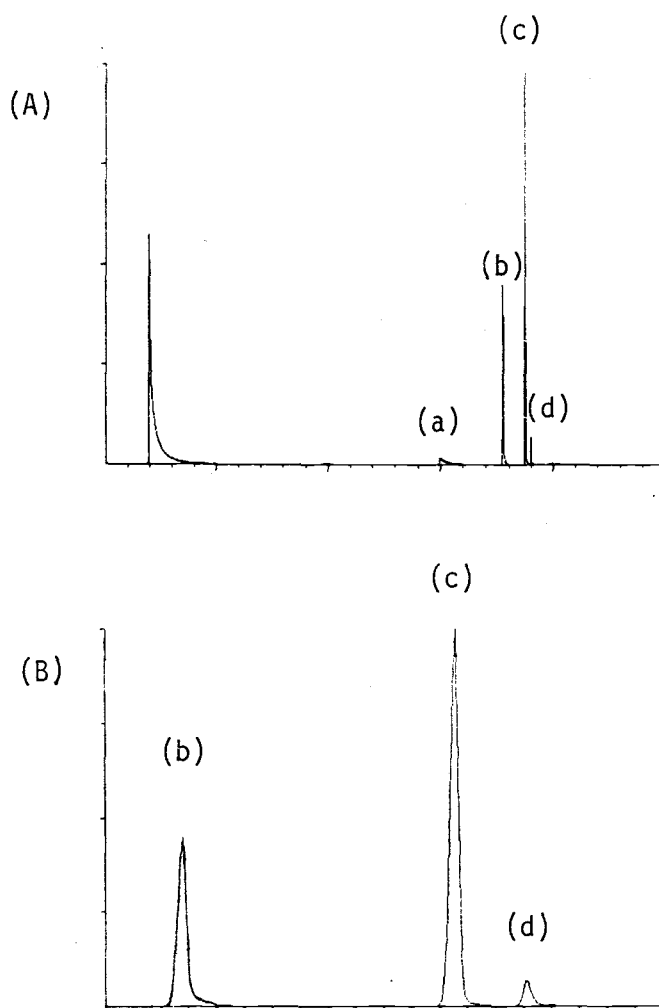


Figure III.6 GC/MS chromatograms of (a) interference, (b) pentazocine, (c) MET1 and (d) MET2: (A). GC/MS chromatogram obtained for collected TLC eluting band before HPLC analysis; (B). Close-up of chromatogram (A).

derivatives are shown in Fig. III.7. MET1 and MET2 are identified as pentazocine metabolites by comparison with the mass spectrum of the pentazocine parent compound trimethylsilylated derivative (Fig. III.8) and tracing their characteristic fragmentation ions<sup>[18]</sup>. Since MET1 and MET2 have virtually the same mass spectra, they must be geometric isomers. The ion peak at  $m/z$  387 in both the MET1 and MET2 mass spectra is the trimethylsilylated derivative molecular ion. Other important ions at  $m/z$  69, 110, 274-6, 304, 319 resemble those of the pentazocine parent compound. It is concluded that MET1 and MET2 are metabolites of pentazocine produced by the additional attachment of a methoxy group to the aromatic ring of the pentazocine parent structure, and the isomerism of MET1 and MET2 is a result of different placement of the methoxy group on the aromatic ring (Fig. III.9).

Fig. III.10 shows a GC/MS chromatogram of the fraction corresponding to MET1 peak collected after the HPLC separation of MET1 and MET2. The appearance of a single peak with the mass spectrum of MET1 confirms that a highly selective separation of isomers MET1 and MET2 is achieved by the chosen HPLC conditions.

## 5. CONCLUSION

The method described has effectively separated a pair of pentazocine metabolic isomers from greyhound urine. The specificity of this separation has been documented by GC/MS, and the separation has been proved fully satisfactory in terms of providing pure NMR spectral quality samples for the subsequence NMR identification of the MET1

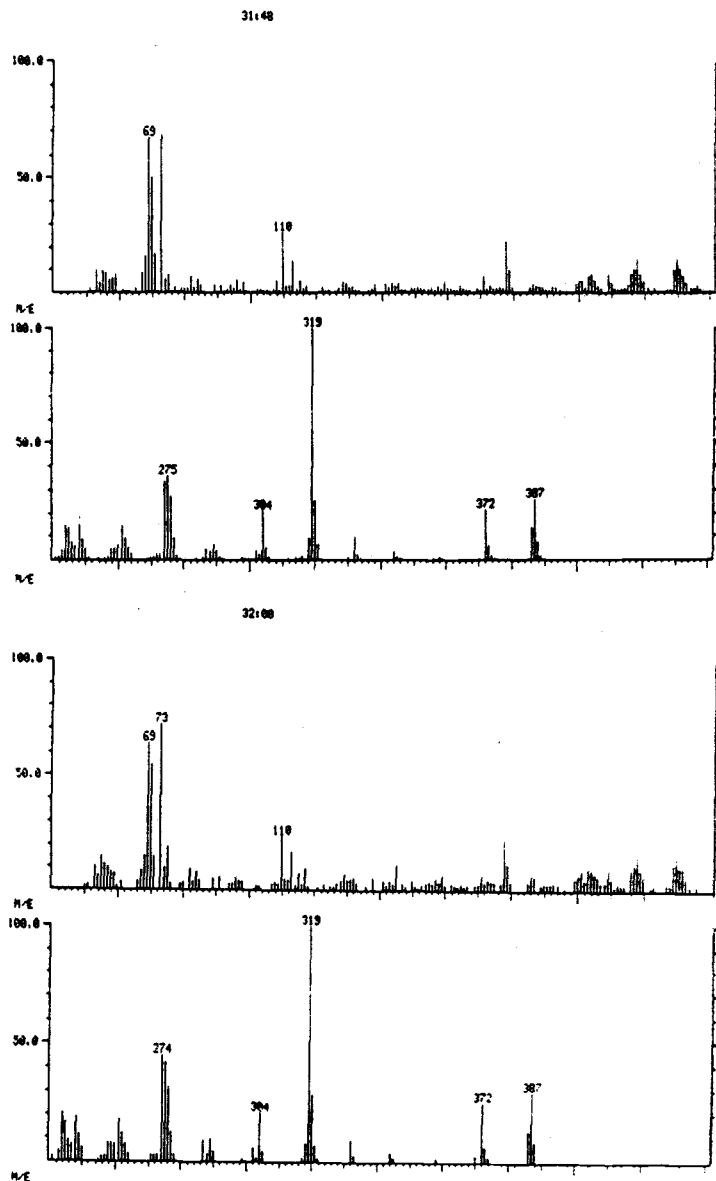


Figure III.7 Mass spectra of pentazocine metabolites MET1 and MET2:  
(a) mass spectrum of pentazocine metabolite MET1 trimethylsilylated derivative; (b) mass spectrum of pentazocine metabolite MET2 trimethylsilylated derivative.

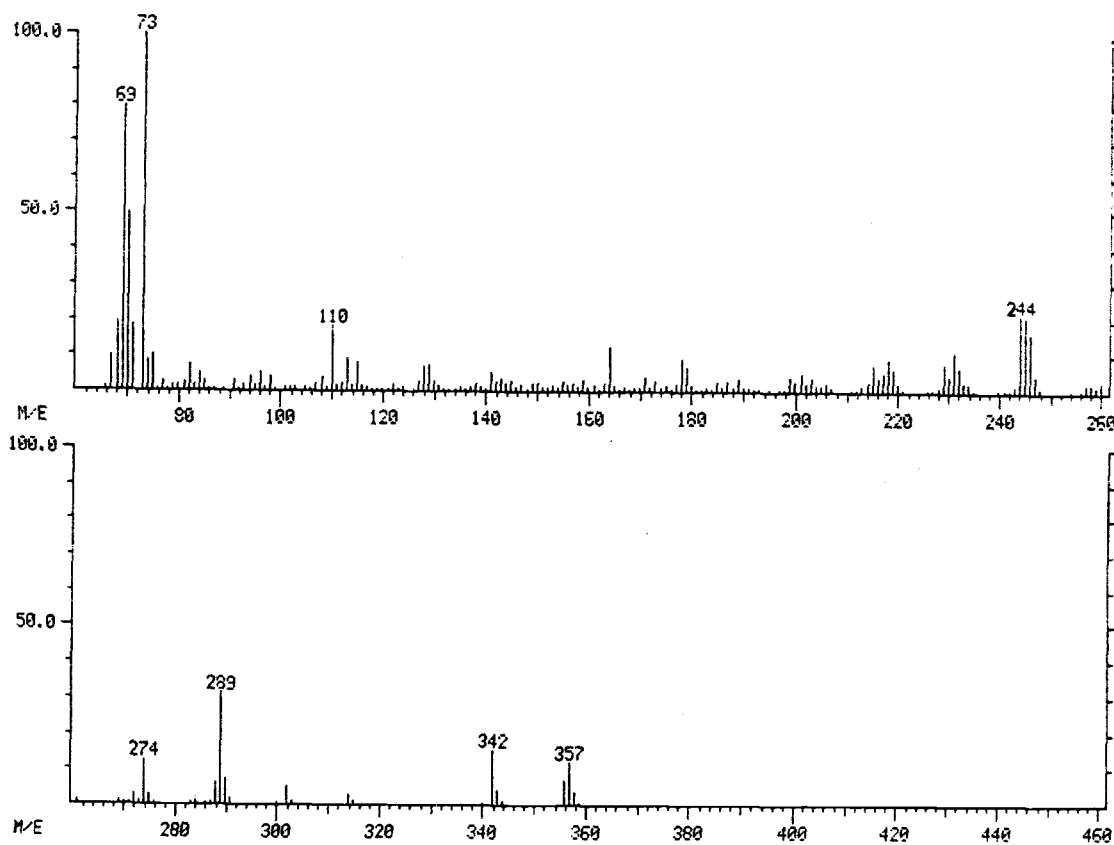


Figure III.8 Mass spectrum of pentazocine trimethylsilylated derivative.

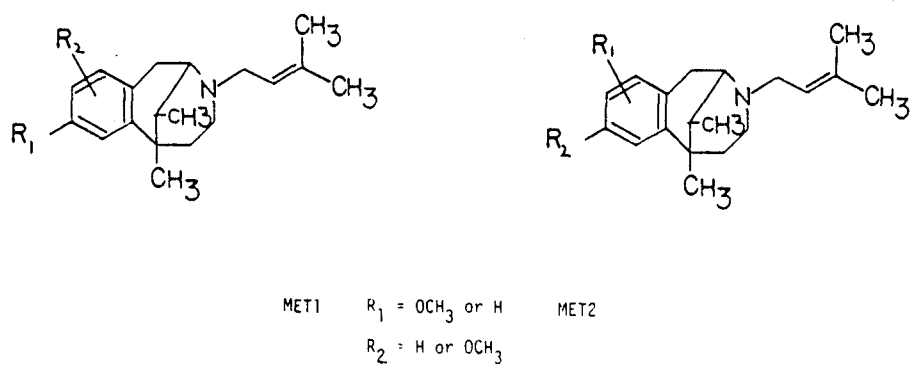


Figure III.9 Structures of pentazocine metabolites MET1 and MET2.

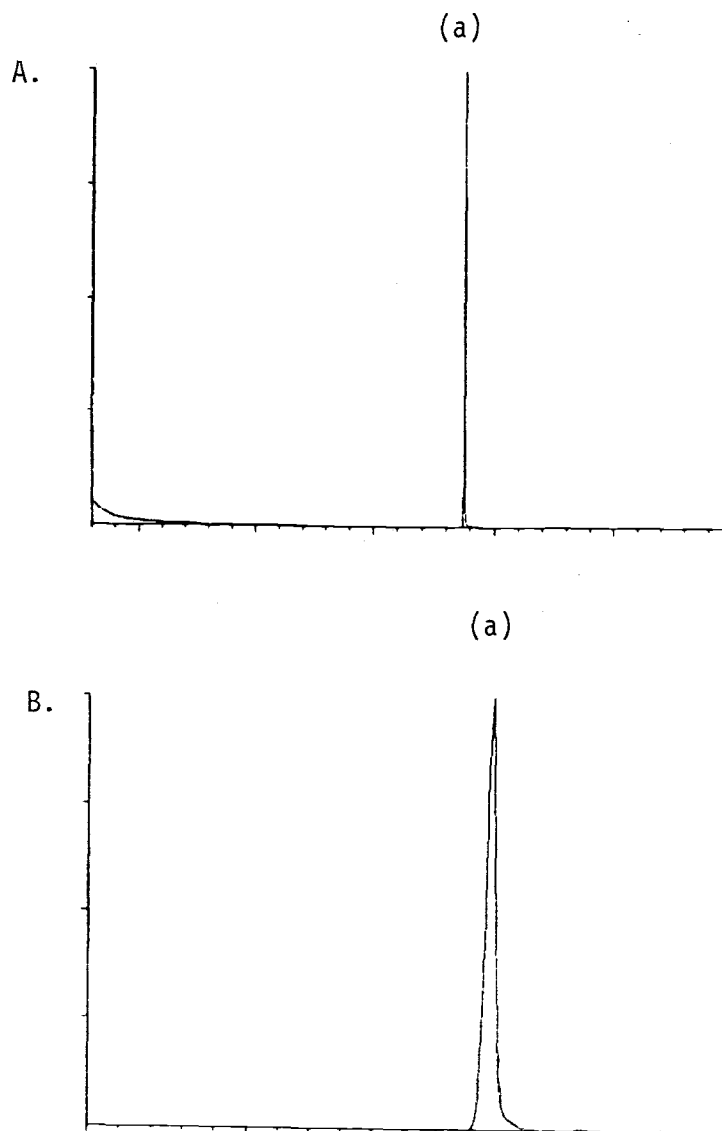


Figure III.10 GC/MS chromatograms of (a) pentazocine metabolite MET1: (A) GC/MS chromatogram obtained for the fraction collected for MET1 after HPLC separation; (B) Close-up of chromatogram (A).

molecular structure. In addition to estimating approximately the necessary polarity of and selectivity of the mobile phase for the subsequence HPLC separation, the initial TLC analysis has also served as a pre-separation step to eliminate very polar interferences which are common in a biological sample analysis, and to reduce the number of analytes to be separated in a single HPLC injection. This is done by collecting the elution band corresponding to the mixture of pentazocine metabolites MET1 and MET2 from the TLC plates, which greatly simplified the selection of subsequence HPLC separation conditions. The strategy applied in the separation has been successful in methods development for the separation of isomers, and the findings in the solvent selectivity implicate the potential and the need for further study in this field.

IV. Structural Characterization of Pentazocine Metabolites  
in The Greyhound by Gas Chromatography/Electron Impact  
Mass Spectrometry

by

Guang Xiao and Edward H. Piepmeier

Department of Chemistry

Oregon State University

Corvallis, OR 97331

and

A. Morrie Craig

School of Veterinary Medicine

Oregon State University

Corvallis, OR 97331

For submission to Organic Mass Spectrometry

## 1. Introduction

Biotransformation is the major factor limiting the intensity and duration of the effects of analgesics, and therefore metabolism studies become the center piece to much of biochemical and pharmacological research. The biotransformation of a drug may result in a diversity of metabolites with widely differing physico-chemical properties. Structural elucidations of these metabolites are further complicated by the fact that they are usually present in trace amounts within a complex biological sample matrix.

As a well established tool for structure elucidation studies, mass spectrometry has been extensively used in the field of metabolite identification. The use of GC/MS in the characterization of metabolites clearly has advantages because GC/MS combines both powerful separation and identification tools into one method, and hence the direct analysis after a simple solvent clean-up procedure by GC/MS is possible without tedious isolation and a large sample size requirement.

Characterization of all of the metabolites derived from a drug present in a complex biological sample matrix is a difficult task. Nonetheless, the inherent difficulties can be somewhat reduced by the fact that the structure of the parent drug is known, and that the metabolites will retain most or at least parts of the original substructure of the parent compound. In an attempt to characterize the structures of pentazocine (Fig. IV.1) metabolites in greyhounds, the present paper studies the fragmentation pathways of trimethylsilylated

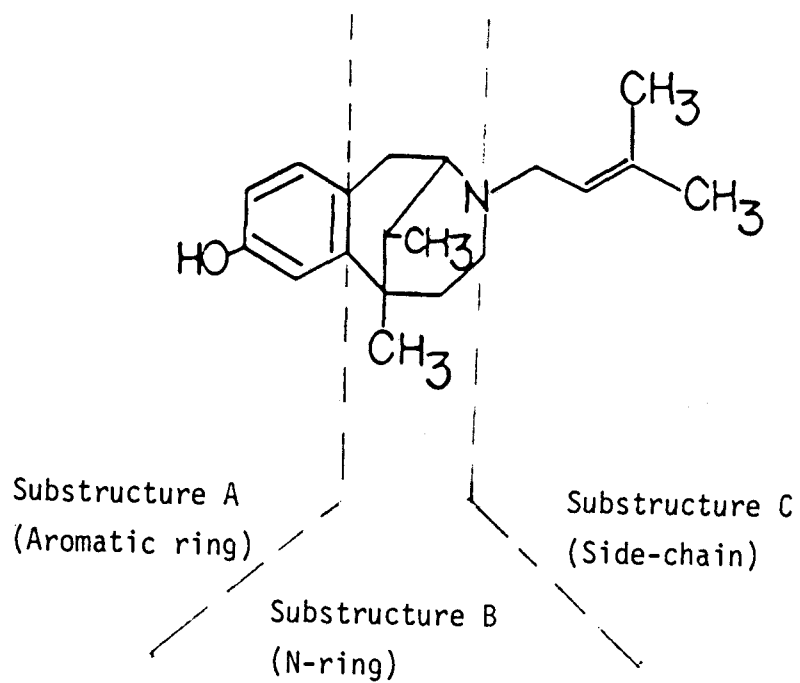


Figure IV.1 Structure of pentazocine.

pentazocine upon electron impact (EI), and then applies these fragmentation pathways to identify metabolites of pentazocine, in particular, to differentiate the positional isomers due to trans- or cis- functional group attachment to the terminal methyl groups of the dimethylallyl side chain of the structure.

## 2. Experimental

Drug administration and sample collection. Four greyhounds were used. After the intravenous administration of 40 mg pentazocine hydrochloride in aqueous solution to each dog, urine samples were collected naturally into a urinal at 0, 2, 4, 6, 8, 12 and 24 hours. All samples were frozen for subsequent experiments. Aliquots of 500 ml urine collected at 4 and 6 hours were combined for gas chromatographic-mass spectrometric analysis of pentazocine metabolites.

Urine sample preparation. A 25-ml volume of combined 4 and 6 hour urine samples was adjusted to pH 6 with acetic acid, and then was incubated with 125,000 units of  $\beta$ -glucuronidase (1,400,000 units/g, Sigma Chemical Company) in 50 ml of 1.0 M acetate buffer (pH 5.0) at 65°C for 3 h for enzymatic hydrolysis. The solution was cooled to room temperature and adjusted to pH 9.5 with 5.0 M sodium hydroxide, and then extracted twice with two 75-ml portions of pre-mixed methylene chloride:isopropanol (3:1, v/v). The combined organic phase was added to 25 ml of aqueous saturated sodium bicarbonate solution and shaken for 3 minutes. After dehydration with anhydrous sodium sulphate, the organic phase was filtered and evaporated to dryness under reduced pressure at 35°C.

After the methylene chloride:isopropanol extraction, the aqueous phase was adjusted to pH 2-4 with acetic acid, taken to one-tenth of the original urine volume by a Lyophilizer, dissolved in about twice the original volume of absolute ethanol, and stood overnight in a freezer. The solutions were taken to dryness under a nitrogen stream after filtering out the precipitate. The residue was taken up in water and submitted to an Amberlite XAD-2 (Eastman Kodak) column. The column was rinsed with water and then eluted with methanol. The eluate was taken to dryness.

Both residues were dissolved in 5 ml of benzene, and a 100- $\mu$ l volume of benzene solution was evaporated to dryness under a nitrogen stream at 45°C. The residues were then dissolved in 10 mg/ml sodium acetate in methanol, and evaporated again under a nitrogen stream. A 100- $\mu$ l volume of Sylon BFT (Supelco) was added, and the solution was heated at 60°C for 25 minutes to form the trimethylsilylated derivatives for gas chromatographic-mass spectrometric (GC/MS) analysis. After the silylation reaction was completed, the solutions were evaporated under a nitrogen stream, and the residues were dissolved in 50  $\mu$ l of methylene chloride.

Identification of pentazocine and its metabolites in urine. For each solution obtained from the previous step, a 2.5- $\mu$ l volume of the trimethylsilylated sample was injected into the gas chromatograph of the GC/MS system (Finnigan 1020B mass spectrometer equipped with a Perkin Elmer Sigma 3B gas chromatograph). The chromatograph was equipped with a 30 m x 0.25 mm i.d. DB-5 capillary column (J & W

Scientific, Inc.). Operating temperatures were as follows: injector, 260°C, GC temperature program was from 165 to 210°C at 3°C/min.; interface, 280°C; source, 80°C. The carrier gas was helium, at a flow-rate of 33 cm<sup>3</sup>/sec. The mass spectra were obtained at an electron ionization energy of 70 eV and scanned from 45 to 500 a.m.u.. Pentazocine was identified by comparison with the mass spectrum of a trimethylsilylated pentazocine standard obtained by direct injection of an analytical standard into GC/MS.

### 3. Results and Discussion

Mass spectrum of pentazocine trimethylsilylated derivative and its fragmentation pathways. It is reasonable to assume that upon electron impact, ionization of a pentazocine molecule should occur by loss of an n-electron of either the nitrogen or oxygen atom, or by loss of a  $\pi$ -electron of the aromatic ring, because of their relatively low ionization energy (favorability for ionization generally is in the order of  $\sigma^- < \pi^- < n$ -electrons<sup>[34]</sup>). Consequently, intermediates with radical and charge sites are generated, which can lead to fragmentation.

The mass spectrum of trimethylsilylated pentazocine along with its structure is shown in Fig. IV.2. The molecular ion is at m/z 357. Other prominent and important fragment ions (m/z) are 342, 289, 274, 244 (245, 246), 110, 73, 69, 68.

The base ion peak at m/z 73 is produced by losing the trimethylsilyl group derivatized to the phenolic functional group. As

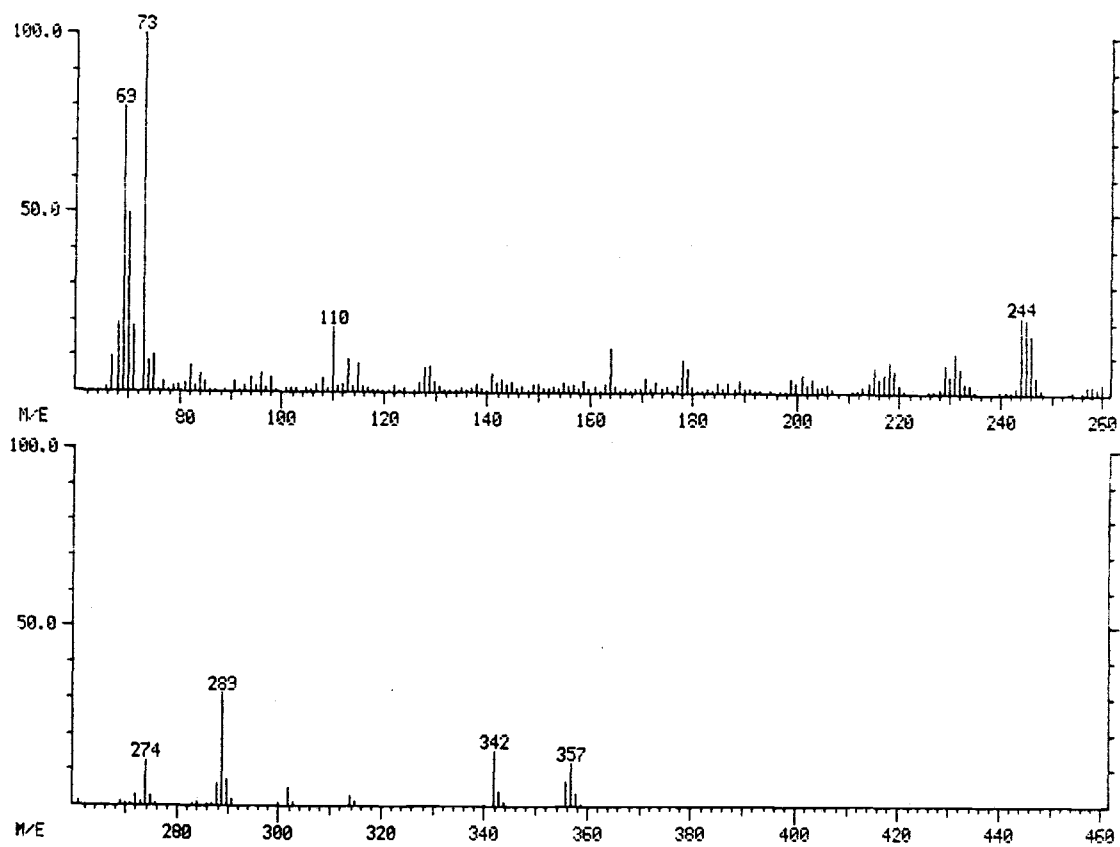


Figure IV.2 Mass spectrum of trimethylsilylated pentazocine

shown in Fig. IV.3, this fragmentation is initiated by the positive charge site at the oxygen atom upon the electron impact, and a pair of electrons can be withdrawn from the adjacent bond<sup>[35]</sup>. Consequently, a cleavage reaction (inductive cleavage, i) results in loss of the trimethylsilylated group with positive charge transferred to the silicon atom, producing a characteristic ion peak at  $m/z$  73. This base peak is expected to show in all metabolite trimethylsilylated derivative mass spectra if the phenolic functional group exists.

The appearance of an ion peak at  $m/z$  289 is one of the characteristic features of the mass spectrum of pentazocine trimethylsilylated derivative. The formation of this ion is probably associated with loss of the fragment I attached to the nitrogen atom of the pentazocine molecule as indicated by Pathway I in Fig. IV.4. As shown in Fig. IV.4, Pathway I involves a intramolecular hydrogen rearrangement initiated by the radical site at the nitrogen atom<sup>[36]</sup>. The new radical site generated by the hydrogen rearrangement can then initiate the cleavage of the nearby C-N,<sup>[36]</sup> and hence, a neutral fragment I ( $C_5H_8$ ) and an ion at  $m/z$  289 are formed.

It should be pointed out that this intramolecular hydrogen rearrangement is favored because of the steric selectivity of the six-membered-ring transition state. Referring to Fig. IV.4, it can be noted that only the hydrogens attached to the methyl group in the cis position at the end of the double bond can have such an orientation. In other words, if there are no hydrogens in the cis position, the intramolecular rearrangement would not take place, and the characteristic ion produced by Pathway I would not exist. This mass

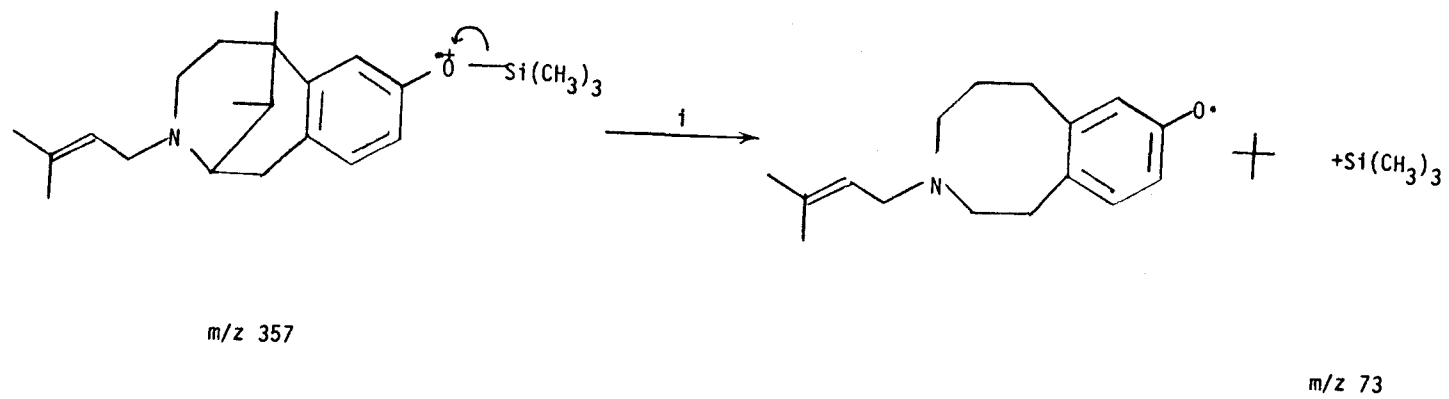


Figure IV.3 Fragmentation pathway producing ion m/z 73.

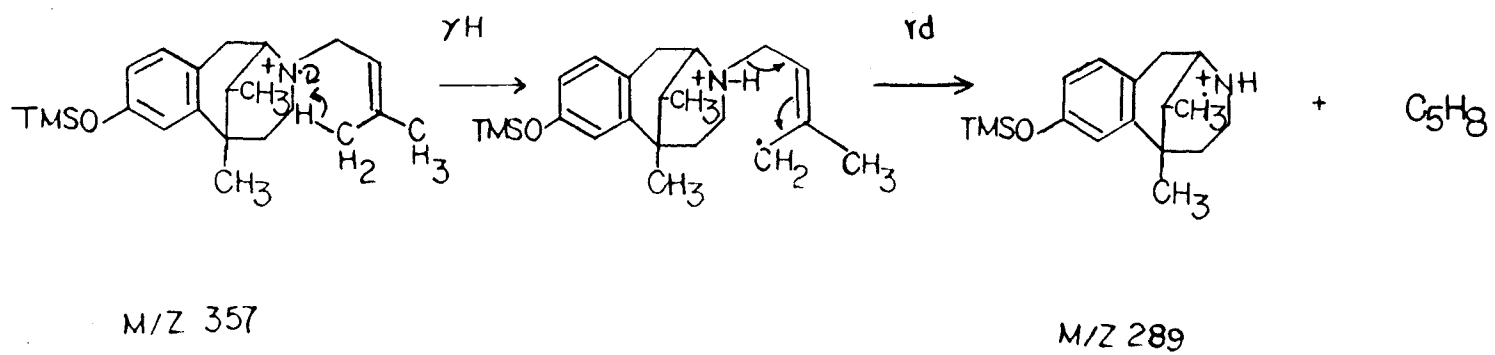


Figure IV.4 Fragmentation Pathway I.

spectral information can be used to distinguish between possible stereoisomers due to trans or cis attachment to the terminal carbons for the double bond.

However, a secondary cleavage reaction is possible for fragment  $m/z$  289, because of the strong tendency for electron pairing at the nitrogen radical site <sup>[36]</sup> remaining in fragment  $m/z$  289. Thus, the odd electron is donated to form a new bond to an atom adjacent to the nitrogen radical site, and accompanied by the bond cleavage of an  $\alpha$ -atom to the same nitrogen atom ( $\alpha$ -cleavage). This secondary fragmentation of the molecular ion  $m/z$  357 is shown in Fig. IV.5a.

After the secondary  $\alpha$ -cleavage reaction, the product ion still has an unpaired electron, which can initiate yet another hydrogen rearrangement ("consecutive" rearrangement <sup>[36]</sup>), accompanied by further secondary  $\alpha$ -cleavage fragmentations. Consequently, two secondary fragment ions are formed. As shown in Fig. IV.5b (Pathway II), one characteristic fragment ion  $m/z$  110 appears in the pentazocine trimethylsilylated derivative mass spectrum as a secondary product of the molecular ion  $m/z$  357, formed by further losing the aromatic moiety from fragment  $m/z$  289. Fragment ion  $m/z$  274 accounts for another secondary product produced by further lose of a methyl group from fragment  $m/z$  289 described as Pathway III in Fig. IV.5c.

The positive charge site at the nitrogen atom can also initiate a cleavage reaction involving attraction of a pair of electrons from the adjacent bond <sup>[36]</sup>. As shown in Fig. IV.6 (Pathway IV), such inductive cleavage will result in losing an entire side-chain part of the pentazocine molecule with the positive charge transferred to the carbon atom bound to the nitrogen in the side-chain. As the result,

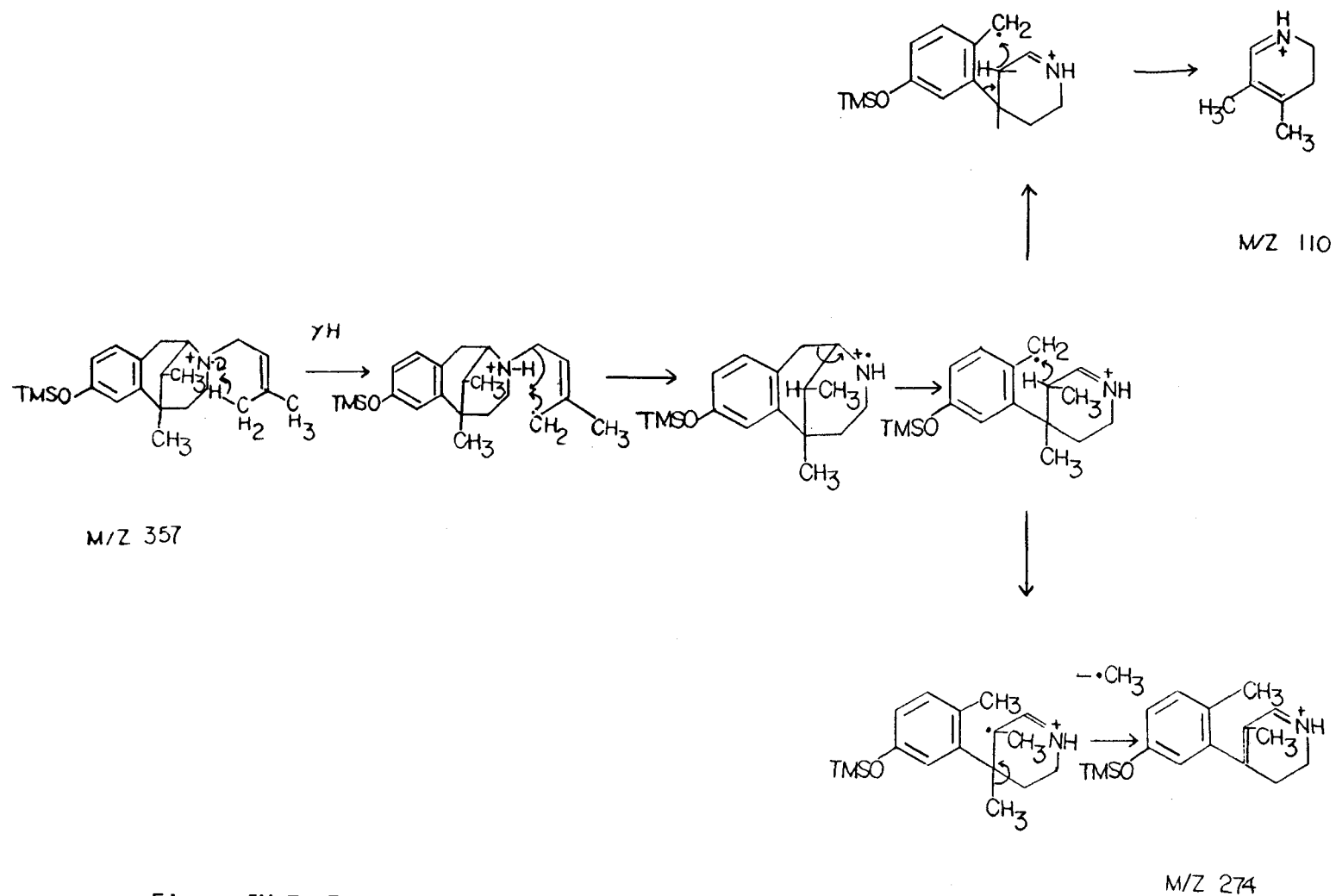


Figure IV.5 Fragmentations of (a) secondary cleavage of ion  $m/z$  357, (b) Pathway II, and (c) Pathway III.

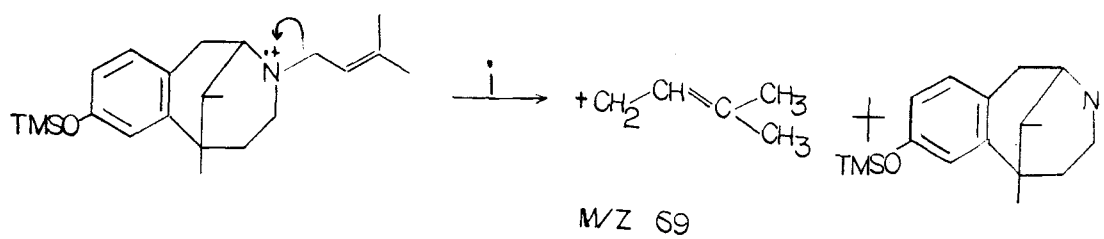


Figure IV.6 Fragmentation Pathway IV.

the characteristic ion peak at  $m/z$  69 is produced.

It is also conceivable that the same inductive cleavage can take place after the intramolecular hydrogen rearrangement described previously (Fig. IV.4). The ion peak at  $m/z$  68 should be produced by this fragmentation as shown in Fig. IV.7 (Pathway V).

It is obvious that the inductive cleavage in Pathway V is competing with the  $\alpha$ -cleavage initiated by the radical site resulting from the hydrogen rearrangement in Pathways I and IV. The fate of fragmentation Pathway V is thus dependant upon whether there is a favorable site to loose a hydrogen for the rearrangement, and the stability of the product ion which contains a radical site (unpaired electron). That is, if the product ion of Pathway V can stabilize the radical site, for example, by resonance-stabilization, then the characteristic ion peak resulting from Pathway V should appear; otherwise Pathway V would be unfavorable, and the characteristic ion produced by Pathway IV (which has one unit of  $m/z$  more than that of Pathway V product ion) may appear with a higher relative abundance. In the case of pentazocine, the fact that the relative abundance of the peak at  $m/z$  69 is higher than that of  $m/z$  68 (67% vs. 16% to the base peak) indicates that fragmentation Pathway IV is favored.

Ion peaks produced by Pathway IV or V are very good indications of changes on the side-chain structure, because their product ions involve only the side-chain. That is, a higher relative abundance of the characteristic ion produced by Pathway V should be the indication of a favorable fragmentation reaction, which should contain a favorable site to loose a hydrogen for the rearrangement, for example, containing a electronegative atom such as oxygen, or result in a stabilized product

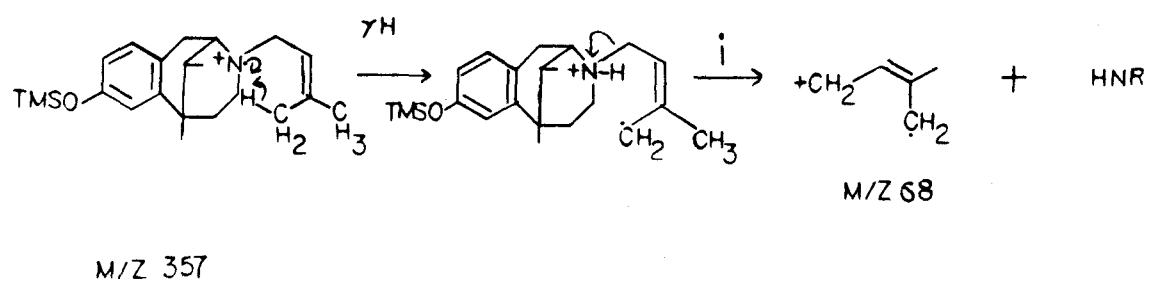


Figure IV.7 Fragmentation Pathway V.

structure with a unpaired electron.

It is also possible that upon electron impact, the radical and charge site occurs at the aromatic ring, which loses a  $\pi$ -electron due to its relatively low ionization energy<sup>[34]</sup>. This radical site would then initiate a series of fragmentations through an intermediate ion<sup>[37]</sup>. A group of characteristic ion peaks at  $m/z$  244, 245 and 246 are the products of such reactions referred to as Pathway VI in Fig. IV.8. As shown at the far left of Fig. IV.8, an  $\alpha$ -cleavage initiated by the radical-site at the aromatic ring takes place first in Pathway VI, which forms an intermediate with the radical site moved to the methylene group near the nitrogen atom. The stabilization of the radical site in this intermediate then drives the secondary fragmentation, which involves radical site rearrangement accompanied by a bond cleavage at the nitrogen atom. As the result, a nitrogen-containing fragment is lost from the intermediate because of the larger electronegativity of the nitrogen atom. Thus, a three-bond cleavage in the intermediate ion will result in losing a neutral fragment II with the radical-site relocated at the aromatic ring (Fig. IV.8a), and the ion  $m/z$  244 will be formed. The ion peak  $m/z$  245 is produced by an ion formed by a double-bond cleavage in the intermediate ion accompanied by losing fragment III (Fig. IV.8b), which is a resonance-stabilized radical product. The ion peak at  $m/z$  246 is from an ion formed by single-bond cleavage in the intermediate ion to lose a neutral fragment IV (Fig. IV.8c), and as a product, the ion  $m/z$  246 itself is a resonance-stabilized

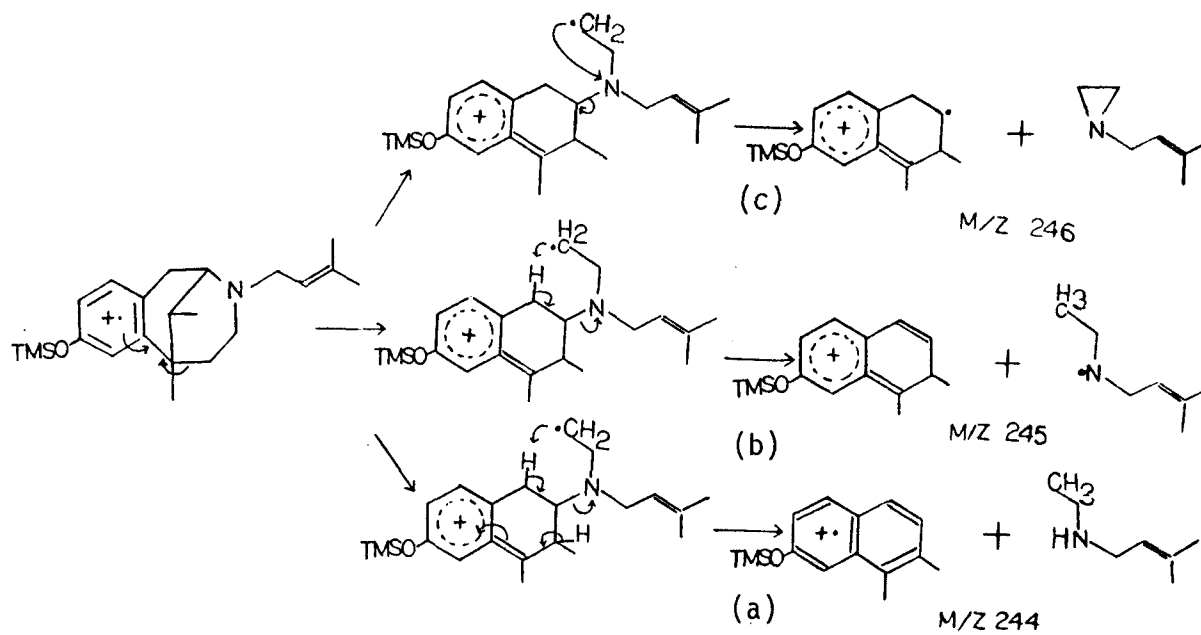


Figure IV.8 Fragmentation Pathway VI: (a) producing ion  $m/z$  244, (b) producing ion  $m/z$  245 and (c) producing ion  $m/z$  246.

radical <sup>1</sup>.

For the purpose of structure elucidation, the characteristic fragment ions in pentazocine trimethylsilylated derivative mass spectrum are put into three classes. As shown in Fig. IV.1, if the pentazocine structure is described as consisting of three parts, substructures A, B and C, then ion peaks at m/z 298 would contain substructures A and B. The characteristic ion peak at m/z 274 represents substructure A and B without a methyl group originally attached to the edge of substructure B. Characteristic ion peak at m/z 110 contains mostly substructure B except for a methylene group (next to substructure A). Characteristic ion peaks at m/z 69 and 68 indicate the existence of substructure C. Finally, the unique appearance of the ion peak groups at m/z 244, 245 and 246 come from substructure A plus half of the substructure B with the nitrogen atom. Thus, the characteristic ion peaks described cover the entire pentazocine molecular structure. Table IV.1 summarizes the fragmentation pathways, their corresponding product ions and the structural implications.

The difficulties of structural characterization of drug metabolites can be greatly reduced by the fact that most of metabolites usually retain a large portion of the structure of their parent drug with additional small functional groups attached. This has been found to be

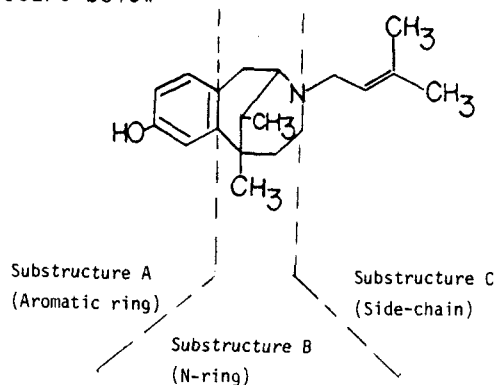
---

<sup>1</sup>As noted for the Pathway V proposed, an important driving force for such reaction is stabilization of the radical site. Hence, the ion m/z 244, whose radical and charge site is located in a stable aromatic ring system, and a stable neutral product fragment II make the particular ion production most favorable. Likewise, the resonance-stabilized radical ion m/z 246 with an unstable fragment IV make this fragmentation reaction least favorable. This also explains the fact that the relative abundance of m/z 244 > 245 > 246.

Table IV.1. Important Mass Spectral Fragment Ions (m/z) and the Structural Implications for the Trimethylsilylated Derivative of Pentazocine \*.

Fragmentation Pathway **	Characteristic Mass Fragments	Structural Implication
M+	357	Molecular Ion
V	69	Substructure C
IV	68	Substructure C - H (H rearrangement)
II	110	Substructure B - CH <sub>2</sub>
VI	244-6	Substructure A + B - C <sub>7</sub> H <sub>13-15</sub> N
III	274	Substructure A + B - CH <sub>3</sub>
I	289	Substructure A + B
TMS	73	TMS Derivative

\* Referring to structure below



\*\* Referring to the fragmentation Pathway responsible for the corresponding fragment ion (see text for details).

the case in the pentazocine metabolism.[6,7,8,9] In GC/MS analysis, such a small functional group attached to a large molecule will only change the mass spectrum of the parent compound by merely increasing the mass of the specific ion fragments which contain this functional group, without changing the relative abundances of these ions to a great extent<sup>[38]</sup> unless this functional group makes the fragmentation pathway more or less favorable or changes the stabilities of the products. Therefore, by tracing the characteristic fragments in a metabolite mass spectrum, one can discover the nature and locations of the additional substituents added to the pentazocine molecular structure. For example, a common feature of the mass spectra of all metabolites is the presence of a characteristic ion peak produced by Pathway I either at  $m/z$  289 or at  $m/z$  319, which indicates that metabolites in greyhound urine may be divided into two categories despite their differences in substructure C in Fig. IV.1. That is, there are those metabolites with a 30 a.m.u. substituent added to either substructure A or B, and those that have the same substructure A and B as the pentazocine structure.

Identification of urinary metabolites. The metabolites were identified with the normalized and background-subtracted mass spectra of their trimethylsilylated derivatives.

The gas chromatographic retention times of the trimethylsilylated derivatives of the metabolites are listed in Table IV.2. The characteristic fragment ions observed in the mass spectra are summarized in Table IV.3, and the relative abundances of the corresponding characteristic ions are shown in Table IV.4.

Fig. IV.9 shows the mass spectrum of the trimethylsilylated

Table IV.2 GC Relative Retention Time<sup>2</sup> of the Trimethylsilylated Derivatives of Petazocine Metabolites.

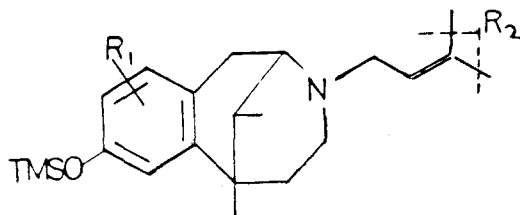
Metabolites	Relative Retention Time
PENT	1.00
MET1	1.06
MET2	1.07
MET3	1.15
MET4	1.19
MET5	1.23
MET6	1.28
MET7 <sup>3</sup>	1.28
MET8	1.40
MET9	1.41

-----  
<sup>2</sup>Retention times of the trimethylsilylated derivatives of the metabolites are relative to the retention time of a trimethylsilylated derivative of pentazocine standard (29.53 min. on DB-5 column).

Table IV.3. Important Fragment Ions (m/z).

Cmpd.	Substituent *		Fragmentation Pathway **										
	R <sub>1</sub>	R <sub>2</sub>	M+	V	IV	II	VI	III	I	IX	VIII	VII	TMS
PENT	H	CH <sub>3</sub>	357	68	69	110	244-6	274	289				73
MET1	OCH <sub>3</sub>	CH <sub>3</sub>	387	68	69	110	274-6	304	319				73
MET2	OCH <sub>3</sub>	CH <sub>3</sub>	387	68	69	110	274-6	304	319				73
MET3	H	-CH <sub>2</sub> OTMS	445	156		110	244-6	274	289			342	73
MET4	H	-CH <sub>2</sub> OTMS	445		157	110	244-6	274	289			342	73
MET5	OCH <sub>3</sub>	-CH <sub>2</sub> OTMS	475	156		110	274-6	304	319			372	73
MET6	OCH <sub>3</sub>	-CH <sub>2</sub> OTMS	475		157	110	274-6	304	319			372	73
MET7	H	-COOTMS	459		171	110	244-6	274	289	314	342	370	73
MET8	OCH <sub>3</sub>	-COOTMS	489		171	110	274-6	304	319	344	372	400	73
MET9	OCH <sub>3</sub>	-COOTMS	489		171	110	274-6	304	319	344	372	400	73

\* Referring to structure below



\*\* Referring to the fragmentation Pathway responsible for the corresponding fragment ion (see text for details).

Table IV.4. Percent Abundances of Important Fragment Ion Peaks Relative to the Base Peak.

Cmpd.	Substituent *		Fragmentation Pathway **										
	R1	R2	M+	V	IV	II	VI	III	I	IX	VIII	VII	TMS
PENT	H	CH3	22	17	75	26	33,32,27	24	55				100
MET1	OCH3	CH3	26	16	67	27	33,35,27	21	100				69
MET2	OCH3	CH3	29	15	63	24	44,42,31	20	100				72
MET3	H	-CH2OTMS	02	39		10	18,17,14	10	26			11	100
MET4	H	-CH2OTMS	05		07	07	14,15,11	07	28			12	100
MET5	OCH3	-CH2OTMS	02	08		13	28,25,18	14	73			09	100
MET6	OCH3	-CH2OTMS	05		08	09	15,16,12	07	55			10	100
MET7	H	-COOTMS	08		07	08	17,17,13	06	22	17	12	03	100
MET8	OCH3	-COOTMS	10		12	11	19,27,16	07	43	14	13	03	100
MET9	OCH3	-COOTMS	10		12	09	23,26,17	05	38	16	10	03	100

\* Referring to the picture attached to Table IV.3.

\*\* Referring to the fragmentation Pathway responsible for the corresponding fragment ion (see text for detail).

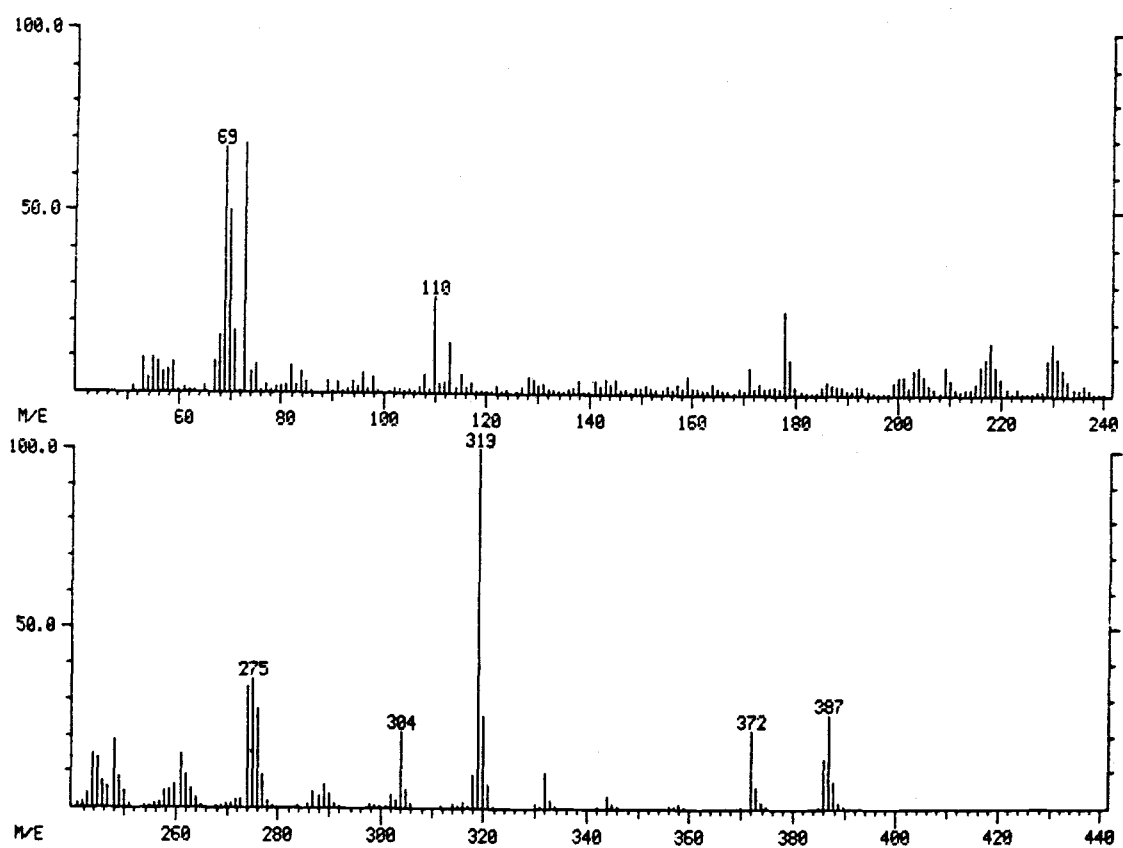


Figure IV.9 Mass spectrum of pentazocine metabolite MET1 trimethylsilylated derivative.

derivative of a metabolite which will be called MET1. The molecular ion peak is at  $m/z$  387, which shows a 30 a.m.u increase comparing to that of the pentazocine trimethylsilylated derivative. Other characteristic ions at  $m/z$  319, 304 and a group of ions at  $m/z$  274, 275, 276 also indicate the same 30 a.m.u increment in each fragment.

A characteristic ion appears at  $m/z$  304, which has a relative abundance of 21% of the base peak. Comparing this with that of the pentazocine trimethylsilylated derivative mass spectrum, it is believed that the ion at  $m/z$  304 should be formed by Pathway III as shown in Fig. IV.5c. Hence, the 30 a.m.u increment, which is equivalent to a methoxy group, should be attached to either substructure A or B as shown in Table IV.1.

An unique appearance of a group of ions at  $m/z$  274, 275, 276 and their relative abundances ( 33% 35% 17% to the base ion peak) suggests that they could be formed by Pathway VI shown in Fig. IV.8. This observation further limits the location of the additional methoxy group to either substructure A or the part of substructure B as indicated in Table IV.1.

The existence of ion peaks at  $m/z$  110 and 69, which should be produced by Pathways II and IV, respectively, indicates that MET1 should have the same substructures B and C as those of pentazocine. Therefore, the structure of MET1 is concluded to be similar to that of pentazocine with an additional methoxy group added to the aromatic ring portion (substructure A).

Metabolite MET2 shows the same trimethylsilylated derivative mass spectrum as MET1 (Fig. IV. 10), but has a different GC retention time (Table IV.2). Fig. IV.11 shows the GC/MS chromatogram of the injection

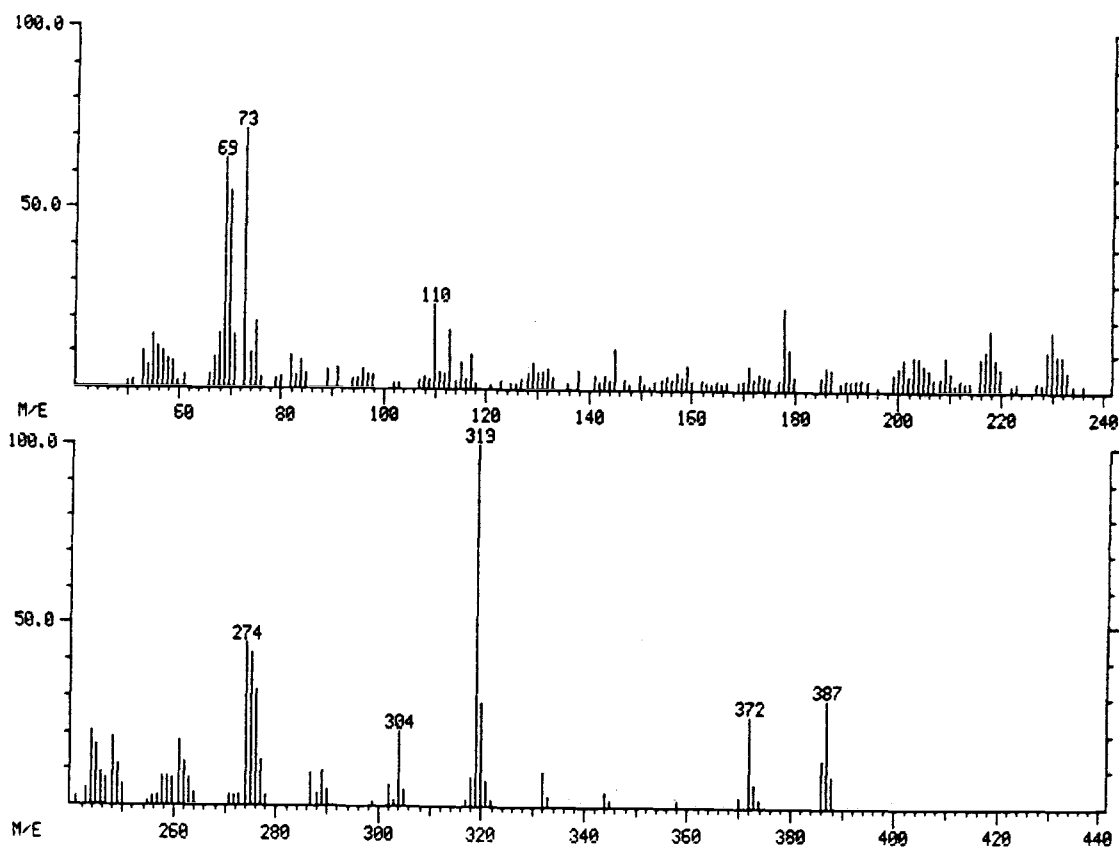


Figure IV.10 Mass spectrum of pentazocine metabolite MET2 trimethylsilylated derivative.

of a mixture of MET1 and MET2. Structures of MET1 and MET2 are shown in Fig. IV.12.

The molecular ion of the trimethylsilylated derivative of metabolite MET3 is at  $m/z$  445. The existence of ion peaks at  $m/z$  110, 244-6, 274, 289 in its mass spectrum (Fig. IV.13) suggests that the structure of MET3 is the same as pentazocine except for substructure C. The absence is noted of ions at  $m/z$  69 and  $m/z$  68, which arise from the side-chain (substructure C) in pentazocine. Instead, a characteristic ion appears at  $m/z$  156 (relative abundance 39%), which could arise from the same Pathway V as the pentazocine ion at  $m/z$  68 (relative abundance 17% in the pentazocine trimethylsilylated derivative mass spectrum). Hence, the ion at  $m/z$  156 is probably responsible for the fragment from substructure C of MET3. An 89 a.m.u increment in ion  $m/z$  156 compared to that of  $m/z$  68 for pentazocine indicates that this additional functional group should be trimethylsilylated with a hydroxyl group.

Similar to the fragmentation described in Fig. IV.3, if there is an additional trimethylsilylated hydroxyl group attached to the end of the side-chain, an inductive cleavage fragmentation should be expected because of the positive charge site at the oxygen atom<sup>[36]</sup>. A characteristic ion peak at  $m/z$  342 appears in the MET3 trimethylsilylated derivative mass spectrum as expected by such a fragmentation (Fig. IV.14, Pathway VII). This information further confirms the proposed hydroxylated metabolite structure.

The fact that ion peak at  $m/z$  156 has a much higher relative

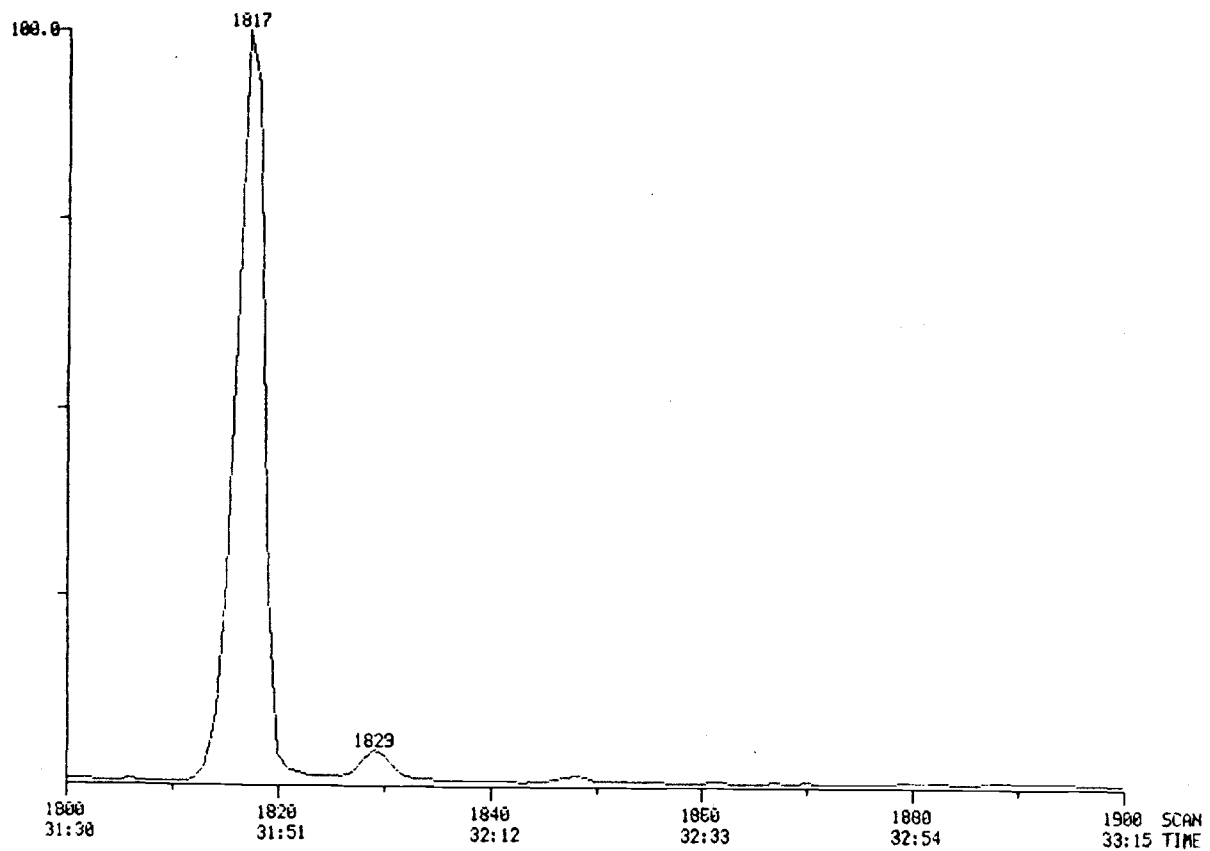


Figure IV.11 GC/MS chromatogram of pentazocine metabolites (a) MET1 and (b) MET2.

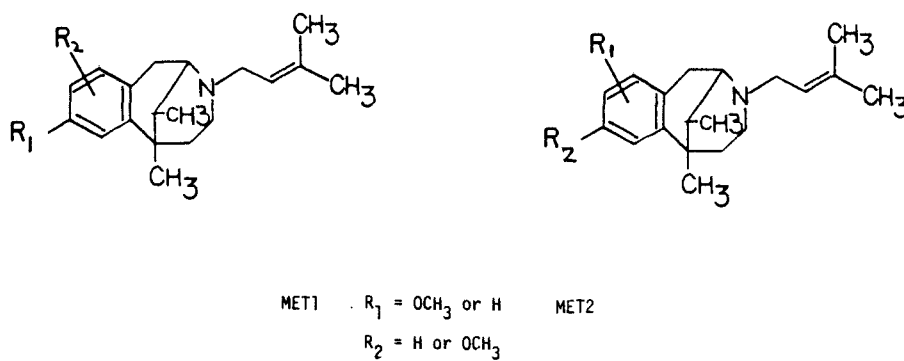


Figure IV.12 Structures of pentazocine metabolites MET1 and MET2.

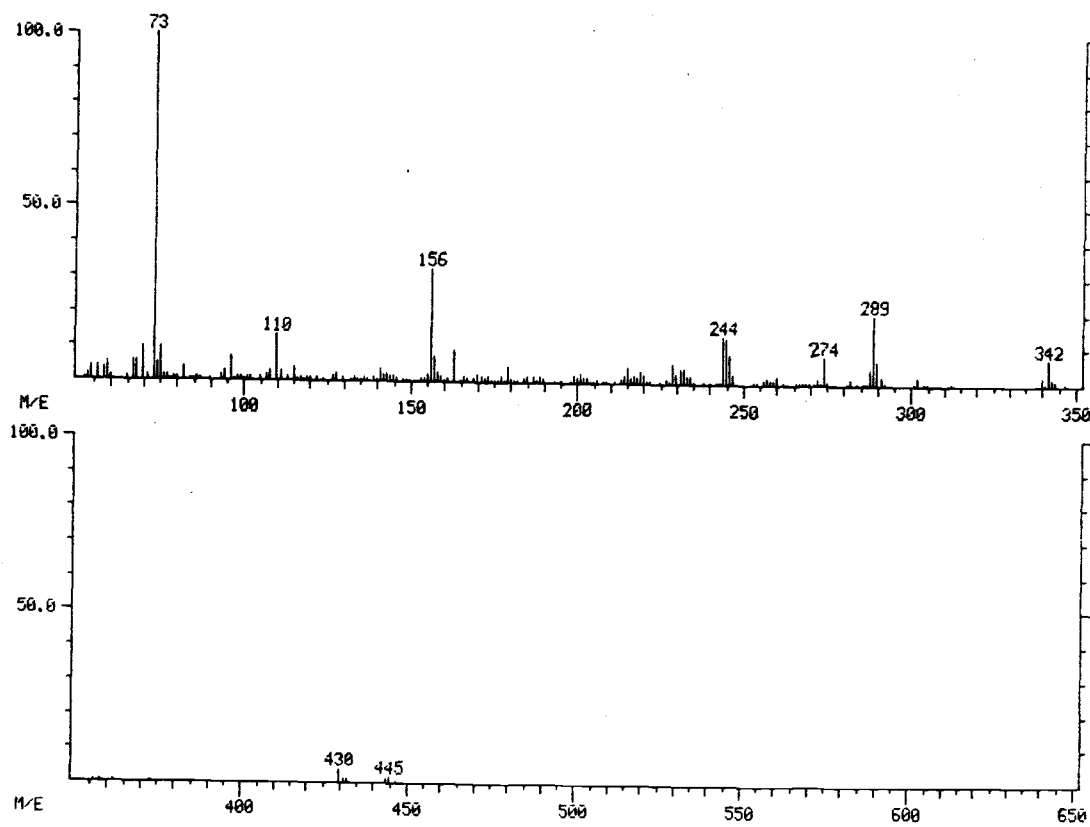


Figure IV.13 Mass spectrum of pentazocine metabolite MET3 trimethylsilylated derivative.

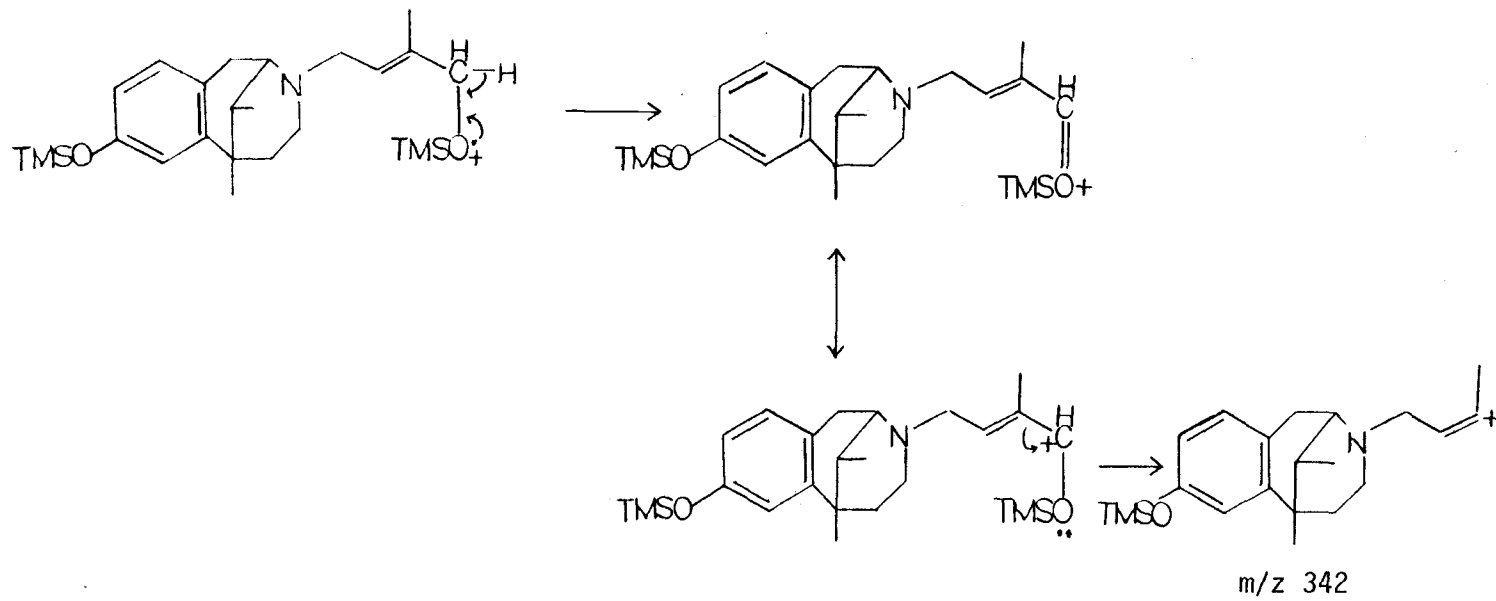


Figure IV.14 Fragmentation Pathway VII.

abundance than that of  $m/z$  157 (39% vs. 8%) indicates a favorable fragmentation reaction Pathway V over Pathway IV. That is, a hydrogen from the carbon cis position to the double bond is favored for the intramolecular hydrogen rearrangement before the charge inductive cleavage (Fig. IV.7, Pathway V). This characteristic ion indicates that the additional hydroxyl group should be attached to the cis carbon at the end of the double bond, which would therefore stabilize the new radical site resulting from losing the hydrogen for the rearrangement. [39,40,41] It is concluded that MET3 is a metabolite of pentazocine due to the oxidation of its side chain (substructure C) to a cis-alcohol.

Metabolite MET4 shows a similar trimethylsilylated derivative mass spectrum (Fig. IV.15) as MET3, except that the characteristic ion peak at  $m/z$  157 has a higher relative abundance than that of  $m/z$  156, and it has a different GC retention time. Since, in this case, fragmentation reaction Pathway IV, which produces the ion at  $m/z$  157, appears to be a bit more favored, like for pentazocine itself, there should be no change in the methyl group cis to the double bond. Therefore it appears that MET4 is an isomer of MET3 with the hydroxyl group attached in the trans position to the double bond. Structures of MET3 and MET4 are shown in Fig. IV.16.

The mass spectrum of the trimethylsilylated derivative of MET5 (Fig. IV.17) shows a molecular ion at  $m/z$  475. Similar to the mass spectrum of MET1, it shows characteristic ion peaks at  $m/z$  319, 304, 110 and a group of ions at  $m/z$  274, 275 and 276. According to proposed fragmentation Pathways I, II, III and VI, these product ions are an indication of a methoxy group added to the aromatic ring portion of

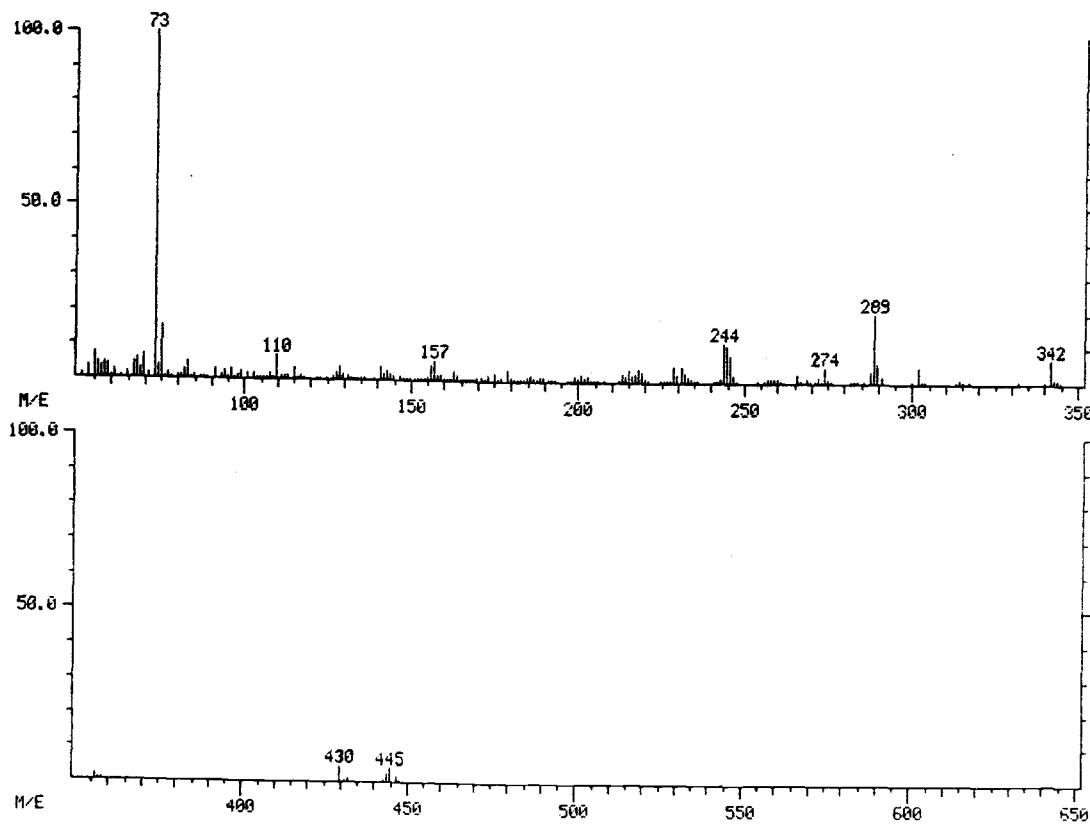
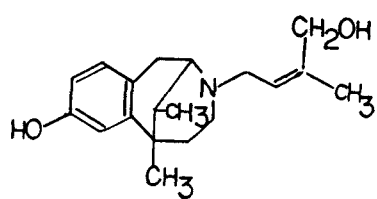
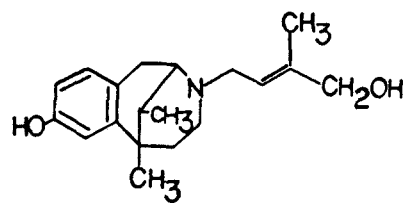


Figure IV.15 Mass spectrum of pentazocine metabolite MET4 trimethylsilylated derivative.



MET3 (cis-OH)



MET4 (trans-OH)

Figure IV.16 Structures of pentazocine metabolites MET3 and MET4.

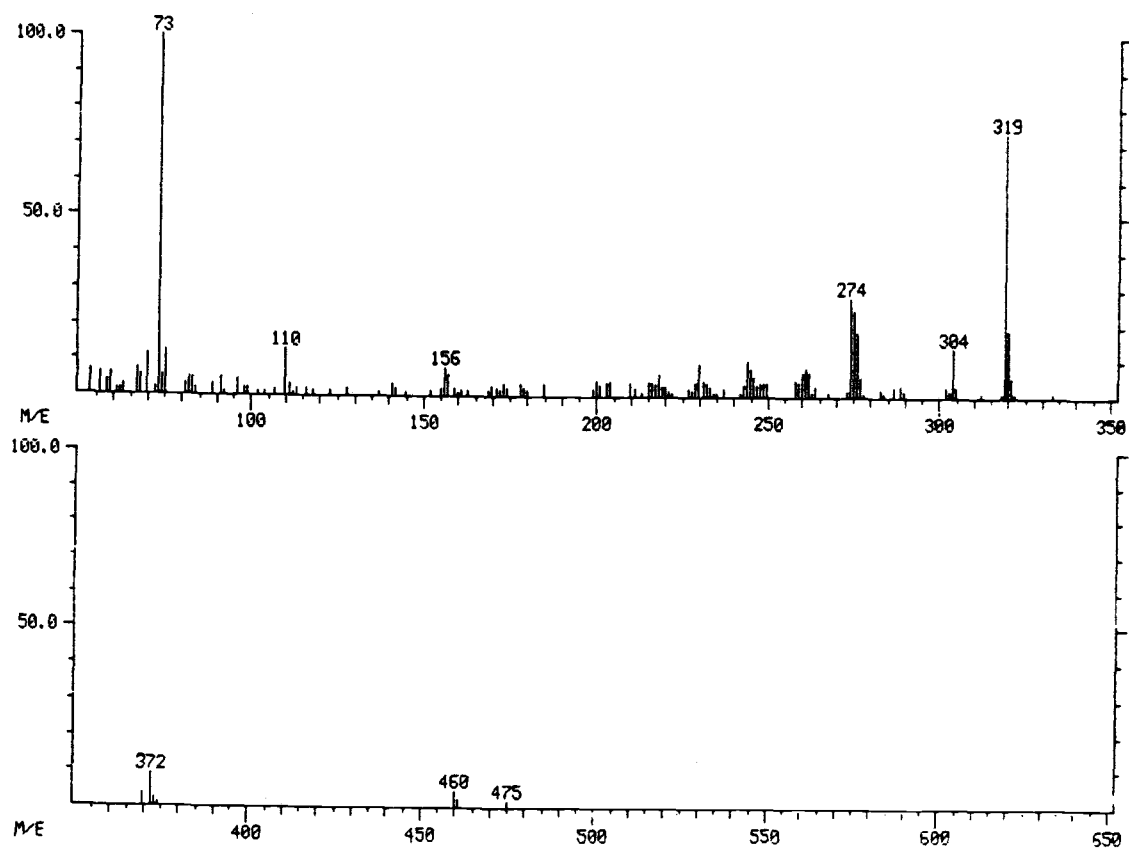


Figure IV.17 Mass spectrum of pentazocine metabolite MET5 trimethylsilylated derivative.

pentazocine as discussed earlier in the MET1 section. The absence of ions at  $m/z$  69, 68, and the appearance of characteristic ions at  $m/z$  372 and 156 suggest the existence of a trimethylsilylated alcohol attached to the cis position of the double bond of the side-chain, as in MET4. It is therefore concluded that MET5 is a secondary metabolite of pentazocine, resulting from the oxidation of the side-chain of MET1 to an alcohol cis to the double bond at the end of the side-chain.

MET6 shows a mass spectrum similar to MET5 (Fig. IV.18), except that the characteristic ion at  $m/z$  157 shows a higher relative abundance than that of  $m/z$  156, and it also has a different GC retention time. Evidently, MET6 is an isomer of MET5, with a hydroxyl group attached to the trans position to the double bond. The structures of MET5 and MET6 are shown in Fig. IV.19.

For MET7, characteristic ion peaks are shown at  $m/z$  110, 244, 245, 246 and 289 in Fig. IV.20. This reveals that part of the MET7 structure should be the same as substructures A and B in pentazocine. The absence of an ion peak at  $m/z$  69 again suggests a different side-chain in MET7. The appearance of an additional characteristic ion peak at  $m/z$  171 (Pathway IV) as well as the molecular ion at  $m/z$  459 indicate that MET7 would most likely be a secondary derivative of MET3 produced by further oxidation of the side-chain to a carboxylic acid.

As a carboxylic acid derivative, the trimethylsilylated MET7 would contain a carbonyl oxygen, a saturated oxygen atom of ester, and both of these oxygen atoms can evolve as the site of a new charge and radical site upon the electron impact<sup>[36]</sup>. These charge or radical sites can then initiate a new series of fragmentations, and their product ions can be used as further indications of the existence of

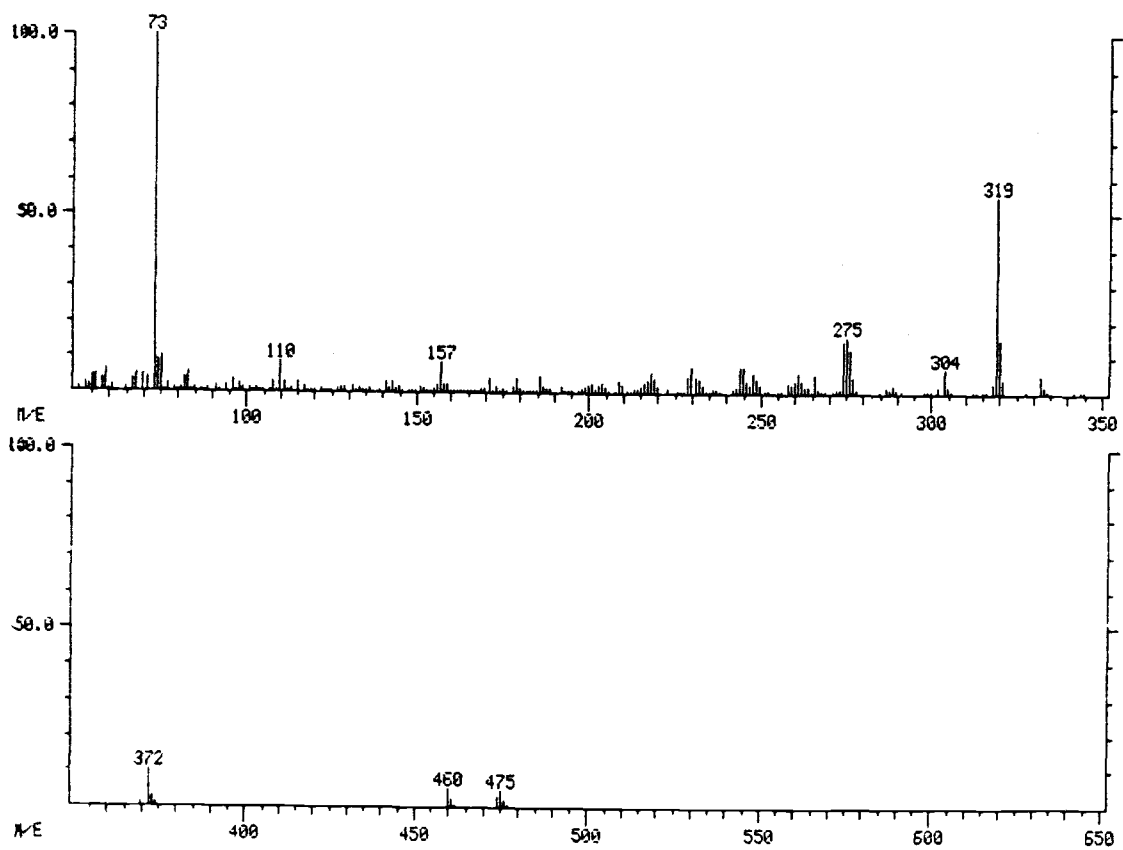
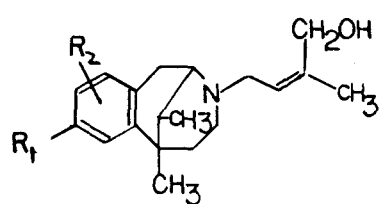
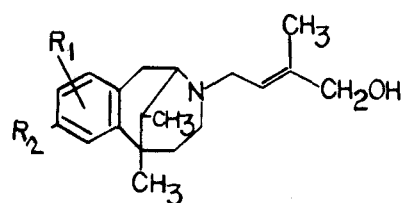


Figure IV.18 Mass spectrum of pentazocine metabolite MET6 trimethylsilylated derivative.



MET5

$R_1 = \text{OCH}_3$  or H  
 $R_2 = \text{H}$  or  $\text{OCH}_3$   
(cis-OH)



MET6

Figure IV.19 Structures of pentazocine metabolites MET5 and MET6.

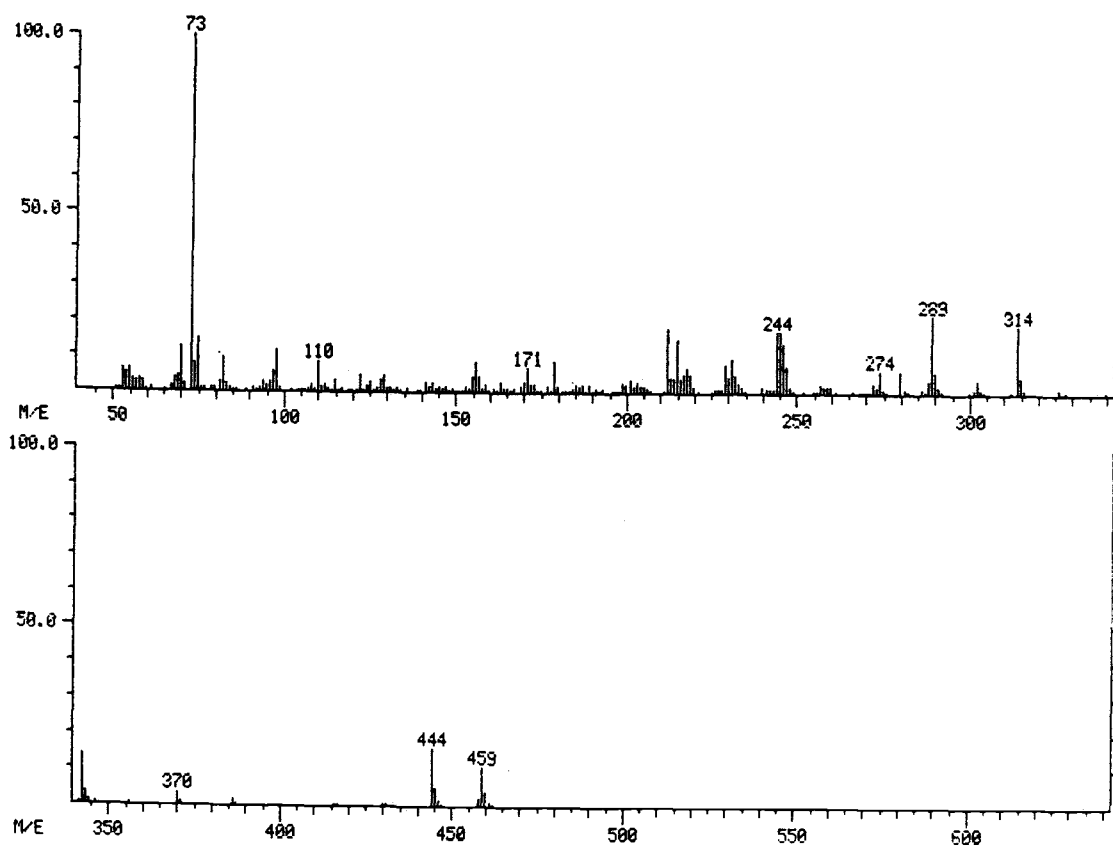


Figure IV.20 Mass spectrum of pentazocine metabolite MET7  
trimethylsilylated derivative.

carboxylic acid functional groups.

For example, the carbonyl group in MET7 can initiate an  $\alpha$ -cleavage<sup>[42]</sup>, producing a characteristic ion at  $m/z$  370 (Fig. IV.21), which has the same net result as the fragmentation Pathway VII shown in Fig. IV.14. The remained charge site in the ion at  $m/z$  370 can also initiate an inductive cleavage<sup>[42]</sup>, resulting in a secondary fragmentation Pathway VIII as shown in Fig. IV.22. The characteristic ion at  $m/z$  342 is thus produced by further loss of the carbonyl group.

As shown in Fig. IV.23, Pathway IX fragmentation involves a  $\gamma$ -hydrogen rearrangement<sup>[36]</sup> after which the resultant radical site causes the double bond to shift its position. Then an inductive cleavage takes place to produce an intermediate and another characteristic ion  $m/z$  at 314 as shown. Although this kind of fragmentation is generally unfavorable<sup>[36]</sup>, the existence of a double bond in the  $\beta$  position to the carbonyl group may promote this reaction.

In the MET7 trimethylsilylated derivative mass spectrum, the existence of a characteristic ion at  $m/z$  289 indicates an intramolecular hydrogen rearrangement (Pathway I, Fig. IV.4) involving the hydrogen attached to the carbon cis to the double bond at the end of the side-chain. Therefore the carboxylic group at the end of the side-chain must be attached to the trans position of the double bond, because otherwise there would be no hydrogens available for the intramolecular rearrangement within a six-membered-ring orientation to the nitrogen atom, and no ion peak at  $m/z$  289 produced by Pathway I. The structure of metabolite MET7 is therefore concluded to be a secondary metabolite produced by further oxidation of the pentazocine side-chain to a trans carboxylic acid (Fig. IV.24).

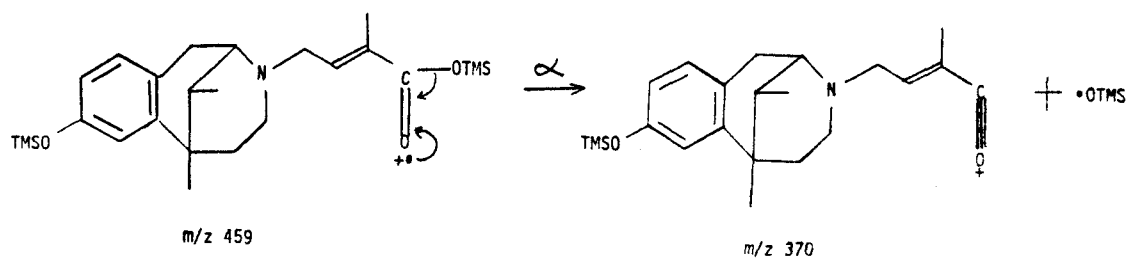


Figure IV.21 Fragmentation pathway producing ion  $m/z$  370 in pentazocine carboxylic acid metabolites.

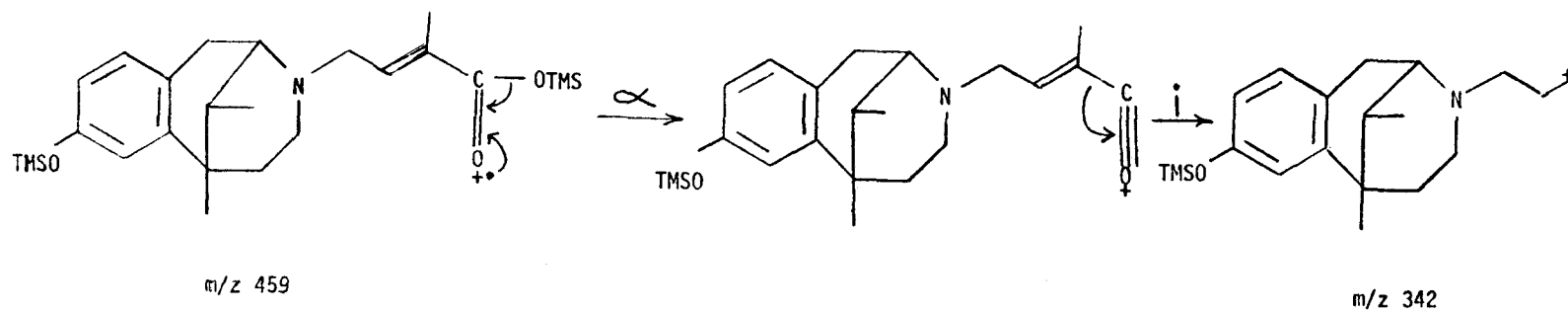


Figure IV.22 Fragmentation Pathway VIII.

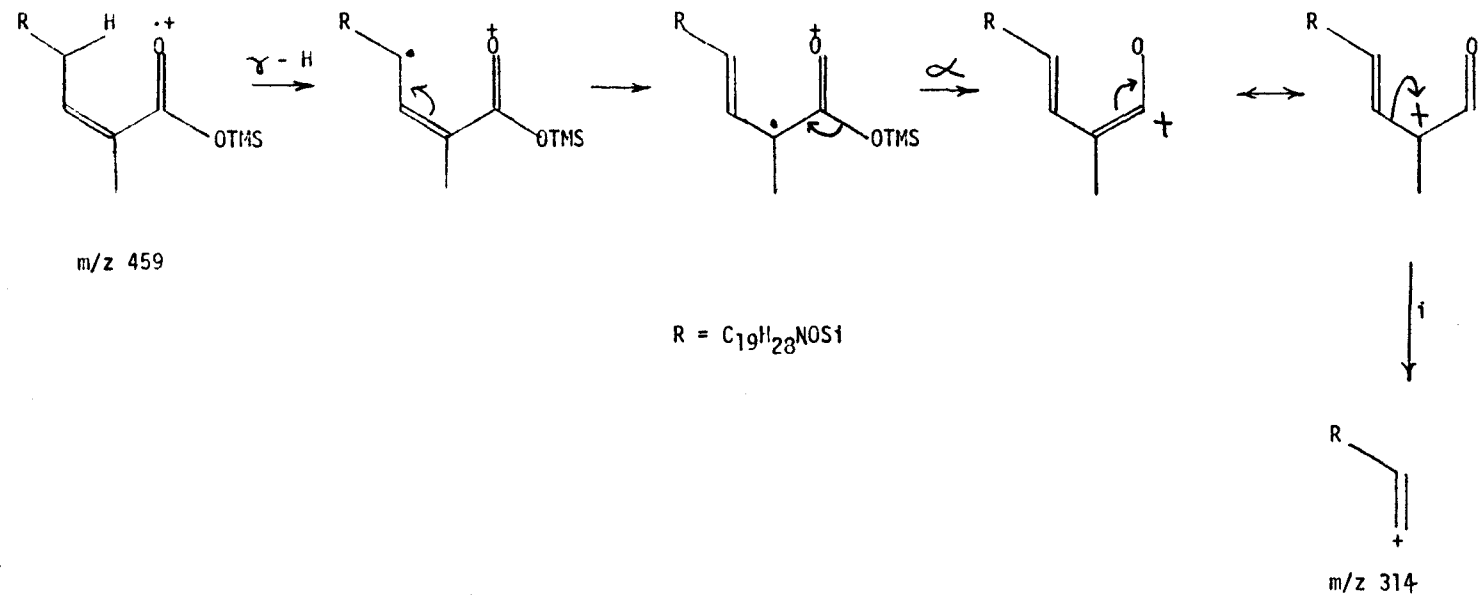
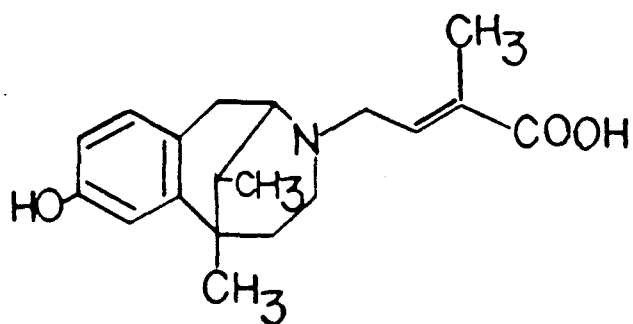


Figure IV.23 Fragmentation Pathway IX.



(trans acid)

Figure IV.24 Structure of pentazocine metabolite MET7.

The mass spectrum of the metabolite MET8 trimethylsilylated derivative is shown in Fig. IV.25. The molecular ion of MET8 is at  $m/z$  389, which has a 30 a.m.u. increment above that of MET7. The characteristic ions of MET8 at  $m/z$  319, 304, 110, 274 275 and 276 resemble those of MET1, MET2, MET5 and MET6, which indicates that a methoxy group is added to the aromatic ring portion of the structure. The ions at  $m/z$  400, 372 and 344 show the distinct character of a carboxylic acid side-chain structure produced by fragmentation Pathways VII, VIII and IX. Again, the 30 a.m.u increment in these fragments compared to those of MET7 are due to the additional attachment of a methoxy group in the aromatic ring. Therefore, MET8 is concluded to be a metabolite of pentazocine caused by further oxidation of either MET5 or MET6 to a carboxylic acid.

Again, the appearance of  $m/z$  319, which is produced by fragmentation Pathway I, indicates that the carboxylic group has to attach to the trans position of the double bond as in MET7.

Metabolite MET9 shows the same trimethylsilylated derivative mass spectrum as MET8 (Fig. IV. 26), but a different GC retention time. It also shows a characteristic ion peak at  $m/z$  319 caused by an ion produced by Pathway I. Therefore MET9 appears to be an isomer of MET8, where the isomerism is due to a different placement of the methoxy group on the aromatic ring. The structures of MET8 and MET9 are shown in Fig. IV.27.

#### 4. Conclusion

Oxidative pentazocine metabolism in the greyhound seems similar to

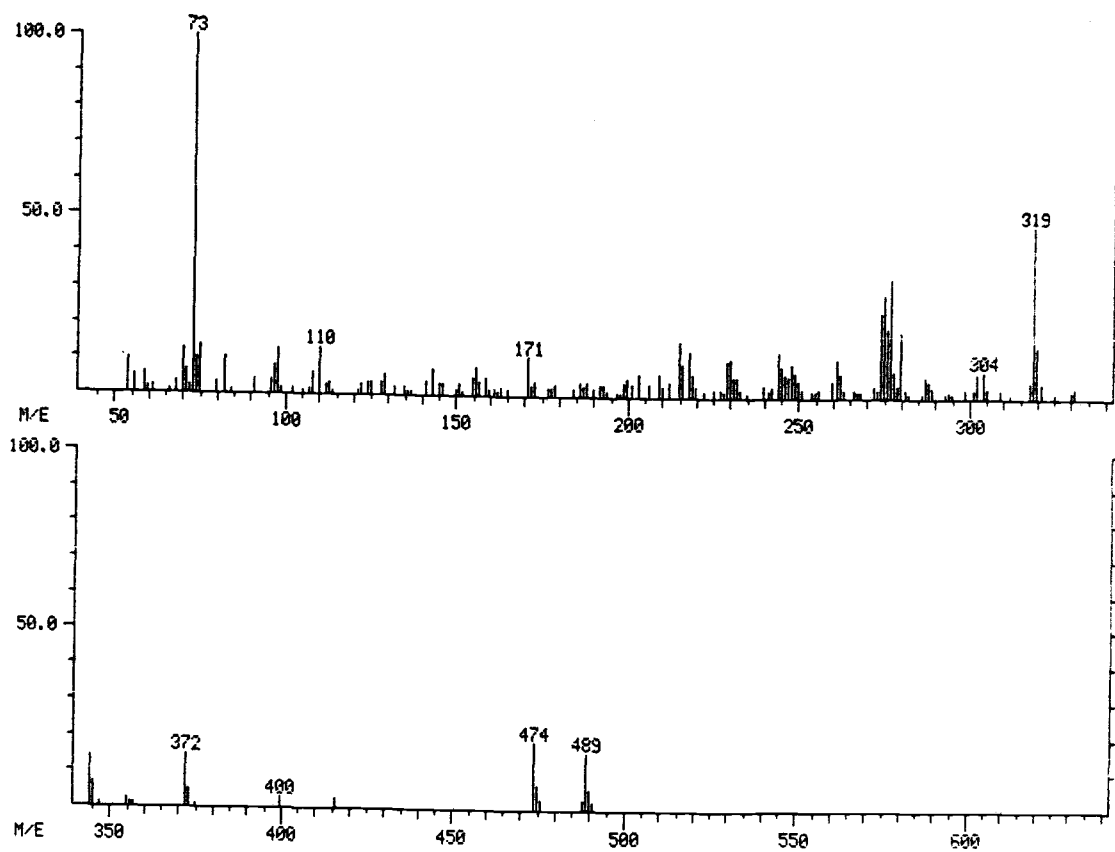


Figure IV.25 Mass spectrum of pentazocine metabolite MET8 trimethylsilylated derivative.

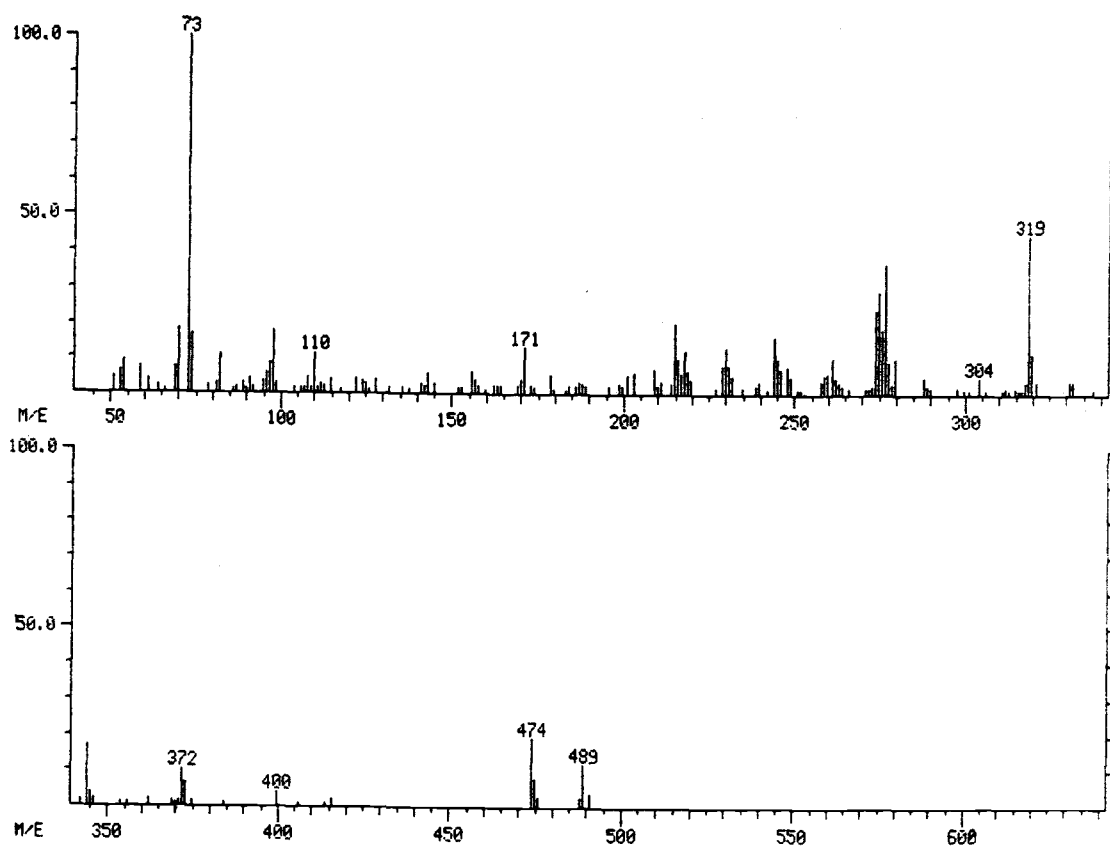
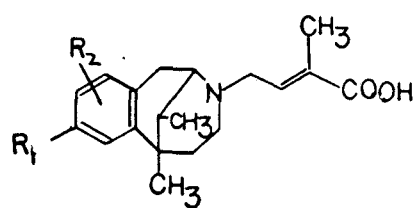
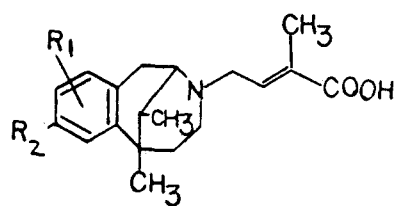


Figure IV.26 Mass spectrum of pentazocine metabolite MET9 trimethylsilylated derivative.



(trans acid)

MET8



(trans acid)

MET9

$R_1 = \text{OCH}_3 \text{ or } \text{H}$   
 $R_2 = \text{H or OCH}_3$

Figure IV.27 Structures of pentazocine metabolites MET8 and MET9.

that in monkey, mouse and rat [6,7,8,9]. In those species, pentazocine is partly converted into either an alcohol or a carboxylic acid at the end of the side-chain (Fig. 8). It was also reported that the metabolites produced by oxidation to an alcohol at the end of the side-chain were isomers due to trans and cis attachment of a hydroxyl group at the end of the side-chain, and there was no isomer for the carboxylic acid metabolite produced by further oxidation at such trans and cis attachments<sup>6,7,8,9</sup>. The finding of metabolites MET3, MET4 and MET7 in this greyhound urine study show the same results for this side-chain oxidation metabolism.

However, both the hydroxylation of pentazocine in the aromatic ring and the methylation of the phenolic group are observed in greyhound metabolism. That is, an aromatic carbon is hydroxylated, and then methylation changes one of the two hydroxyl groups attached to the aromatic ring to a methoxy group. As the result of this metabolism, another branch of pentazocine metabolites are formed: metabolites produced by oxidation and methylation of the aromatic ring only, MET1 and MET2. Then further oxidation of MET1 and MET2 at the end of the side-chain to an alcohol produces MET5 and MET6, and further oxidation of the alcohol group to carboxylic acid produces MET8 and MET9.

Although the GC/MS study has not shown the exact location of the methoxy group attached to the aromatic ring for the hydroxylated and methylated metabolites, a study of fragmentation has enabled the determination of the isomerism due to the trans and cis attachment of an additional function group to the end of the side-chain without further spectroscopic assistance. It is found that in greyhound urine, the carboxylic acid metabolites MET8 and MET9 are both trans acids, and

are isomers due to a different attachment of a methoxy group in the aromatic ring. This is in agreement with previous studies which indicated that only the trans acid would be produced by the oxidative metabolism on the side-chain. It is also noted that there is only one pair of cis/trans alcohol isomers, MET5 and MET6, found in the greyhound urine.

The relative gas chromatographic retention times (Table IV.2) of metabolite isomers MET1 and MET2 are found to be different by 0.01. Gas chromatographic relative retention time difference are also found to be 0.01 for isomers MET8 and MET9. This further supports the findings from the interpretation of the mass spectra that isomerism for both pairs are due to a different attachment of the methoxy group in the aromatic ring. GC retention time data (Table IV.2) also indicates that the isomerism for MET5 and MET6 is the same as MET3 and MET4, which are both due to cis and trans attachment of a hydroxyl group to the end of the side-chain.

This GC/MS study of pentazocine metabolites in greyhound urine has established a network of pentazocine metabolism. The key question remaining for the structural determination is the location of the methoxy group in the aromatic ring, which will be determined by NMR techniques and described later.

V. INTRODUCTION AND GENERAL THEORY OF TWO-DIMENSIONAL NMR

by

Guang Xiao

Department of Chemistry

Oregon State University

Corvallis, OR 97331

## 1. Introduction

In the GC/MS study discussed in the previous chapter, characteristic fragmentation pathways were applied to identify the positional isomers due to the cis- and trans- functional group attachment at the end of the dimethylallyl side chain of pentazocine metabolic isomers. However, the position of the methoxyl group in the aromatic ring in the metabolites produced by hydroxylation and methylation metabolism cannot be clarified, and the use of NMR techniques to facilitate accurate and complete structural characterization is necessary.

NMR study of a complex molecule is a formidable task, which can be further complicated if no synthetic reference is readily available. Through the years, due to the fast growing two-dimensional NMR techniques, it is now possible to characterize a molecular structure with little prior knowledge about its structure. In the field of drug metabolite analysis, the fact that the structure of the metabolites will retain some or most of the original substructure of the parent drug further reduces the inherent difficulty since the parent drug can be used as a reference for the metabolite analysis.

As part of this NMR study, a description of the theoretical and experimental aspects of high-resolution NMR in a simple conceptual fashion with illustrative data will prove beneficial, and this chapter is thus dedicated to this purpose. The intention herein is merely to assist the practicing chemist who has a real need but little experience

in the areas of two-dimensional (2D) and other multi-pulse NMR procedures, and to explore potentially useful experiments for the structural characterization of pentazocine metabolites and hence drug metabolite analysis in general.

## 2. $^1\text{H}$ and $^{13}\text{C}$ NMR Fundamentals

General theory and FT-NMR. Like other forms of spectroscopy, NMR studies the energy gaps between states of different energy. However, unlike most other forms of spectroscopy, the phenomenon requires the presence of an external magnetic field and concerns nuclei rather than electrons [43, 44].

Every proton has charge as well as spin, and hence behaves as if it were a small magnet. This magnetization is called the MICROSCOPIC MAGNETIZATION VECTOR,  $\mu$ . Once a group of nuclei such as protons is placed in a magnetic field,  $B_0$ , they will precess about the direction of this field with the LARMOR PRECESSION FREQUENCY,  $\omega_0$

$$\omega_0 = \gamma B_0$$

where  $\gamma$  is called the MAGNETOGYRIC RATIO and is a constant for all nuclei of a given isotope. Also, microscopic magnetization vectors will split into two states: those aligned with the magnetic field  $B_0$  are in the LOW ENERGY STATE, those aligned against the field are in the HIGH ENERGY STATE. When equilibrium exists, the population of the low energy state ( $N_-$ ) is greater than that of the high energy state.

( $N_+$ ) according to the Boltzmann equation.

$$N_+ / N_- = e^{-\partial E / kT}$$

where  $\partial E$  is the energy difference between states,  $k$  is the Boltzmann constant and  $T$  is the absolute temperature.

The NMR spectrometer basically consists of a magnet, an radio frequency (rf) transmitter, a receiver, and a recording system. An intense external magnetic field is applied to the sample, which results in the generation of two energy states for nuclei. The nuclei will also precess in a gyroscopic manner at the Larmor frequency. Transitions between these energy states are stimulated by the rf field from a wire coil positioned perpendicular to the magnetic field and connected to the rf transmitter, tuned to the Larmor frequency. Subsequent transitions between energy states produce rf signals which are received by an antenna coil positioned perpendicular to both the rf coil and the magnetic field.

When a molecule is placed in the external magnetic field, the nucleus in the molecule is shielded to a small extent by its electron cloud whose density varies with the environment. This variation alters the gap between the two energy states, and gives rise to a different frequency absorption by the nuclei. The shift in frequency in the NMR spectrum is usually described by the CHEMICAL SHIFT. Since there are several types of NMR spectrometers with different magnetic field strengths, it is helpful when the position of a resonance signal is given in units which are independent of the field of the magnet. The relative frequency shift  $\delta$  is used for this purpose and is defined as

$$\delta = (\nu_S - \nu_{\text{TMS}}) \times 10^6 / \nu_{\text{TMS}}$$

where  $\nu_S$  is the nuclei transition Larmor frequency, in Hz, and  $\nu_{\text{TMS}}$  is the resonance frequency, in Hz, of tetramethylsilane.

NMR spectra consist not only of individual lines, but also of groups of lines known as MULTIPLETS. The multiplet structure arises from interactions between nuclei which cause further splitting of nuclear energy levels, and hence several lines in place of the single line expected otherwise. This type of interaction is called SPIN-SPIN COUPLING, J COUPLING, or SCALAR COUPLING [45]. The J coupling phenomenon occurs because there is some tendency for a bonding electron to pair its spin with the spin of the nearest nucleus. The spin of a bonding electron having been thus influenced, the electron will affect the spin of another bonding electron and so on through to the next nucleus. In this way the spin direction of a proton on one carbon atom can influence the magnetic field experienced by a proton on an adjacent carbon atom. The J coupling information is carried by intervening bonding electrons through chemical bonds, not through space. (Possible exceptions have been suggested, especially with nuclei other than hydrogen, in which J coupling takes place not through bonding electrons but through space.)

The appearance of the multiplet is usually referred to as the SPLITTING PATTERN. Simple splitting patterns that are produced by the coupling of protons that have very different chemical shifts are called FIRST-ORDER splitting patterns [46]. These can usually be

interpreted by using two rules:

1. The multiplicity of a proton absorption split by surrounding coupling protons is  $n + 1$ , where  $n$  is the number of equivalent protons causing the coupling.

2. The relative intensities of the peaks of a multiplet may be obtained from "Pascal's Triangle" as shown in Fig. V.1.

The information from a first-order splitting pattern is one of the major aids to successful proton assignments.

As the complexity of a chemical system increases, chemical shifts for different coupling protons may become close to one another, and first-order rules may then no longer apply. The splitting pattern may now become unrecognizable, because nearly adjacent multiplets may coalesce to give fewer peaks than would be expected in a first-order situation, or the multiplets may appear to have more peaks caused by neighboring protons which have different chemical shifts. This phenomenon is illustrated in Fig. V.2, which is a downfield portion of a pentazocine proton NMR spectrum. Resonances k, l and m represent aromatic protons in the pentazocine structure. If the first-order splitting rules apply here, resonances k and m would couple to each other, which in turn would show as two doublets, and resonance l would be a singlet if it were not coupled with any other proton. But a closer examination shows that both resonances l and k are doublets, and resonance m is a quartet although it is only coupled with two other resonances k and l. That is, because of the complexity of this coupling system, the first-order coupling rules no longer apply in this case (e.g., instead of showing a triplet according to first-order coupling rules, resonance m is a quartet although it only coupled with

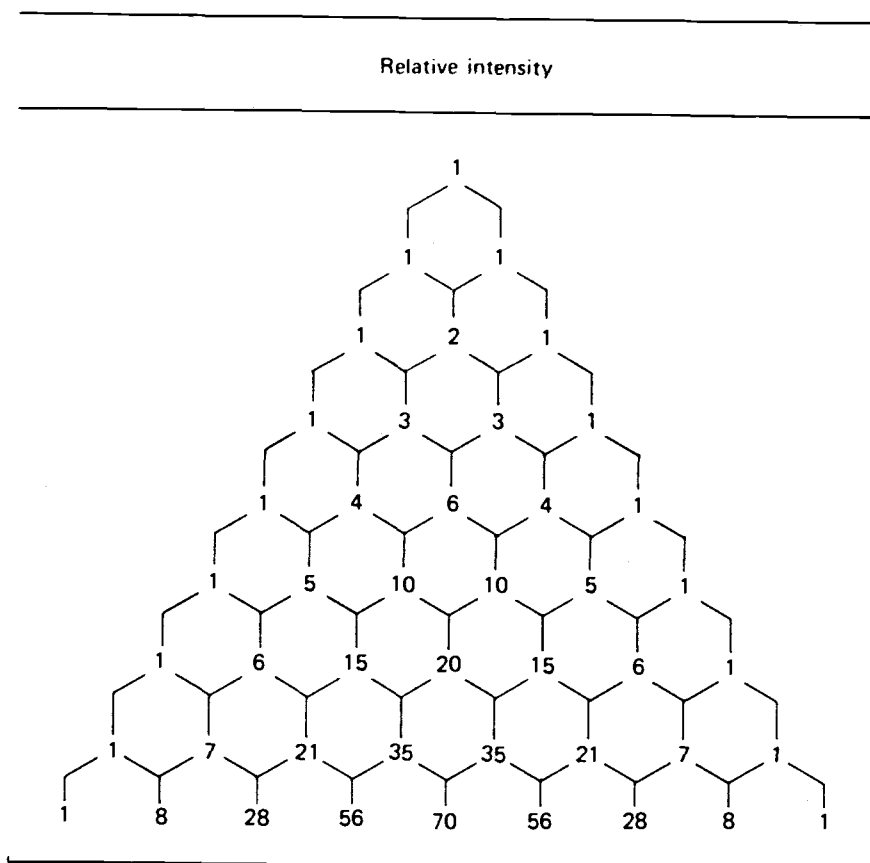


Figure V.1 Pascal's triangle for relative intensities of first-order multiplets (Adapted from reference [56]).

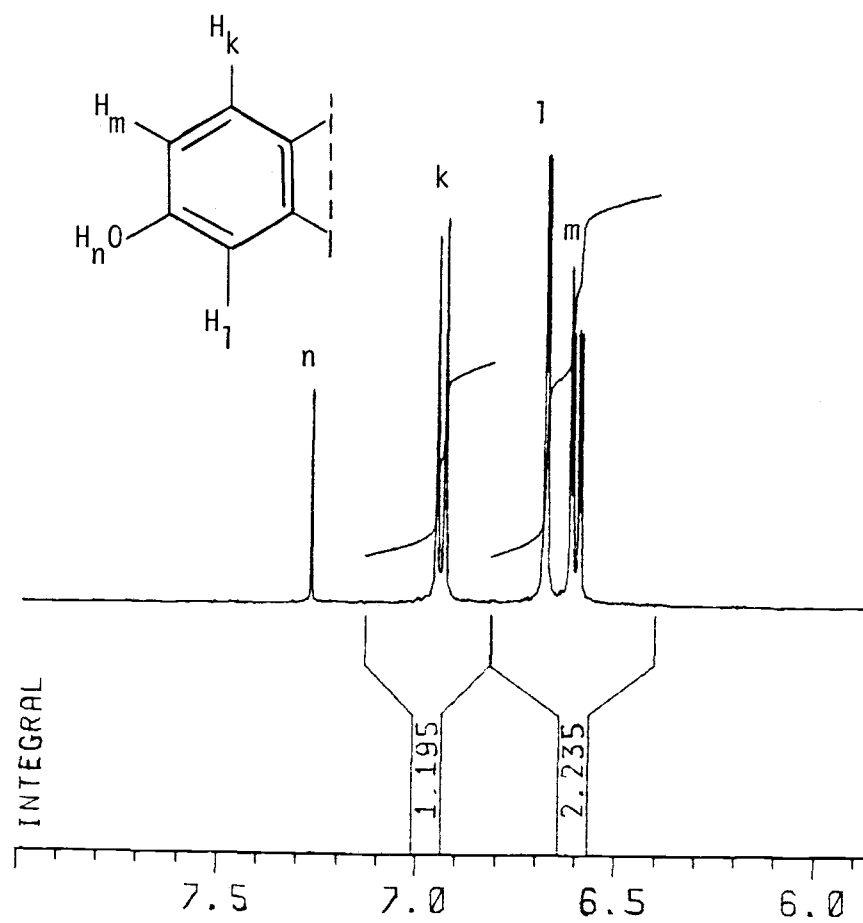


Figure V.2  $^1\text{H}$  NMR spectrum of aromatic protons in pentazocine.

two other protons). This example shows clearly that it would be very difficult and sometimes impossible to extract useful information from the splitting pattern other than a first-order one.

There is another kind of coupling phenomenon, known as DIPOLE-DIPOLE COUPLING, which is caused by an interaction between the magnetic dipole moments of two nuclei [47]. It can be described as the direct coupling of nuclei spins through space. Developed on the basis of this type of dipole-dipole interaction, the NOE technique (nuclear Overhauser effect) observes the intensity change of one nuclear resonance when the magnetization of a nearby nucleus is perturbed. For protons, a good approximation of the initial rate of intensity change observed for a nucleus when perturbed by the magnetization of another nucleus is given by:

$$\kappa = [ 34.2\tau_C / ( 1 + 4\omega^2\tau_C^2 ) - 5.7\tau_C ] * 10^{10}\gamma^{-6}$$

where  $\gamma$  is the distance between protons concerned,  $\omega$  is the angular proton resonance frequency, and  $\tau_C$  is the correlation time of the molecule (approximately the time it takes the molecule to tumble, on average, through an angle of 1 radian). This expression shows that the NOE buildup rate,  $\kappa$ , is proportional to  $\gamma^{-6}$ , and that measurement of  $\kappa$  directly determines the interproton distance,  $\gamma$ , if  $\tau_C$  is known. One can also use two protons at a known distance as an internal reference to determine  $\tau_C$ , if  $\tau_C$  is not known.

The nuclear Overhauser effect (NOE) has been known for a long time and has been used extensively. In the classical NOE experiment [47], the magnetization of one nucleus is perturbed selectively by

irradiation with a weak radio frequency (rf) field, and the changes in the intensities of other resonances in the spectrum are then monitored. Structure elucidation is aided because the response of dipole-dipole interactions is a function of the distance between dipoles, so that information on the spatial orientation of the nuclei might be extracted in favorable cases. It is worthwhile to note that confirmatory NOE evidence always leads to greater confidence in the spectral and conformational assignments, but the lack of an observable NOE response cannot be used as conclusive evidence for the absence of a certain spatial orientation.

There are two types of NMR spectrometers: continuous wave (CW) and pulsed Fourier transform (FT). In CW NMR, the rf oscillator frequency is normally kept constant and the magnetic field gradually changed. As the various values of the magnetic field at which transitions of different protons at that particular frequency occur are reached, absorption signals are observed. The disadvantage in this method is that at any one time there is only one field which is being observed. Thus, for complex molecules like pentazocine and its metabolites, CW NMR may take a very long time to scan, and perhaps give a largely unresolved spectrum, because the complicated nuclear environments in these molecules result in overlapped nuclear transitions and very complicated splitting patterns. To improve spectral resolution and the signal-to-noise ratio (S/N ratio), an unreasonably large amount of sample and experimental time would be required.

A totally different approach to NMR is called pulsed high resolution Fourier transform NMR (FT-NMR) [48], in which a strong pulse of energy containing the whole range of frequencies of interest

is applied while the magnetic field is kept constant. As a result, all nuclei are flipped to their upper state from which, over time (evolution time), they will return (decay) to the lower state. By collecting the resulting rf signal as a function of time, a complex pattern called the free-induced decay (FID) is obtained.

The FID signal is the result of so-called PHASE MODULATION of the NMR signal [49]: each precessing nuclear magnetization with different chemical shift and spin-coupling constants will generate different resonance frequencies in the magnetic field; thus, a compound with different nuclei will produce an interference pattern consisting of different resonance frequencies; these individual frequencies will get out of phase with each other after a certain evolution time, and this phenomenon (continuing change in phase) is referred to as phase modulation of the NMR signal.

After FID signals are obtained, a mathematical manipulation, the FOURIER TRANSFORM, is applied to convert FID information (time domain) into a spectrum virtually identical to a regular absorption spectrum (frequency domain). The idea of the Fourier transform is that any function,  $y = f(t)$ , can be represented as a sum of sinusoids of appropriate frequency, phase and amplitudes. Mathematically, this can be expressed by a series of the form

$$y = a_0/2 + \sum a_n \cos(\omega t) + \sum b_n \sin(\omega t)$$

which is known as a Fourier series. The appropriate phase shift of each sine wave is accounted for by including both a sine and cosine term for each frequency. In FT-NMR, FID information obtained is

represented by the function  $v = f(t)$ , where  $v$  is voltage and  $t$  is time. Because of the validity of the Fourier series, FID information consists of a sum of cosine and sine functions, each with its own amplitude ( $a_n$  and  $b_n$ ), and a constant ( $a_0/2$ ), as shown in Fig.

V.3a. Thus, the varying voltage can also be viewed as a sum of frequencies, each with its own amplitude, as shown in Fig. V.3b. This sum can then be expressed as another function,  $a = f(\omega)$ , where  $a$  is amplitude and  $\omega$  is frequency. The function  $a = f(\omega)$  is obtained from  $v = f(t)$  by applying the Fourier transform. Therefore, a frequency domain, regular absorption spectrum can be finally obtained, as shown in Fig. V.3c. This process may also be visualized as the reverse of phase modulation described above.

The most important advantage of FT spectroscopy concerns an increase in the signal-to-noise ratio (S/N) by means of TIME AVERAGING or TIME-DOMAIN FILTERING [50]. By taking advantage of a very basic and important difference between the spectral signal and noise, time averaging improves the sensitivity by increasing the signal-to-noise ratio, S/N. If the NMR scan measurement is repeated  $n$  times, by adding one noisy spectrum to another, the signal will increase in direct proportion to the number of scans,  $n$ , but the random noise will increase only as the square root of  $n$  [50]. Thus, the S/N after  $n$  scans is  $\sqrt{n}$  times better than the S/N obtained after one scan:

$$(S/N)_n = nS/\sqrt{n}N = \sqrt{n}S/N = \sqrt{n}(S/N)_1$$

It seems that to improve the signal-to-noise ratio by time averaging would be at the expense of the time required to obtain the

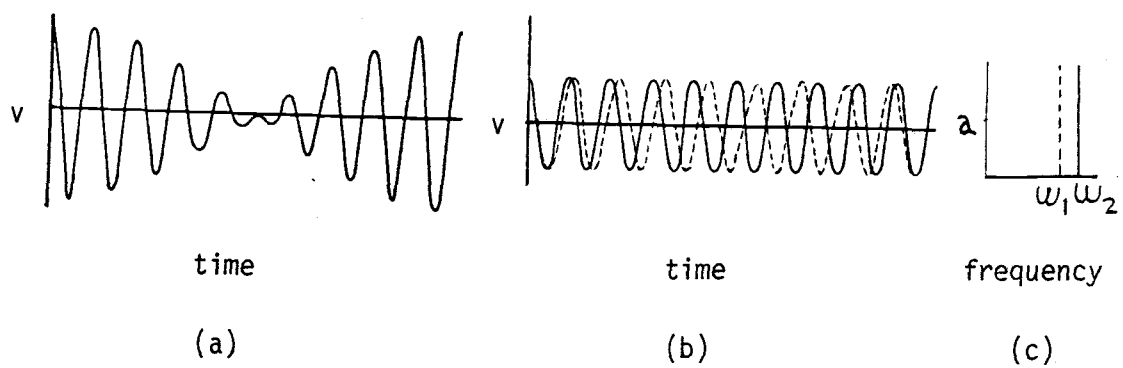


**Figure V.3** Different representations of two NMR signals received simultaneously: (a) the sum of two sine waves; (b) two separate sine waves; (c) the Fourier transform of (a).

spectrum. Bare in mind that the time needed for collecting a FID in pulsed NMR is of the order of seconds, whereas the time needed for a CW scan of the same nuclei is of the order of minutes. Thus, during the time taken for a CW scan, the computerized FT-NMR can accumulate about a hundred scans and add them up in memory. Ultimately, FT-NMR represents about an order of magnitude increase in the signal-to-noise ratio over CW NMR with the same measurement time. Today, quite literally, it is possible for a FT-NMR spectrometer aided with a modern computer to run an unknown quantity of an unknown compound through a set of experiments that are automatically optimized to provide satisfactory sensitivity [51].

<sup>13</sup>C NMR. The direct observation of the carbon skeleton as well as the carbon atoms in carbon-containing functional groups is the obvious motivation for using carbon-13 NMR on top of proton NMR [52,53,54]. The combination of both forms the basis of a modern NMR structural analysis. Many of the advantages of carbon-13 NMR relate to its spectral resolution because of the wide range of chemical shifts it covers, 600 ppm, comparing to only about 20 ppm for that of proton NMR [55]. It is therefore not unusual in carbon-13 NMR to be able to identify individual resonances for each carbon in a relatively high molecular weight compound. In such complex molecules, conventional proton NMR may be useful only for "fingerprint" identification, because so many different resonances lay in such a narrow range, that is, the spectrum may consist of many overlapping peaks. However, the overall sensitivity of carbon-13 NMR compared with proton NMR is about 1/5700 because of the lower natural abundance of carbon-13 and other technical problems [56]. Thus, even with the availability of FT carbon-13 NMR,

in reality a larger sample size and longer acquisition time are still essential for a successful carbon-13 NMR experiment.

Because of spin-spin coupling with bonded and with more distant nuclei, usually protons, the intensity of a carbon signal is distributed among several multiplet lines. Signal splitting, added to the unfavorable nuclear properties of carbon-13, further decreases the sensitivity of Carbon-13 NMR. Furthermore, the multiplets may overlap in molecules with several kinds of carbon, which complicates the interpretation. Therefore, it is common to employ a DECOUPLING technique whereby the spin-spin interactions of carbon-13 nuclei with neighboring magnetic nuclei, protons, are eliminated [57]. Thus, the spectra normally consist entirely of singlet signals, and the interpretation of the spectra involves the assignment of specific signals to the various nonequivalent carbons without the aid of the multiplets found in proton NMR spectra.

Unlike proton NMR whose absorption peak area is proportional to the numbers of protons involved, carbon-13 nuclei, whose relaxation times vary over a wide range compared to the acquisition time in FT-NMR, cannot be integrated to give the correct number of carbon atoms [56]. Fortunately, almost all carbons in a molecule will likely have a different chemical shift because of their different chemical environments; that is, the number of carbons represented by a spectral peak would be less important.

### 3. Two-dimensional NMR

General information about a molecule, such as the number of

distinct protons and carbons, can be obtained by so called 1D NMR (one-dimensional) spectra (signal vs. ppm). Preliminary assignments may be made by inspection of these spectra, by taking into consideration gross chemical shift arguments, and by matching spectral splitting. These information can be also useful for "fingerprint" identification if a synthetic reference can be obtained for comparison. But, as molecular complexity increases, peak assignment may become impossible due to the problems arising from overlapped peaks. This creates a serious problem for the structural analysis of drug metabolites, in which the individual nuclear resonances of a new metabolite have to be assigned, while usually only parent drug but no synthetic reference of the metabolite is available. However, 2D (two-dimensional) NMR spectroscopy, which employs two-dimensional Fourier transformation and two-dimensional plots in data presentation, offers dramatic improvements in spectral resolving and correlating power by spreading out information in two frequency dimensions and by revealing interactions between nuclei [58,59,60,61,62,63,64]. Thus, definite resonance assignments, and hence accurate structural interpretation can be made even without a particular synthetic reference.

In order to understand the basic aspects of 2D NMR, it is best to start with the description of the concept of the "rotating frame" [59,60,64], which simplifies the study of the motion of the nuclear spins.

As shown in Fig. V.4a, if a standard set of Cartesian axes is arranged with the z axis along the direction of the magnetic field  $B_0$ , then individual microscopic magnetic vectors will precess clockwise in the frame with more vectors pointing up (low energy state)

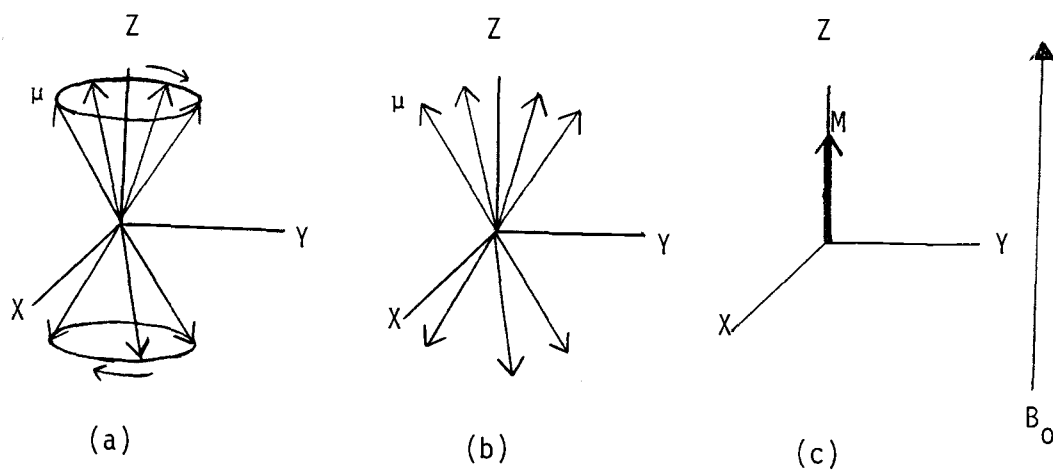
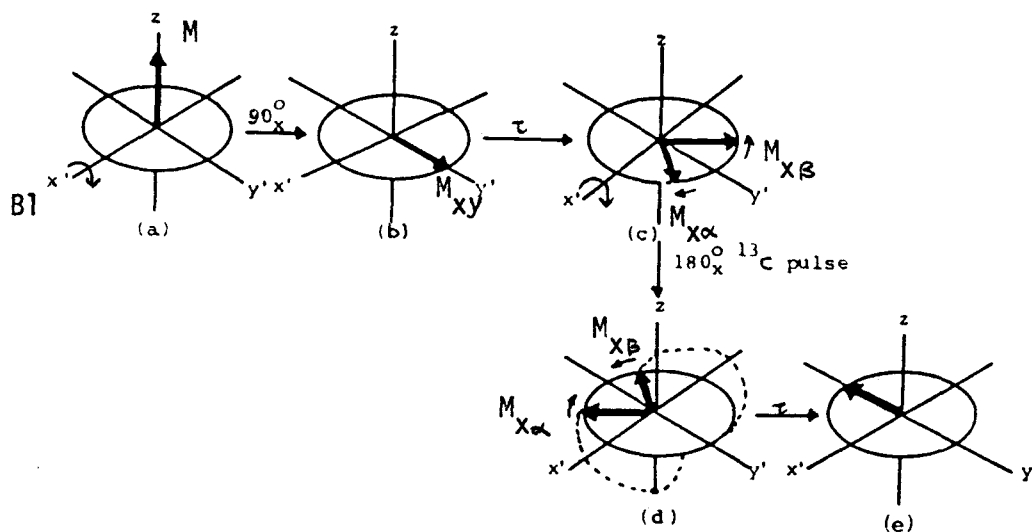


Figure V.4 The microscopic ( $\mu$ ) and macroscopic ( $M$ ) magnetizations in the stationary and rotating frames.

than down (high energy state). If the frame is imagined to rotate at the same speed and in the same direction as the microscopic magnetization vectors, then in this "ROTATING FRAME", the microscopic magnetization vectors are stationary and are not rotating. This is shown in Fig. V.4b. In the real chemical sample situation, because a large number of microscopic magnetization vectors exist, the sum of these vectors is only along the z axis and points up (+z direction). This vector sum is labeled M in Fig. V.4c, and is called the MACROSCOPIC MAGNETIZATION VECTOR. The changes in the macroscopic magnetization vector are observed in a NMR experiment. Magnetization vectors can only be observed when they lay in the xy plane, because of the position of the detector coil.

Take as an example a heteronuclear system containing two different nuclei A and X which are coupled to each other. In the NMR experiment, a linearly oscillating magnetic field,  $B_1$ , produced by a radio frequency transmitter, is set along the x axis as shown in Fig. V.5a. This field will make the macroscopic magnetization vector of nucleus A precess clockwise around  $B_1$ . That is, the macroscopic magnetization vector M of nucleus A in the AX system will tip away from the z axis towards the xy plane. Thus a transverse vector component in the xy plane is generated,  $M_{xy}$ , which in turn produces TRANSVERSE MAGNETIZATION. If the  $B_1$  field is turned off just as M reaches the xy plane, then  $M_{xy}$  will be at its maximum value, as shown in Fig. V.5b. A pulse of  $B_1$  that causes this  $90^\circ$  rotation of M is referred to as a  $90^\circ$  pulse.

An individual micromagnetization vector (nuclear spin) cannot be measured. However, the effect of a  $90^\circ$  pulse is to generate a

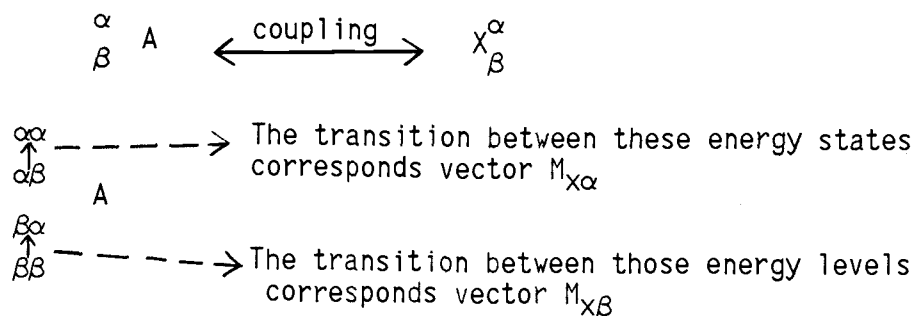


**Figure V.5** Schematic representations of the Spin-echo experiment for a simple AX system: (a) macromagnetization vector before applying the  $90^\circ$  pulse; (b) application of the  $90^\circ$  pulse transverses magnetization; (c) transversed magnetization splits into its components; (d) application of the  $180^\circ$  pulse causes interchange of magnetizations; and (e) Spin-echo information after time  $\tau$  due to refocusing of magnetizations (Adapted from reference [58]).

transverse macromagnetic vector  $M_{xy}$  in  $xy$  plane, which is an ensemble of individual microscopic magnetization vectors. Keep in mind that  $M_{xy}$  is stationary in the rotating frame, that is, it rotates at  $\omega_0$  about  $B_0$  ( $z$  axis). As  $M_{xy}$  rotates, it cuts through the turns of a receiver coil mounted with its axis along the  $y$  axis and induces a radio frequency current in this coil. This rf current is the NMR signal, and is produced only when  $B_1$  is stationary in the rotating frame, that is, when the Larmor and transmitter frequencies are the same.

In fact, the macroscopic magnetization  $M$  of nucleus  $A$  consists of two components  $M_{x\alpha}$  and  $M_{x\beta}$ , because nucleus  $A$  will experience the effects of nearby nucleus  $X$ , which is in two different energy states,  $\alpha$  and  $\beta$ <sup>3</sup>, and part of the total population of  $X$  has its spin in direction that adds to the magnetic field experienced by  $A$ . The magnetizations  $M_{x\alpha}$  and  $M_{x\beta}$  will now precess about the applied field  $B_0$  at different rates in the  $xy$  plane, because their Larmor frequencies are different and, as a consequence, the macroscopic magnetic vector  $M$  now splits into its components  $M_{x\alpha}$  and  $M_{x\beta}$  as shown in Fig. V.5c. That is, if the Larmor frequency of the

-----  
3



magnetization vector  $M_{x\beta}$  is very near the reference frequency (the frequency of the "rotating frame"), the vector  $M_{x\beta}$  will precess slowly in the rotating frame, whereas a Larmor frequency of  $M_{x\beta}$  that is further away from the reference frequency, will precess more rapidly. This process is referred as DEPHASING or DEFOCUSING. <sup>4</sup>

If another oscillating magnetic field is now applied, which rotates all magnetization vectors  $180^\circ$  around the x axis, then the microscopic magnetization vectors will adopt mirror image positions across the x axis, that is, the direction of each microscopic vector is unchanged although its position changes<sup>5</sup>, as shown in Fig. V.5d. This applied oscillating magnetic field pulse is called a  $180^\circ$  pulse, and is applied at time  $\tau$  after dephasing begins. After an additional time  $\tau$  after the  $180^\circ$  pulse, since the faster moving vector  $M_{x\alpha}$  now lies behind the slower moving vector  $M_{x\beta}$ , these magnetization vectors will be REFOCUSED along the -y axis generating a "spin echo signal" as shown in Fig. V.5e. It should be noted that the  $180^\circ$  pulse applied here is selective for the A nucleus and does not affect the spin states of the heteronuclear X. Therefore, the amplitude of the spin echo signal differs from the initial value only through true relaxation

-----  
<sup>4</sup>The fact that some vectors go left and others go right in the rotating frame is because the frequency of the rotating frame is set so that the frequencies of some vectors are "faster" than this rotating frame frequency and others are "slower", so if one "sat" on the rotating frame, one would see one vector going clockwise, the other going counterclockwise.

<sup>5</sup>Bear in mind that this is a heteronuclear system. The  $180^\circ$  pulse is selective in this case; that is, only nucleus A is affected, its magnetization vector components will thus adopt the mirror image only; the state of nucleus X is unchanged.

losses, which allow the nuclei to relax back to their original state. The situation will be different in the case of a homonuclear system to be discussed below<sup>6</sup>.

The experiment described is usually called a SPIN-ECHO experiment [65], which is the basis of two-dimensional NMR. When the spin-echo experiment was first documented, the author noted that "...if only one of two coupled nuclei is subjected to resonance...no echo envelope modulation will appear for either of such coupled nuclei, although the steady state resonance will still reveal the J splitting." [65] Herein lies the concepts of 2D NMR.

In a 1D NMR experiment, a single pulse is used to excite all nuclei of one type. The resulting transverse magnetization (which is obtained with respect to only one time variable, say  $t_2$ ) contains information relating both to the chemical shifts and coupling constants of the nuclei being irradiated and represents a time-domain signal,  $S(t_2)$ . Fourier transformation converts it into a frequency-domain spectrum  $S(\omega)$ :

$$S(t_2) \xrightarrow{\text{F.T.}} S(\omega)$$

where  $t_2$  represents the times at which successive signals are acquired. The production of transverse magnetization by the short  $90^\circ$  pulse may be called the PREPARATION PERIOD and the recording of the FID

---

<sup>6</sup>See discussion in 2D homonuclear J-resolved NMR section.

the DETECTION PERIOD. The idea of 2D NMR is to introduce a second time period ( $t_1$ ) between the preparation and detection periods, which is called the EVOLUTION PERIOD. During this evolution period the NMR receiver is not active but the nuclear motions are made to undergo some prescribed motions which eventually influence the signal  $S(t_2)$ .

The time axis in a 2D NMR experiment may therefore be divided into three (sometimes four) periods (Fig. V.6), during which a sequence of pulses is applied as in the spin-echo experiment. The preparation period allows the nuclei to reach thermal equilibrium and to establish reproducible starting conditions. Then one or more rf pulses are applied, which disturb the thermal equilibrium established in the preparation period. 2D NMR gains a second dimension by varying the duration of the subsequent evolution period,  $t_1$ , which causes a periodic change in signal amplitudes. During this evolution period, the x, y, and z components of the magnetization are allowed to evolve under the forces acting on the nuclei, which include spin coupling interactions between the coupled nuclei. These interactions appear as additional peaks in a 2D spectrum, as we will see later, and help in interpreting molecular structure.

At the end of the evolution period,  $t_1$ , the existing magnetization is recorded in the form of an FID during the detection period,  $t_2$ . The evolution period  $t_1$  is increased gradually and for each  $t_1$ , a separate FID is recorded. That is, an array of one-dimensional time functions  $f(t_2)$  is collected as a function of the time period  $t_1$ ,  $f(t_1, t_2)$ , and the Fourier transform is then performed twice, first along  $t_1$ , then, for that result, in the direction of  $t_2$ , to obtain a two-dimensional frequency spectrum,

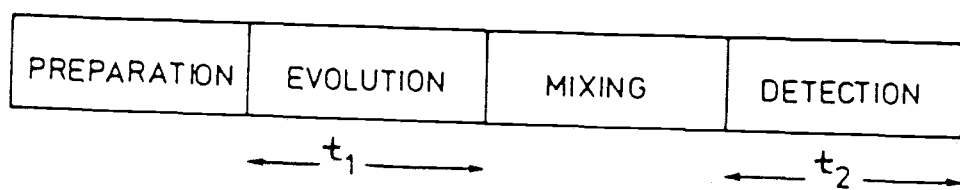


Figure V.6 Timing sequence for 2D NMR spectroscopy.

$F(\omega_1, \omega_2)$ . By applying such a sequence of pulses, the scalar coupling information or the interactions between nuclei can be spread out in two dimensions, which will now be discussed in detail along with different 2D (two-dimensional) NMR techniques.

The original graphic display of 2D NMR data is three-dimensional [66]. However, the so-called contour plot is in more frequent use. A contour plot is a cross-section through the three-dimensional plot parallel to the x,y-plane at a chosen height. If contours at periodically spaced heights are obtained, a clearly arranged diagram of contour lines can be plotted, which is easier to interpret.

2D NMR spectroscopy can be divided into three broad categories by the kind of information it provides: 2D-resolved, 2D-correlated, and 2D-exchange spectroscopies [67].

Two-dimensional J-resolved NMR. [62,68] 2D-resolved (J-spectroscopy) aids the interpretation of even highly overlapping resonances, resolving them into readily interpretable multiplets, and permits peak assignments to be made in a simple and direct manner.

2D J-resolved NMR has been applied extensively for NMR analysis of very large and complex molecules such as proteins, where severely overlapped J coupling peaks are very difficult to assign [13]. Fortunately this is not the case for pentazocine and its metabolites. NMR analysis using this technique is therefore only briefly described here for the sake of completeness.

A 2D-resolved pulse sequence, as shown in Fig. V.7A, results in the generation of a transverse magnetization at time  $t_1$  after the initial  $90^\circ$  pulse. The effect of this sequence on the two magnetization components  $H_A$  and  $H_B$  representing a proton X coupled

to another proton A with two different spin states  $\alpha$  and  $\beta$  can be briefly described as follows: the  $90^\circ$  pulse puts both the  $H_A$  and  $H_B$  components into the xy plane (Fig. V.7-B1). During the subsequent  $t_1/2$  period, the two vectors move away from one another in the xy plane because of their different Larmor frequencies (Fig. V.7-B2). The  $180^\circ$  pulse rotates the  $H_A$  and  $H_B$  vectors so that they adopt mirror image position across the x axis (Fig. V.7-B3). Unlike the case of the heteronuclear system<sup>7</sup> where only one of two coupled nuclei is subjected to a  $180^\circ$  pulse, the situation for the homonuclear system is that both coupled protons now experience the  $180^\circ$  pulse. Therefore, as well as rotating the vectors  $180^\circ$  about the x axis, the vectors are interchanged with each other (Fig. V.7-B3). The two transitions of proton X are EXCHANGED (A - B) as coupled proton A changes its spin state ( $\alpha - \beta$ ) as shown in Fig. V.7-B3 and Fig. V.7-B4. That is, if  $H_A$  was coupled to the  $\alpha$  state of the neighboring proton before the  $180^\circ$  pulse, it switches over to a state (i.e.,  $H_B$  before  $180^\circ$  pulse) in which it is coupled to  $\beta$  of the neighboring proton after the  $180^\circ$  pulse (Fig. V.7-B4). Thus, the faster vector  $H_B$  continues to move away from the slower vector  $H_A$ , and a difference in phase is created (Fig. V.7-B5). These signals are then said to be J-MODULATED. This phase difference during the second  $t_1/2$  period applies only to the vectors of the multiplet (coupled) component. For two vectors that are not connected by spin coupling (Fig. V.7-C1), no exchange of their Larmor frequencies takes place after the  $180^\circ$  pulse (Fig. V.7-C2). The faster

---

<sup>7</sup>Referring to the Spin-echo experiment for comparison.

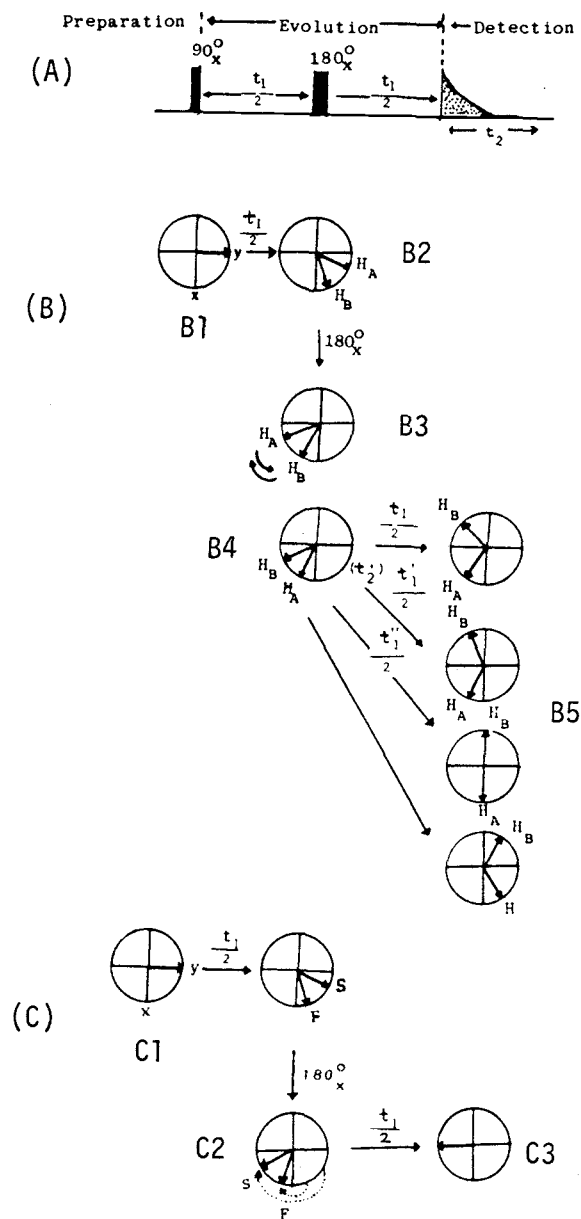


Figure V.7 Pulse sequence and its effect on magnetization components in homonuclear 2D J-resolved spectroscopy: (A) Pulse sequence in homonuclear 2D J-resolved spectroscopy; (B) Effect of the pulse sequence on a  $^1\text{H}$  doublet; and (C) Effect of the pulse sequence on two magnetization components that are not coupled to each other (Adapted from reference [58]).

non-coupled vector will therefore catch up with the slower one during the subsequent  $t_1/2$  period, producing a spin-echo (Fig. V.7-C3); that is, only the chemical shift effects are refocused to produce an echo and not spin-spin coupling cases. The overall result is a modulation in phase of the signals by  $J$ , as a function of  $t_1$ .

As a function of the evolution time  $t_1$ , after Fourier transformation, frequency  $\omega_1$  is recorded, which is determined only by multiplet components that are  $J$ -modulated. As a function of the detection time  $t_2$ , frequency  $\omega_2$  is determined by both the chemical shift and the coupling. Therefore, 2D  $J$ -resolved NMR separates the proton chemical shift along the  $\omega_2$  frequency axis and the homonuclear  $J$  coupling along the  $\omega_1$  frequency axis in the spectrum. As schematically shown in Fig. V.8, individual multiplets lie along parallel lines which make an angle of  $45^\circ$  with the  $\omega_2$  axis<sup>8</sup>. The chemical shift for a multiplet is the value of  $\omega_2$  at the intersection of the  $45^\circ$  line containing the multiplet and the horizontal line at  $J = 0$ . Overlapped multiplets are thus resolved.

Two-dimensional Correlated NMR. [62,68,69] After the multiplet pattern for each nucleus is recognized, maybe with the aid of a 2D  $J$ -resolved NMR spectrum, it is most important to find out next which nearby nuclei cause such multiplet patterns. 2D-correlated NMR (homonuclear or heteronuclear correlation spectroscopy) was therefore developed to correlate spins which are related to each other as a

-----  
<sup>8</sup>The  $45^\circ$  angle is due to the way the computer system performs data acquisition, which can be actually "corrected" by "tilting" the data matrix.

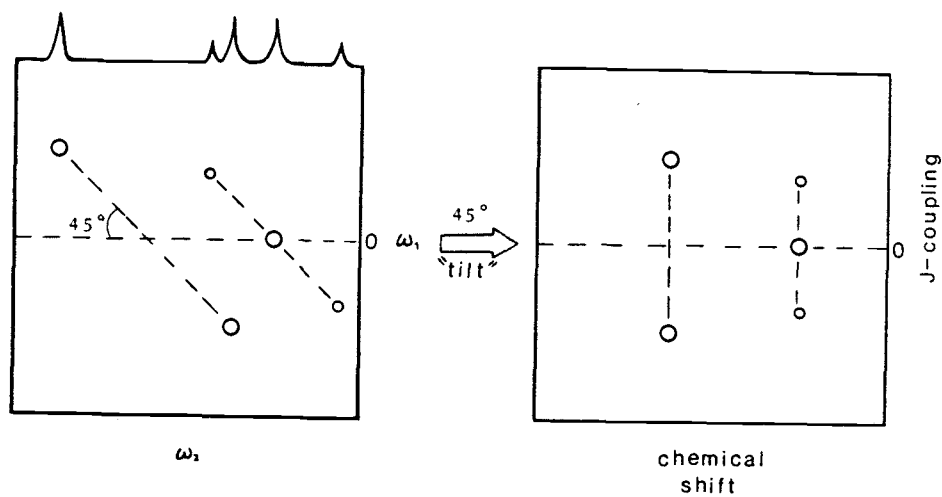


Figure V.8 Schematic representation of a 2D J-resolved spectrum for a proton spectrum containing two overlapped doublets (Adapted from reference [68]).

consequence of J coupling, thus identifying spin-coupled networks of nuclei (C-H, H-H, etc.), or allowing information from one spectrum to help in the assignment of the other spectrum (C-H, e.g., HETCOR).

1. COSY. In a one-dimensional NMR experiment, to find out which protons are responsible for the observed coupling and where their chemical shift is, simple homonuclear (e.g., proton vs. proton) spin-decoupling of a specific proton may be applied by simply irradiating this proton at its frequency with an rf field and observe whether other nuclei are affected by the decoupling from this irradiated proton. That is, if proton A is "decoupled", the multiplicity of proton X changes (sharpens or collapses) [70]. But this procedure can get tedious for a complex spectrum, and sharpening of complex overlapping multiples is often difficult to confirm. COSY, homonuclear COrrrelated SpectroscopY, has been developed to reveal interconnections between structural fragments of a entire molecule on the basis of proton-proton spin coupling networks [63].

The pulse sequence for COSY is shown in Fig. V.9. The first  $90^\circ$  pulse creates transverse magnetization in the xy plane. During the evolution time period,  $t_1$ , the magnetization vectors will precess in the xy plane according to their Larmor frequency and their spin coupling constant, J. Thus, as a function of the evolution time  $t_1$ , after Fourier transformation, the frequency of the magnetization vectors,  $\omega_1$ , is recorded which is determined by the initial precession frequency of those vectors. The second  $90^\circ$  pulse causes

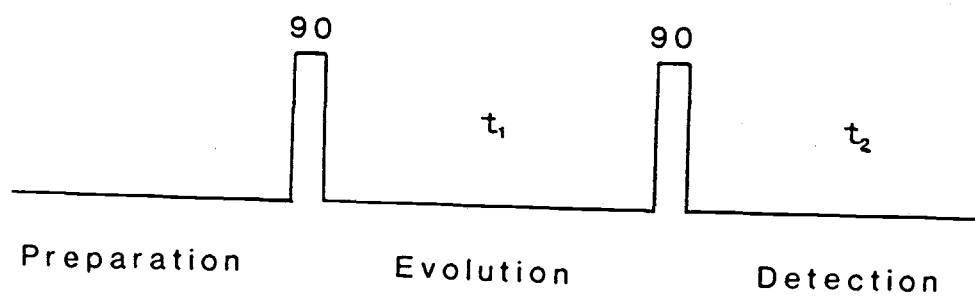


Figure V.9 Pulse sequence for COSY.

magnetization exchange <sup>9</sup> between spins that are J coupled (just like the function of the 180° pulse in 2D J-resolved NMR), whereas spins that are not J coupled retain their initial frequency. The final precession frequency,  $\omega_2$ , is measured during the detection period,  $t_2$ . A COSY spectrum is then plotted of intensity versus  $\omega_2$  and  $\omega_1$ . Those spins that do not couple to one another have the same initial and final frequencies. Hence, DIAGONAL PEAKS occur along the DIAGONAL LINE, which is defined by  $\omega_1 = \omega_2$ . Those protons that exchange magnetization due to J coupling have a final frequency that is different from their initial frequency. This exchange generates pairs of OFF-DIAGONAL peaks, which are symmetric about the diagonal line, connecting spin-spin coupled resonances.

COSY can be displayed in the form of a two-dimensional contour plot, as shown in Fig. V.10, for example. The diagonal contours correspond to an overhead view of the 1D NMR spectral peaks with the

-----  
<sup>9</sup>It can also be said that this second 90° pulse transfers magnetization among all the possible transitions in the coupled spin system, and the magnetization transfer between transitions of noncoupled nuclei and coupled nuclei would result in different appearances in the COSY spectrum (see later discussions for COSY spectrum appearance). But this "all possible transitions in the coupled spin system" also implies the transitions involved here are not only "single quantum" transitions, but also "double" and "zero" quantum transitions, which cannot be simply explained by this so-called vector description. In fact as far as the COSY experiment is concerned, the only successful explanation lies in the quantum theory itself, for example, the "density matrix" description, which is beyond the main concern here, since the intention with this chapter is merely to identify and illustrate potentially useful NMR experiments.

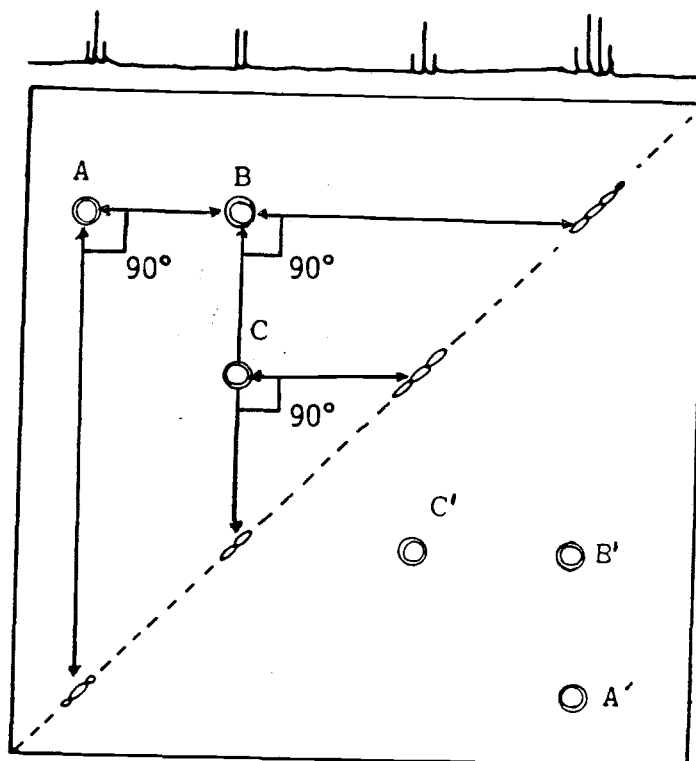


Figure V.10 Example of COSY spectrum. Cross peaks A, B and C establish the proton-proton connectivities (Adapted from reference [58]).

upfield chemical shifts at the top end of the diagonal line. Off-diagonal contours in symmetric pairs represent the coupling interactions between the protons. In order to bring out the many couplings involved, a tracing of the diagonal contours and off-diagonal contours are made by drawing the lines at  $90^\circ$  from each other. In Fig. V.10, three symmetric pairs of off-diagonal contour peaks, A-A', B-B' and C-C' represent the coupling proton peaks. The straight lines at  $90^\circ$  from each other linking diagonal and off-diagonal contour peaks indicate the coupling correlations. The chemical shifts of the coupled protons are obtained from either the horizontal or the vertical axes. A complete coupling network in a molecule can be thus established.

2. Heteronuclear Chemical Shift Correlation Spectroscopy (direct C-H bond). [62,68,71] HETeronuclear chemical shift CORrelation spectroscopy, HETCOR, is another type of the 2D correlated technique which identifies the resonances in the proton and carbon-13 spectra that arise from the coupled proton and carbon-13 nuclei, through either  $^1J_{C-H}$  scalar coupling (direct C-H bond) or  $^2J_{C-H}$ ,  $^3J_{C-H}$  long range scalar coupling (H-C-C, H-C-C-C) [72].

The pulse sequence employed for this technique is shown in Fig. V.11A. The first proton  $90^\circ$  pulse causes the protons to precess at their characteristic frequencies in the xy plane (Fig. V.11-B1). During the subsequent  $t_1/2$  period, two vectors representing a proton which is coupled to its bound C (one vector in which the protons are bound to C nuclei in the  $\alpha$  spin state and the other in which the

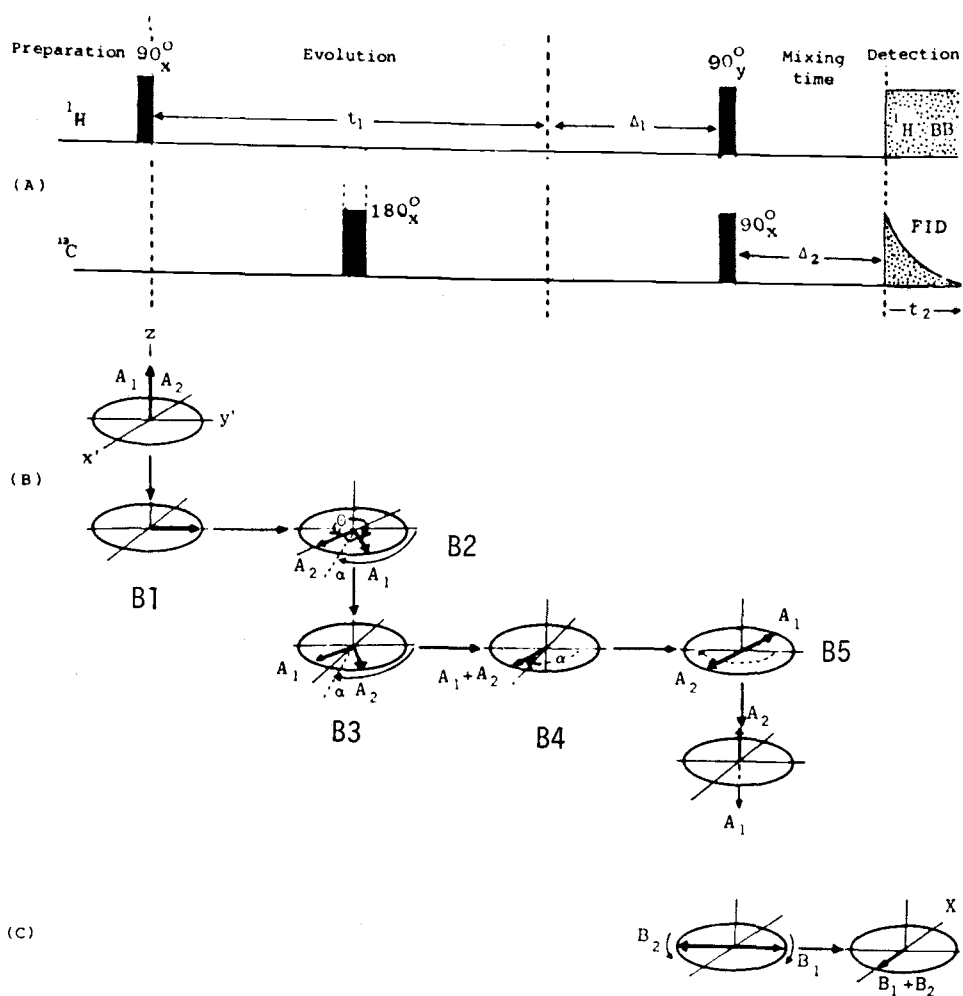


Figure V.11 Pulse sequence and its effect on magnetization components in heteronuclear 2D-shift correlated experiment: (A) Pulse sequence in heteronuclear 2D-shift correlated experiment; (B) Effect of the pulse sequence on a  $^1\text{H}$  doublet coupled with a bound C; and (C) Effect of the pulse sequence on the bound  $^{13}\text{C}$  magnetization component (Adapted from reference [58]).

protons are bound to C nuclei in the  $\beta$  spin state) move away from one another due to different Larmor frequencies (Fig. V.11-B2). The heteroatom (carbon-13)  $180^\circ$  pulse reverses the populations of the C states<sup>10</sup>, resulting in a corresponding interchange of the frequencies of the two vectors representing its coupled proton (Fig. V.11-B3). Then, in the next  $t_1/2$  period, instead of moving away from one another, the two vectors representing the coupled proton are refocused at the end of the evolution period (Fig. V.11-B4). Hence, the precession frequency  $\omega_1$  during the evolution period  $t_1$  depends only on the proton chemical shift. Simultaneous application of the second  $90^\circ$  pulses on both nuclei causes exchange of magnetization between protons and their coupled carbon (just as the second  $90^\circ$  pulse does to two coupled protons in COSY) and significantly enhances the sensitivity of the C signal. The resultant heteronuclear signal is detected during the detection period  $t_2$  (Fig. V.11-B5 & V.11C). If proton decoupling is employed during the detection period,  $t_2$ , the final frequency  $\omega_2$

-----  
<sup>10</sup>Referring to the Fig. V.4. It can be pictured that if the vector M were rotated  $180^\circ$  pointing in the  $-z$  direction, then more microscopic magnetization vectors would have to point in the  $-z$  direction (contrary to Fig. V.4b). Bare in mind that the  $-z$  direction represents a higher energy state in that case, while the  $+z$  direction is a lower energy state, and the number of microscopic magnetization vectors representing the population of the energy state. That is, after M is rotated  $180^\circ$  (by applying a  $180^\circ$  pulse to the nucleus), the population of the higher energy state is more than that of the lower state, which is the reversed case before M is rotated. So, it is said that the " $180^\circ$  pulse reverses the populations of the C states".

will depend only on the heteronuclear chemical shift. Unlike homonuclear correlated spectra, there are no diagonal peaks in a heteronuclear correlated spectrum; all peaks are CROSS PEAKS.

3. Long-Range Heteronuclear Shift Correlation Spectroscopy, LR HETCOR. [73] As shown in Fig. V.11, there are two delay times,  $\Delta_1$  and  $\Delta_2$ , following evolution time  $t_1$  and the second  $90^\circ$  pulse, respectively. The function of the delay times is to allow time for the cross-correlated signal to build up. The delay times can be adjusted to the mean C-H coupling constant,  $J_{C-H}$ . After the first delay time is adjusted to  $\Delta_1 = 1/(2J)$ , the two vectors representing a proton in Fig. 14 are found to be oriented on the  $y'$ -axis in opposite directions. During the  $\Delta_2 = 1/(2J)$ , the carbon-13 vectors refocus. Hence, the value of the coupling constant  $J_{C-H}$  determines the final outcome of the experiment, and two main types of 2D-heteronuclear shift correlated spectra can be recorded. If  $J_{C-H}$  is set between 125-140 Hz, then direct C-H couplings are observed. If the value is set at 5-10 Hz, then the longer range couplings via H-C-C, or H-C-C-C can be identified.

The result of HETCOR is often presented as an intensity contour plot, in which cross peaks indicate partial magnetization transfer between a specific carbon atom and its coupling proton via the  $J_{C-H}$  coupling. In this way, the cross peaks correlate the resonance of each carbon atom to the corresponding proton resonance of its coupling protons. This is illustrated in the HETCOR spectrum of ethanol presented in Fig. V.12.

In Fig. V.12,  $J_{C-H}$  is set to be 140 Hz, the two peaks on the horizontal axis are the carbon-13 chemical shifts of  $CH_3$  and  $CH_2$

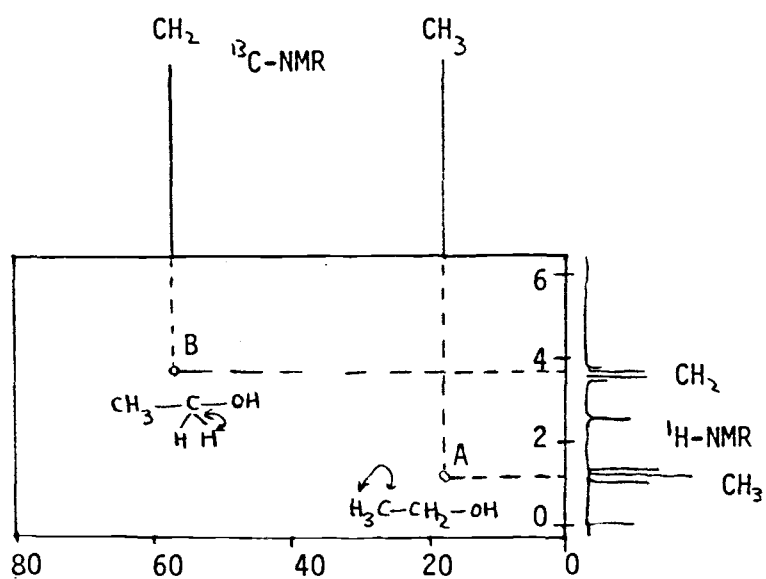


Figure V.12 Schematic representation of the HETCOR spectrum of ethanol (Adapted from reference [58]).

groups while the vertical axis contains the proton NMR spectrum. The cross peak A below the carbon-13 signal for the methyl group corresponds horizontally with the methyl protons in the proton NMR spectrum of ethanol. The second cross peak B similarly establishes a one-bond coupling correlation between the methylene carbon atom and the methylene protons. Thus, protons may be assigned based on known carbon chemical shifts or carbons based on known proton chemical shifts.

In Fig. V.13,  $J_{C-H}$  is set to be 7 Hz, therefore it only shows long range couplings. A two-bond long range coupling interaction in the range of 7 Hz exists between the methyl carbon and the methylene protons results in the cross peak C. The cross peak D establishes a long range coupling between the methylene carbon and the methyl protons. The long range C-H coupling information would be particularly useful when the direct coupling information is not enough, especially when the number of such couplings is less than that of long range couplings. In the case of the pentazocine metabolite MET1 analysis, in which only two protons directly attach to the aromatic ring, the long range C-H coupling information becomes very helpful in establishing the structure.

Two-dimensional exchange NMR. 2D-exchange, such as NOESY (Nuclear Overhauser and Exchange Spectroscopy), offers a new way to obtain the same Overhauser effect information for all nuclei in a molecule by a single experiment and without prior knowledge of the peak assignments or molecule structure [74,75].

In a conventional 1D NOE experiment, if measurement of NOE for a large number of different protons is to be made, an equally large number of such 1-D experiments are needed. Moreover, in complex proton

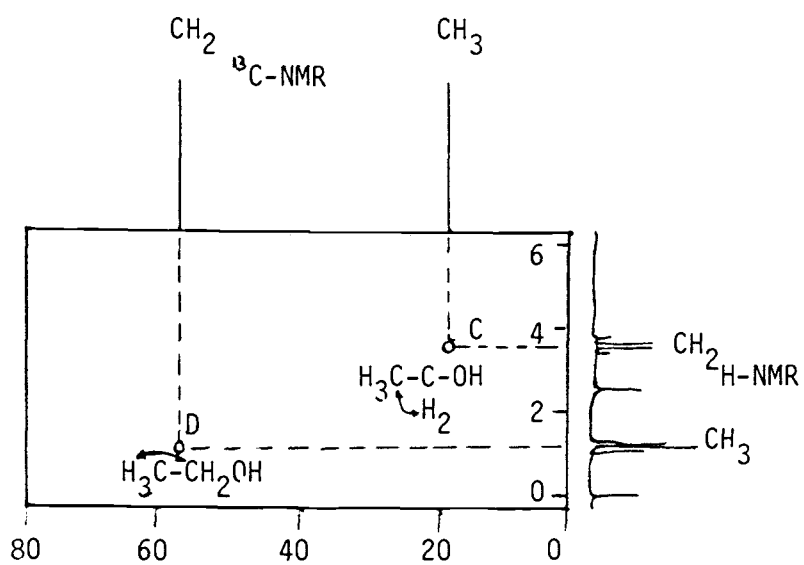


Figure V.13 Schematic representation of LR HETCOR spectrum of ethanol (Adapted from reference [58]).

spectra, a truly selective perturbation is often impossible because of spectral overlap. 2D NOE, NOESY, overcomes such problems by measuring all interproton distances simultaneously and by spreading the overlapping spectrum in two frequency dimensions. NOESY will be used later in the structural elucidation of metabolite MET1.

The pulse sequence for 2D-exchange NMR is shown in Fig. V.14. The first  $90^\circ$  pulse transverses the net magnetization vector to the  $xy$  plane and causes each spin to precess at its characteristic frequency during the evolution time period,  $t_1$ . This is followed by the second  $90^\circ$  pulse (mixing pulse). During the subsequent mixing time,  $\tau_m$ , magnetization exchange due to dipolar interactions <sup>11</sup> is allowed to take place. The third  $90^\circ$  pulse serves to transform the  $z$  magnetization produced into transverse magnetization, which is detected.

The resultant NOESY spectrum is similar in appearance to a COSY spectrum. That is, protons that do not dipole-dipole couple to one another have a final frequency equal to the initial frequency. This gives rise to a set of peaks along the DIAGONAL LINE, which is defined by  $\omega_1 = \omega_2$ . Those protons that exchange magnetization during the mixing period due to dipole-dipole coupling have a final frequency that is different from the initial frequency; symmetrical pairs of OFF-DIAGONAL peaks connecting such protons thus arise.

A NOESY spectrum of pentazocine metabolite MET1 is shown in Fig.

---

<sup>11</sup>Again, like for the COSY experiment, a satisfactory explanation of the NOESY is impossible without the so-called "density-matrix formalism", and even the density-matrix becomes rather confusing when considering more than two or three spins.

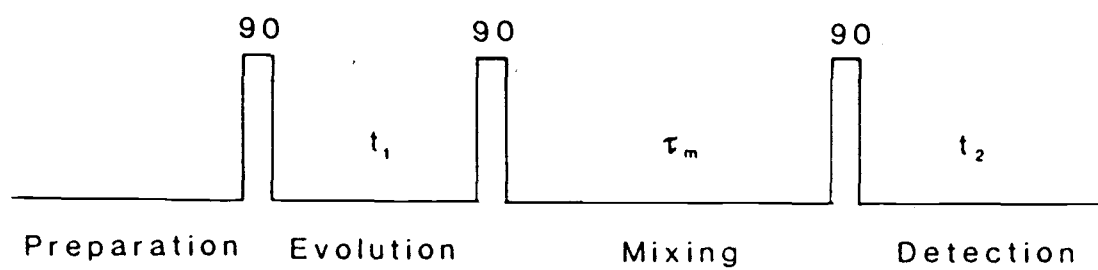


Figure V.14 Pulse sequence for NOESY.

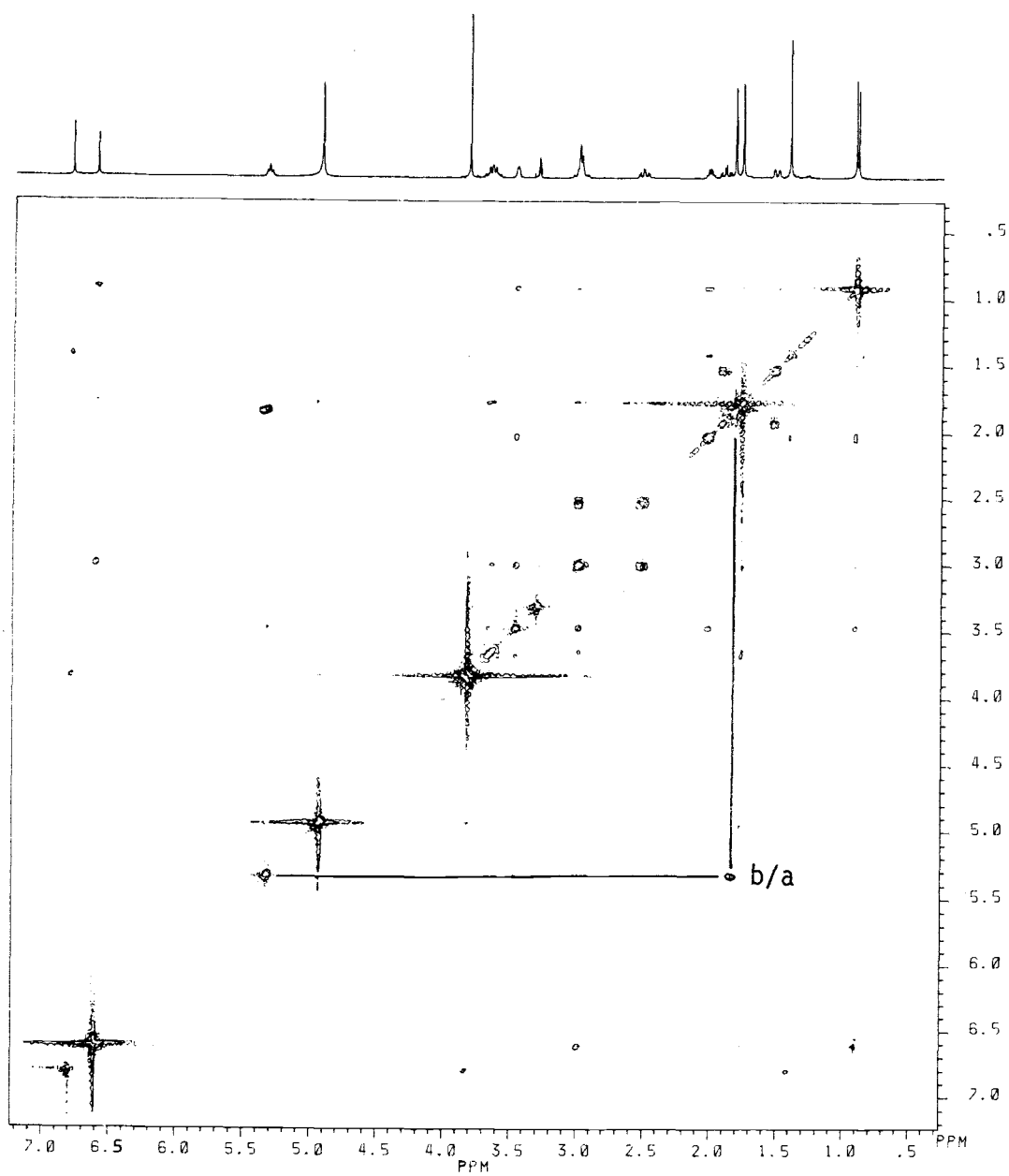


Figure V.15 NOESY spectrum of pentazocine metabolite MET1.

V.15. A 1D proton NMR spectra is drawn on one of the two axes of the 2D plot. The contours represent NOE interactions between protons. The cross peak marked with red ink shows the NOE interactions between the methyl group protons  $H_a$  attached to  $C_{20}$  and the proton  $H_b$  attached to  $C_{17}$ , which indicates that  $H_a$  is cis to  $H_b$ <sup>12</sup>.

#### 4. Experimental

<sup>1</sup>H NMR and <sup>13</sup>C NMR spectra were recorded on a Bruker AM-400 spectrometer. All <sup>13</sup>C NMR spectra were broadband decoupled. All NMR spectra were obtained using 5 mm NMR tubes. Samples were prepared in CDCl<sub>3</sub>, C<sub>3</sub>D<sub>6</sub>O or CD<sub>3</sub>O and the chemical shifts are reported in parts per million (ppm) relative to external tetramethylsilane (SiMe<sub>4</sub>, 0.00 ppm).

All two-dimensional spectra were recorded at ambient temperature with a Bruker AM-400 spectrometer equipped with an Aspect 3000 computer operating in the Fourier transform mode with quadrature detection. Standard Bruker pulse programs were used.

Solvents for the acquisition of NMR spectra were purchased from Aldrich Chemical Company, Inc. (Milwaukee, WI). Pentazocine standard was obtained from Steiling, USA.

-----  
<sup>12</sup>This information confirms the assignment suggested in the pentazocine model compound NMR analysis, because this part of the structure is the same for both pentazocine and MET1, although NOE is not performed in pentazocine NMR analysis.

## 5. Conclusion

In conclusion, there have been a large number of the NMR techniques developed along with the advancement in NMR instrumentation in recent years. The use of these high-resolution 2D NMR is also becoming more and more popular especially in the field of organic chemistry. In this chapter, several 2D NMR techniques have been introduced in a very simple and illustrative fashion only because of their potential in the structural analysis of drug metabolites. The intention in this chapter is to, hopefully, assist in the acceptance of 2D NMR in the area of drug metabolites identification, in which the structure of a metabolite may be very similar to its parent drug but the synthetic reference of this metabolite may not be available. In the following discussion, some of the introduced NMR techniques are used for pentazocine structural analysis to explore the potential of the combination of these techniques in the structural analysis of a metabolite without any synthetic reference.

The required depth of analysis will depend on various factors, such as the complexity of the molecule and how much is known about it. One thing that should be kept in mind is that refined experiments are often more difficult to perform than basic experiments. Thus, there is always merit in attempting the basic experiments first, and resorting to specialized ones only when difficulties present themselves or when questions remain unanswered. In the proposed study, an investigation of the pentazocine model molecule is conducted first to yield an effective structural analysis strategy for the ultimate structural

identification of a metabolite using a combination of both 1D and 2D NMR techniques without any synthetic references.

VI. NUCLEAR MAGNETIC RESONANCE STUDY OF PENTAZOCINE

by

Guang Xiao and Edward H. Piepmeier

Department of Chemistry

Oregon State University

Corvallis, OR 97331

and

A. Morrie Craig

School of Veterinary Medicine

Oregon State University

Corvallis, OR 97331

Chapter VI and VII will be combined for submission to  
the Journal of American Chemical Society

## 1. Introduction

One of the common tasks of NMR analysis is the confirmation of a proposed structure by the assignment of the peaks in proton or carbon-13 spectra, usually with the help of NMR data from related model molecules. This might be accomplished with a 1D  $^1\text{H}$  NMR spectrum, backed up by  $^{13}\text{C}$  NMR data or by some information from proton-proton as well as proton-carbon spin coupling. When there is no suitable model compound (synthetic reference), the NMR resonance assignments are then dependent upon the additivity rules (for example, in a  $^{13}\text{C}$  spectrum) perhaps backed up by more sophisticated 2D NMR techniques. Additional information is obtained by matching similar nuclear environments for the regional proton spectrum, using cross-peak assignments from Heteronuclear Shift-Correlated NMR, and finally doing an entire network tracing by H-C-C-H connectivity through NOE.

In any case, before attempting to apply various NMR techniques to complex molecules like a metabolite of pentazocine, a thorough assessment of each technique using a single model compound will always be beneficial. Based on the fact that pentazocine and its metabolites are structurally similar, such an assessment can be done by using pentazocine as a model compound. The purpose of the NMR study of pentazocine described in the following chapter is to assign, as far as possible, all  $^1\text{H}$  and  $^{13}\text{C}$  signals of pentazocine (Fig. VI.1), through which an analysis protocol for later structural characterization of metabolite MET1 is also devised. Furthermore, this

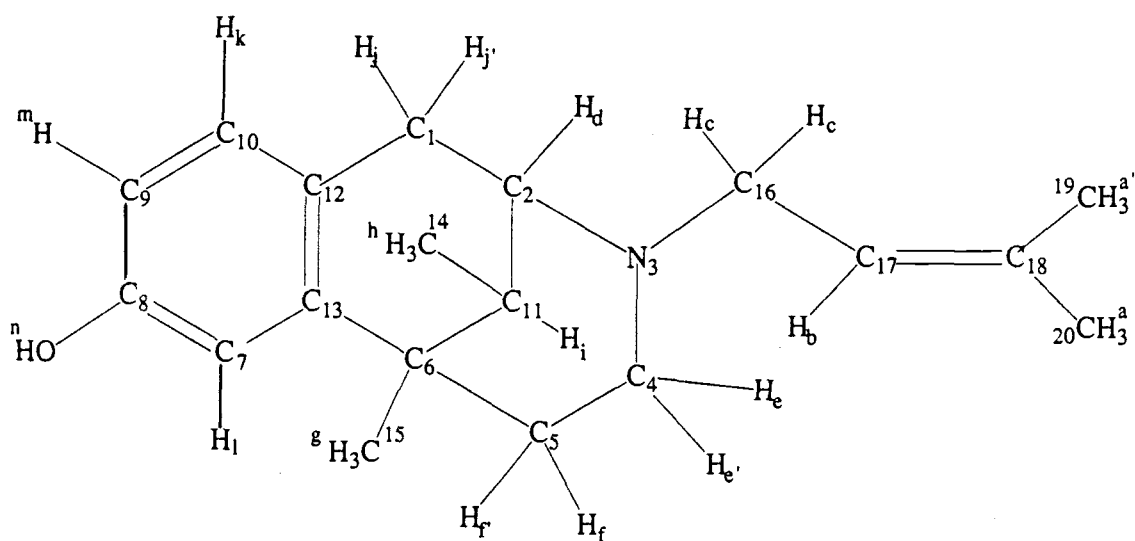


Figure VI.1 Pentazocine molecular structure.

initial investigation of pentazocine also provides a broad base of expertise and experience, which makes the subsequent metabolite study more efficient and, perhaps, the descriptions of the metabolite NMR data analysis correspondingly concise.

## 2. Discussion and Results

Proton NMR. Fig. V.2 shows a 400-MHz proton NMR spectrum of pentazocine in D-chloroform. As pointed out earlier, the assignments in the "one-dimensional" proton NMR spectrum are only preliminary. Most of the assignments are made by matching with published chemical shifts for protons in the same or similar nuclear environments, and will have to be confirmed by spectral information obtained from "two-dimensional" NMR unless stated otherwise.

The normalized intensity of resonance b at 5.28 ppm amounts to only one proton, or a methine group. Its splitting pattern appears to be a triplet. Thus, if the splitting pattern of resonance b follows the first-order, it should be coupled with two nearby protons. This assumption would eliminate the possible assignments of this resonance to methine protons  $H_d$  and  $H_i$ , because their neighboring coupling protons are two  $H_j$  and a  $H_i$  for  $H_d$  protons, and three  $H_h$  and a  $H_d$  for  $H_i$  protons; that is, for both of them neighboring coupling protons are more than two. Resonance b can be therefore assigned to the only other methine protons  $H_b$  attached on  $C_{17}$ , whose triplet splitting pattern arises from coupling with the two nearby  $H_c$  protons on  $C_{15}$ . The chemical shift of  $H_b$  can also be calculated by

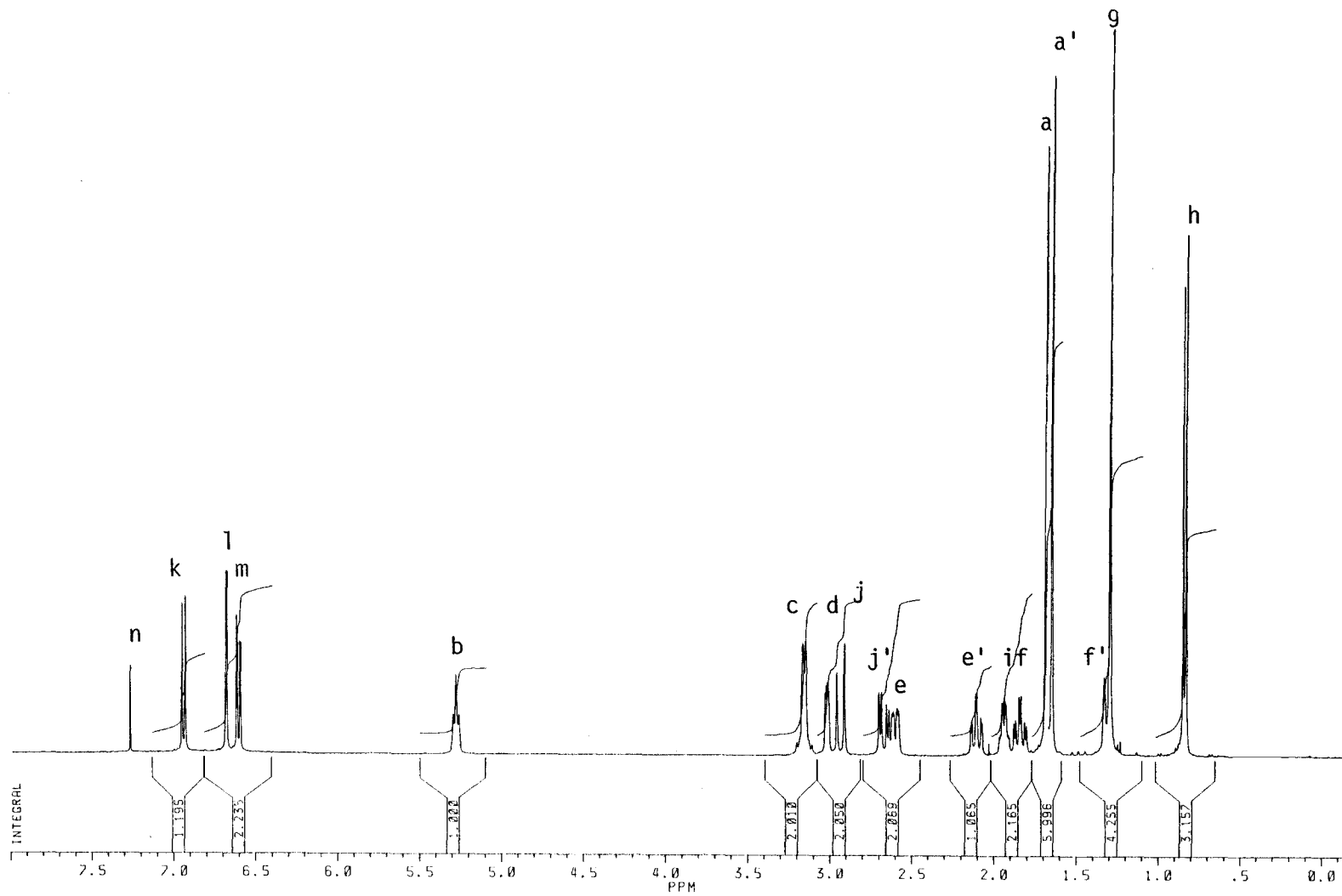
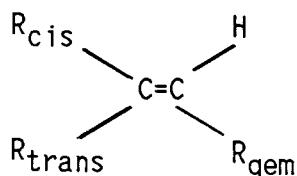


Figure VI.2 400-MHz  $^1\text{H}$  NMR spectrum of pentazocine in D-chloroform.

$$\delta = 5.28 + Z_{\text{gem}} + Z_{\text{cis}} + Z_{\text{trans}}$$

where  $Z$  is the substituent constant [56] for the chemical shift of substituted ethylenes in  $\text{CCl}_4$  as shown in the formula



where  $R_{\text{cis}} = R_{\text{trans}} = \text{Alkyl}$

$R_{\text{gem}} = -\text{NRR}'$

Thus using values from Table I, appendix d. in reference [9],

$$\delta = 5.28 + 0.66 - 0.26 - 0.29 = 5.39 \text{ ppm}$$

This calculated value is fairly close to the observed resonance b at 5.28 ppm, which further confirms its assignment.

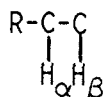
Resonances a and a' at 1.64 and 1.68 ppm integrate to have 3 protons each. Therefore, they should belong to two methyl groups. The singlet appearance of both resonances further implies that there is an adjacent quaternary carbon (no protons directly attached to cause splitting) such as  $\text{C}_{18}$ . Since the chemical shift in the literature for methyl protons such as  $\text{H}_a$  and  $\text{H}_{a'}$  attached to a carbon on a double bond is within the range of 1.6-1.65 ppm [56], it is reasonable to assume that resonances a and a' at 1.64 and 1.68 ppm are

responsible for the  $H_a$  and  $H_{a'}$  protons attached to  $C_{20}$  and  $C_{19}$ , which are in turn attached to the quaternary carbon  $C_{18}$ . But these assignments still need to be confirmed, because it is based on the assumption of first-order coupling and the comparison of chemical shifts in the similar but not identical environments.

Resonance g at 1.29 ppm is also integrated to a methyl group and has a singlet appearance, which also indicates a quaternary carbon attachment (the single side peak f' at 1.326 ppm should belong to another proton from somewhere else, because the total integration for both peaks is four, which is more than the maximum number of protons that can be attached to a carbon, except for methane). In pentazocine, the methyl group with protons  $H_g$  attached to  $C_{15}$  is connected to a quaternary carbon  $C_6$ . The chemical shift for such protons can be calculated according to Curphey-Morrison additivity constant [76]:

$$\delta = \text{Methyl group basic value} + R$$

in the formula,



where R in this case is  $\beta$ -Aryl.

Hence, using values from the Curphey-Morrison additivity constant table in reference [76]

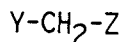
$$\delta = 0.90 + 0.35 = 1.25 \text{ ppm}$$

This calculated value is pretty close to the observed resonance g at 1.29 ppm. Thus, resonance g at 1.29 ppm is assigned to  $H_g$  attached on  $C_{15}$ .

The doublet appearance of resonance h at 0.84 ppm, which has an area equivalent to 3 protons, accounts for another methyl group, probably consisting of the  $H_h$  protons attached to  $C_{14}$ . The literature chemical shift for such an environment is 0.87 ppm [56], and its direct attachment of the methine group (a  $H_i$  proton attached to  $C_{11}$ ) also fits the doublet splitting pattern.

Up to this point, assignments for all methyl groups still remain uncertain, because they are heavily dependent upon the assumption that a first-order system applies. These assignments should be confirmed by further study, such as a COSY spectrum, which will establish the coupling network for the entire molecule.

The chemical shift for the methylene protons such as  $H_c$  can also be calculated from the Curphey-Morrison additivity constants based on the formula [56]:



where  $Y = -NRR'$  and  $Z = -C=C-$

Hence, by using Table I, appendix b, in reference [56]

$$\delta = 1.20 + 1.33 + 0.75 = 3.28 \text{ ppm}$$

Therefore, it is logical to assign resonance c at 3.20 ppm to  $H_c$ , which integrates to two protons and appears to be approximately a doublet probably arising from nearly first-order coupling with the only nearby proton  $H_b$ . It is also evidence that in this case "first-order" coupling does not strictly apply, because resonance c appears to have a more complicated splitting pattern than a doublet, caused perhaps by the long range coupling with methyl group protons on the other side of the double bond, which makes this assignment suspicious.

Other methylene protons  $H_e-H_{e'}$ ,  $H_f-H_{f'}$  and  $H_j-H_{j'}$  are impossible to assign at this point, because those protons are diastereotopic, or chemically nonequivalent protons [56], arising from asymmetrical rigid structures. Very briefly, although these protons, for example  $H_e$  and  $H_{e'}$  are attached on the same carbon  $C_4$ , their chemical shifts are different due to their uninterchangeable position (i.e., the  $-C_4-$  bond cannot be rotated), and hence these protons are in different nuclear magnetic environments.

Based on their chemical shifts, the proton resonances k, l and m in the 6.5-7.0 ppm region (normalized intensity accounts for a total of three protons) are assigned to protons on the benzene ring structure. The splitting patterns of resonances k and m are doublets, and resonance l is a quartet at 6.614, 6.608, 6.594 and 6.587 ppm [attached

proton NMR print-out resonance report] although it appeared very much like a singlet. Because of the complexity of this coupling system, the first-order coupling rules no longer apply, and the specific assignment of individual protons in this aromatic moiety thus relies largely on later 2D NMR analysis, which will clearly show the coupling relationships among these protons.

Table VI.1 shows the probable proton NMR peak assignments so far with their observed and calculated resonances. Again, most assignments made at this point are based on assumptions of a first-order splitting pattern, and comparisons to the available chemical shifts cited from well studied similar proton environments. Other than these, the complete proton resonance assignment cannot be done with 1D proton NMR.

Carbon-13 NMR. Fig. VI.3 shows the proton broadband-decoupled Carbon-13 NMR spectrum of pentazocine in D-chloroform. The possible assignments comparing the observed chemical shift to calculated or literature published ones are listed in Table VI.2.

It was recognized at an early stage in the development of NMR that chemical shift assignments could be made by means of additivity effects [80]. Specifically, the affects of substituents upon the chemical shifts of carbon in monosubstituted compounds could be algebraically added to predict the chemical shifts in compounds with two or more of these substituents. Thus, in Table II, the calculation of the chemical shifts of carbons in the aromatic moiety, C<sub>7</sub>-C<sub>10</sub>, C<sub>12</sub> and C<sub>13</sub> are based on unsubstituted benzene absorptions at 128.5 ppm in D-chloroform [56], and chemical shift increments of polysubstituted benzene can be predicted by assuming that increments in chemical shifts of carbon

Table VI.1 The probable pentazocine  $^1\text{H}$  NMR resonance assignments.

Possible Assignment	Observed	Calculated	Reference
	ppm	ppm	
Aromatic Protons	6.939 6.676 6.601	6-7	[56]
$\text{H}_b$	5.28	5.14	[56]
$\text{H}_a$ or $\text{H}_{a'}$	1.645 1.682	1.6-1.65	[56]
$\text{H}_h$	0.828	0.87	[56]
$\text{H}_g$	1.290	1.25	[76]
$\text{H}_c$	3.163	3.28	[56]

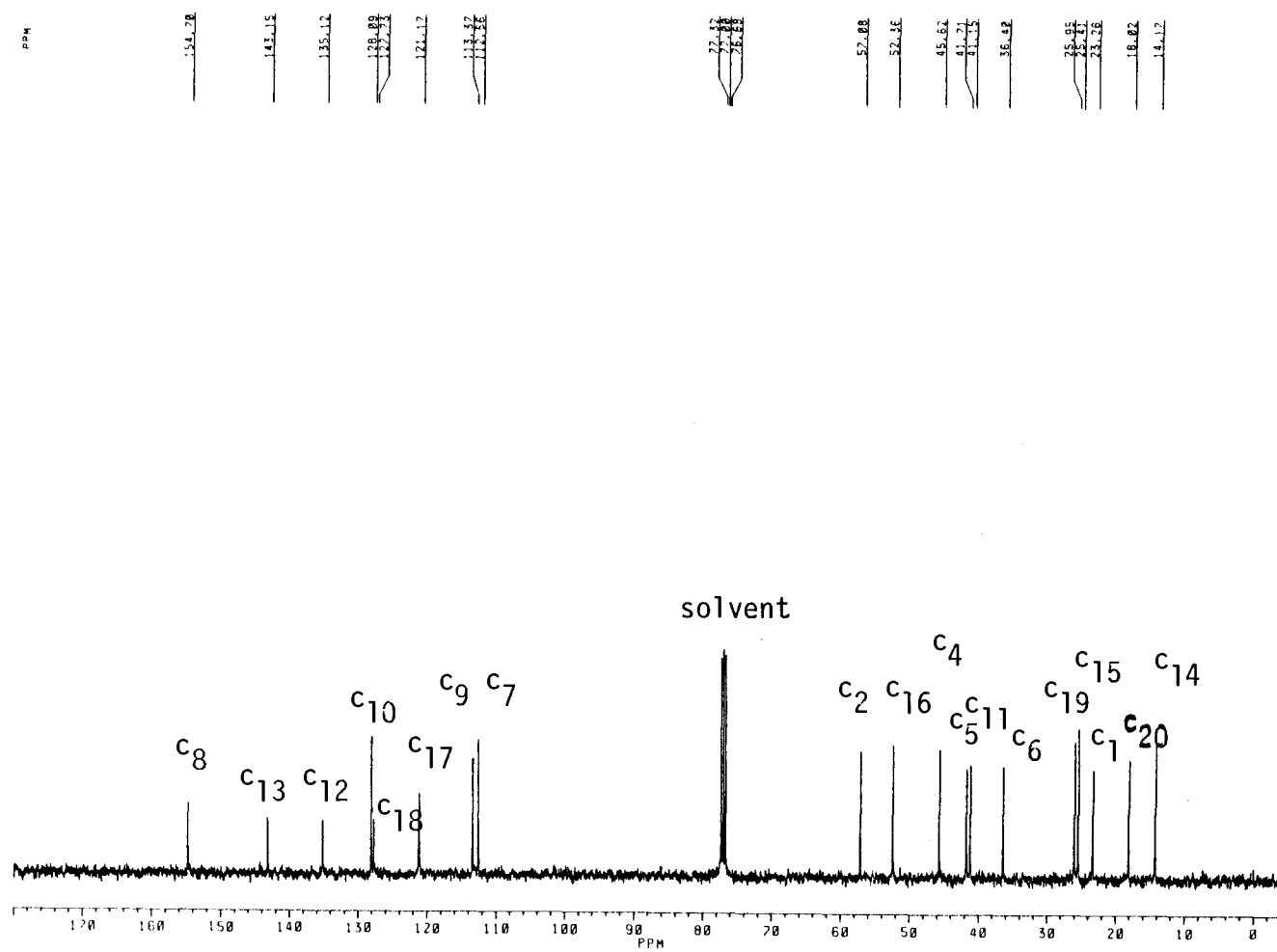


Figure VI.3 Proton broadband-decoupled  $^{13}\text{C}$  NMR spectrum of pentazocine in D-chloroform.

Table VI.2 The possible assignments of  $^{13}\text{C}$  NMR resonances of pentazocine.

Carbon Assignment	Observed	Calculated	Reference
	ppm	ppm	
C <sub>8</sub>	154.70	152.4	[56]
C <sub>7</sub> *	112.56	111.9	[56]
C <sub>13</sub>	143.15	144.5	[77]
C <sub>12</sub>	135.12	136.5	[56]
C <sub>10</sub> **	128.09	129.0	[56]
C <sub>9</sub> *	113.37	112.7	[56]
C <sub>4</sub>	45.62	46.5-48.2	[55],[56],[78]
C <sub>5</sub>	41.71	35.4	[56],[78],[79]
C <sub>6</sub>	36.40	34.5	[56]
C <sub>18</sub> **	127.73	133.9	[56]
C <sub>20</sub>	25.95	25.3	[56]

\* The assignments of C<sub>7</sub> and C<sub>9</sub> are based on the fact that calculated chemical shift for C<sub>9</sub> is further downfield than that of C<sub>7</sub>, although they are really close to each other. These assignment can be confirmed the results of HETCOR, which showed the correlation between H<sub>m</sub> (quartet) and C<sub>9</sub>, H<sub>1</sub> (doublet) and C<sub>7</sub>.

\*\* The calculated chemical shift of C<sub>10</sub> is very close to the observed one; the relatively small intensity of resonance 18 in carbon-13 NMR shows the characteristic of quaternary carbon (the decreased peak height is due to lacks of the bound proton and thus suffers from a longer T<sub>1</sub> and a diminished NOE [56]), which leaves C<sub>20</sub> assignment inevitable based on the comparison of the calculated chemical shift and the observed one.

atoms in monosubstituted benzene derivatives are additive [77].

Based on the same principle, to assign the carbon-13 NMR spectrum of a large molecule, appropriate smaller molecules can be chosen in such a way that they are, or contain, parts of the larger molecule and have carbon-13 signals which have been assigned previously. Then certain carbon-13 resonances can be assigned either by the direct comparison of a similar carbon environment in an appropriate smaller molecule [81], or by manipulating carbon-13 resonances of several similar carbon environments in more than one smaller molecule to lead a preliminary assignment. Such a method enables the assignments of  $C_4$  and  $C_5$  demonstrated as follows.

As shown in Fig. VI.4, five similar nuclear environments (1)-(5), which have been studied by carbon-13 NMR, are extracted from references [55], [78] and [79]. Comparing these smaller molecules to the pentazocine structure shown on the upper left corner (the similar positions for  $C_4$  and  $C_5$  in these smaller molecules are indicated in parentheses), chemical shifts  $\delta_4$  and  $\delta_5$  for  $C_4$  and  $C_5$  can be extracted as follows.

By inspecting the pentazocine structure, it is easy to note that  $C_4$  and  $C_5$  are in a part of the structure that is close to piperidine, structure (1). The direct comparison of pentazocine with piperidine would have a chemical shift for  $C_4$  equal to 47.3 ppm, which is reasonably close to the carbon resonance  $C_4$  at 45.62 ppm (see Fig. VI.4). Substitutions on the piperidine ring shown by structures 2-4 give similar chemical shifts for  $C_4$ . Therefore resonance 4 is assigned to  $C_4$ .

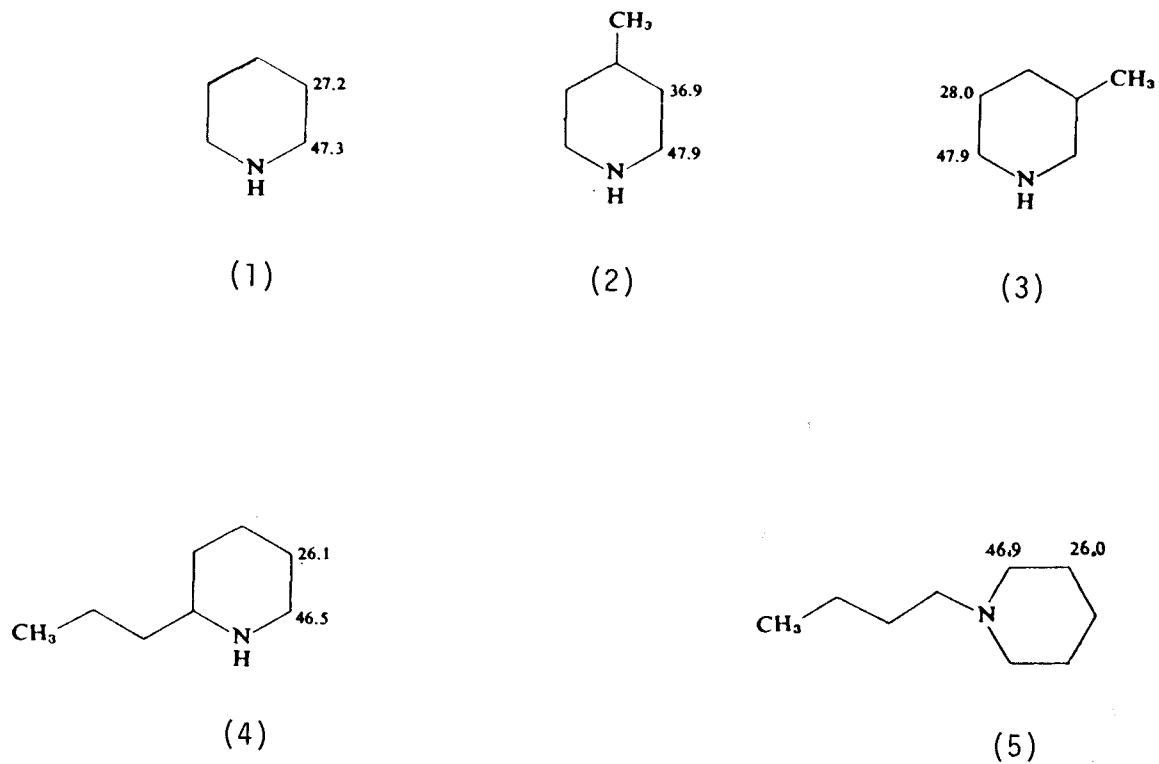


Figure VI.4 Structures of five smaller molecules with similar nuclear environments to that of N-ring portion in pentazocine: (1) piperidine; (2)-(5) piperidine derivatives.

Such a direct comparison leads to an ambiguous assignment of  $C_5$  because of the difference between the 36.9 ppm shift in structure (2) in Fig. VI.4 and the shifts for the other three structures which are close to each other and average 27.1 ppm. Other substituents attached to the N-ring structure in pentazocine may make the  $C_5$  environment very different from the corresponding ones in the piperidine and other reference structure. Therefore the influences of the substituents attached to the N-ring on structures (2)-(5) are estimated by using the data in Table III. Comparing piperidine to structure (2), there is an additional methyl group next to the  $C_5$  position, while in the pentazocine structure, there is a methyl and a phenol both attached next to the  $C_5$ . Unfortunately, a carbon-13 shift for a smaller molecule close to this structure with both a methyl and phenol is not available in the literature. The calculation of the carbon-13 resonance for  $C_5$  could then be ambiguous because of this difference, but the calculation of carbon-13 chemical shift for  $C_4$  should be less affected. If  $C_4$  is to be considered first, the increment in the carbon-13 resonance for the carbon in piperidine corresponding to  $C_4$ ,  $\delta_{4(2)}$ , due to the additional methyl group attachment on the  $\beta$ -position could be calculated by

$$\delta_{4(2)} = 47.9 - 47.3 = 0.6 \text{ ppm}$$

where 47.3 ppm is the carbon-13 resonance for the carbon corresponding to  $C_4$  in piperidine, and 47.9 is the carbon-13 resonance for the

carbon corresponding to C<sub>4</sub> in structure (2) in which a methyl group is attached to the β position to C<sub>4</sub>.

Similarly, comparison of piperidine to structure (3) with an additional methyl group in the β position to C<sub>5</sub>, would lead to a change in the carbon-13 resonance for C<sub>4</sub> of

$$\delta_{4(3)} = 47.9 - 47.3 = 0.6 \text{ ppm}$$

and an attachment of a three-carbon alkyl chain, structure (4), would cause a change in the carbon-13 resonance of C<sub>4</sub> of

$$\delta_{4(4)} = 46.5 - 47.3 = -0.8 \text{ ppm}$$

Finally, a N-alkyl, structure (5), would change for the carbon-13 resonance of C<sub>4</sub> by

$$\delta_{4(5)} = 46.9 - 47.3 = -0.4 \text{ ppm}$$

Therefore, adding these results together, the overall changes due to attachments to the N-ring structure in pentazocine for the carbon-13 resonance of C<sub>4</sub> would be approximately

$$\partial\delta_4 = -0.8 + 0.6 + 0.6 - 0.4 = 0 \text{ ppm}$$

Adding this total change to the base value of the carbon-13 resonance of the equivalent C<sub>4</sub> position in piperidine, the calculated chemical shift can be obtained

$$\delta_4 = 47.3 + 0 = 47.3 \text{ ppm}$$

Similarly, for C<sub>5</sub>, the structural differences between piperidine and structure (2) would make an increment in the carbon-13 resonance of

$$\delta_{5(2)} = 36.9 - 27.2 = 9.7 \text{ ppm}$$

and the changes in the carbon-13 resonance for C<sub>5</sub> due to an additional methyl group in the  $\beta$  position to C<sub>5</sub>, can be calculated by the comparison of piperidine to structure (3),

$$\delta_{5(3)} = 28.0 - 27.2 = 0.8 \text{ ppm}$$

The changes for C<sub>10</sub> resulting from an attachment of a three-carbon alkyl chain, structure (4), would be

$$\delta_{5(4)} = 26.1 - 27.2 = -1.1 \text{ ppm}$$

and the comparison of piperidine to structure (5) would make changes of

$$\delta_{5(5)} = 26.0 - 27.2 = -1.2 \text{ ppm}$$

Thus the overall changes due to the N-ring structure in pentazocine for the carbon-13 resonance of C<sub>5</sub> would be

$$\delta\delta_{5a} = -1.1 + 0.8 + 9.7 - 1.2 = 8.2 \text{ ppm}$$

and the calculated chemical shift for C<sub>5</sub> would be the corresponding chemical shift of the C<sub>5</sub> position in piperidine plus the changes due to additional attachments to piperidine

$$\delta_5 = 27.2 + 8.2 = 35.4 \text{ ppm}$$

There are observed carbon-13 resonances at 41.71 ppm, 36.40 ppm and 41.15 ppm in pentazocine. Apparently, all of these carbon-13 resonances can be candidate for C<sub>5</sub> assignment. Although the carbon-13 resonance at 36.40 ppm is very close to the calculated one, its low intensity indicates the possibility of a corresponding quaternary carbon [56]. If that were the case, then this resonance should be assigned to the C<sub>6</sub> which has a calculated resonance of 34.5 ppm [56]. Obviously, the assignment of C<sub>5</sub> up to this point still remains ambiguous, and further 2D NMR information is needed. Also bear in mind that the calculated carbon-13 resonance for C<sub>5</sub> shown here could be in error, because the smaller molecules used in the calculation do not very closely resemble the pentazocine environment. But, it shows how the C<sub>4</sub> resonance is affected very little by other attachments to the N-ring.

Because only limited information is available from the carbon-13 NMR analysis of pentazocine-like compounds, only certain carbons have

been assigned, others such as  $C_1$ ,  $C_2$ , and  $C_{14}$ - $C_{20}$  still remain ambiguous from the information presented so far; their assignments can be completed with help from 2D NMR methods such as HETCOR.

COSY, Proton-Proton Chemical Shift Correlation. Beyond the assignment of the  $H_b$  attached to  $C_{17}$ , little can be done directly with the proton NMR spectrum as far as specific and unambiguous assignments are concerned. One solution to this problem is to seek assistance from extracting the proton coupling pattern and interpreting it in terms of the number of nearby protons. This can be done easily under the assumption that the splitting patterns observed are due to first-order coupling as demonstrated above. When it comes to a complicated molecule like pentazocine, where couplings other than the first-order coupling also exist, either making a first-order coupling assumption seems unreasonable (e.g., proton resonance c, Fig. VI.2), or the splitting pattern simply becomes uninterpretable (e.g., proton resonances e and e' arising probably from a pair of diastereotopic methylene protons). But, if we can find out which protons are responsible for the observed couplings, and where they are to be found in the chemical shift spectrum, we should still be able to assign one resonance based on other coupled resonances that may be assigned previously on the basis of other theoretical grounds (e.g., resonance b). In this case, a COSY experiment is performed for such a purpose.

A COSY spectrum of pentazocine in D-chloroform is shown in Fig. VI.5, and Table VI.3a lists J-couplings between protons in pentazocine observed by the COSY experiment. Beginning with the  $H_b$  resonance unambiguously identified from the 1D proton NMR spectrum, which appears as the response on the diagonal line corresponding to 5.28 ppm, two

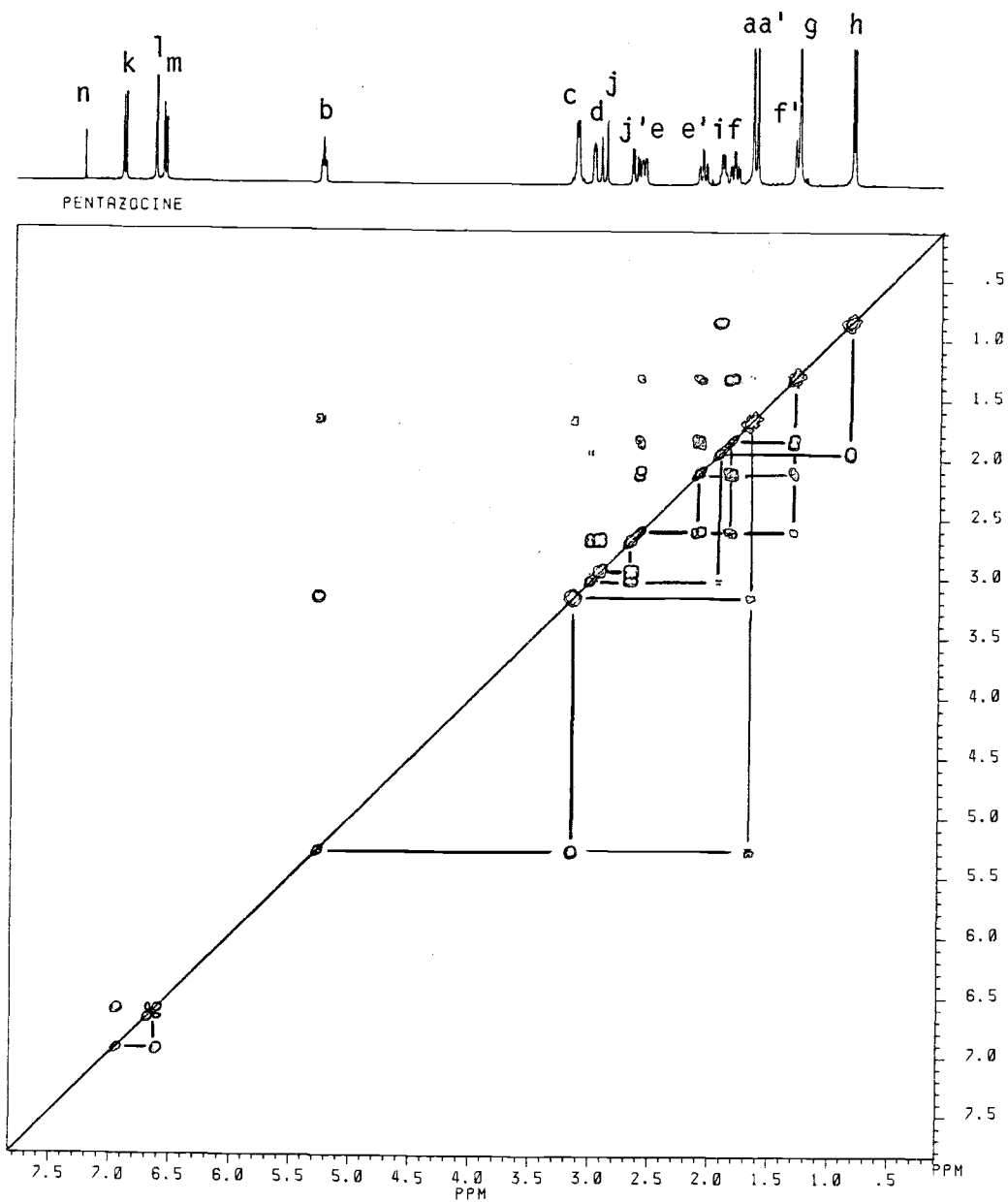


Figure VI.5 COSY spectrum of pentazocine in D-chloroform.

Table VI.3a Proton J-couplings in pentazocine observed by COSY experiment.

Normal Couplings	Very Weak Couplings
a/b, a/c	a'/f'
b/a, b/c	
c/a, c/b	
d/j'	d/i
e/e', e/f, e/f'	
e'/e, e'/f, e'/f'	
f/e, f/e', f/f'	
f'/e, f'/e', f'/f	f'/a'
h/i	
i/h	i/d
j/j'	
j'/d, j'/j	
k/m	
	l/m
m/k	m/l

pairs of off-diagonal elements can be observed, labeled c/b and b/a, which correlate with resonances c and a, at 3.16 ppm and 1.682 ppm. At this point, logical possibilities, to which  $H_b$  is correlated, are methylene protons  $H_c$  attached to  $C_{16}$ , and one of the methyl proton groups,  $H_a$  or  $H_{a'}$ , whichever yields stronger  $J_{H-H}$  coupling with  $H_b$  (see Fig. VI.1 for the pentazocine structure).

Since resonance c is integrated to two protons, a methylene group, it is therefore concluded that resonance c at 3.163 ppm belongs to  $H_c$  protons. Although J coupling is usually not a spatial effect, it will be assumed at this point that  $H_a$  protons, which account for a methyl group and are cis to  $H_b$ , may be coupled with  $H_b$  (The  $H_{a'}$  protons are trans to  $H_b$  and therefore farther away). Thus, resonance a at 1.684 ppm is assigned to  $H_a$  and resonance a' at 1.645 ppm is assigned to  $H_{a'}$ . The assignments of  $H_a$  and  $H_{a'}$  are confirmed for metabolite MET1, as discussed later by a NOE experiment, which identifies those protons that are coupled through space <sup>13</sup>.

The upfield resonance h at 0.828 ppm, which is a doublet accounting for three protons, is correlated with resonance i at 1.93 ppm that accounts for one proton, and resonance i has a weak coupling with further downfield resonance d at 3.146 ppm, which also accounts

-----  
<sup>13</sup>The primary reason for the assignments of resonance a and a' is the fact that only resonance a is coupled with resonance b. It was mentioned in chapter V that the J coupling is indeed carried out through bonding electrons, but with possible exceptions. If it were one of these exceptions in this case, it would be the best choice to assign resonance a to the protons that are cis to the proton b; that is, assuming J coupling is carried out through space in here. The NOE was not performed for pentazocine itself, but performed on its metabolite. Evidently, the MET1 NOE result confirmed the above assumption (see discussion in chapter VII.)

for one proton. Again, resonance h at 0.828 is responsible for a methyl group <sup>14</sup>, which could correspond to the H<sub>h</sub> protons attached to C<sub>14</sub>. If this is the case, then resonance i is responsible for H<sub>i</sub> attached to C<sub>11</sub>. Those predictions will be further confirmed by the following results.

The COSY spectrum of pentazocine also shows off-diagonal responses indicating the coupling correlations between resonances f, f' at 1.845 ppm and 1.326 ppm, e, e' at 2.579 ppm and 2.108 ppm, as well as j, j' at 2.910 ppm and 2.697 ppm. From their coupling constants, Table VI.3b, it can be seen that these pairs of couplings should be the results of the geminal couplings (two protons attached to the same carbon but coupled to each other, due to their unexchangeable positions in a rigid structure) between protons in each pair [56]. Thus, the assignment of these resonances has to be among H<sub>j</sub>-H<sub>j'</sub>, H<sub>e</sub>-H<sub>e'</sub>, and H<sub>f</sub>-H<sub>f'</sub> (attached to C<sub>1</sub>, C<sub>4</sub> and C<sub>5</sub>, respectively). These geminal coupling phenomena are clearly identified in the later C-H correlated spectrum. Furthermore, two pairs of resonances f, f' at 1.845 ppm and 1.326 ppm, as well as e, e' at 2.579 ppm and 2.108 ppm are also coupled to each other (see f/e, f/e', f'/e, and f'/e' in Fig. VI.2). Based on structural considerations, the off-diagonal response correlates resonances f at 1.845 ppm and e' at 2.108 ppm, for example, must result from vicinal coupling between one proton attached to C<sub>4</sub> (H<sub>e</sub> or H<sub>e'</sub>) and another proton attached to C<sub>5</sub> (H<sub>f</sub> or

---

<sup>14</sup>Resonance h belongs to a methyl group because it integrated to three protons. But, there are four methyl groups all together, and which one is responsible for resonance h is uncertain from the result of 1D proton NMR.

Table VI.3b Proton J-coupling constants observed in pentazocine.

Proton	Coupled Proton (Coupling Constant, Hz)	Multiplicity*
H <sub>a</sub>		s
H <sub>a'</sub>		s
H <sub>b</sub>	H <sub>c</sub> (7.2)	t
H <sub>c</sub>	H <sub>b</sub> (7.2)	d
H <sub>d</sub>	H <sub>i</sub> (2.9), H <sub>j'</sub> (5.5)	q
H <sub>e</sub>	H <sub>e'</sub> (12.1), H <sub>f</sub> (3.0)	q
H <sub>e'</sub>	H <sub>e</sub> (12.1), H <sub>f</sub> (12.1) H <sub>f'</sub> (3.0)	m
H <sub>f</sub>	H <sub>f'</sub> (12.8), H <sub>e</sub> (3.0) H <sub>e'</sub> (12.1)	m
H <sub>f'</sub>		m
H <sub>g</sub>		s
H <sub>h</sub>	H <sub>i</sub> (7.0)	d
H <sub>i</sub>	H <sub>h</sub> (7.0), H <sub>d</sub> (2.9)	m
H <sub>j</sub>	H <sub>j'</sub> (18.3)	d
H <sub>j'</sub>	H <sub>j</sub> (18.3), H <sub>d</sub> (5.5)	q
H <sub>k</sub>	H <sub>m</sub> (8.2)	d
H <sub>l</sub>	H <sub>m</sub> (2.5)	d
H <sub>m</sub>	H <sub>k</sub> (8.2), H <sub>l</sub> (2.5)	q

\* Only those of the multiplicities observed in 1D Proton NMR : s-singlet, d-doublet, t-triplet, m-multiplet.

$H_{f'}$ ). The pair of resonances,  $j$ ,  $j'$  at 2.910 ppm and 2.697 ppm, which are correlated to each other due to geminal coupling and not apparently correlated with any upfield resonance (e.g., resonances  $e$ , and  $e'$  or  $f$ , and  $f'$ ), is therefore assigned to  $H_j$  and  $H_{j'}$ , both attached to  $C_1$ . Continuing from the resonance  $j'$  at 2.697 ppm, there is another off-diagonal response that correlates with resonance  $d$  at 3.146 ppm. Based on the assignment of  $H_{j'}$  to resonance  $j'$ , resonance  $d$  at 3.146 ppm is thus assigned to  $H_d$  attached to  $C_2$ , which is next to  $H_{j'}$  attached to  $C_1$  in the pentazocine structure. Because of the correlations among  $d$ ,  $i$  and  $h$  discussed previously, resonances  $i$  and  $h$  at 1.930 ppm and 0.828 ppm are also concluded to belong to  $H_i$  and  $H_h$  protons attached to  $C_{11}$  and  $C_{14}$ , respectively. This is also analogous to the previous assignments of resonances  $d$ ,  $i$  and  $h$  from the earlier discussion of the COSY NMR spectrum, and of course, resonance  $g$  at 1.290 ppm which accounts for a methyl group and appears to be a singlet (has no off-diagonal response to any other resonances, which indicates a probable quaternary carbon attachment) should belong to  $H_g$  protons attached on  $C_{15}$ .

The downfield resonances  $m$ ,  $l$  and  $k$  at 6.601 ppm, 6.676 ppm and 6.939 ppm are attributed to the protons on the aromatic ring according to the previous discussion. As far as the coupling network is concerned, they are isolated from the rest of the molecule, which becomes obvious from their location in the lower left hand corner of the COSY spectrum. The off-diagonal response correlates resonances  $k$  and  $m$  at 6.939 ppm and 6.601 ppm; the doublet appearance of resonance  $k$  also indicates that resonance  $m$  is the only coupling proton to resonance  $k$ . Resonances  $l$  and  $m$  at 6.676 ppm and 6.601 ppm are also

correlated, possibly due to long range coupling between them. This also explains the doublet appearance of resonance l and the quartet appearance of resonance m (coupling to both k and l). Resonances l and k at 6.676 ppm and 6.939 ppm are not coupled. The logical suggestion based on structural considerations would be that resonance l at 6.676 ppm is responsible for  $H_l$ , resonance m at 6.601 ppm arises from  $H_m$ , and resonance k at 6.939 ppm is the result of  $H_k$ , but further confirmation is still needed for such specific assignments. A carbon-proton correlated NMR experiment is therefore conducted to confirm these assignments and to assign proton resonance n.

Table VI.3c summarizes the couplings observed between protons in pentazocine and the assignments confirmed at this stage.

Correlation of the Proton NMR and Carbon-13 NMR Resonances Using Heteronuclear Chemical Shift Correlation Spectroscopy. Despite the progress made in proton resonance assignments with assistance from COSY, there are still some proton resonances remaining unassigned or their assignments are questionable. Also, some of carbon-13 resonances have not yet been assigned. But it can be noted that between each bonded pair of C-H there is at least one of the nuclei (either C or H) that has been assigned. To take advantage of this complementarity, HETCOR is performed, which correlates the resonance of each carbon atom to the corresponding proton resonance of its directly bonded protons, as discussed earlier in the Background section. Thus, it enables cross-assignment for proton or carbon-13 resonance assignments, such as the chemically nonequivalent methylene protons  $H_e-H_{e'}$  and  $H_f-H_{f'}$  in pentazocine.

The contour plot of the proton/carbon-13 shift-correlated 2D NMR

Table VI.3c The  $^1\text{H}$  resonance assignments of pentazocine supported by COSY experiment.

Proton Assignments	Observed	Calculated	Multiplicity*
	ppm	ppm	
H <sub>a</sub>	1.645	1.6-1.65	s
H <sub>a'</sub>	1.682	1.6-1.65	s
H <sub>b</sub>	5.28	5.14	t
H <sub>c</sub>	3.163	3.33	m
H <sub>d</sub>	3.146	2.88	m
H <sub>g</sub>	1.290	1.22	s
H <sub>h</sub>	0.828		d
H <sub>i</sub>	1.930	1.55	m
H <sub>j</sub>	2.910		d
H <sub>j'</sub>	2.697	2.73	d
H <sub>e</sub> /H <sub>e'</sub> or H <sub>f</sub> /H <sub>f'</sub>	2.579/2.108 1.845/1.326	2.53 1.86	m m
H <sub>k</sub>	6.939	6-7	d
H <sub>l</sub>	6.676	6-7	d
H <sub>m</sub>	6.601	6-7	m

\* Only those of the multiplicities observed in 1D Proton NMR : S-singlet, D-doublet, T-triplet, M-more than Triplet observed .

spectrum (HETCOR) of pentazocine in D-chloroform is shown in Fig. VI.6. Table VI.4 shows the correlations observed between carbons and their directly bonding protons as well as the assignments established by these correlations.

In Fig. VI.6, three carbon-13 resonances in the downfield part of the carbon-13 resonance axis as well as resonances at 127.73 ppm and 36.40 ppm do not show cross peaks to proton resonances. This finding indicates the absence of  $J_{C-H}$  coupling and that these carbon-13 resonances originate from quaternary carbon atoms, which is analogous to the previous assignments of  $C_8$ ,  $C_{13}$ ,  $C_{12}$ ,  $C_6$  and  $C_{18}$  from Table VI.2.

It is noted that resonance 6 observed at 36.40 ppm, although it is close to that of the calculated  $C_5$  resonance, is assigned to  $C_6$ , because the HETCOR spectrum indicates that  $C_6$  has the characteristic of a quaternary carbon. In fact, the calculated carbon-13 resonance for  $C_6$  is 34.5 ppm [56], which is also in favor of the assignment of  $C_6$  to the observed resonance at 36.40 ppm.

In the previously discussed carbon-13 spectrum assignments, the resonance at 112.56 ppm was assigned to  $C_7$ . This resonance has a cross peak with proton resonance l at 6.617 ppm in the HETCOR spectrum as shown in Fig. VI.6. Also  $C_{10}$  at 128.09 ppm,  $C_9$  at 113.37 ppm are also correlated to proton resonances k, m at 6.939 ppm and 6.601 ppm, respectively. Thus, proton resonances l, k, m at 6.676 ppm, 6.939 ppm, 6.601 ppm are assigned to  $H_l$ ,  $H_k$ ,  $H_m$  attached on  $C_7$ ,  $C_{10}$  and  $C_9$ , respectively. These assignments are also supported by previous interpretation of the COSY spectrum.

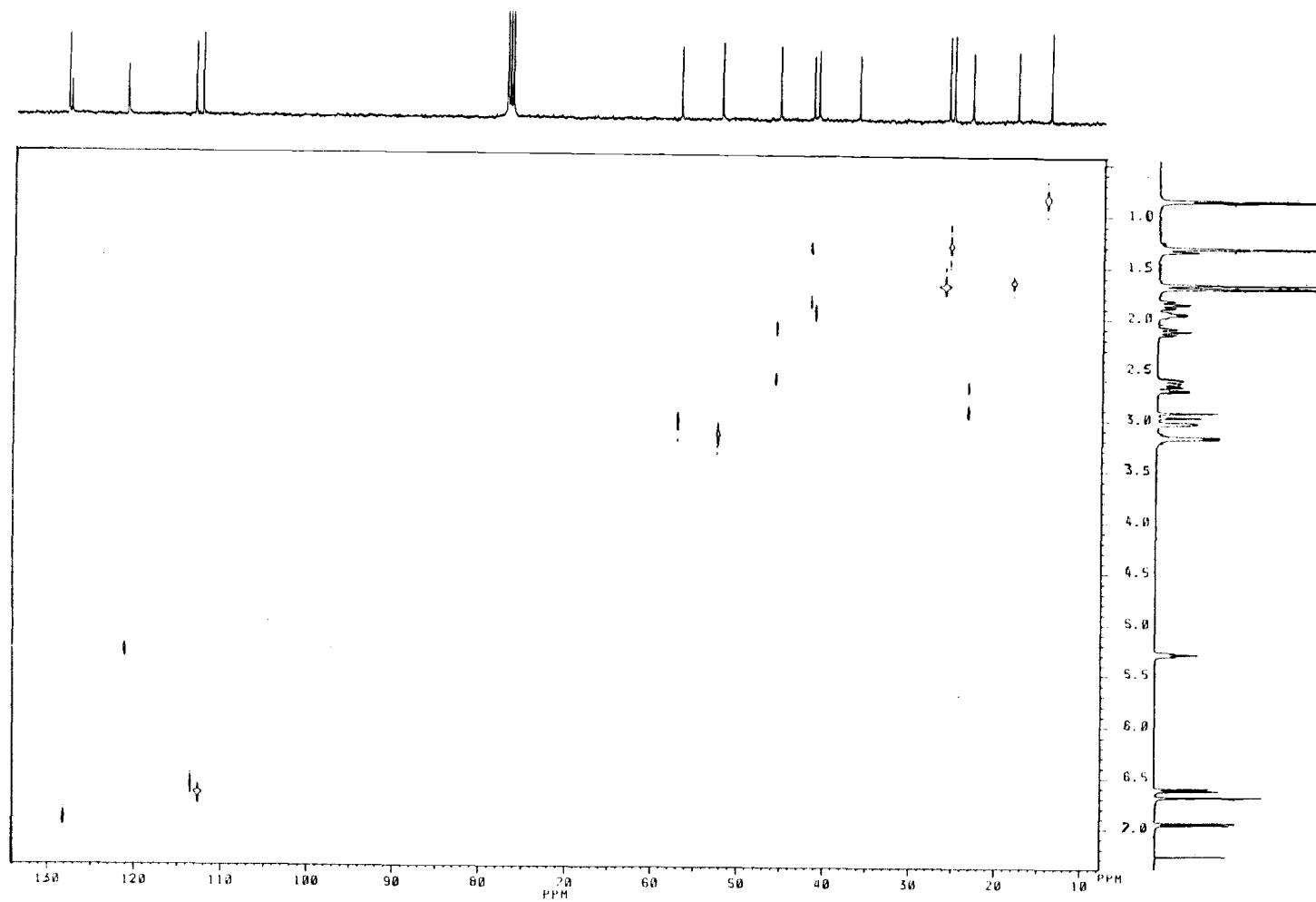


Figure VI.6 Heteronuclear shift correlated (direct C-H bond) spectrum of pentazocine in D-chloroform.

Table VI.4 Heteronuclear chemical shift correlation (direct C-H bond) NMR results for pentazocine.

Chemical Shifts		
Carbon	Proton	Assignments
ppm	ppm	
154.70	---	C <sub>8</sub>
143.15	---	C <sub>13</sub>
135.12	---	C <sub>12</sub>
36.40	---	C <sub>6</sub>
127.73	---	C <sub>18</sub>
112.56	6.617	H <sub>l</sub> -C <sub>7</sub>
128.09	6.679	H <sub>k</sub> -C <sub>10</sub>
113.37	6.594	H <sub>m</sub> -C <sub>9</sub>
45.62	2.579 2.108	H <sub>e</sub> /H <sub>e'</sub> -C <sub>4</sub>
41.71	1.845 1.362	H <sub>f</sub> /H <sub>f'</sub> -C <sub>5</sub>
121.17	5.280	C <sub>17</sub> -H <sub>b</sub>
25.95	1.645	C <sub>20</sub> -H <sub>a</sub>
18.02	1.682	C <sub>19</sub> -H <sub>a'</sub>
52.36	3.163	C <sub>16</sub> -H <sub>c</sub>

Also referring to the carbon assignments of  $C_4$  and  $C_5$ , specific proton resonance assignments are possible between  $H_e-H_{e'}$  and  $H_f-H_{f'}$ . Because they all have cross peaks with corresponding carbons in the HETCOR spectrum (Fig. VI.6), it is concluded that  $H_e-H_{e'}$  are at 2.579 ppm and 2.108 ppm, while  $H_f-H_{f'}$  are at 1.845 ppm and 1.362 ppm.

In the mean time, according to the proton resonance assignment of  $H_b$  at 5.28 ppm, which has a cross peak with the carbon-13 resonance at 121.17 ppm in the contour plot in Fig. VI.3, the resonance at 121.17 ppm is assigned to  $C_{17}$ . Also, the pair of proton resonances at 2.910 ppm and 2.697 ppm previously assigned to  $H_j-H_{j'}$  are correlated to the same carbon-13 resonance at 23.26 ppm by cross peaks, which in turn is assigned to  $C_1$ . Furthermore, carbon-13 assignments follow directly from the knowledge of the proton resonance assignments enabling carbon-13 resonance assignments of 25.95 ppm, 18.02 ppm, 52.36 ppm, 14.17 ppm, 41.15 ppm, 25.41 ppm and 57.08 ppm to  $C_{20}$ ,  $C_{19}$ ,  $C_{16}$ ,  $C_{14}$ ,  $C_{11}$ ,  $C_{15}$  and  $C_2$ , respectively.

There is no cross peak link to any carbon resonance for the proton resonance n at 7.264 ppm. This leaves the assignment of resonance n to the proton attached to the hydroxyl group -OH in the aromatic moiety.

A complete tabulation of all resonance assignments, calculated versus observed, for both proton and carbon-13 are gathered in Table VI.5.

Table VI.5  $^1\text{H}$  and  $^{13}\text{C}$  NMR resonance assignments for pentazocine in D-chloroform.

Proton NMR Resonance		Carbon-13 NMR Resonance		Assignments	
Obs'd	Calc'd	Obs'd	Calc'd	Proton	Carbon
ppm	ppm	ppm	ppm		
1.645	1.6-1.65	18.02	16.9	H <sub>a</sub>	C <sub>19</sub>
1.682	1.6-1.65	25.95	25.3	H <sub>a'</sub>	C <sub>20</sub>
5.280	5.14	121.17	130	H <sub>b</sub>	C <sub>17</sub>
3.163	3.28	52.36	55.4	H <sub>c</sub>	C <sub>16</sub>
3.146	2.88	57.08	56-58	H <sub>d</sub>	C <sub>2</sub>
2.579	2.53	45.62	46-48	H <sub>e</sub>	C <sub>4</sub>
2.108				H <sub>e'</sub>	
1.845	1.86	41.71	35.4	H <sub>f</sub>	C <sub>5</sub>
1.326				H <sub>f'</sub>	
1.290	1.22	25.41	22.1	H <sub>g</sub>	C <sub>15</sub>
0.828	0.87	14.17	19.6	H <sub>h</sub>	C <sub>14</sub>
1.937	1.55	41.15	31.5	H <sub>i</sub>	C <sub>11</sub>
2.697	2.73	23.26	20.2	H <sub>j'</sub>	C <sub>1</sub>
2.910				H <sub>j</sub>	
6.939	6-7	128.09	129	H <sub>k</sub>	C <sub>10</sub>
6.676	6-7	112.56	111.9	H <sub>l</sub>	C <sub>7</sub>
6.601	6-7	113.37	112.7	H <sub>m</sub>	C <sub>9</sub>
7.264	7			H <sub>n</sub>	-OH
		154.70	152.4	-	C <sub>8</sub>
		143.15	150.1	-	C <sub>13</sub>
		135.12	136.5	-	C <sub>12</sub>
		36.40	34.5	-	C <sub>6</sub>
		127.73	117.5	-	C <sub>18</sub>

### 3. Strategic Implications for Metabolite NMR Analysis

Bearing in mind that pentazocine metabolite structural analysis is the ultimate goal, several conclusions can be drawn from this study. First, neither 1D nor 2D techniques alone provided the complete assignments for pentazocine, but in combination a total spectral analysis is possible. Based on this experience, a general strategy for the complete NMR analysis of metabolites is suggested in Fig. VI.7.

As the starting point, an integrated, 1D spectrum of the compound is essential, and with as many assignments as possible. Although assignments at this stage are preliminary, some very useful information such as the number of protons in each region of the spectrum can be obtained, which provides a guideline for further analysis.

The next step is a COSY spectrum to indicate the J coupling pathways, that is, to identify coupled multiplets, in which different methylene groups, for example, can be distinguished and further structural information can therefore be extracted. At this point in the analysis it is worthwhile to establish SPIN-POCKETS in the molecule, that is, sets of spins coupled to one another directly or indirectly, but with no J coupling between the sets. These fragments will contribute to the structure of an entire molecule once the breaks in coupling continuity, at the N atom or the quaternary carbon center that isolates the aromatic moiety in case of pentazocine, are characterized.

An HETCOR spectrum would then give all the carbon-13 assignments,

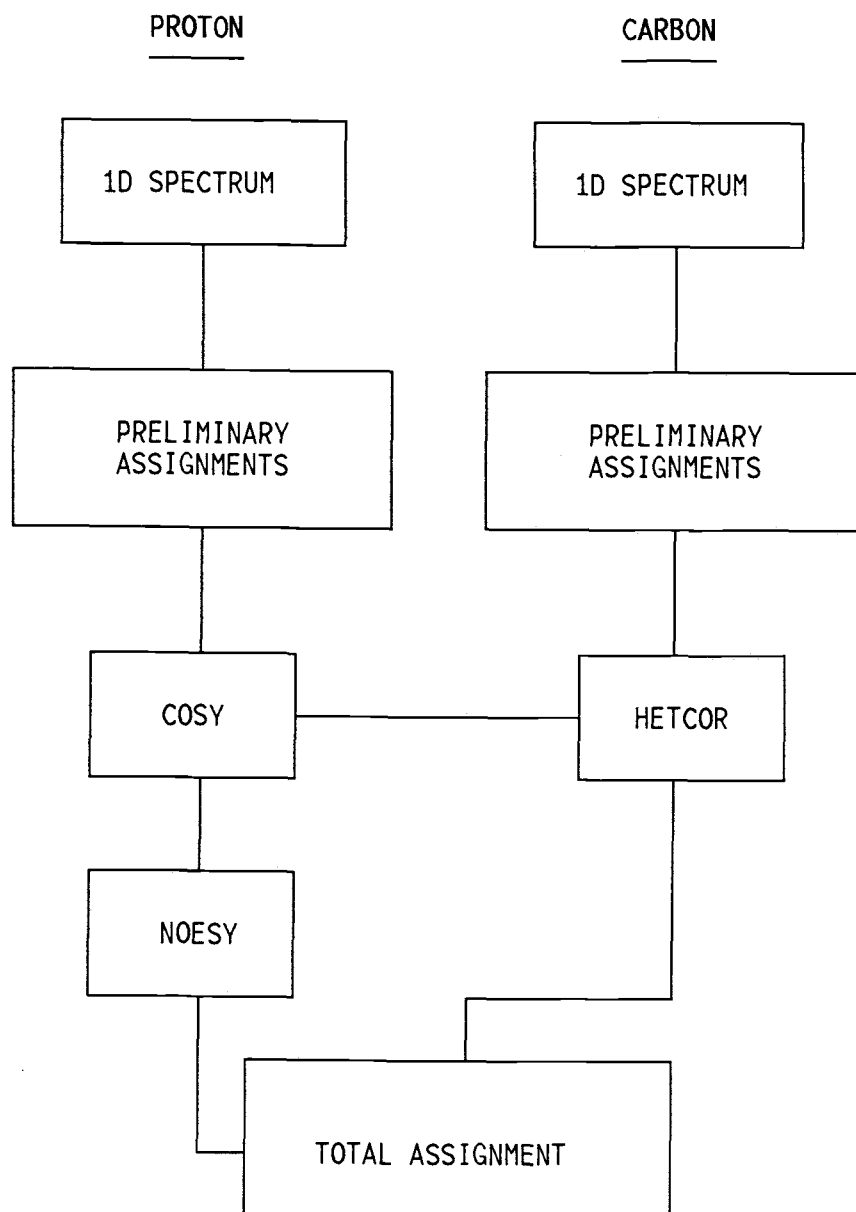


Figure VI.7 Schematic representation of the assignment strategy for the complete NMR analysis of pentazocine metabolite.

and in those cases where some parts of the carbon-13 spectrum are more readily assigned than the proton spectrum, then the assignment may be made in the reverse order.

Although not used in the pentazocine analysis, an NOE experiment would be necessary for the metabolite analysis where the structural information is limited. NOE provides information about the connection between "isolated" substructures through the coupling effect "through space" and conformational details.

Pentazocine was chosen to be the model compound for this pilot analysis because of its structural similarity to its metabolites. It should not be surprising that most of the assignments for pentazocine can be readily applied to its metabolites, which makes metabolite analysis easier even though the quantity and stability of a metabolite is limited. NMR instrumental time is very expensive, and some 2D experiments could become financially disastrous if they are not carefully chosen. Thus, the guidelines established are very important, and they function as the key to successful metabolite analysis.

D-chloroform was used as a solvent in this analysis, mainly because most literature chemical shifts for similar nuclear environments were studied in this solvent, whereas different solvents may change certain chemical shifts [56]. In addition, D-chloroform is very well known for its excellent purity and solubility for most organics: pentazocine is easily dissolved in it. Unfortunately, this choice was found to cause trouble in metabolite analysis, which will be discussed later.

#### 4. Experimental

$^1\text{H}$  NMR and  $^{13}\text{C}$  NMR were recorded on a Bruker AM-400 spectrometer. All  $^{13}\text{C}$  NMR spectra were broadband decoupled. All NMR spectra were obtained using 5 mm NMR tubes. Samples were prepared in  $\text{CDCl}_3$  and the chemical shifts are reported in parts per million (ppm) relative to external tetramethylsilane ( $\text{SiMe}_4$ , 0.00 ppm).

All two-dimensional spectra of pentazocine were recorded at ambient temperature with a Bruker AM-400 spectrometer equipped with an Aspect 3000 computer operating in the Fourier transform mode with quadrature detection. Standard Bruker pulse programs were used.

The two-dimensional  $^1\text{H}$ - $^1\text{H}$  shift correlated (COSY-45) data for pentazocine was acquired at a sweep width of 3105.6 Hz (1024 data points) in the  $F_2$  domain; 256 FIDs (8 scans plus 2 dummy scans for each FID) were accumulated with 322- $\mu\text{sec}$  increments and a 3- $\mu\text{sec}$  starting delay. A 1 sec recycle delay was inserted between scans to allow spin relaxation. The digital resolution was 3.033 Hz/pt in both dimensions. A sinebell window function was applied to the Fourier transformation to enhance resolution. The COSY was then summarized about the diagonal line.

The heteronuclear  $^1\text{H}$ - $^{13}\text{C}$  shift correlated (HETCOR) experiment for pentazocine was performed with a 16129 Hz (4096 data points) spectral width in the  $^{13}\text{C}$  ( $F_2$ ) dimension and a  $\pm 1450$  Hz (512 data points) window in the  $^1\text{H}$  ( $F_1$ ) dimension; 256 FIDs (128 scans plus 2 dummy scans each) were acquired with 172- $\mu\text{sec}$  increments and a 3- $\mu\text{sec}$  starting delay. A 1 sec recycle delay was used between scans. The

digital resolution for the  $^{13}\text{C}$  ( $F_2$ ) and  $^1\text{H}$  ( $F_1$ ) dimensions were 3.938 and 5.664 Hz/pt, respectively. A Gauss notification was applied to both dimensions before Fourier transformation to enhance resolution ( $F_2$ : LB=-4, GB=0.9;  $F_1$ : LB=-5, GB=0.5).

## VII. COMPLETE STRUCTURAL ELUCIDATION OF A PENTAZOCINE METABOLITE

by

Guang Xiao and Edward H. Piepmeier

Department of Chemistry

Oregon State University

Corvallis, OR 97331

and

A. Morrie Craig

School of Veterinary Medicine

Oregon State University

Corvallis, OR 97331

Chapter VI and VII will be combined for submission to  
the Journal of American Chemical Society

## 1. Introduction

During the course of the separation and GC/MS studies, it has been found that hydroxylation and methylation metabolic transformations have taken place in the aromatic ring of the pentazocine molecule. It is also clear that, in the mean time, some of the metabolites that have undergone hydroxylation and methylation have also undergone side-chain oxidative metabolic transformation, from which trans-OH, cis-OH or trans-COOH at the end of the side-chain are produced. Consequently, besides the isomers resulted from trans- or cis-OH at the end of the side-chain, an additional methoxyl group is attached to the aromatic ring of each of these metabolites produced, and two different placements of the methoxyl group in the aromatic ring cause pairs of isomers among these metabolites (Fig. IV.11 and IV.27). This isomerism is also found in a pair of isomers of metabolites, MET1 and MET2, whose structures are the same as pentazocine except that an additional methoxyl group is attached to different positions in the aromatic ring. Although the structure changes on the side-chain of pentazocine after the biotransformation can be characterized by GC/MS study, the position of the methoxyl group in the aromatic ring remains unclear. Therefore, the identification of the methoxy group position in the metabolites by more powerful spectroscopic tools such as NMR is needed for the complete structural characterization of the metabolite MET1.

Complete and accurate structural characterization of a molecule as complex as pentazocine metabolite MET1 by  $^1\text{H}$  and  $^{13}\text{C}$  NMR is a formidable task. Nevertheless, NMR study of the parent compound pentazocine described in the previous chapter laid the groundwork for the structural analysis of MET1, through which a two-dimensional NMR analysis protocol has been devised. In the NMR study of metabolite MET1 described in this chapter, one-dimensional  $^1\text{H}$  and  $^{13}\text{C}$  NMR spectra are used to obtain general information about MET1, such as the numbers of distinct protons and carbons. Subsequently,  $^1\text{H}$  and  $^{13}\text{C}$  NMR spectral information are correlated to each other via direct and long-range  $J_{\text{C-H}}$  couplings in HETCOR and LR HETCOR. Moreover, spin-pockets are established by using COSY. These spin-pockets are then identified on the basis of their  $^1\text{H}$  and  $^{13}\text{C}$  chemical shift data. Finally, NOE experiments are performed to obtain spatial information about the molecule, and the structural elements thus obtained are assembled using NOSEY, yielding the complete structure of the metabolite MET1.

Most of the structural characterization of metabolites by NMR is complicated by the fact that the synthetic reference is not readily available. The inherent difficulty of this task is somewhat reduced by the fact that the structure of the metabolites will retain some or most of the original substructure of the parent compound, which can be used as a model compound. By taking this advantage, the previous assignments of the  $^1\text{H}$  and  $^{13}\text{C}$  NMR spectra of pentazocine can be used as a reference in the MET1 NMR analysis. Nonetheless, differences especially in the aromatic region do exist. As will be seen, because

of solvent effects, some of the NMR data analysis, such as carbon-13 resonance assignments could even become the subject of "pattern recognition". Thus, some parts of MET1 NMR analysis rely on powerful two-dimensional NMR techniques where little structural information needs to be known prior to the analysis.

## 2. Discussion and Results

Solvent selection. Solvent selection plays an important role in the NMR study: not only must the spectral resolution provided by the chosen solvent be excellent, but also the solubility of the analyte in the chosen solvent should be good. In the model compound pentazocine NMR study, D-chloroform is chosen as the solvent because it provides excellent solubility and well resolved spectra, and it is also the solvent for most of the published chemical shifts for well-studied similar nuclear environments. D-chloroform was also selected at first for metabolite MET1 NMR study because of its similarity with the pentazocine parent compound.

Fig. VII.1 shows a 400-MHz proton NMR spectrum obtained for MET1 in D-chloroform under the same instrumental conditions as those used for the pentazocine analysis. In Fig. VII.1, although certain characteristics of MET1 predicted by GC/MS are shown (for example, the resonance peak at 7.264 ppm shows the presence of a hydroxyl group -OH in the molecule), the spectrum obtained is rather noisy and individual assignments are difficult. In a "semi-quantitative" study of metabolites by GC/MS, it is concluded that the most concentrated metabolite in greyhound urine is MET1, whose concentration is only

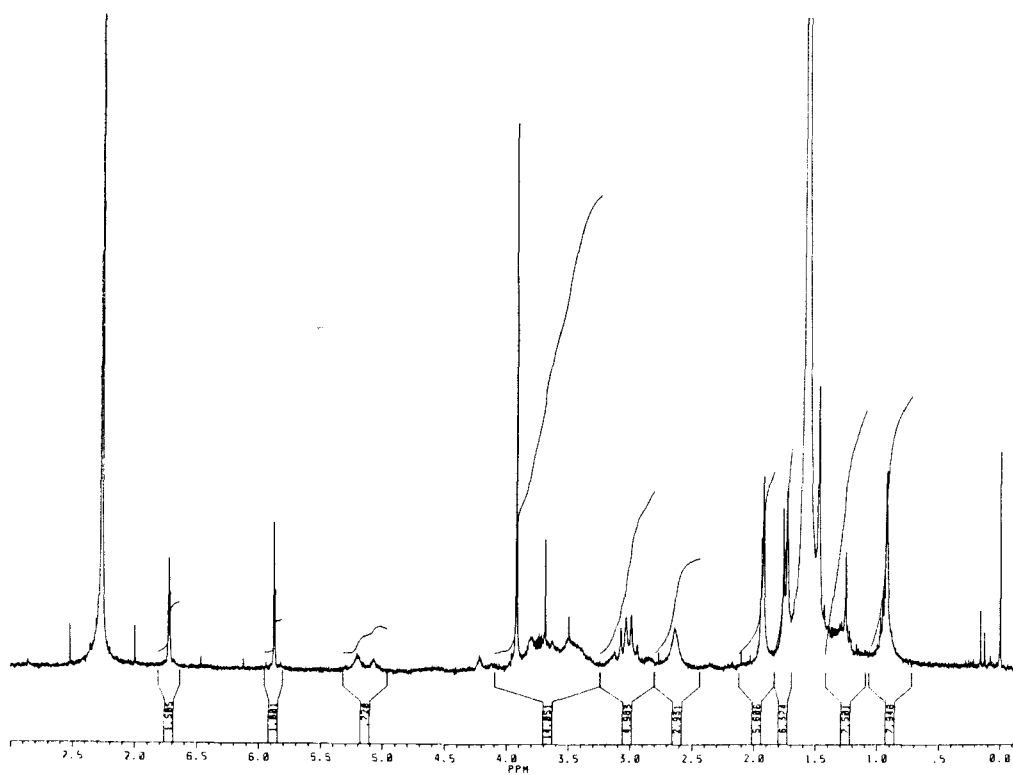


Figure VII.1 400-MHz  $^1\text{H}$  NMR spectrum of pentazocine metabolite MET1 in D-chloroform.

about 1/20 of the unchanged pentazocine concentration in the urine, and the stability of the metabolites is also uncertain. Hence, the small amount of the MET1 sample could be the major reason for such poor spectral appearance, although the estimated amount of MET1 collected right before dissolving in D-chloroform was above 7 mg using the "weigh-by-difference" method.

A massive effort to collect a larger sample size was made, and the collected amount was estimated to be about 5 times larger than that of the previous collection. In the mean time, the solvent selection was reconsidered.

It is well known that the polarities of metabolites are usually higher than that of their parent drug [14]. Therefore a more polar solvent D-acetone was chosen. Fig. VII.2 shows 400-MHz proton, and carbon-13 spectra of MET1 in D-acetone. The spectra obtained are obviously better, but the carbon-13 spectrum is still noisy with unresolved peaks. It is noted that D-acetone may be saturated since some white crystals precipitated. D-methanol, an even more polar solvent was then used to provide better solubility than that of D-acetone.

Fig. VII.3 shows 400-MHz proton NMR spectrum for MET1 in D-methanol. Clearly, despite the fact that the resonance responsible for the hydroxyl function group becomes ambiguous, and the residual H<sub>2</sub>O in D-methanol is noticeable in the spectrum, it provides much better solubility and spectral resolution.

<sup>1</sup>H NMR. Similar arguments for the proton resonance assignments of the MET1 proton NMR spectrum (Fig. VI.3) can be imposed as those used in the pentazocine model molecule analysis. All carbons and

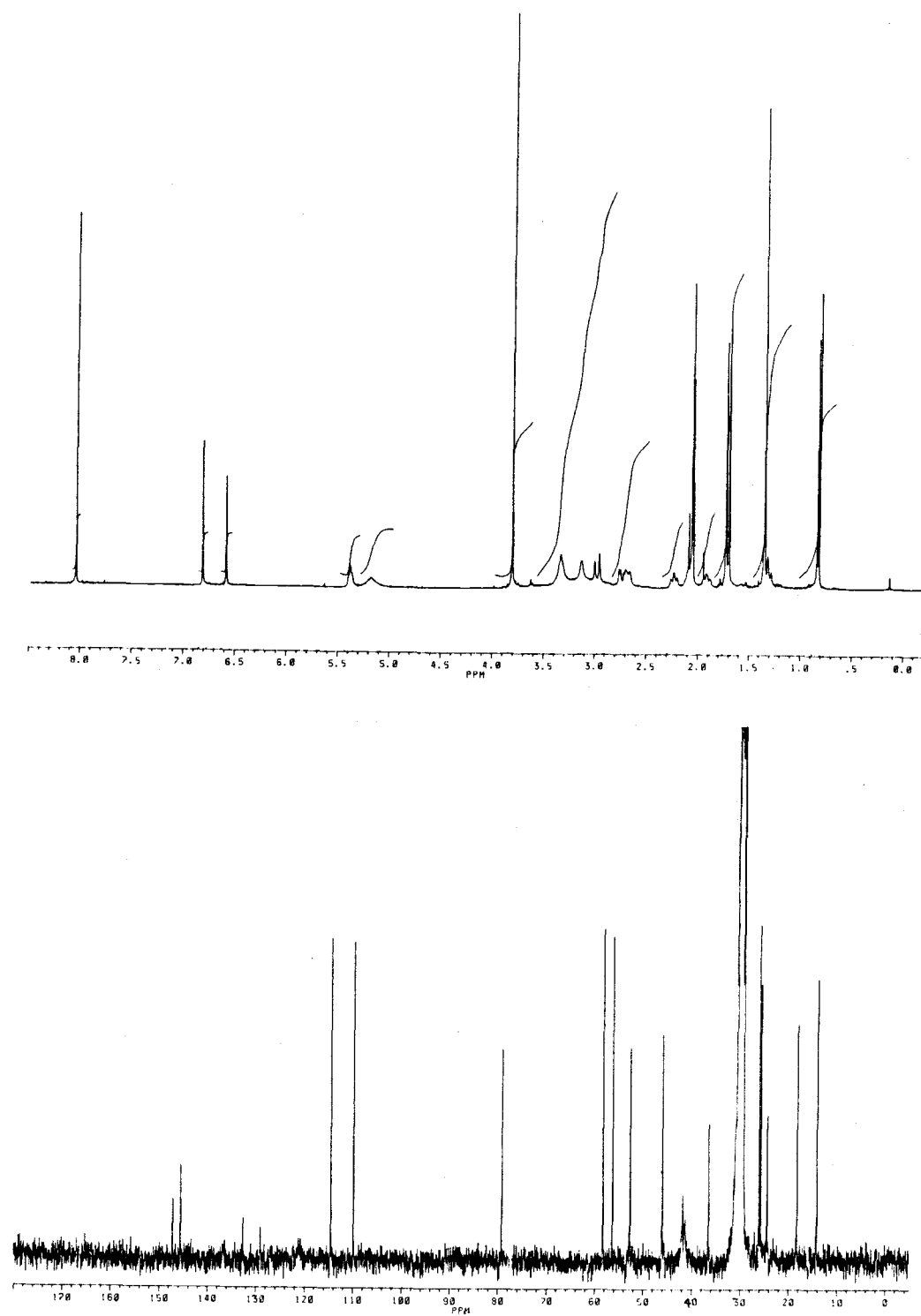


Figure VII.2 NMR spectra of pentazocine metabolite MET1 in D-acetone: (a) 400-MHz  $^1\text{H}$  NMR spectrum and (b)  $^{13}\text{C}$  NMR spectrum.

protons in MET1 will be designated with the same number as those in reference compound pentazocine (Fig. VI.1) if they are in the same nuclear environments. Table VII.1 lists the possible resonance assignments for the 1D proton NMR spectrum of MET1 (Fig. VII.3) made by the direct comparison with those of pentazocine at this stage.

It is noticed that the overall chemical shifts are further downfield for MET1 in D-methanol compared with pentazocine in D-chloroform. Since the MET1 structure is predicted to be similar to that of pentazocine except for the aromatic moiety, the differences here are presumably due to using a different solvent, D-methanol, as well as small structural differences.

It was demonstrated at an early stage in the development of the NMR technique that when a polar molecule is dissolved in a relatively polar solvent, it induces a reaction field which then tends to increase the shielding constant, and thus a downfield-shift [82,83]. That is, the higher polarity of D-methanol has an overall increase in shielding effect, and hence protons in the same nuclear environment would have further downfield chemical shifts in D-methanol than those in the less polar solvent D-chloroform.

The proton resonances of MET1 observed in three different solvents are summarized in Table VII.2. As can be seen there is indeed an overall further downfield shift with an increase in solvent polarity from D-Chloroform to D-Methanol. The differences between the MET1 proton resonances and the calculated ones listed in all of the tables are also due to the fact that most of the calculated chemical shifts are cited from literature values based on the use of D-chloroform as the solvent.

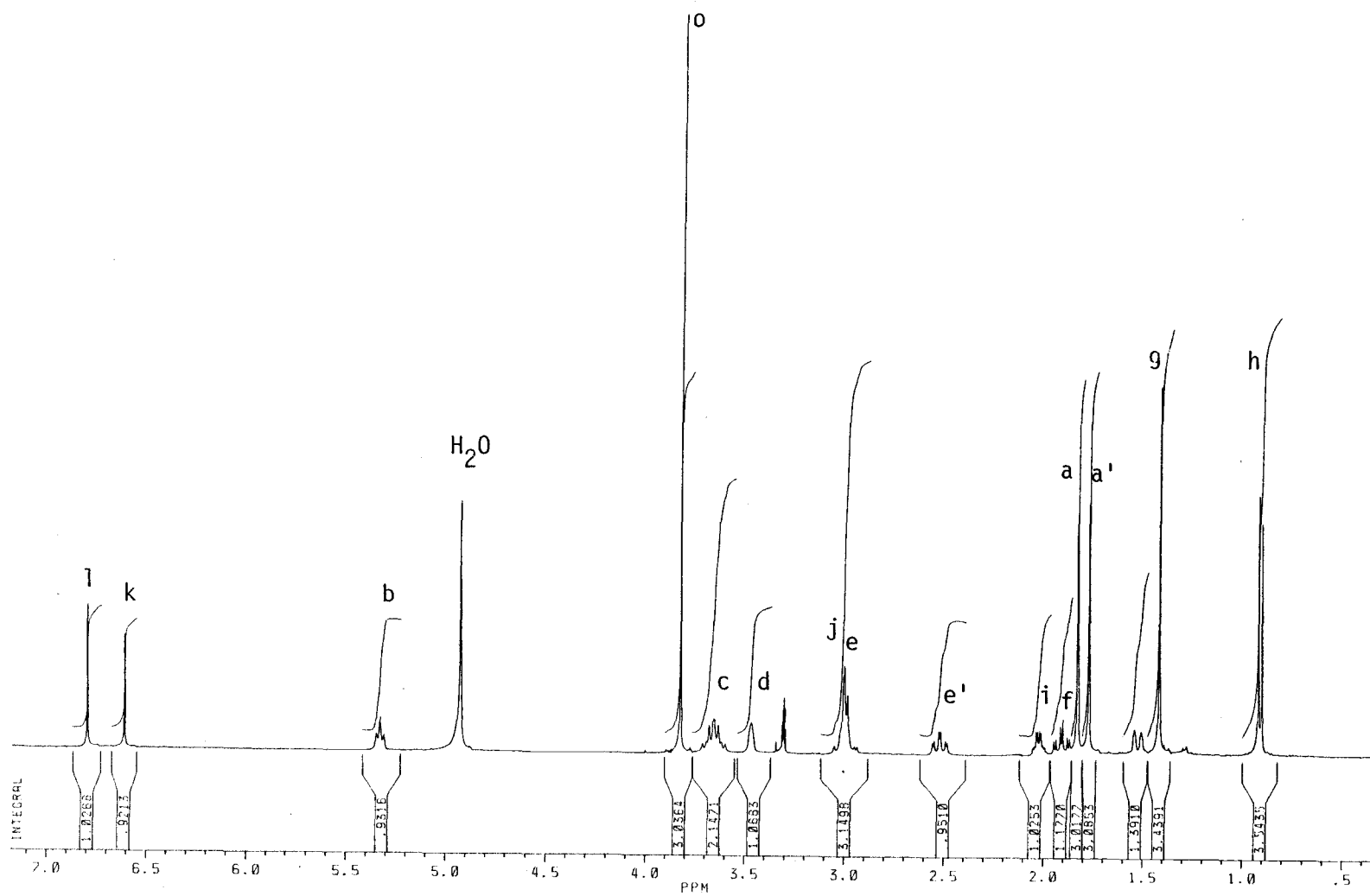


Figure VII.3 400-MHz  $^1\text{H}$  NMR spectrum of pentazocine metabolite MET1 in D-methanol.

Table VII.1 The probable  $^1\text{H}$  NMR resonance assignments for pentazocine metabolite MET1.

Possible Assignment	Obs.(ppm)		Cal.(ppm)	Ref.
	PENT	MET1		
Aromatic Protons	6.939 6.676 6.601	6.792 6.607	6-7	[56]
H <sub>b</sub>	5.28	5.324	5.14	[56]
H <sub>a</sub> or H <sub>a'</sub>	1.645 1.682	1.768 1.826	1.6-1.65	[56]
H <sub>h</sub>	0.828	0.909	0.87	[56]
H <sub>g</sub>	1.290	1.414	1.25	[76]
H <sub>c</sub>	3.163	3.648	3.20	[56]
H <sub>o</sub>		3.818	3.86	[56]

Table VII.2 The observed  $^1\text{H}$  NMR resonance of pentazocine metabolite MET1 in three different deuterated solvents.

Resonances Observed	Proton NMR Chemical Shift of MET1 in Three Different Deuterated Solvents (ppm)		
	<u>D-Methanol</u>	<u>D-Acetone</u>	<u>D-Chloroform</u>
a	1.826	1.726	
a'	1.768	1.698	
b	5.324	5.375	5.235
c	3.648	3.329	
d	3.462	3.130	
e	2.982	2.755	
e'	2.518	2.691	
f	1.905	1.914	
f'	1.520		
g	1.414	1.350	
h	0.909	0.828	
i	2.028	2.229	
j	3.021	3.002	
j'		2.956	
k	6.607	6.583	5.877
l	6.792	6.810	6.742
n		8.034	7.263
o	3.818	3.803	3.920

Resonance  $\delta$  at 3.818 ppm integrates to three protons and shows the distinct character of the methoxy group [56],  $-\text{OCH}_3$ , which amounts to 30 mass units, and is in agreement with the results from GC/MS analysis. Resonance  $\delta$  at 3.818 ppm is therefore assigned to protons attached to a methoxy group ( $\text{H}_\text{o}$ ).

Another important feature of 1 D proton NMR spectrum of MET1 is that the total number of aromatic protons amount to two in MET1 instead of three in pentazocine, indicating an additional attachment in the aromatic portion in the MET1 structure. It will be shown later that the absence of this aromatic proton in MET1 results from the attachment of the methoxy group on the aromatic ring.

$^{13}\text{C}$  NMR. In the proton broadband-decoupled carbon-13 NMR spectrum of MET1 in D-acetone (Fig. VII.2b), although the upfield carbon-13 resonances appear to be similar to those of the pentazocine model compound, the downfield carbon-13 resonances are quite different, and the total number of recognizable carbon-13 signals is less than what would be expected.

The proton broadband-decoupled carbon-13 NMR spectrum of MET1 in D-methanol was also taken, and is shown in Fig. VII.4. Again, since a more polar solvent is used in this case, the precise match of MET1 carbon-13 resonances to those of pentazocine is not expected for most parts of the molecule, although their structures are predicted to be similar.

The comparison of the carbon-13 spectrum of MET1 and that of pentazocine shows again the overall further downfield shifts. It is also noticeable that the upfield portion of the MET1 carbon-13 spectrum ( $\delta < 100$  ppm) shows a similar pattern to that of pentazocine.

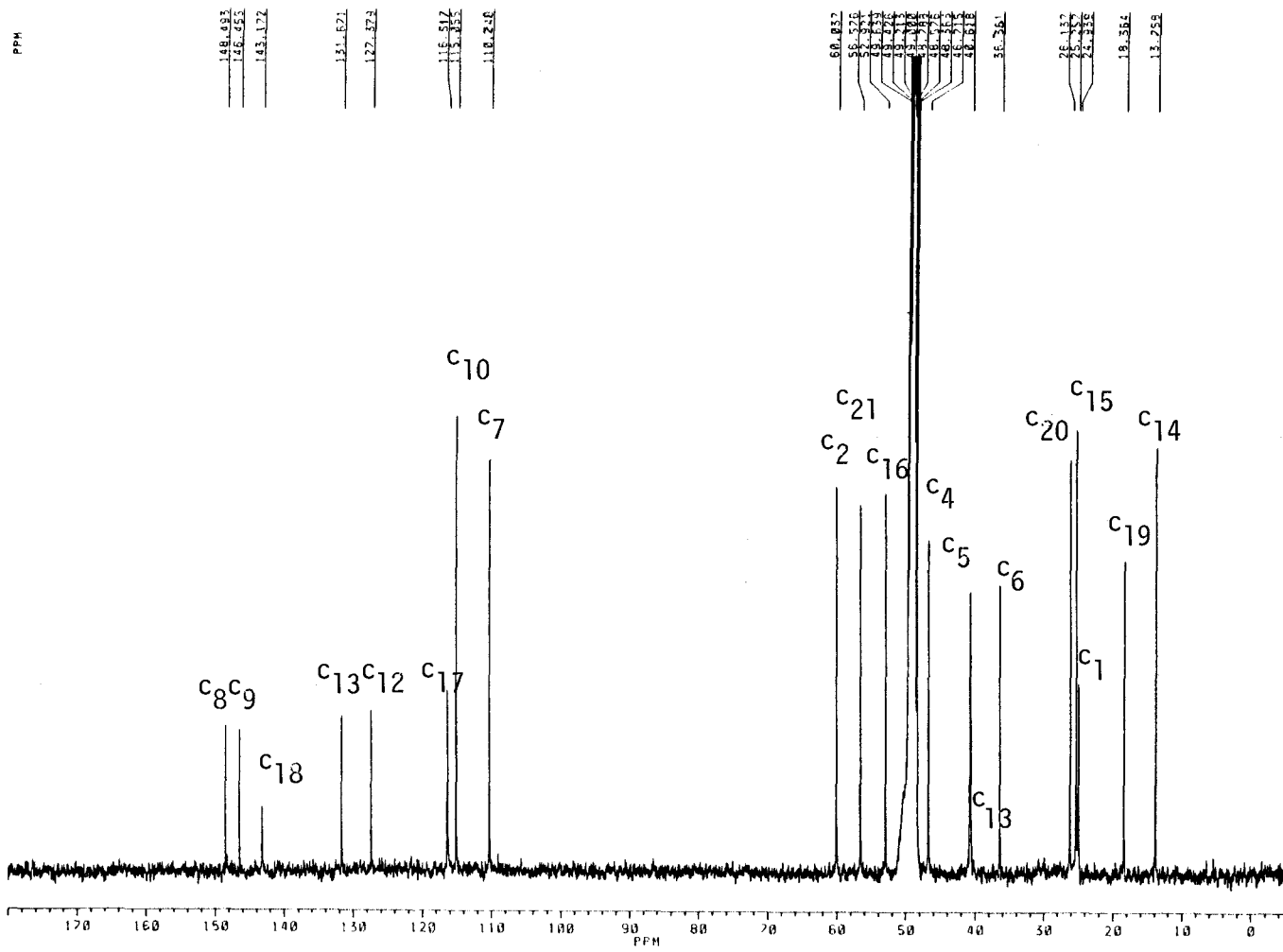


Figure VII.4 Proton broadband-decoupled  $^{13}\text{C}$  NMR spectrum of pentazocine metabolite MET1 in D-methanol.

Therefore, some preliminary carbon-13 resonance assignments for  $\delta < 100$  ppm for MET1 are made by means of pattern similarities. Table VII.3 shows the results of the carbon-13 resonances assignments for MET1 along with those of corresponding pentazocine carbons for comparison.

Since the exact position of where the methoxy group is attached to the aromatic ring is uncertain at this point, the calculation of the carbon-13 resonances for the carbons in the MET1 aromatic ring portion by the additivity rule is impossible. Also, because of the attachment of the methoxy group to the aromatic ring in MET1, carbon-13 resonances for the carbons in this portion of the molecule are expected to show a great deal of difference to those of the corresponding carbons in pentazocine. Hence, assignments based on a direct comparison would be impossible. That is, the structure of the aromatic portion of MET1 cannot be elucidated from carbon-13 resonance study alone. Therefore, besides the preliminary assignments made from 1D proton and carbon-13 NMR, the elucidation of the MET1 structure is heavily dependent upon the assistance of 2D NMR techniques, even though a model compound pentazocine is available.

COSY,  $^1\text{H}$ - $^1\text{H}$  shift correlation NMR. Although the model compound is available for the MET1 NMR analysis, 1D proton and carbon-13 NMR provided little unambiguous information about the MET1 structure except the existence of a methoxy group attached on the aromatic ring. All the assignments made for both the 1D spectra are preliminary.

In order to get an accurate structural elucidation of MET1, a COSY experiment is performed for MET1, which determines the proton coupling

Table VII.3 The possible assignments of  $^{13}\text{C}$  resonances of pentazocine metabolite MET1 based on the direct comparison to  $^{13}\text{C}$  resonance of pentazocine.

Preliminary Carbon Assignment	Carbon-13 NMR Resonance		
	Pentazocine		MET1
	<u>Obs'd(ppm)</u>	<u>Calc'(ppm)</u>	<u>Obs'd(ppm)</u>
C <sub>1</sub>	23.26	20.2	24.94
C <sub>2</sub>	57.08	56-58	60.04
C <sub>4</sub>	45.62	46.5-48.2	46.72
C <sub>5</sub> *	41.71	35.4	40.62
C <sub>6</sub>	36.40	34.5	36.36
C <sub>15</sub>	25.41	22.1	25.26
C <sub>11</sub> *	41.15	31.5	40.69
C <sub>14</sub>	14.17	19.6	13.76
C <sub>16</sub>	52.36	55.4	52.92
C <sub>20</sub>	25.95	25.3	26.14
C <sub>19</sub>	18.02	16.9	18.36
C <sub>21</sub>	-----	54.1 **	56.58

\* Although Carbon-13 resonances for C<sub>5</sub> and C<sub>11</sub> appear to be unresolved in the carbon-13 spectrum for MET1 in D-methanol, the "close-up" and proton/carbon-13 correlated NMR (see Table V) show 0.07 ppm difference for these two resonances.

\*\* Cited from reference [56] table VII in page 265.

patterns and helps in the interpretation of its structure in terms of the number of nearby protons.

A COSY spectrum of MET1 in D-methanol is shown in Fig. VII.5. Table VII.4 summarizes J-couplings observed in the MET1 COSY spectrum. Beginning with the resonance b identified from the 1D NMR spectrum as responsible for  $H_b$ , which is located as the response on the diagonal line corresponding to 5.324 ppm, three pairs of off-diagonal elements can be observed, labeled a/b, a'/b and b/c, which correlate with resonances a, a' and c at 1.768, 1.826 and 3.648, respectively. At this point, logical possibilities, to which  $H_b$  is correlated, are methylene protons  $H_c$  attached to  $C_{16}$ , and two methyl groups attached to the end of the double bond,  $H_a$  and  $H_{a'}$ .

Since the integral of resonance c indicates two protons, a methylene group, it is concluded that resonance c at 3.648 ppm belongs to the  $H_c$  protons. It is noticed that instead of showing coupling correlation with only one of two terminal methyl groups in the COSY spectrum of pentazocine, both  $H_a$  and  $H_{a'}$  are coupled with  $H_b$  and  $H_c$  in this case. That is, no specific assignments for  $H_a$  and  $H_{a'}$  can be done at this point, and an NOE experiment is necessary.

The upfield resonance h at 0.909 ppm, which accounts for three protons, is correlated with resonance i at 2.028 ppm that accounts for one proton, and resonance i is coupled with the farther downfield resonance d at 3.462 ppm, which is also accounts for a single proton. Since it is responsible for a methyl group, resonance h at 0.909 ppm could be the  $H_h$  protons attached to  $C_{14}$  as suspected from 1D proton NMR. If this were the case, then resonance i would be responsible for  $H_i$  attached to  $C_{11}$ .

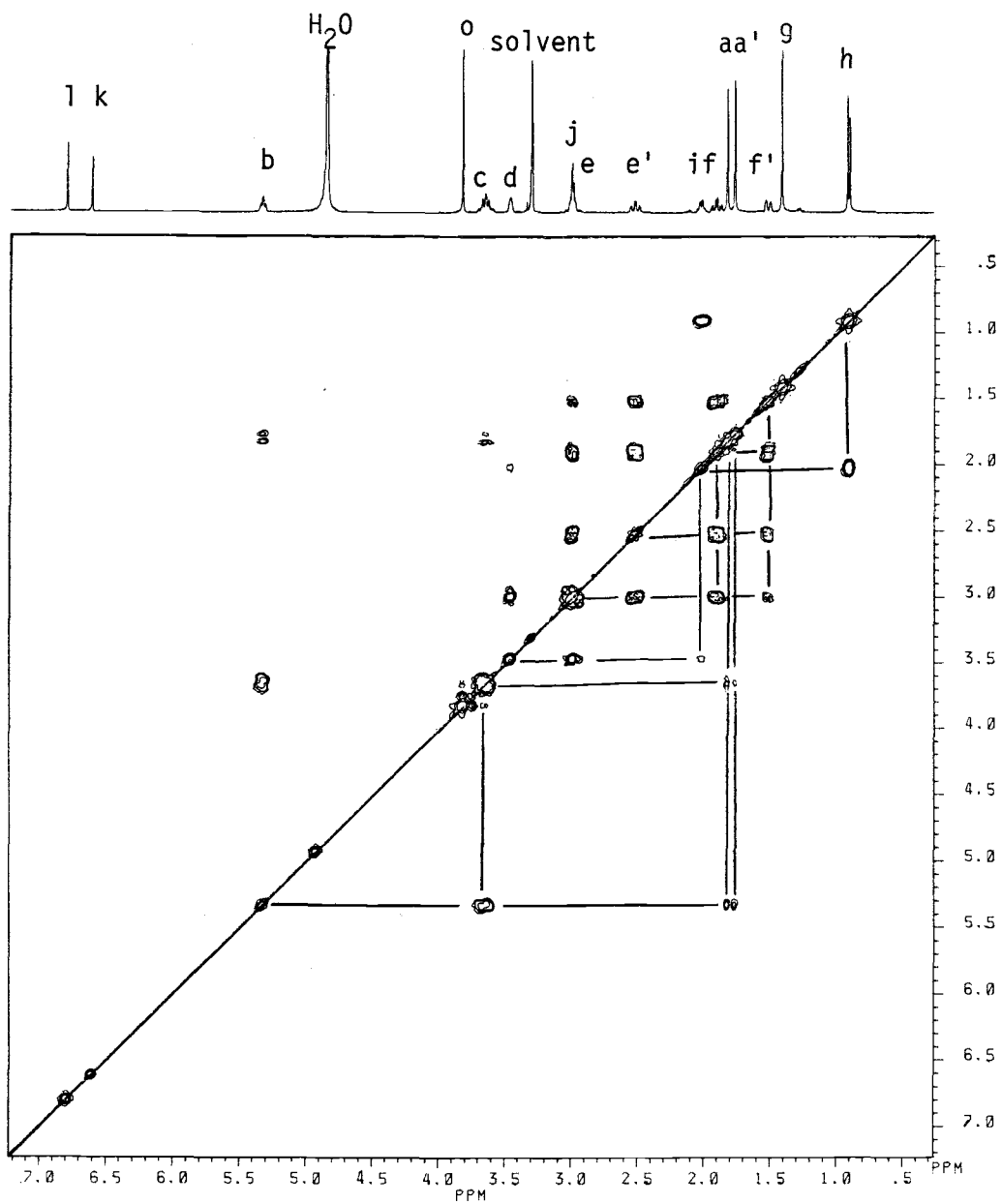


Figure VII.5 COSY spectrum of pentazocine metabolite MET1 in D-methanol

Table VII.4a Proton J-couplings in pentazocine metabolite MET1 observed by COSY experiment.

<u>Normal Couplings</u>		<u>Weak Couplings</u>	
Pentazocine	MET1	Pentazocine	MET1
a/b, a/c	a/b, a/c a'/b, a'/c		
b/a, b/c	b/a, b/c b/a'		
c/a, c/b	c/a, c/a', c/b		
d/j'	d/j	d/i	d/i
e/e', e/f, e/f'	e/e', e/f, e/f'		
e'/e, e'/f, e'/f'	e'/e, e'/f, e'/f'		
f/e, f/e', f/f'	f/e, f/e', f/f'		
f'/e, f'/e', f'/f	f'/e, f'/e', f'/f		
h/i	h/i		
i/h	i/h	i/d	i/d
j/j'	---		
j'/d, j'/j	---		
k/m	---		
		l/m	--
m/k	---	m/l	--

Just like for pentazocine, the COSY spectrum for MET1 shows off-diagonal responses indicating coupling correlations between resonances f, f' at 1.905 ppm and 1.520 ppm, e, e' at 2.982 ppm and 2.518 ppm. J-coupling constants for f-f' and e-e' (Table VII.4b) also indicate that both of them should arise from the geminal coupling. Furthermore, two pairs of resonances f and f', as well as e and e' are also coupled to each other (off-diagonal responses f/e, f/e', f'/e and f'/e' in Fig. 6). Thus, the assignment for resonances f, f', e, e' have to be among methylene protons in the N-ring portion of the structure, H<sub>f</sub>-H<sub>f'</sub> and H<sub>e</sub>-H<sub>e'</sub>. Continuing from resonance j at 3.021 ppm, which accounts for two protons and is overlapped with resonance e at 2.982 ppm, there is another off-diagonal response, d/j, that correlates with resonance d at 3.462 ppm. Unlike for pentazocine, the off-diagonal response d/j is the only coupling correlation for resonance j, which accounts for two protons, in MET1. Again, resonance d is also coupled with i at 2.028 ppm, which is responsible for a methine proton. If the previous suggestion were true that resonance i at 2.028 ppm belongs to H<sub>i</sub> attached to C<sub>11</sub>, then resonance d would have to be responsible for the only other unassigned methine proton H<sub>d</sub>, and therefore resonance j at 3.021 ppm would be responsible for the methylene protons H<sub>j</sub> and H<sub>j'</sub>, although they are magnetically nonequivalent protons appearing as two well resolved resonances for pentazocine in D-chloroform.

Resonance g at 1.414 ppm has no off-diagonal response correlating to any other resonances, and it accounts for a methyl group. The reasonable assignment of resonance g at this point appears to be H<sub>g</sub> attached to C<sub>15</sub>.

Table VII.4b Proton J-coupling constants observed in pentazocine metabolite MET1

Proton	Coupled Proton (Coupling Constant, Hz)	Multiplicity*
H <sub>a</sub>		s
H <sub>a'</sub>	H <sub>b</sub> (<1)	d
H <sub>b</sub>		m
H <sub>c</sub>		m
H <sub>d</sub>		bs
H <sub>e</sub>		m
H <sub>e'</sub>	H <sub>e</sub> (13), H <sub>f</sub> (13) H <sub>f'</sub> (4)	m
H <sub>f</sub>	H <sub>f'</sub> (13), H <sub>e</sub> (3)	m
H <sub>f'</sub>	H <sub>e'</sub> (13) H <sub>f</sub> (13), H <sub>e'</sub> (3)	m
H <sub>g</sub>		s
H <sub>h</sub>	H <sub>i</sub> (7)	d
H <sub>i</sub>	H <sub>h</sub> (7), H <sub>d</sub> (3)	m
H <sub>j</sub> (H <sub>j'</sub> )		bs
H <sub>k</sub>		s
H <sub>l</sub>		s
H <sub>o</sub>		s

\* Only those of the multiplicities observed in 1D Proton NMR : s-singlet, d-doublet, t-triplet, m-multiplet.

The downfield resonances k and l at 6.607 ppm and 6.792 ppm are known to be attributed to the protons on the aromatic ring according to the previous discussion. As far as the coupling network is concerned, they are not only isolated from the rest of the molecule, but also isolated from each other. There could be no unambiguous assignment for resonances k and l based on the COSY spectrum of MET1.

Like in the case of pentazocine, COSY spectral information has established a similar coupling network for MET1. That is, four "spin-pockets" consist of an aromatic ring, side-chain, methyl group H<sub>g</sub>, and the rest of the molecule. Each one of these spin pockets may have couplings within itself, but each is isolated from the others. Again, the coupling continuity breaks at either the nitrogen atom or the quaternary carbon center. Hence, as predicted from the GC/MS analysis, MET1 has a similar molecular skeleton as that of pentazocine.

Unlike that of pentazocine, the COSY spectrum for MET1 shows less confirmative information about the aromatic ring portion, which is nonetheless the main suspected difference between the MET1 and pentazocine structures. For other parts of the molecule, although direct comparisons can still enable some of the proton assignments, most of them are still only suggestions, which need to be confirmed by further investigations. It is thus necessary to conduct NOE experiments to establish the connections between the "spin-pockets", to locate the methoxyl group in the aromatic ring.

HETCOR, <sup>1</sup>H-<sup>13</sup>C heteronuclear shift correlation (direct C-H bond) NMR. Although the structural information for MET1 extracted from the NMR analyses so far shows a great deal of similarity to its model

compound pentazocine as was expected from GC/MS analysis, it is noted that important differences do exist. Most of the assignments so far are made by pattern comparisons, since the directly calculated chemical shifts especially for carbon-13 NMR are not available. As proposed in the analysis protocol along with the pentazocine analysis, the next step would be to use proton/carbon-13 heteronuclear shift-correlation NMR to explore the connections between carbons and their coupling protons, and thus establish a more complete picture of the molecule.

Fig. VII.6 presents the proton/carbon-13 shift-correlated 2D NMR spectrum of MET1 in D-methanol in the form of a contour plot. The cross peaks in the contour plot indicate partial magnetization transfer between a specific carbon atom and its directly bound proton via  $^1J_{C-H}$  (one C-H bond) scalar coupling. In this way the cross peaks correlate the resonance of each carbon atom to the corresponding proton resonance of its directly bound protons.

Table VII.5 shows the correlations observed between carbons and their directly bound protons in MET1 as well as the possible assignments made by these correlations.

In Fig. VII.6, five carbon-13 resonances in the downfield part of the carbon-13 resonance axis ( $\delta = 127.38, 131.67, 143.17, 146.46,$  and  $148.49$  ppm) as well as the resonance at  $36.36$  ppm do not show cross peaks to proton resonances. This finding implies the absence of  $^1J_{C-H}$  coupling; that is, these carbon-13 resonances originate from quaternary carbon atoms. The direct comparison with pentazocine would enable the assignment of the carbon-13 resonance at  $34.50$  ppm to  $C_6$  in MET1, and the resonance at  $143.17$  ppm to  $C_{18}$ .

As discussed in the 1D proton NMR data analysis section, the

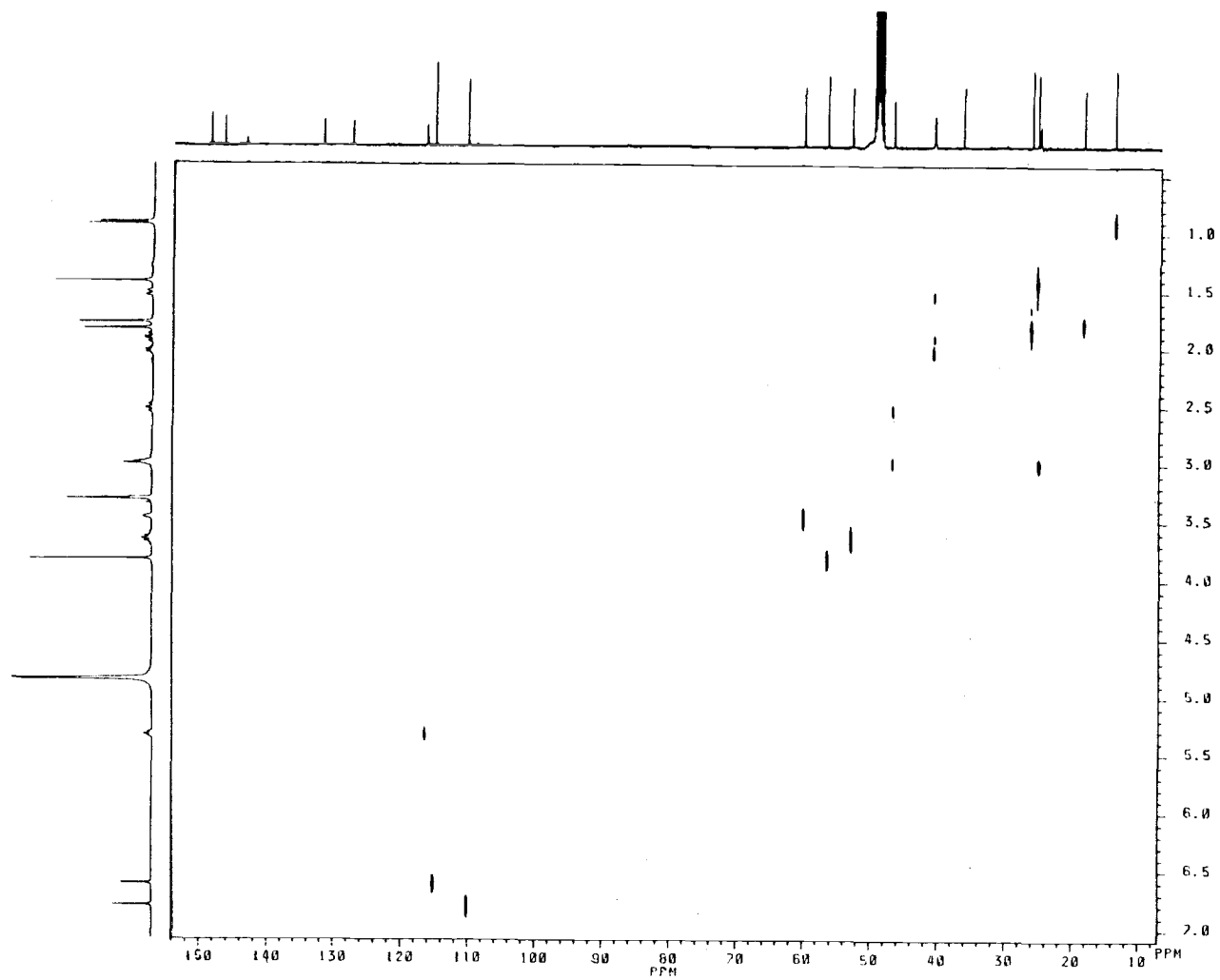


Figure VII.6 Heteronuclear shift correlated (direct C-H bond) spectrum of pentazocine metabolite MET1 in D-chloroform.

Table VII.5 Heteronuclear chemical shift correlation (via coupling through direct C-H bond) NMR results for pentazocine metabolite MET1.

Chemical Shifts				
Carbon ppm		Proton ppm		Assignments
MET1	PENT	MET1	PENT	
148.49	154.70	----	----	C <sub>8</sub>
146.46	143.15	----	----	C <sub>13</sub>
127.38	127.73	----	----	C <sub>12</sub>
36.36	36.40	----	----	C <sub>6</sub>
143.17	135.12	----	----	C <sub>18</sub>
110.25	112.56	6.792	6.617	H <sub>l</sub> -C <sub>7</sub>
115.06	128.09	6.607	6.679	H <sub>k</sub> -C <sub>10</sub>
46.72	45.62	2.983	2.579	H <sub>e</sub> /H <sub>e'</sub>
		2.518	2.108	-C <sub>4</sub>
40.62	41.71	1.905	1.845	H <sub>f</sub> /H <sub>f'</sub>
		1.520	1.326	-C <sub>5</sub>
24.94	23.26	3.021	2.910	H <sub>i</sub> /H <sub>j'</sub>
			2.697	-C <sub>1</sub>
116.32	121.17	5.324	5.280	C <sub>17</sub> -H <sub>b</sub>
26.14	25.95	1.826	1.645	C <sub>20</sub> -H <sub>a</sub>
18.36	18.02	1.768	1.682	C <sub>19</sub> -H <sub>a'</sub>
52.92	52.36	3.648	3.163	C <sub>16</sub> -H <sub>c</sub>
60.04	57.08	3.462	3.146	C <sub>2</sub> -H <sub>d</sub>
24.94	25.41	1.414	1.290	C <sub>15</sub> -H <sub>g</sub>
13.76	14.17	0.909	0.828	C <sub>14</sub> -H <sub>h</sub>
40.69	41.15	2.028	1.937	C <sub>11</sub> -H <sub>i</sub>

direct comparison of MET1 and pentazocine spectra suggested the assignment of  $H_b$  at 5.324 ppm, which has a cross peak with the carbon-13 resonance at 116.32 ppm in the contour plot in Fig. VII.7. Thus the carbon-13 resonance at 116.32 ppm should be responsible for  $C_{17}$ . Similarly, since proton resonances at 0.909, 1.414, and 3.648 ppm show cross peaks with carbon-13 resonances at 13.76, 25.26, and 52.92 ppm, these carbon-13 resonances are thus assigned to  $C_{14}$ ,  $C_{15}$  and  $C_{16}$ , respectively. Carbon-13 resonances at 18.36 and 26.14 ppm have cross peaks with proton resonances at 1.768 and 1.826 ppm, respectively; they thus belong to  $C_{19}$  and  $C_{20}$ . It is found that, in general, cis -CH=CH- carbon-13 resonance signals are upfield from those of corresponding trans groups [56]. If this were the case for MET1, then the resonance at 18.36 ppm would correspond to  $C_{19}$ , which is cis to  $C_{16}$ , and the resonance at 26.14 would be  $C_{20}$ , which is trans to  $C_{16}$ . Consequently, proton resonances at 1.768 and 1.826 ppm would belong to  $H_{a'}$  and  $H_a$ , respectively. These assignments are further confirmed by the NOESY experiment discussed later.

It is also concluded that the proton resonance at 3.818 ppm is responsible for the protons in the methoxy group,  $-OCH_3$ , which in turn has a cross peak linking to the carbon-13 resonances at 56.58 ppm; this peak is therefore assigned to  $C_{21}$  in  $-OCH_3$ . It is also noted that the published carbon-13 resonance for such a carbon in the methoxy group attached to the benzene ring would have a chemical shift at 54.1 ppm [56], which is fairly close to the observed value. This helps to confirm that MET1 has a structure similar to that of pentazocine, except for an additional methoxy group attached to the aromatic moiety, as is also indicated by the GC/MS analysis.

Both proton resonances f, f' at 1.905 ppm and 1.520 ppm are

correlated to the same carbon-13 resonance at 40.618 ppm by cross peaks. There is another pair of proton resonances e (appears to be overlapped with proton resonance j), e' at 2.982 ppm and 2.518 ppm showing correlations with a single carbon-13 resonance at 46.72 ppm. Combined with the previous findings in COSY and carbon-13 NMR studies, it is concluded that proton resonances f and f' are responsible for a pair of geminal protons belonging to the same methylene group, namely, protons f and f' are attached to the carbon which has a similar environment as C<sub>5</sub> in pentazocine; proton resonances e and e' are assigned to the protons attached to C<sub>4</sub> as was done for pentazocine.

Proton resonance i at 2.028 ppm, which is previously assigned to a methine proton i, shows a correlation with the carbon-13 resonance at 40.685 ppm. The Carbon-13 resonance at 40.685 ppm is therefore assigned to be a methine carbon as that of C<sub>11</sub> in pentazocine. In Fig. VII.7, it is obvious that the cross peak for i/C<sub>11</sub> is not on the same vertical line linking cross peaks f, f'/C<sub>5</sub>. This shows again that there are two different carbon-13 resonances at 40.618 ppm and 40.685, although they appear to be unresolved.

Unlike for pentazocine in D-chloroform, which shows two different proton resonances for protons H<sub>j</sub> and H<sub>j'</sub> belonging to the same methylene group attached to C<sub>1</sub>, MET1 in D-methanol shows a single proton resonance j at 3.021 ppm, which accounts for two protons, correlating with a carbon-13 resonance at 24.94 ppm. Combining observations from both COSY and carbon-13 NMR, proton resonance j is assigned to methylene protons attached to C<sub>1</sub> as was done for pentazocine.

The suspected aromatic proton resonances at 6.792 and 6.607 ppm

have cross peaks with carbon-13 resonances at 110.25 and 115.06 ppm, respectively. But the connections in this case do not suggest any better assignments than in the carbon-13 NMR data analysis, because the proton resonances concerned have not been specifically assigned previously.

LR HETCOR, long-range  $^1\text{H}$ - $^{13}\text{C}$  heteronuclear shift correlation NMR. As predicted from the GC/MS data analysis, the MET1 structure should have an additional methoxy group attached to the aromatic ring of the pentazocine structure, but it is questionable as to where it is attached. The proton/carbon-13 resonance correlation for the direct bounding C-H also has failed to provide enough information to elucidate the detailed MET1 structure, because there are only two direct bounding protons attached to the aromatic ring, and the specific assignments for these protons and their bound carbons are not possible. To obtain more connectivity information about the aromatic ring, another proton/carbon-13 correlated 2D NMR experiment is conducted with emphasis on the correlations through small coupling constants, that is, long range proton/carbon-13 coupling via two or three bonds, H-C-C or H-C-C-C. Since each aromatic proton has two more possible couplings via  $^2\text{J}_{\text{CH}}$ , and two more via  $^3\text{J}_{\text{CH}}$ , examination of the two different kinds of spectra allows many more correlations to be identified than with a single spectrum, and a complete picture of the molecular skeleton can thus be obtained.

Fig. VII.7 shows the proton/carbon-13 chemical shift correlation spectrum with long range proton/carbon-13 coupling only.

Table VII.6 shows the observed correlations between proton and carbon-13 via long range coupling in MET1.

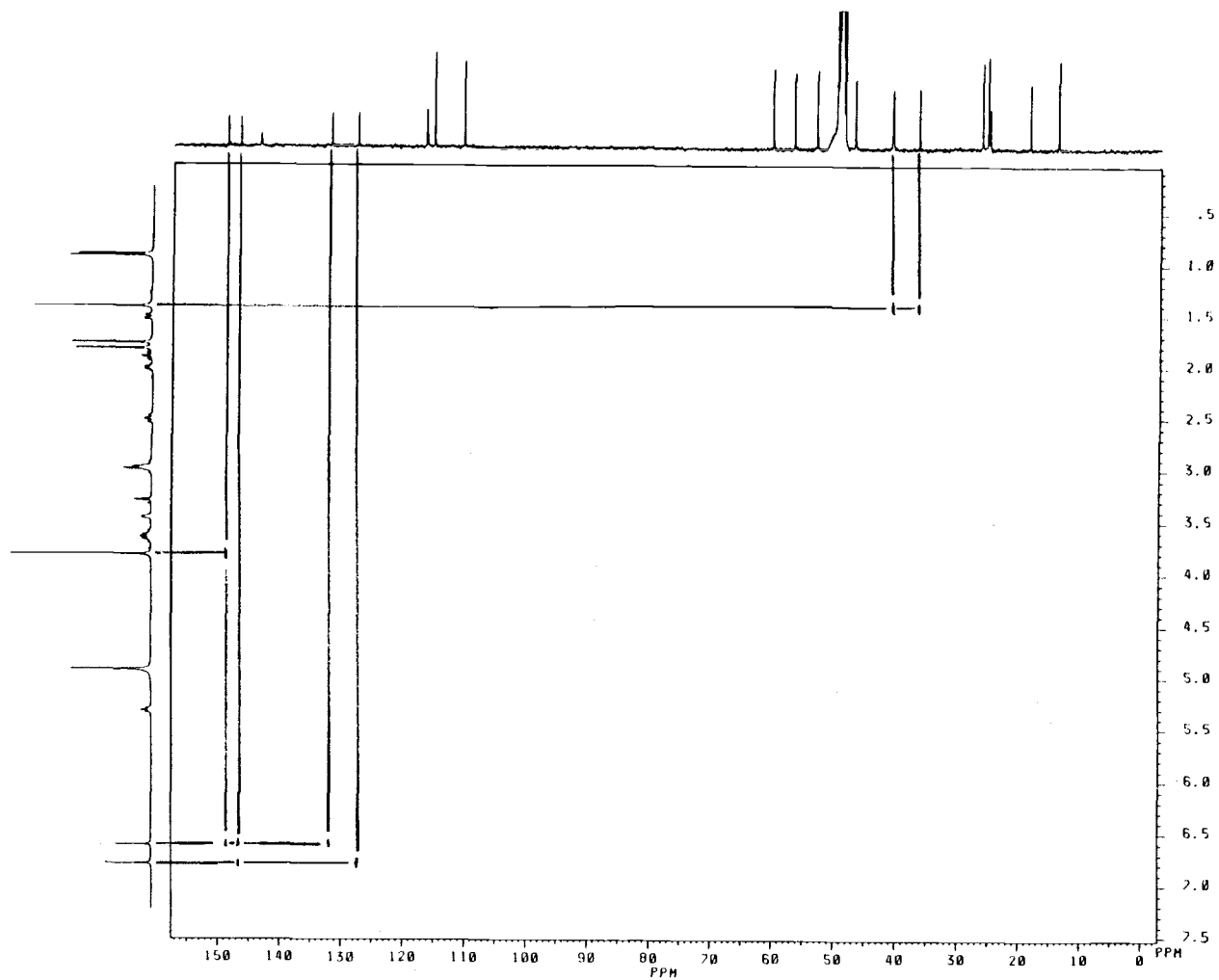


Figure VII.7 Heteronuclear shift correlated (long range C-H coupling) spectrum of pentazocine metabolite MET1 in D-methanol.

Table VII.6 Heteronuclear chemical shift correlation (long range C-H coupling) NMR results for pentazocine metabolite MET1.

Chemical Shifts				
Carbon ppm		Proton ppm		Assignments
MET1	PENT	MET1	PENT	
148.49	154.70	3.818	----	C <sub>8</sub> \H <sub>o</sub>
148.49	154.70	6.607	6.939	C <sub>8</sub> \H <sub>k</sub>
146.46	113.37	6.607	6.939	C <sub>9</sub> \H <sub>k</sub>
146.46	113.37	6.792	6.676	C <sub>9</sub> \H <sub>l</sub>
131.67	143.15	6.607	6.939	C <sub>13</sub> \H <sub>k</sub>
127.38	135.12	3.021	2.910	C <sub>12</sub> \H <sub>j</sub>
127.38	135.12	6.792	6.676	C <sub>12</sub> \H <sub>l</sub>
36.36	36.40	1.414	1.290	C <sub>6</sub> \H <sub>g</sub>
40.69	41.15	1.414	1.290	C <sub>11</sub> \H <sub>g</sub>
40.62	41.71	1.414	1.290	C <sub>5</sub> \H <sub>g</sub>

The proton resonance at 3.818 ppm, which represents the protons attached to the methoxy group, has a cross peak correlating to carbon-13 resonance 21 at 148.49 ppm. The implication is that the carbon-13 resonance at 148.49 ppm is responsible for the carbon that is directly attached to the methoxy group in the aromatic moiety.

Proton resonance g at 1.414 ppm has two cross peaks correlating to carbon-13 resonance 6 at 36.36 ppm, and either one or both of the carbon-13 resonances 5 or 11 at 40.62 ppm and 40.685 ppm.

Proton resonance j has a cross peak correlated with carbon-13 resonance 12 at 127.38 ppm. As discussed earlier the carbon-13 resonance at 127.38 ppm is responsible for an aromatic carbon, and the proton resonance j belongs to protons attached to the N-ring structure. Thus, this cross peak virtually shows the linkage between those two segments of the MET1 structure. Most likely, if the suggestion in the previous proton NMR discussion were applied, that is, proton resonance j were responsible for proton j attached to C<sub>1</sub>, then carbon-13 resonance 15 at 127.34 ppm should belong to C<sub>15</sub> in the aromatic ring, which would lead to the strongest  ${}^2J_{C-H}$  coupling with protons j.

Proton resonance l has two cross peaks indicating long range C-H coupling with carbon-13 resonances 12 and 9 at 127.34 and 146.46 ppm, respectively. Proton resonance k has cross peaks correlated with carbon-13 resonances 8, 13 and 9 at 148.49, 131.67 and 146.46 ppm, respectively. Those C-H couplings could rise from either "two bond" or "three bond" proton/carbon-13 coupling.

Since the coupling constant  $J_{CH}$  is not available, it is impossible to distinguish whether an observed cross peak is due to

"three bond", H-C-C-C, or "two bond", H-C-C coupling. But usually, "three bond" proton/carbon-13 coupling is stronger than those of "two bond" coupling due to the electron configuration in the molecule [84], which makes "three bond" coupling more visible. However, because of the unique structure of the benzene ring, there are only two "two bond" and two "three bond" connectivities for each proton attached to the ring. Thus, if there are only two cross peaks correlating each proton with different carbons, it is very likely that both of them are due to the same connectivity, that is, either "two bond" or "three bond", and this is the case for proton resonance l. Nonetheless, the fact that there are three cross peaks for proton resonance k indicates that there is one cross peak arising from different connectivity than the other two. Therefore, no matter what a kind of proton/carbon-13 coupling is responsible for the correlation observed, the logical structure in the aromatic portion for proton l and k would be as shown in Fig. VII.8. In any case, the specific assignments of proton resonances l and k would need more conclusive results from experiments such as NOE, which will be discussed in the following section.

Carbon-13 resonance 8 at 148.49 ppm is determined to be responsible for the carbon that is directly bound to a methoxy group. Combining this with all of the other information leads to the aromatic portion of the MET1 structure as shown in Fig. VII.9.

NOE experiments. In order to assemble the major parts of MET1 into a complete structure, especially the final structure of the aromatic portion and the linkage between the aromatic portion and the N-ring portion, NOE experiments are conducted.

As discussed along with the pentazocine NMR study, in the classic

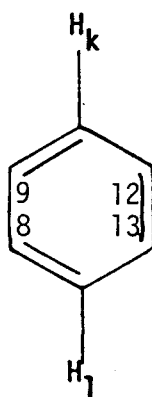


Figure VII.8 The possible structure of the aromatic ring portion of pentazocine metabolite MET1 based on long range C-H coupling information.

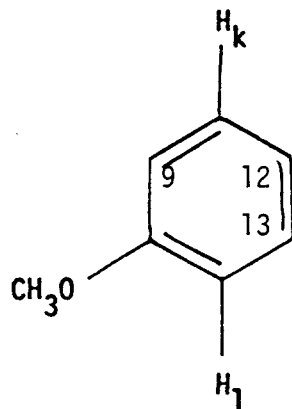


Figure VII.9 The possible structure of the aromatic ring portion of pentazocine metabolite MET1 based on heteronuclear shift correlated spectral information.

NOE experiment, the magnetization of one nucleus is perturbed selectively by irradiation with a weak radio frequency field, and the changes in the intensities of other resonances in the spectrum are monitored. Such changes indicate the dipole-dipole interactions between nearby nuclei through space.

If the suggestion based on the previous study were true, that is, most of parts of MET1 structure are the same as that of pentazocine, except the aromatic portion, then proton resonances responsible for the protons nearby the aromatic ring become the key for the NOE study.

Selectively irradiating proton resonance j at 3.021 ppm, the intensity changes of other proton resonances are shown in Fig. VII.10, in which (a) shows the proton NMR difference spectrum of MET1 in D-methanol obtained by subtracting the off-resonance spectrum (b) from the on-resonance irradiation of proton resonance j.

Irradiation of resonance j <sup>17</sup> results in an intensity increase in proton resonance k (3.9% relative to the intensity of irradiating resonance), while intensity change in proton resonance l is not observed. Thus, resonance k is assigned to the aromatic protons closer to j in space. Other perceptible increases in intensities are also observed for resonances e' (8.0%), d (3.7%), and c (2.9%), which all support the previous assignment of resonance j to the methylene protons attached to the same position as C<sub>1</sub> in the pentazocine structure.

-----  
<sup>17</sup>Since proton resonances j and e are not well resolved, the irradiation of resonance j is not very selective. That is, both resonance j and e are likely to be perturbed in this case. This is why an increase in intensity is also observed for resonance e', because e' and e are geminal protons.

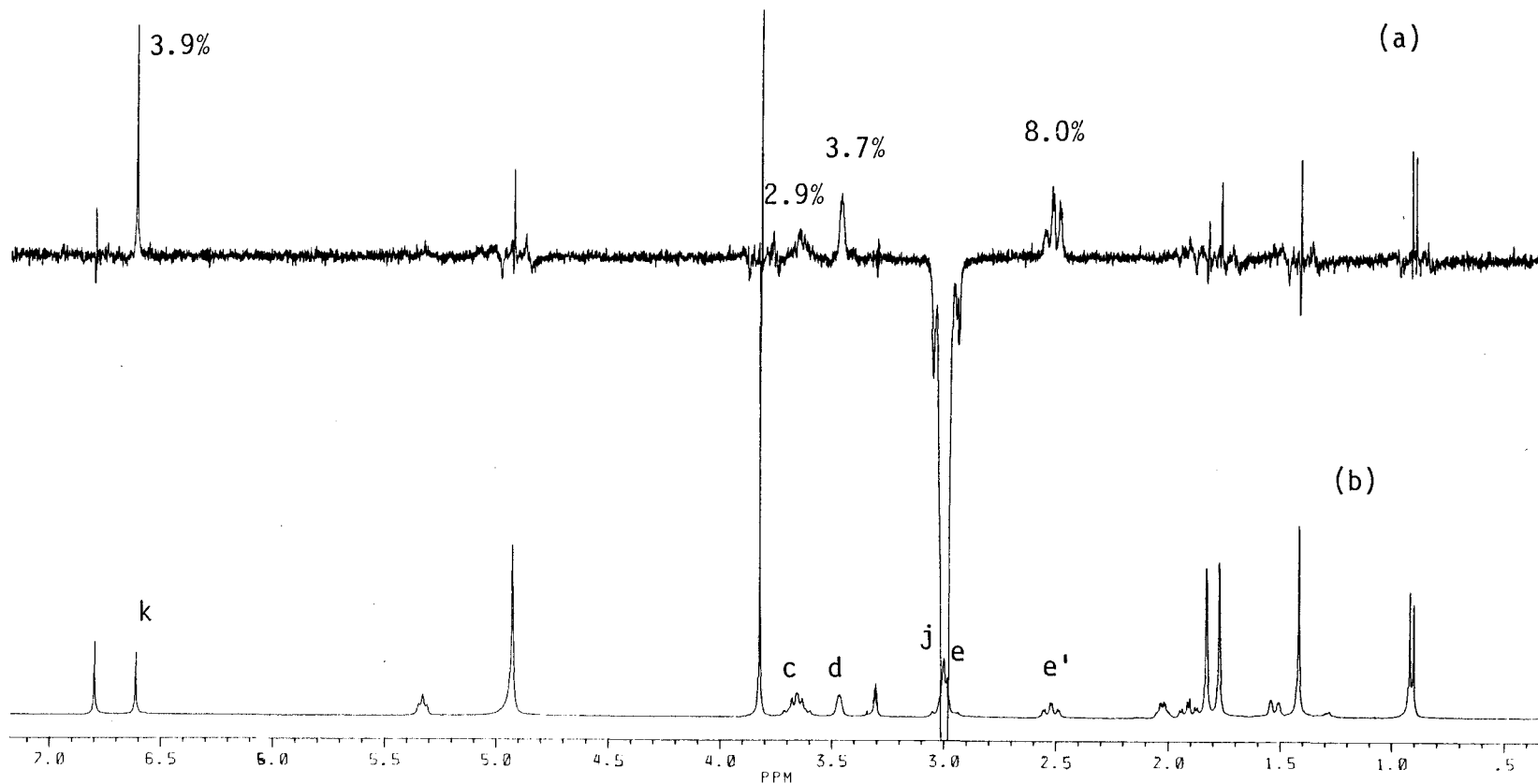


Figure VII.10  $^1\text{H}$  NMR difference spectrum of pentazocine metabolite MET1 in D-methanol (irradiation of resonance j & e): (a) proton difference spectrum of MET1 in D-methanol; (b) off-resonance proton NMR spectrum of MET1 in D-methanol.

Fig. VII.11 (a) and (b) are proton NMR difference spectra of MET1 in D-methanol obtained by subtracting the off-resonance spectrum (c) from the on-resonance irradiation of proton resonances k and l, respectively.

In Fig. VII.11 (a), irradiation of resonance k clearly results in an intensity increasing in resonance j (5.6% relative to the intensity of irradiating resonance), but has no affect on resonances o, g and h. On the contrary, irradiation of resonance l, as shown in Fig. VII.11(b) results in an intensity increase in resonances o (9.1%), g (6.8%), and has no influence on resonance j. It is also noted that the selective irradiation of resonance l or k does not result in any intensity change in each other.

The most likely conclusion from these NOE results would be that aromatic proton k is adjacent to protons j in space; whereas aromatic proton l is close to both methyl group protons g <sup>18</sup> and the methoxy group attached to the aromatic ring.

Fig. VII.12 (a) and (b) illustrate the proton NMR difference spectrum obtained by subtracting the off-resonance carbon-13 NMR spectrum of MET1 in D-methanol from the on-resonance irradiation of resonances g and o, respectively.

The irradiation of resonance g gives a strong NOE signal for resonance l (5.2% relative to the intensity of the irradiating resonance), while the intensity changes in resonance h (1.9%) and i (1.5%) are also observed, which confirms that resonance g is

-----

<sup>18</sup>Proton l is close to proton g in space as can be seen easily in 3-D molecular model.

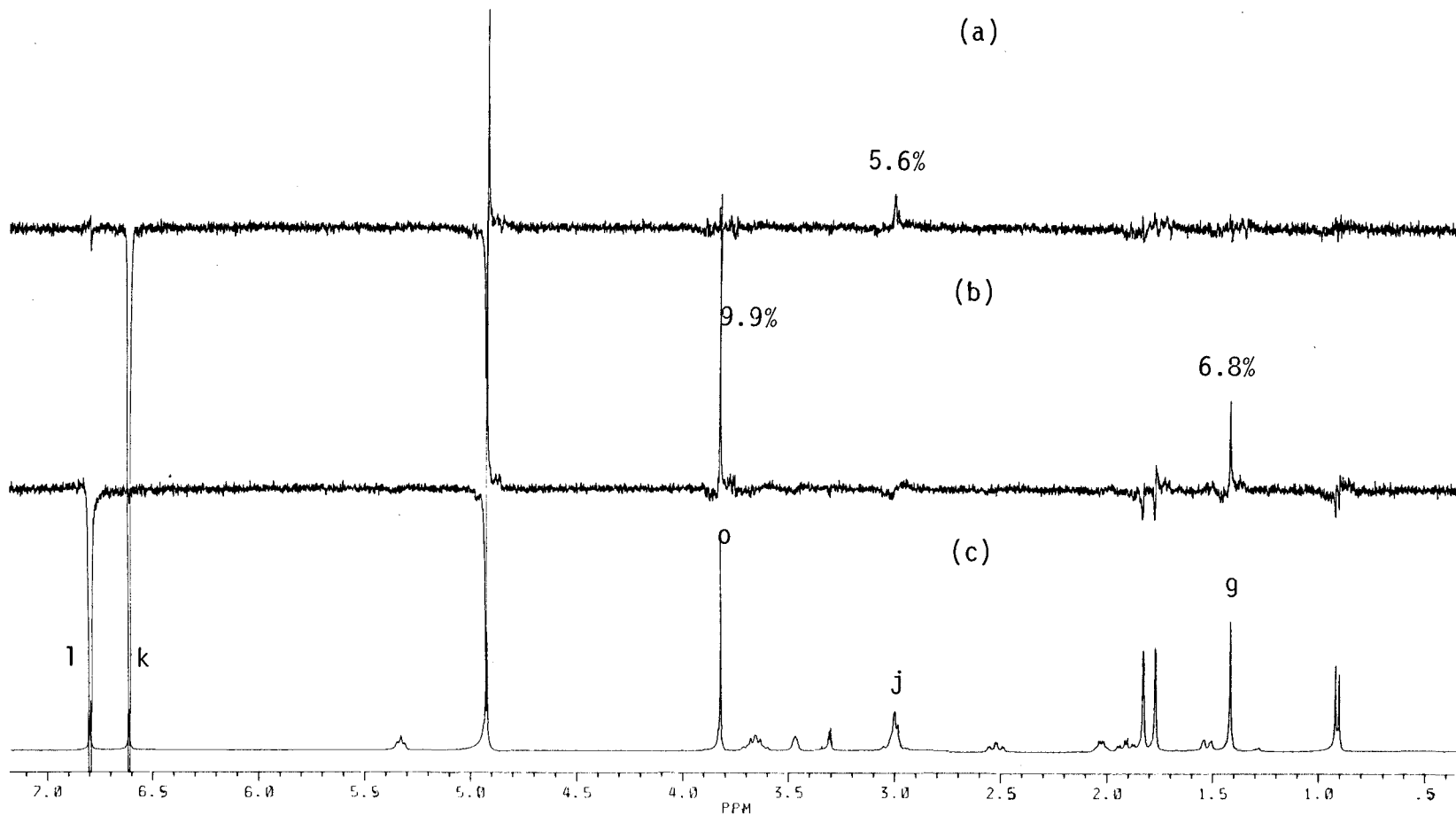


Figure VII.11  $^1\text{H}$  NMR difference spectrum of pentazocine metabolite MET1 in D-methanol (irradiation of resonance k,l): (a) proton difference spectrum of MET1 in D-methanol (upon irradiation of k); (b) proton difference spectrum of MET1 in D-methanol (upon irradiation of l); and (c) off-resonance proton NMR spectrum of MET1 in D-methanol

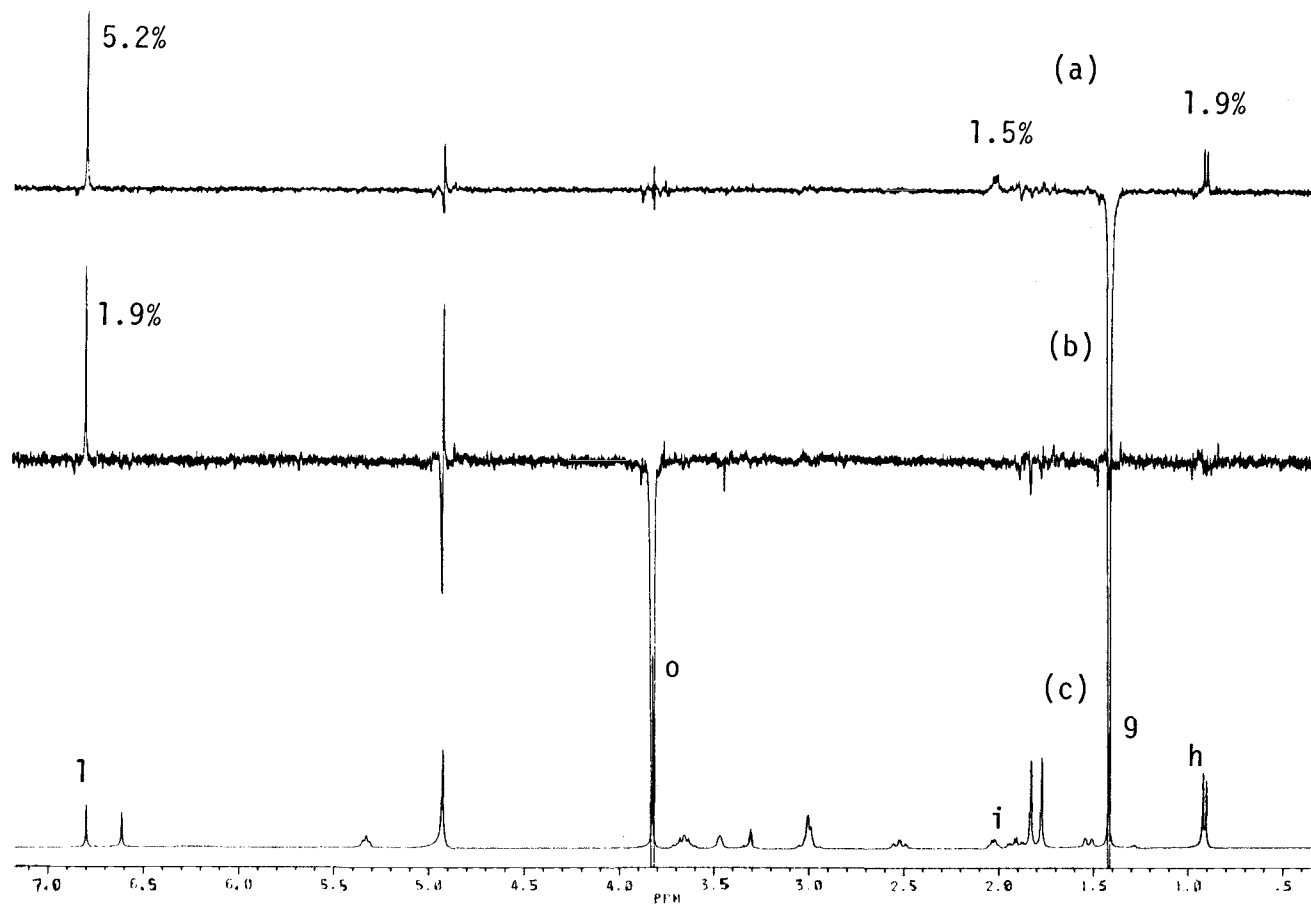


Figure VII.12  $^1\text{H}$  NMR difference spectrum of pentazocine metabolite MET1 in D-methanol (irradiation of resonance g,o): (a) proton difference spectrum of MET1 in D-methanol (upon irradiation of g); (b) proton difference spectrum of MET1 in D-methanol (upon irradiation of o); and (c) off-resonance proton NMR spectrum of MET1 in D-methanol

responsible for methyl group protons attached to the same position as C<sub>15</sub> in pentazocine, which is close to proton i attached to C<sub>11</sub> and proton j attached to C<sub>14</sub>. Thus, proton g should be adjacent to the aromatic proton l in space.

Irradiation of resonance o, which is responsible for the protons in the methoxy group attached to the aromatic ring (Refer to proton NMR assignments), again gives a NOE signal for resonance l (1.9% relative to the intensity of the irradiating resonance), and not for resonance k, which further indicates that resonances l and k are not meta to each other with the -OCH<sub>3</sub> group in between. Since resonances l and k are not ortho to each other either, which was concluded from Fig. VII.11, it is inevitable that aromatic protons l and k are in the para position to each other with the methoxy group attached to the aromatic ring next to proton l.

Again, the -OCH<sub>3</sub> group is attached to the C<sub>8</sub> carbon responsible for carbon-13 resonance 8, whereas two other quaternary carbons have to be used to connect with the N-ring portion of the structure. It is thus inevitable that the only other quaternary carbon C<sub>9</sub> in the aromatic ring, responsible for carbon-13 resonance 9 at 146.46 ppm, has to be the carbon that has the hydroxyl group -OH attached to it. It is noted that there is no proton resonance corresponding to -OH observed for the proton NMR of MET1 in D-methanol, due to the rapid exchange of -OH between the MET1 molecule and the D-methanol solvent molecule, although the existence of -OH is evident in proton NMR of MET1 in both D-chloroform and D-acetone.

The results of above NOE experiments are summarized in Table VII.7. The structure of aromatic ring portion of MET1 and its

Table VII.7 Intensity changes observed by NOE experiments upon selective proton resonance irradiation.

Resonance Irradiated	Observed Intensity Changes (%)									
	<u>Proton Resonance</u>									
	c	d	e'	g	h	i	j	k	l	o
j, e	2.9	3.7	8.0					3.9		
k							5.6			
l				6.8						9.1
g					1.9	1.5			5.2	
o										1.9

\* The intensity changes observed are related to the intensity of the irradiating proton resonance as 100%.

connection to the N-ring derived from the above data is presented in Fig. VII.13.

NOESY, two-dimensional NOE. In order to assemble the complete structure of MET1, and establish conformational details of the entire molecule, a NOESY, two-dimensional NOE, spectrum is recorded as shown in Fig. VII.14. Table VII.8 shows the coupling observed in NOESY (through space) comparing with those obtained in COSY (through bonds). Starting from the proton resonance l, cross peaks are found for the resonances o and g. Moreover, starting from resonance k connectivity is found to j and h. Hence the aromatic moiety is next to the protons H<sub>j</sub> and H<sub>g</sub> attached on the N-ring, and the aromatic protons k and l in para positions to each other with l next to the methoxy group, -OCH<sub>3</sub>. Proton resonance g, which is responsible for methyl group protons, shows no correlation with any other proton in the COSY spectrum. That is, this methyl group must attach to a quaternary carbon, yet close to the aromatic proton l in space according to the NOE results. The logical structure for this part of the molecule is thus concluded to be as shown in Fig. VII.15.

Resonance b shows cross peaks to resonances d and a <sup>19</sup>, which indicate trans positions of the methyl group H<sub>a</sub> at the end of the double bond, and the configuration of the methine proton H<sub>b</sub> and the other methine proton H<sub>d</sub> attached to the N-ring is on space to each other.

Resonance c shows cross peaks to resonances d, e and a'. It is

-----  
<sup>19</sup>H<sub>c</sub> and H<sub>b</sub> may point to opposite directions in a 3-D model; that is, they are not close to each other in space.

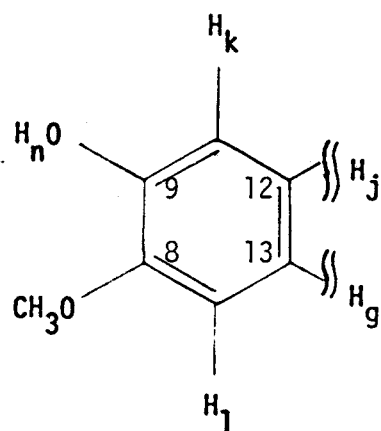


Figure VII.13 The structure of aromatic ring portion of pentazocine metabolite MET1 deduced from NOE experiments.

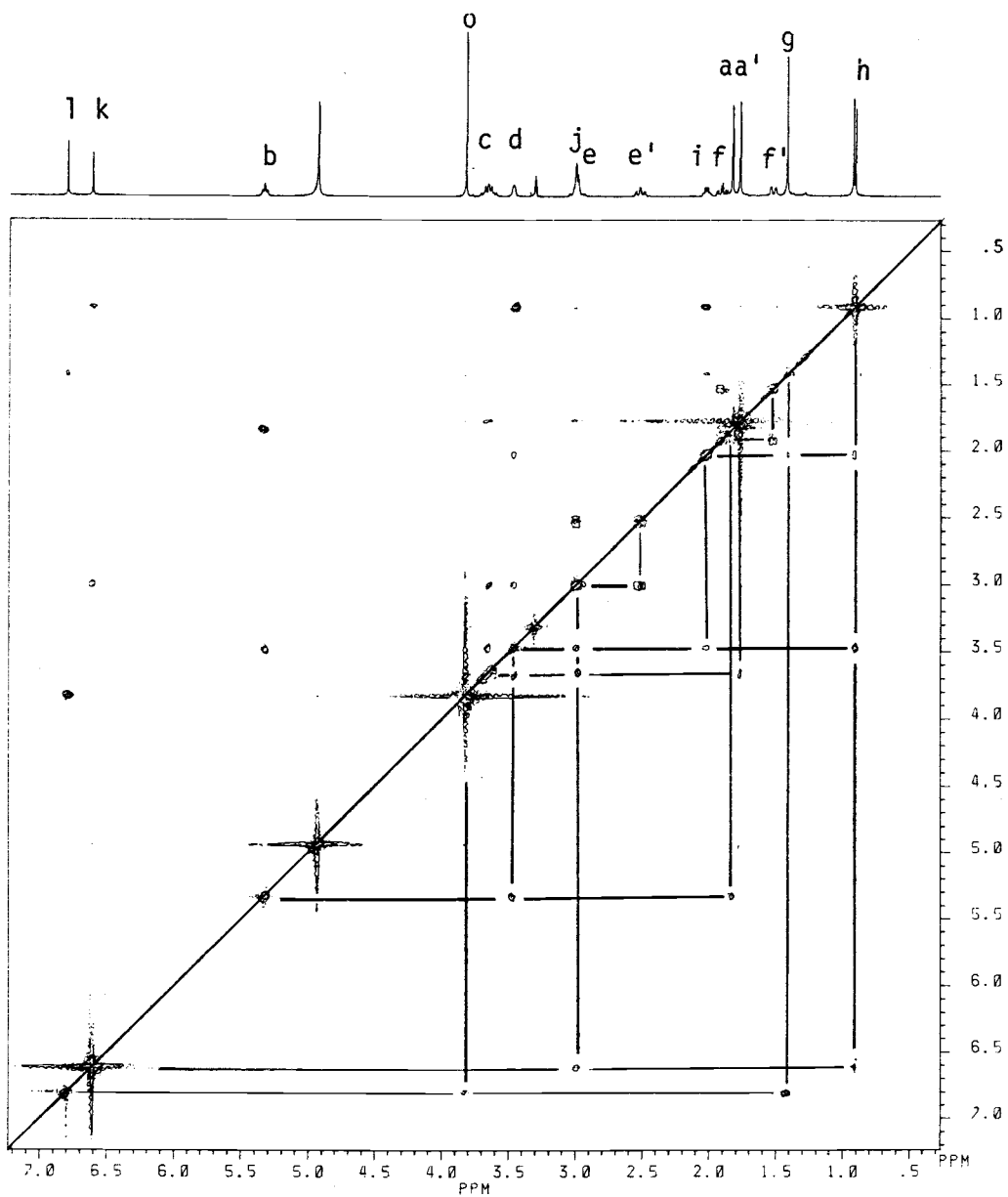


Figure VII.14 NOESY spectrum of pentazocine metabolite MET1 in D-methanol.

Table VII.8 Proton couplings observed by both NOESY and COSY experiments for pentazocine metabolite MET1.

<u>Dipole-Dipole</u>	<u>Spin-Spin</u>
NOESY	COSY
a/b	a/b, a/c
a'/c	a'/b, a'/c
b/a, b/d	b/a, b/c
	b/a'
c/a', c/d, c/e	c/a, c/a', c/b
d/j, d/i, d/h	d/j, d/i
e/e', e/c	e/e', e/f, e/f'
e'/e	e'/e, e'/f, e'/f'
f/f'	f/e, f/e', f/f'
f'/f	f'/e, f'/e', f'/f
g/i, g/l	
h/d, h/i, h/k	h/i
i/h, i/g	i/h, i/d
j/d, j/k	
k/j, k/h	
l/g, l/o	

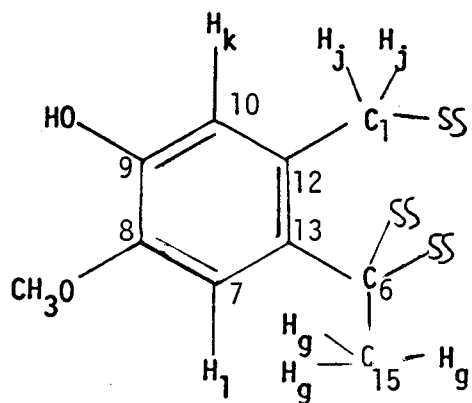


Figure VII.15 The structure of aromatic ring portion of pentazocine metabolite MET1 and its connection to the rest of the molecule deduced from both COSY and NOESY spectral information.

therefore concluded that methylene protons  $H_C$  are cis to the terminal methyl group proton  $H_{a'}$  upon the double bond, and  $H_C$  are on a carbon that is attached to the nitrogen atom with nearby protons  $H_D$  and  $H_e$  on both sides in the N-ring.

The connectivity between the proton resonances d, j, e-e', f-f', g, h and i indicate that these protons reside in the same part of MET1, that is, the N-ring portion. This finding is in accordance with other 2D NMR results, which suggest the same structure for both MET1 and pentazocine in the N-ring portion.

The above analysis of the NOESY spectrum completes the structure elucidation of MET1 as 8-methoxy pentazocine (Fig. VII.16). Table VII.9 summarizes the assignments for the MET1 NMR data. For the sake of completeness, it is noted that the cross peaks in the NOESY spectrum which are not addressed in this study are in full accordance with the proposed structure.

### 3. Experimental

$^1H$  NMR and  $^{13}C$  NMR were recorded on a Bruker AM-400 spectrometer. All  $^{13}C$  NMR spectra were broadband decoupled. All NMR spectra were obtained using 5-mm NMR tubes. Samples were prepared in  $CDCl_3$ ,  $C_3D_6O$  or  $CD_3O$  and the chemical shifts are reported in parts per million (ppm) relative to external tetramethylsilane ( $SiMe_4$ , 0.00 ppm).

All two-dimensional spectra of pentazocine metabolite MET1 were recorded at ambient temperature with a Bruker AM-400 spectrometer equipped with an Aspect 3000 computer operating in the Fourier

Table VII.9 Comparison of  $^1\text{H}$  and  $^{13}\text{C}$  NMR spectra data obtained for pentazocine in D-chloroform and pentazocine metabolite MET1 in D-methanol.

Proton NMR Resonance		Carbon-13 NMR Resonance		Assignments	
PENT.	MET1.	PENT.	MET1.	Proton	Carbon
ppm	ppm	ppm	ppm		
1.645	1.826	25.95	26.14	H <sub>a</sub>	C <sub>20</sub>
1.682	1.768	18.02	18.36	H <sub>a'</sub>	C <sub>19</sub>
5.280	5.324	121.17	116.32	H <sub>b</sub>	C <sub>17</sub>
3.163	3.648	52.36	52.92	H <sub>c</sub>	C <sub>16</sub>
3.146	3.462	57.08	60.04	H <sub>d</sub>	C <sub>2</sub>
2.579	2.982	45.62	46.72	H <sub>e</sub>	C <sub>4</sub>
2.108	2.518			H <sub>e'</sub>	
1.845	1.905	41.71	40.62	H <sub>f</sub>	C <sub>5</sub>
1.326	1.520			H <sub>f'</sub>	
1.290	1.414	25.41	25.26	H <sub>g</sub>	C <sub>15</sub>
0.828	0.909	14.17	13.76	H <sub>h</sub>	C <sub>14</sub>
1.937	2.028	41.15	40.69	H <sub>i</sub>	C <sub>11</sub>
2.697	-----	23.26	24.94	H <sub>j'</sub>	C <sub>1</sub>
2.910	3.021			H <sub>j</sub>	
6.939	6.607	128.09	115.06	H <sub>k</sub>	C <sub>10</sub>
6.676	6.792	112.56	110.25	H <sub>l</sub>	C <sub>7</sub>
6.601	-----	113.37	146.46	H <sub>n</sub> *	C <sub>9</sub>
-----	3.818	-----	56.58	H <sub>o</sub>	C <sub>21</sub>
-----	-----	143.15	131.67	---	C <sub>13</sub>
-----	-----	135.12	127.34	---	C <sub>12</sub>
-----	-----	36.40	34.5	---	C <sub>6</sub>
-----	-----	127.73	143.17	---	C <sub>18</sub>
-----	-----	154.70	148.49	---	C <sub>8</sub>

\* Proton H<sub>n</sub> in the hydroxy group attached to the aromatic ring is not shown in the proton NMR spectrum of MET1 in D-methanol because of the rapid exchange of -OH between MET1 and the solvent molecules. Existence of the -OH is indicated in the proton NMR spectrum of MET1 in both D-chloroform and D-acetone.



transform mode with quadrature detection. Standard Bruker pulse programs were used.

The two-dimensional  $^1\text{H}$ - $^1\text{H}$  shift correlated (COSY-45) data for pentazocine metabolite MET1 was acquired at a sweep width of 2793 Hz (1024 data points) in the  $F_2$  domain; 256 FIDs (8 scans plus 2 dummy scans for each FID) were accumulated with 352  $\mu\text{sec}$  increments and a 3- $\mu\text{sec}$  starting delay. A 1-sec recycle delay was inserted between scans to allow spin relaxation. The digital resolution was 2.727 Hz/pt in both dimensions. A sinebell window function was applied to the Fourier transformation to enhance resolution. The COSY was then summarized about the diagonal line.

The heteronuclear  $^1\text{H}$ - $^{13}\text{C}$  shift correlated (HETCOR) experiment for pentazocine metabolite MET1 was performed with a 16129 Hz (4096 data points) spectral width in the  $^{13}\text{C}$  ( $F_2$ ) dimension and a  $\pm 1450$  Hz (256 data points) window in the  $^1\text{H}$  ( $F_1$ ) dimension; 128 FIDs (64 scans plus 2 dummy scans each) were acquired with 167- $\mu\text{sec}$  increments and a 3- $\mu\text{sec}$  starting delay. A 1-sec recycle delay was used between scans. The digital resolution for the  $^{13}\text{C}$  ( $F_2$ ) and  $^1\text{H}$  ( $F_1$ ) dimensions were 3.938 and 11.328 Hz/pt, respectively. A Gauss multiplication was applied to both dimensions before Fourier transformation to enhance resolution ( $F_2$ : LB=-4, GB=0.9;  $F_1$ : LB=-5, GB=0.5).

The long-range heteronuclear shift correlated (LR HETCOR) spectral data of pentazocine metabolite MET1 were acquired with sweep widths of 161290 Hz (4096 data points) in the  $F_2$  ( $^{13}\text{C}$ ) domain and  $\pm 1500$  Hz (512 data points) in the  $F_1$  ( $^1\text{H}$ ) domain. The digital resolution in  $F_1$  and  $F_2$  domains were 5.860 and 3.938 Hz/pt, respectively; 256

FIDs were accumulated of 128 scans plus 2 dummy scans each, with an incremental delay of 333  $\mu$ sec and starting delay of 3  $\mu$ sec. A 1-sec recycle delay between scans was used. A Gauss multiplication was applied to both domains to enhance resolution ( $F_2$ : LB=-7, GB=0.9;  $F_1$ : LB=-5, GB=0.5).

The two-dimensional NOE (NOESY) data for pentazocine metabolite MET1 was acquired at a sweep width of 2793 Hz (1024 data points) in the  $F_2$  domain; 256 FIDs with 32 scans plus 2 dummy scans for each FID were accumulated with 179- $\mu$ sec increments and a 3- $\mu$ sec starting delay. A 1-sec recycle delay was inserted between scans. The digital resolution was 2.728 Hz/pt in both dimensions. The NOE mixing time was 1.3 sec randomized with a range of  $\pm$  26 msec. A Gauss multiplication was applied to both domains to enhance resolution ( $F_2$ : LB=-5, GB=0.9;  $F_1$ : LB=-5, GB=0.5). The NOESY was then summarized about the diagonal line.

A Bruker pulse program (NOEDIFF.AUR) was used in all one-dimensional NOE experiments for pentazocine metabolite MET1. All data were acquired at a sweep width of 2793 Hz (16000 data points); 64 scans were accumulated for each FID. A 1.5-sec recycle delay was used. NOE irradiation time was 1.5 sec.

## VIII. CONCLUSION

A drug metabolism study, as in many other scientific fields, requires good methodology with special skills. The diversity of interest in metabolism studies also requires the successful coordination of multi-disciplinary activities. However, analytical chemistry methodology and skills are critical in most, if not every part, of drug metabolism studies. That is, it is most important in drug metabolism studies to have a good appreciation of the analytical chemistry used so as to ensure that it is applied thoughtfully and the data obtained are interpreted accurately. On the other hand, the problems that need to be solved for "real sample analysis" in metabolism studies are often direct challenges to analytical chemists, and their solutions can be used as guidelines for the further development of analytical techniques in general.

In this project, analytical chemistry methodology and specific skills in the field such as chromatography and spectroscopy have been extensively studied and tested through the study of pentazocine metabolism in the greyhound following intravenous administration. The study shows that after enzymatic hydrolysis, nine metabolites and unchanged pentazocine were isolated from the urine samples by solvent extraction and XAD-2 column isolation. These compounds were further separated by TLC, HPLC, GC, and characterized by electron impact mass spectrometry, as well as various two-dimensional  $^1\text{H}$  and  $^{13}\text{C}$  NMR techniques.

In the GC/MS study, the electron-impact-induced fragmentations of pentazocine, 1,2,3,4,5,6-Hexahydro-6,11-dimethyl-3-(3-methyl-2-butenyl)-2,6-methano-3-benzazocine-8-ol (Fig. VIII.1a), and its nine metabolite trimethylsilylated derivatives have been described. The different fragmentation pathways have been applied to establish ion structures of metabolites found in greyhound, and in particular, to identify the positional isomers of metabolites produced by oxidative metabolism of the terminal methyl groups of the dimethylallyl side chain of pentazocine. As a result, metabolite MET3 was determined to be 1,2,3,4,5,6-Hexahydro-8-hydroxy- $\alpha$ ,6,11-trimethyl-2,6-methano-3-benzazocine-3-cis-2-buten-1-ol (cis-alcohol) by GC/MS (Fig. VIII.1b). Metabolite MET4 (Fig. VIII.1c) was identified as 1,2,3,4,5,6-Hexahydro-8-hydroxy- $\alpha$ ,6,11-trimethyl-2,6-methano-3-benzazocine-3-trans-2-buten-1-ol (trans-alcohol), and metabolite MET7 as 1,2,3,4,5,6-Hexahydro-8-hydroxy- $\alpha$ ,6,11-trimethyl-2,6-methano-3-benzazocine-3-crotonic acid (trans-acid) (Fig. VIII.1d). These findings agreed with the side chain oxidative metabolism for pentazocine in most other species<sup>[5,6]</sup>. However, norpentazocine, a metabolite produced by N-dealkylation<sup>[7]</sup>, and pentazocine hydrate<sup>[9]</sup>, another metabolite resulting from reductive metabolism were not found in the greyhound.

Moreover, six other metabolites found to be three pairs of isomers were also detected in the greyhound urine, and an additional methoxyl group attachment was responsible for this new branch of pentazocine metabolites. The structure of metabolite MET1 was then positively identified by subsequent high resolution NMR (including various 2D

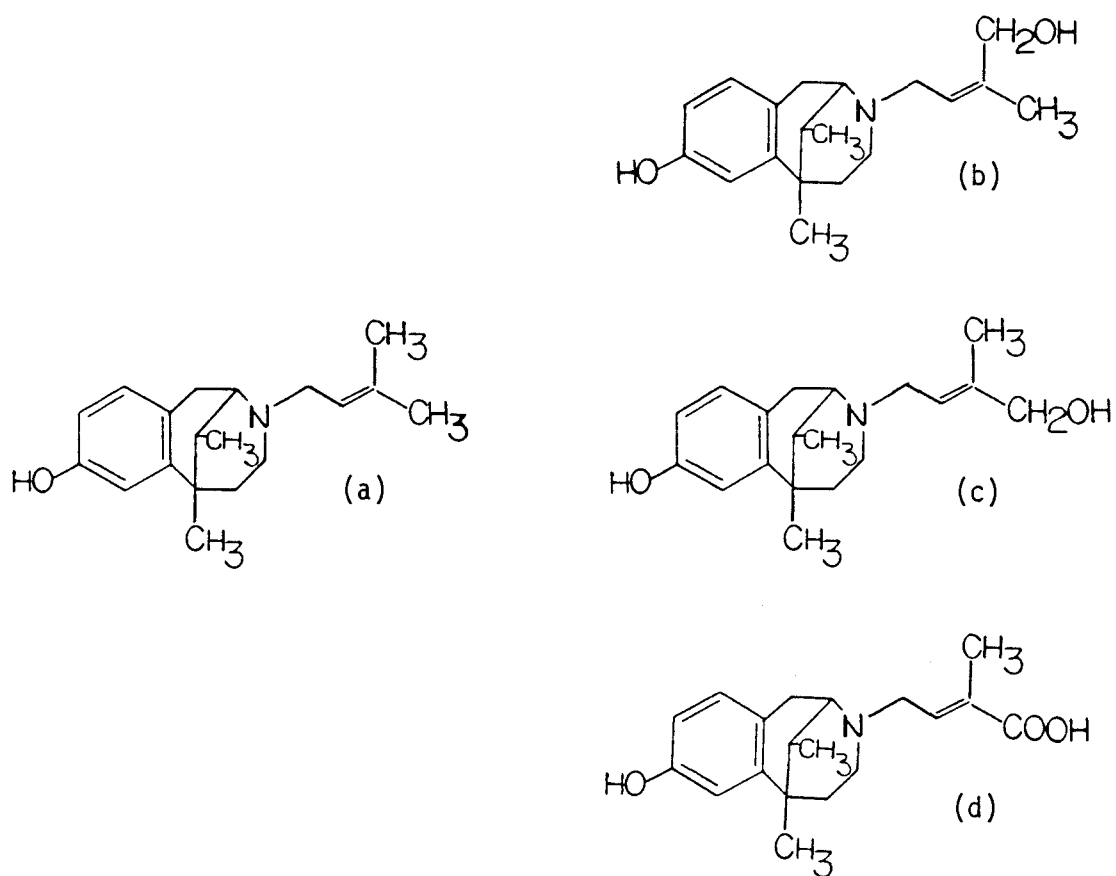
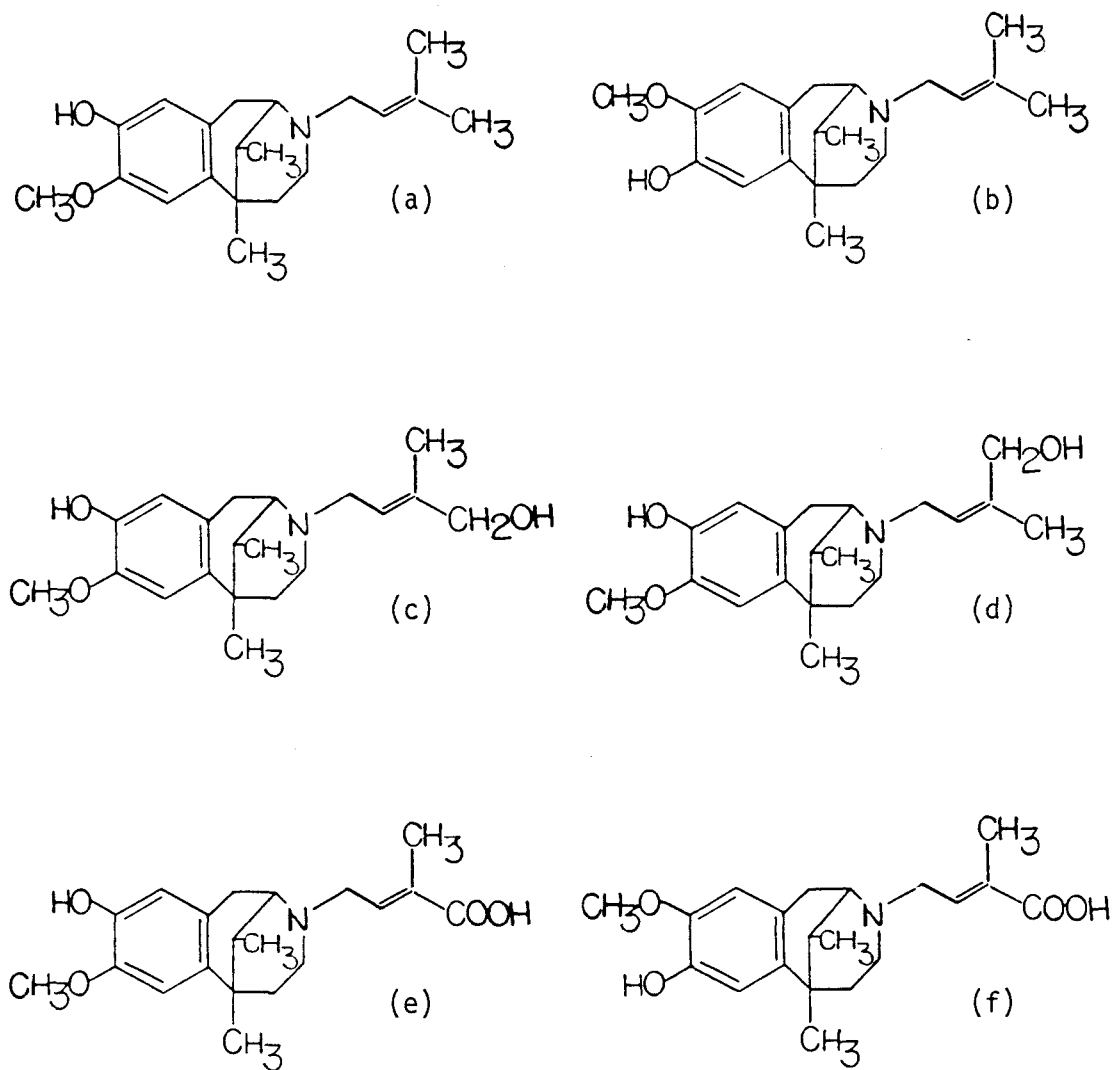


Figure VIII.1 Structures of pentazocine and its metabolites produced by the side chain oxidative metabolism in the greyhound: (a) pentazocine, (b) metabolite MET3 (cis-alcohol), (c) MET4 (trans-alcohol), and (d) MET7 (trans-acid)

experiments) as 1,2,3,4,5,6-Hexahydro-6,11-dimethyl-8-methoxyl-3-(3-methyl-2-butenyl)-2,6-methano-3-benzazocine-9-ol (8-methoxy pentazocine) (Fig. VIII.2a). This finding is in complete agreement with an anticipated hydroxylation metabolism of the pentazocine aromatic ring, which in theory [85,86] can only lead to an additional hydroxyl group attached to the position (9-position) ortho to the original phenolic group at the 8-position. The resulting two vicinal hydroxyl groups then establish a necessary condition for the subsequent methylation, which leads to only one of the hydroxyl groups being methylated [87,88] to methoxyl pentazocine. Metabolite MET2, which was identified as a geometric isomer of MET1 by GC/MS, is therefore concluded to be 1,2,3,4,5,6-Hexahydro-6,11-dimethyl-9-methoxyl-3-(3-methyl-2-butenyl)-2,6-methano-3-benzazocine-8-ol (9-methoxy pentazocine) (Fig. VIII.2b).

The difference in gas chromatographic retention times between metabolic isomers MET1 and MET2 is the same as the difference in retention times between another pair of pentazocine metabolic isomers MET8 and MET9 (Table IV.2). This further supports the findings from mass spectra interpretation that isomerism for both pairs is due to a different attachment of the methoxyl group in the aromatic ring (8 or 9 position), and that MET8 and MET9 are both trans-acid (Fig. VIII.2e,f). GC retention time data (Table IV.2) also indicates that the isomerism for MET5 and MET6 is the same as MET3 and MET4, which are both due to cis and trans attachment of a hydroxyl group to the end of the side-chain (Fig. VII.2c,d).

These results clearly reveal that, in addition to the side chain



**Figure VIII.2** Structures of pentazocine metabolites produced by hydroxylation and methylation of aromatic ring and oxidation of side chain metabolism in the greyhound: (a) metabolite MET1, (b) MET2, (c) MET5, (d) MET6, (e) MET8 and (f) MET9.

oxidative metabolism, pentazocine has also undergone hydroxylation and methylation in the aromatic ring in the greyhound. As a result of this metabolism mechanism, another group of pentazocine metabolites is formed: metabolites produced by hydroxylation and methylation of the aromatic ring only, MET1 and MET2; metabolites produced by hydroxylation and methylation of the aromatic ring as well as the side-chain oxidation to alcohols, MET5 and MET6; and metabolites produced by hydroxylation and methylation of the aromatic ring and further oxidation of the side-chain to carboxylic acid, MET8 and MET9. The probable metabolic pathway of pentazocine in the greyhound is shown in Fig. VIII.3.

The comparison of chromatographic results of extracts obtained after enzymatic hydrolysis with those obtained before hydrolysis reveals that pentazocine and its metabolites are excreted in both glucuronide conjugated forms and non-conjugated forms in greyhound urine. The conjugation was found to be extensive. It is also shown that the excretion rate of pentazocine and its metabolites reaches a maximum around 6 h, and a trace of pentazocine is still detectable 24 h after the administration.

This study also indicates that unchanged pentazocine is the major form excreted, although nine other metabolites are present in greyhound urine. The relative amounts of these metabolites are: MET1  $\gg$  MET2, MET1 > MET3 > MET4, MET5 > MET6, MET7 > MET8 = MET9. These facts demonstrate not only qualitative but also quantitative differences in pentazocine metabolism in greyhound compared to those in other species.

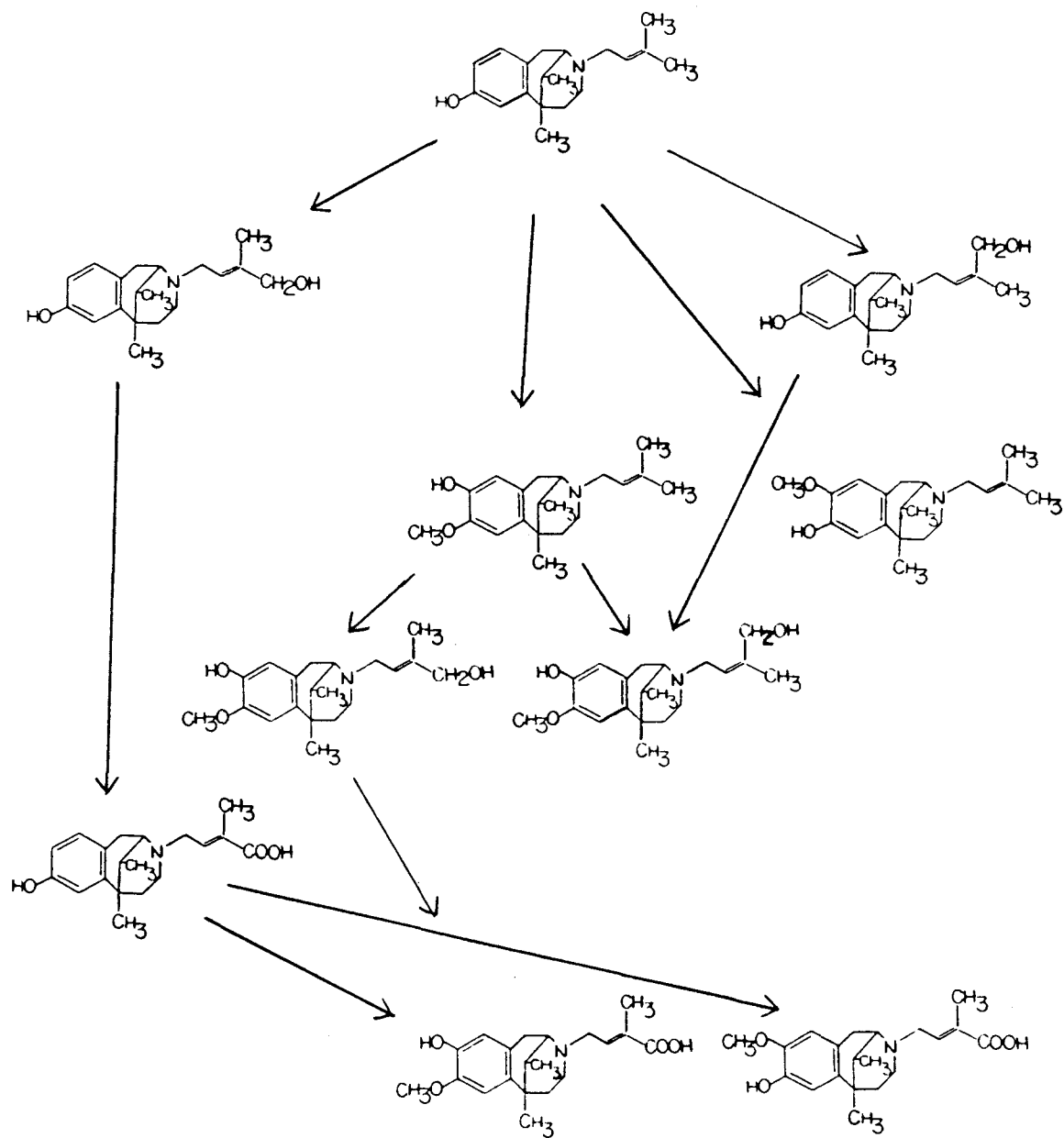


Figure VIII.3 The probable metabolic pathway of pentazocine in the greyhound.

## IX. REFERENCES

1. J. P. Payne, *Drugs*, 5, 1 (1973).
2. R. N. Brogden, T. M. Speight and G. S. Avery, *Drugs*, 5, 6 (1973).
3. T. Cox, M. R. Jacobs, A. E. Leblanc and J. A. Marshman, "Drugs and Drug Abuse ", Alcoholism and Drug Addiction Research Foundation, Toronto, 1983.
4. A. Sullivan, "Statistical Summaries from the Association of Official Racing Chemist", AORC. Reports, (1989).
5. B. A. Berkowitz and E. L. Way, *Clin. Pharmacol. Ther.*, 10, 681 (1969).
6. K. A. Pittman, D. Rosi, R. Cherniak, A. J. Merola and W. D. Conway, *Biochem. Pharmacol.*, 18, 1673 (1969).
7. S. D. James, G. C. Paugh and R. H. Waring, *Xenobiotica*, 4, 521 (1974).
8. R. K. Lynn, R. G. Smith, R. M. Leger, M. L. Deinzer, D. Griffin and N. Gerber, *Drug Meta. Dispos.*, 5, 47 (1977).
9. W. Gielsdorf and M. Tummers, *Int. J. Mass Spec. Ion Phys.*, 48, 133 (1983).
10. E. L. Way and T. K. Adler, *Bull. World Health Organization*, 25, 227 (1962).
11. R. T. Williams, "Detoxication Mechanisms", 2nd Ed., Chapman & Hall, London, 1959.
12. B. Testa and P. Jenner, "Drug Metabolism: Chemical and Biochemical Aspects", Marcel Dekker Inc., New York & Basel, 1976.

13. J. B. Tomazewski, D. M. Jerina and J. W. Daly, *Biochemistry*, 14, 2024 (1975).
14. F. T. William, "Oxidative Functionalization Reaction" in "Concepts in Drug Metabolism", P. Jenner and B. Testa, ed., Vol. 10, Chap. 3, Marcel Dekker, Inc., New York and Basel, 1980.
15. A. M. El-Mazati and E. L. Way, *J. Pharmacol. Exp. Ther.*, 177, 332 (1971).
16. D. P. Vaughan and A. J. Beckett, *J. Pharm. Pharmacol.*, 25, 895 (1973).
17. A. Stolman, *Clin. Toxicol.*, 10, 49 (1977).
18. G. Xiao, E. H. Piepmeier and A. M. Craig, *Org. Mass Spec.*, submitted for publication.
19. G. Xiao, A. M. Craig and E. H. Piepmeier, *Vet. Pharmacol. Ther.*, submitted for publication.
20. R. D. Anderson and K. F. Ilett, *J. Chromatogr.*, 227, 239 (1982).
21. T. D. Wilson, *J. Chromatogr.*, 243, 99 (1982).
22. S. T. Walker, *J. Assoc. Off. Anal. Chem.*, 68, 539 (1985).
23. S. Shibasaki, Y. Imamura, T. Itoh, K. Ishikawa, Y. Noda, S. Yazaki and H. Suzuki, *J. Chromatogr.*, 421, 425 (1987).
24. G. G. Skellern, *Proc. Anal. Div. Chem. Soc.*, 13, 357 (1976).
25. B. A. Bidlingmeyer, S. N. Deming, W. P. Price, Jr., B. Sachok and M. Petrusek, *J. Chromatogr.*, 186, 419 (1979).
26. B. L. Karger and R. W. Giese, *Anal. Chem.*, 50, 1048A (1978).
27. L. R. Snyder and J. J. Kirkland, "Introduction to Modern Liquid Chromatography", 2nd Ed., Wiley-Interscience, New York, 1979.
28. L. D. Olsen and R. J. Hurtubise, *J. Chromatogr.*, 482, 347 (1989).
29. L. R. Snyder, J. L. Glajch and J. J. Kirkland, *J. Chromatogr.*,

- 218, 299 (1981).
30. S. R. Abbott, *J. Chromatogr. Sci.*, 18, 540 (1980).
  31. W. C. Still, M. Kahn and A. Mitra, *J. Org. Chem.*, 43, 2923 (1978).
  32. L. R. Snyder and H. Poppe, *J. Chromatogr.*, 184, 363 (1980).
  33. L. R. Snyder, *J. Chromatogr. Sci.*, 16, 223 (1978).
  34. H. M. Rosenstock, B. W. Steiner and J. T. Herron, *J. Phys. Chem. Ref. Data* 6, Suppl. 1. (1977).
  35. G. Petersson, *Org. Mass Spec.* 6, 565 (1972).
  36. F. W. McLafferty, "Interpretation of Mass Spectra", 3rd Ed., University Science Books, California, 1980.
  37. H. Nakata, Y. Hirata, A. Taematsu, H. Tada and Y. Sawa, *Tetrahedron Letts.*, 13, 829 (1965).
  38. K. Biemann, "Mass Spectrometry: Organic Chemical Applications", McGraw-Hill, New York, 1962.
  39. I. Fleming, "Frontier Orbitals and Organic Reactions", Wiley, New York, 1976.
  40. L. Stella, Z. Janousek, R. Merenyi and H. G. Veihe, *Angew. Chem. Int. Ed. Engl.*, 17, 691 (1978).
  41. H. G. Veihe, R. Merenyi, L. Stella and Z. Janousek, *Angew. Chem. Int. Ed. Engl.*, 18, 917 (1979).
  42. E. Stenhagen, in "Biochemical Applications of Mass Spectrometry", G. R. Waller, Ed., Wiley-Interscience, New York, 1972.
  43. F. Bloch, W. W. Hansen and M. Packard, *Phys. Rev.*, 69, 127 (1946).
  44. E. M. Purcell, H. C. Torrey and R. V. Pound, *Phys. Rev.*, 69, 37 (1946).
  45. D. F. Ewing, *Nucl. Magn. Reson.*, 11, 71 (1982).

46. J. A. Pople, W. G. Schneider and H. J. Bernstein, "High-Resolution Nuclear Magnetic Resonance", McGraw-Hill, New York, 1959.
47. J. H. Noggle, J. H. and S. Schirmer, "The Nuclear Overhauser Effect", Academic Press, New York, 1971.
48. R. R. Ernst and W. A. Anderson, Rev. Sci. Instr., 37, 93 (1966).
49. T. C. Farrar, Anal. Chem. 59, 679A (1987).
50. J. D. Ingle and S. R. Crouch, "Spectrochemical Analysis", Prentice-Hall, New Jersey, 1988.
51. D. Shaw, "Fourier Transform NMR Spectroscopy", Elsevier, Amsterdam, 1984.
52. P. C. Lauterbur, J. Chem. Phys., 21, 217 (1957).
53. C. H. Holm, J. Chem. Phys., 21, 707 (1957).
54. G. C. Levy, R. L. Lichter and G. L. Nelson, "Carbon-13 Nuclear Magnetic Resonance Spectroscopy", 2nd Ed., Wiley-Interscience, New York, 1980.
55. G. C. Levy, "Topics in Carbon-13 NMR Spectroscopy", Vol. 3, Wiley, New York, 1979.
56. R. M. Silverstein, G. C. Bassler and T. C. Morrill, "Spectrometric Identification of Organic Compounds", 4th Ed., Wiley, New York, 1981.
57. E. Breitmaier and G. Bauer, Pharmazie in Unserer Zeit, 5, 97 (1976).
58. Atta-ur-Rahman, "Nuclear Magnetic Resonance", Springer-Verlag, New York, 1986.
59. R. Benn and H. Gunther, Angew. Chem. Int. Ed. Engl., 22, 350 (1983).

60. D. L. Turner, *Prog. Nucl. Magn. Reson. Spectrosc.*, 17, 281 (1985).
61. A. Bax and L. Lerner, *Science*, 232, 960 (1986).
62. W. R. Croasmun and R. M. K. Carlson, "Two-Dimensional NMR Spectroscopy", VCH, New York, 1987.
63. W. P. Aue, E. Bartholdi and R. R. Ernst, *J. Chem. Phys.*, 64, 2229 (1976).
64. R. Freeman and G. A. Morris, *Bull. Magn. Reson.*, 1, 5 (1979).
65. E. L. Hahn and D. E. Maxwell, *Phys. Rev.*, 88, 1070 (1952).
66. G. Bodenhausen and R. R. Ernst, *J. Am. Chem. Soc.*, 104, 1304 (1982).
67. R. R. Ernst, *ACS Symp. Ser.*, 191, 47(1982).
68. M. B. Bruch, in "NMR Spectroscopy Techniques", C. Dybowski and R. L. Lichter, Ed., Marcel Dekker, New York, 1987.
69. A. Bax and R. Freeman, *J. Magn. Reson.*, 44, 542 (1981).
70. Y. Takeuchi and A. P. Marchand, "Applications of NMR Spectroscopy to Problems in Stereochemistry and Conformational Analysis", VCH, Florida, 1982.
71. A. Bax and G. A. Morris, *J. Magn. Reson.*, 42, 501 (1981).
72. A. A. Maudsley and R. R. Ernst, *J. Magn. Reson.*, 28, 463 (1977).
73. H. Kessler, C. Griesinger and J. Lautz, *Angew. Chem., Int. Ed. Engl.*, 23, 444 (1984).
74. J. Jeener, B. H. Meier, P. Bachman and R. R. Ernst, *J. Chem. Phys.*, 71, 4546 (1979).
75. S. Macura and R. R. Ernst, *Molec. Phys.*, 41, 95 (1980).
76. P. L. Fuchs, "Carbon-13 NMR based on Organic Spectral Problems", Wiley, New York, 1979.

77. E. Breitmaier and G. Bauer, "Carbon-13 NMR Spectroscopy A Working Manual with Exercises", Harwood, Chur, 1984.
78. E. Wenkert, J. S. Bindra, C-J. Chang, D. W. Cochran and F. M. Schell, *Acc. Chem. Res.*, 7, 46 (1974).
79. H. Booth, and D. V. Griffiths, *J. Chem. Soc. Perkin II*, 842 (1973).
80. D. M. Grant and E. G. Paul, *J. Am. Chem. Soc.*, 86, 2984 (1964).
81. E. Breitmaier and W. Voelter, "Carbon-13 NMR Spectroscopy: Methods and Applications", "Monographs in Modern Chemistry", Vol. 5, H. E. Ebel, Ed., Verlag Chemie GmbH, Weinheim, 1978.
82. A. D. Buchingham, *Can. J. Chem.*, 38, 300 (1960).
83. A. D. Buchingham, T. Schaefer and W. G. Schneider, *J. Chem. Phys.*, 32, 1227 (1960).
84. J. L. Marshall, "Carbon-Carbon and Carbon-Proton NMR Couplings: Applications to Organic Stereochemistry and Conformational Analysis", Verlag Chemie International, Florida, 1983.
85. J. W. Daly, D. M. Jerina and B. Witkop, *Experientia*, 28, 1129 (1972).
86. D. M. Jerina, N. Kawbisich and J. W. Daly, *Proc. Nat. Acad. Sci. U. S.*, 68, 2545 (1971).
87. J. K. Seydel, *J. Pharm. Sci.*, 57, 1455 (1968).
88. S. H. Wan, B. von Lehmann and S. Riegelman, *J. Pharm. Sci.*, 61, 1288 (1972).